Università degli Studi di Ferrara

DOTTORATO DI RICERCA IN

"Scienze della Terra"

CICLO XXX

COORDINATORE Prof. Massimo Coltorti

Smart Sensor Technology for Environmental Monitoring Applications

Settore Scientifico Disciplinare GEO/09

Dottorando

Dott. Ilie Ana Maria Carmen

Ana MC Ilie

Tutore

Prof.ssa Vaccaro Carmela

Prof. Hannigan Michael

(University of Colorado at Boulder, USA)

Anni 2014/2017

Acknowledgements

I would like to express my deepest gratitude to my supervisor, Prof. Dr. Carmela Vaccaro for offering me this opportunity to undergo my PhD research under her guided assistance. Her words of encouragement have been very helpful throughout my research work, and gave me a huge opportunity on having an International research project, 6 months at LNEC – Lisbon, and 11 months at Mechanical Engineering Department, University of Colorado at Boulder, USA; as well as in Denmark, Copenhagen DTU Nanotech amd University of Michigan, USA so that I could improve my knowledge in Smart Sensor Technology. I thank Francesco Droghetti, Paolo Chiarelli, Umberto Tessari and Renzo Tassinari for a field and laboratory technical support.

I would also like to thank Prof. Dr. Michael Hannigan to accepted me in his research group and for all the support for the Research. I really appreciate the support and assistance of my colleagues: Joanna G. Casey, Evan Coffey, Ricardo Piedrahita, Ashely Colier, Drew, Rebecca Bullard, during most of the field campaigns, laboratory technical support, programming software used in the Y-PODs nodes in this research.

Thanks to my little sister Nicoletta Abbondandolo, and to my housemates in Boulder and most importantly, my beloved family and to a special person in my life Ayush Rastogi, I appreciate their words of encouragement throughout my study.

TABLE OF CONTENTS

LIST OF FIGURES

II. SMART SENSORS TECHNOLOGY

III. ENVIRONMENTAL MONITORING APPLICATIONS

Peer reviewed publications

LIST OF FIGURES:

Chapter 1
I. INTRODUCTION

Research Project focused on developing innovative devices using the low-cost sensors to obtain the concentrations of greenhouse gases (GHGs) epecially carbon dioxide (CO2) and methane (CH4); devices suitable to measure water parameters related to gas migration by diffusion in aquifers. Intelligent remote managed systems of the Global Navigation Satellite System (GNSS) are integrated with the new generation sensors for environment monitoring applications. In addition to sensor calibration, the multi-parameter monitor prototype has been tested in several contexts: a) Laboratory scale with natural soil columns, to figure out the sensor response under controlled conditions. The predefined parameters of porosity, permeability and physical-mechanical properties that control the hydraulic conditions have allowed to describe the gas diffusion into porous media. b) Field scale in many geological contexts, for Air-Soil quality: Natural Gas Storage Site in Minerbio, Italy; Drilling and Hydraulic Fracturing activities in Greeley, CO, USA; for Water Quality: Wastewater Treatment Plant in Algarve, Portugal. The monitoring system provides a huge set of data for which can be used statistical analysis, management and processing (Big DATA). The source identification of greenhouse gas emissions is identified in several IPCC reports that climate change is the major emergency for the socio / economic / environmental equilibrium of Earth planet.

I.1 Natural Gas Storage Site Monitoring System in Minerbio, Italy

I.1.1 Problem statement

Monitoring is an essential element of geologic carbon storage (GCS) risk assessment, management and communication framework recommended by IEAGHG, and described in frameworks proposed by government agencies and authoritative organizations (IEA, 2009). Moreover, GCS monitoring plans have to be able to meet regulatory requirements, include various monitoring tools and approaches, and support site-specific risk assessment (Hovorka SD, 2012). A general and simpler model-based framework of Bayesian belief network was also proposed for CO2 leak detection at geologic sequestration sites and illustrated using ZERT-test-based near-surface CO2 seepage simulations and soil gas monitoring techniques (Yang et al, 2012). Besides these system frameworks, the detectability and spatial resolutions for several monitoring technologies have been evaluated using simulations of potential leakage response, such as near-surface soil flux and tracer measurement (Yang et al, 2012), pressure monitoring at different depths (Sun et al, 2013; Wang et al, 2014; Azzolina et al, 2014; Keating et al, 2014) and shallow groundwater monitoring (Keating et al, 2014, Dai et al, 2014; Yang et al, 2015). Among these, the concept of detection coverage or detection probability, typical objectives in groundwater monitoring network (Meyer et al, 1994; Reed PM et al, 2004; Bode et al, 2015), has been applied to evaluate GCS monitoring network design, such as the detection probability of a monitoring network for a leakage event (Yang at el, 2012), monitoring effectiveness (ME) of a shallow groundwater wellbore leakage event (Yang et al, 2015)

and the overall detection probability (Keating et al, 2014) for stochastic simulations of groundwater wellbore leakage. In Minerbio city, a Methane Gas storage site is developed, so that soil-atmosphere measurements of methane and radon gas, at 10cm and 1m depth was the main purpose of the PhD research project. Measurements have been taken for radon concentrations with a Durridge RAD7 Company, Inc., USA instrument. It was used for atmosphere and soil gas monitoring system three Biogas ETG (Etg Risorse e Tecnologia, Italy) instruments, with nondispersive infrared sensor (NDIR) CH_4 gas sensor. The measurements started in March 2016 and continued in July-August-September 2016, to determine methane and radon gas concentrations, their distribution and to understand the relationship among gases and atmospheric conditions. What distinguishes this study from those conducted at other gas storage site is the methodology used, the monitoring system was done in the same time in atmosphere and at different depths into the soil (10 cm and 1m depth) to understand the differences of methane gas concentration between atmosphere and soil.

I.1.2 Geology Settings of Pianura Padana, Minerbio (BO), Italy

It is well established that a thick clastic sequence fills the Po Plain flexural basin, burying the outermost thrust sheets of the Northern Apennines fold-and-thrust belt and the southernmost thrust sheets of the Southern Alps. Due to the combination of fast sedimentation rates and low deformationrates, the thrusts are buried and the surface evidence of their activity is faint and elusive. The tectonic setting of the buried Northern Apennines is characterized by three adjoining arcs: Monferrato, Emilia and Ferrara-Romagna, respectively from west to east (fig. 1).

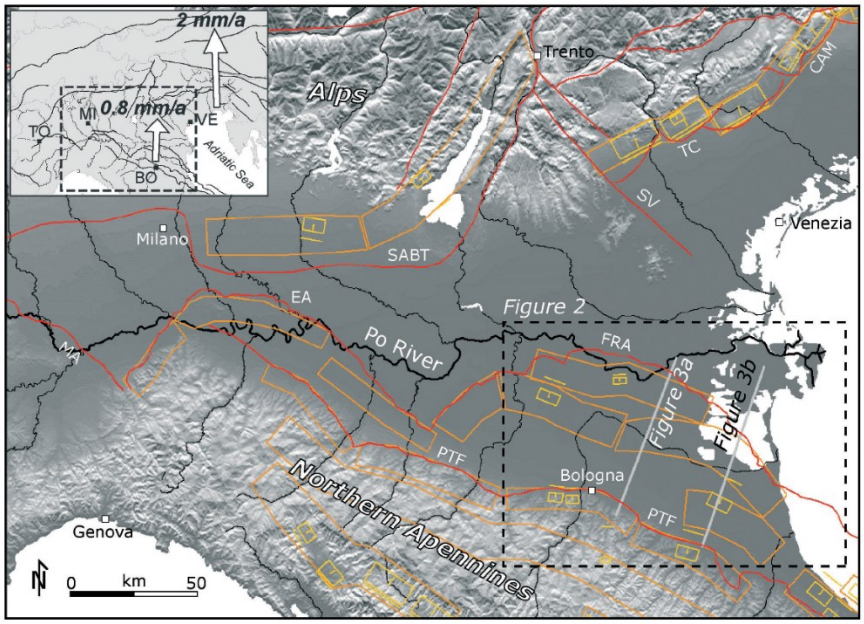

Fig. 1 - Simplified tectonic map of the Po Plain and surrounding regions, showing the Northern Apennines and Southern Alps main thrusts and faults as red lines. Yellow and orange polygons: individual seismogenic sources and seismogenic areas, respectively,

from DISS database (DISS WORKING GROUP, 2007; BASILI *et alii*, 2008). Structures: Monferrato Arc, MA; Emilian Arc, EA; Ferrara-Romagna Arc, FRA; Pedeapenninic Thrust Front, PTF; Western Southern Alps buried thrust, SABT; Schio-Vicenza line, SV; Thiene-Conegliano thrust front, TC; Cansiglio- Maniago thrust front, CAM. GPS vectors in the inset are from SERPELLONI *et alii* (2005).

The Ferrara-Romagna arc is further subdivided into three second order structures: Ferrara, Romagna and Adriatic (BIGI *et alii*, 1990). These buried surfaces develop over large areas and are deformed in synclines and anticlines; these latter located above the ramps of the blind thrusts. From the deepest (oldest) to the shallowest (youngest), the most continuous surfaces are: 1) the bottom of the Pliocene marine deposits, a first order stratigraphic marker (fig. 2) overlain by sediments varying in age within the Pliocene succession at the scale of the entire Po Plain; 2) the bottom of the Quaternary continental deposits, which coincides with the bottom of the lower alluvial unit (ca. 0.65 Ma); and 3) the bottom of the upper alluvial unit (traditionally dated ca. 0.35-0.45 Ma). The overall sedimentary evolution of the Po Plain follows a regressive trend, from an open marine environment in the Pliocene to shallow marine, paralic and continental environments throughout the Quaternary. The Upper Quaternary sedimentary bodies are separated by major unconformities related to glacio-eustatic cycles (AMOROSI *et alii*, 2004). In cross-section, the sedimentary bodies defined by the regional marker surfaces exhibit growth strata on the limbs of the anticlines, thus testifying the synsedimentary activity of these folds. Growth strata have been effectively used to quantify deformation rates after careful removal of differential compaction effects (SCROCCA *et alii*, 2007).

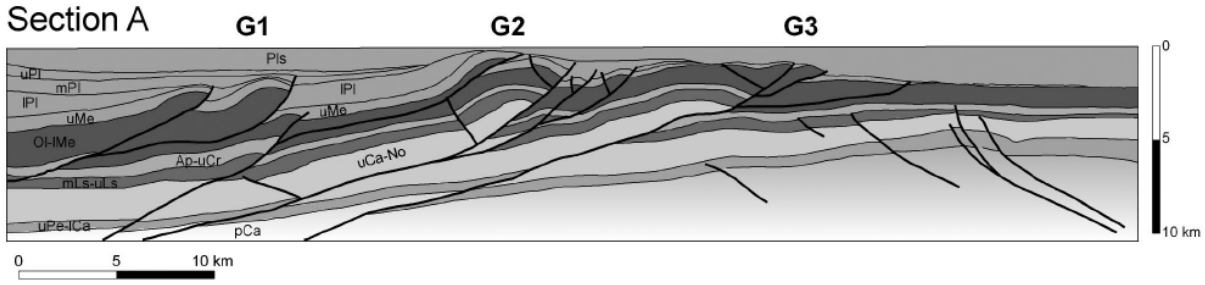

Fig. 2 - Schematic structural sections across the study area. Section A (Bologna-Ferrara, see trace in fig. 2) has been interpreted and depthconverted from seismic data; section B was redrawn after MASSOLI *et alii* (2006). Labels: Pls=Pleistocene; uPl=Upper Pliocene; mPl=Middle Pliocene; lPl=Lower Pliocene; uMe=Upper Messinian; Ol-lMe=Oligocene-Lower Messinian; Ol=Oligocene; Ap-uCr=Aptian-Upper Cretaceous; mLs-uLs=Middle-Upper Lias; uCa-No=Upper Carnian-Norian; uPe-lCa=Upper Permian Lower Carboniferous; pCa=pre-Carboniferous. group of ramp anticlines G1=group 1 of structures; G2=group 2; G3=group 3.

No faults involve the bottom of the Quaternary deposits, which appear to seal the brittle structures that were

active up to the end of the Pliocene. All the observed structural features join each other to form a main and wider structural arc, as highlighted also by the third group of ramp anticlines (group G3, fig. 10). This group includes the outermost thrusts, which again show the same structural style on both sections, with a deeper thrust and associated secondary structures.

I.1.3 Natural Gas Storage site

The Minerbio field, discovered in July 1956, lies under the Minerbio village, around 25 Km from Bologna and it is the most important underground Natural Gas Storage in Italy and Europe. The hydrocarbon bearing zone (seven pools) was discovered in the middle-upper Pliocene sediments at a depth of around 1300 meters. The filling of the Pliocene-Pleistocene Apennine foredeep has been estimated to exceed 7,000 meters in the thickest depocenters (Pieri and Groppi, 1981). Production started in March 1959 and continued until 1972. In the production period around 12.8 billion cubic meters were produced, equal to 90% of the original gas in place. The static pressure declined from the original 153.0 Kg/cmq to 30 Kg/cmq. The water table rose to 1260 meters. Gas injection started in April 1975; only three of sixteen existing wells were utilized. The stage of primary production of the field lasted until 1971, with the drilling of 36 wells, including 24 productions. Subsequently, in 1975, four levels, of which the most important are the ones called C1 and C2, were interested in converting storage activities, which currently employs 51 injection / supply wells arranged in clusters and 6 light-wells for monitoring reservoir pressures; all other wells drilled in the primary production were closed, (Fig. 3).

Fig.3 Natural Gas Storage Site, Minerbio, BO, Italy. (www.stogit.com)

I.1.4 Methodologies

All the measurements have been done surrounding Minerbio city (fig.4) and nearby gas storage wells. Air-Soil samples have been taken at the same daytime on each sampling visit between 9am to 4pm (U.T). Three instruments were used for the gas survey within Minerbio area, (fig. 5). A stainless-steel probe, diameter 6.4mm, was used for the soil gas monitoring and the holes were augered to a depth of 1m. The air pump into the instruments was used to draw the soil gas about 1L/min. A new device was built with low-cost sensors to measure the air quality and water parameters, (fig.6). Further information about the methodologies are specified in the Articles (on page 95, 101).

Fig.4 Gas survey measurement, Minerbio area. The yellow color specify all locations under gas monitoring control, the green color specify the Wells used for the Gas Storage activities, all of them surrounding the Minerbio city.

Fig.5 Instruments used during gas survey measurement, for methane and radon concentrations. The three ETG devices were used for methane concentrations and the Durridge RAD7 device with the drierite was used for radon concentrations.

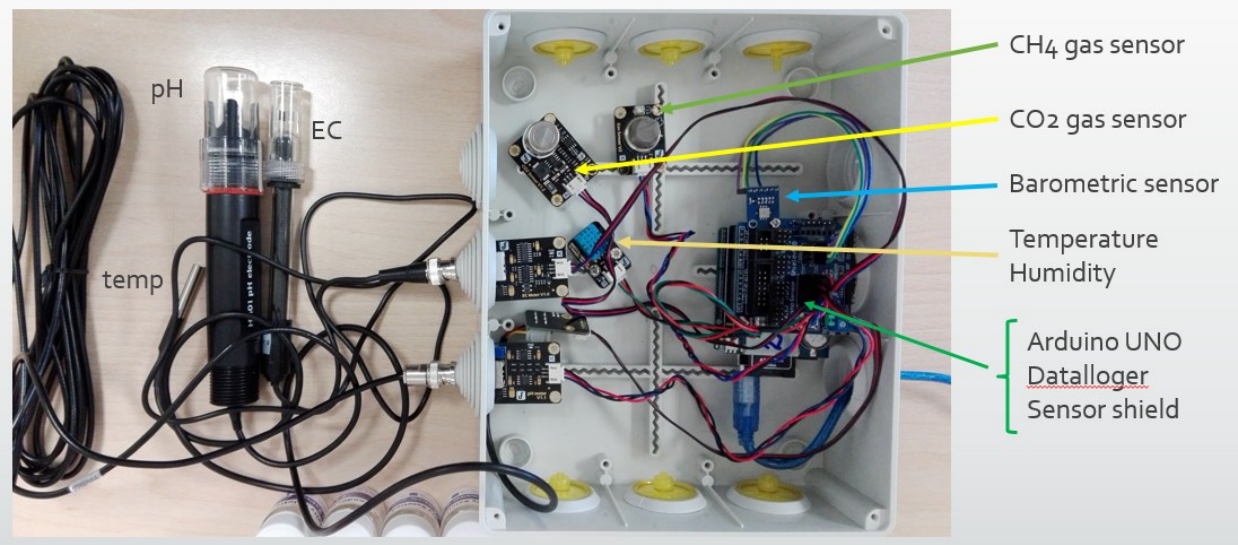

Fig.6 Device that measure Air and Water Quality continuously, by using new low-cost sensors. This new Prototype was built at the University of Ferrara, Earth Sciences Department during my PhD research program. It was built and programmed in C++ language for Arduino microcontroller and Python for RaspberryPi3 micrcontroller for data transmission. It was presented at the International Conference in Texas, USA – Session Co-Chairs: NASA.

I.1.5 Results

The gas measurement survey carried out throughout the Minerbio area, no outliers have been identified. The measurements continued in March-July-August-September 2016, almost at the same time in the same place around the gas storage site, for fifteen minutes for each sampling. At a depth of 1 meter, the maximum soil radon gas concentration was about 1770 ±±582 Bq/m3, the soil consists of 64.31% sand, 20.75% silt and 14.94% clay, and with 0.526 ppm of Uranium. The maximum concentration of methane was about 0.06% in September, into the soil at a depth of 1m, soil characterized by 83% sand, 8.96% silt and 7.89% clay and in atmosphere we had the same value. For the other months, the values have been on the range of 0.01% to 0.03% CH4. Further information is specified on the Article (on page 101).

I.1.6 Discussions

The research focused on soil-atmosphere measurements of methane and radon. A possible methane gas leak detection can be imediatley understood my obtaing the methane concentrations into the soil and atmosphere. It is well known that we should expect higest concentrations of methane into the soil, considering the microbial soil activities as well. Methane (CH4) is formed in the final step of anaerobic microbial degradation of organic matter and is released from wetlands via different transport mechanisms. The most important transport mechanism in this context is diffusion along the concentration gradient between wetland

soil and atmosphere. As this process is very slow it allows up to more than 90 % of the available CH4 to be oxidized by methanotrophic bacteria to carbon dioxide (CO2) before it reaches the soil surface (Sundh et al. 1995, Roslev and King 1996). Aerobic microbial CH4 oxidation is considered as one of the key processes regulating wetland CH4 fluxes (Segers 1998, Whalen 2005). The extent to which the produced CH4 is oxidized, the CH4 oxidation efficiency, is controlled by the key factors: 1) rate of microbial oxidation (Wang et al. 2004) and 2) rate of diffusion of CH4 (Dueñas et al. 1994, Curry 2009). These rates are mainly governed by the abundance and composition of methane-oxidizing microbial communities and the environmental factors CH4 and oxygen (O2) availabilities, soil air-filled porosity and soil-water content. The reason why I focused on methane gas measurments, was because of Minerbio City surrounded by so many wells for the Gas Storage activities and mostly methane is an important greenhouse gas with a radiative efficiency of 3.7 x 10-4 W m-2 ppb1. OH radicals oxidize 85-90 % of atmospheric CH4 to CO2 with the loss of CH4 reducing OH density (O'Connor et al. 2010). This feedback mechanism increases its atmospheric lifetime of 8.4 yrs to a perturbation lifetime of 12 yrs (Denman et al. 2007).

I.1.7 Recommendations

The Phd research focused on the new technology monitoring system, for methane especially. Three ETG commercial instruments were used for methane measurements, in order to understand all issues that these instruments could show up on a geologic field campaign. The idea was to build my own instrument, prototype, after the geologic field campaign. Most of the commercial instruments can be used for several hours, not continuously, since the battery need to be recharged. The instruments used were working for no more than 5 hours, so it meant I would never obtained diurnal variations of methane concentrations by using these devices. The first thing was to build my own prototype with a good battery, rechargeable by solar panel, or by using directly the electricity with 5V in output. The ETG devices showed on a digital screen the CO2%, CH4%, temperature and atmospheric pressure and the issue was that all data saved on USB did not present the temperature and pressure values, so I lost all meteorological data and I could not consider the methane values related to the temperature, humidity or pressure in that specific location, I had to obtain the data from a meteorological station in Minerbio. Furthermore, the microcontroller was programmed in order to obtain the gas concentration levels up to tenth decimal place value, instead of hundredth. This lead to the rounding off of the measurements and yielded incorrect results. For example a values of 0.14% was rounded to 0.1%. This issue also led to an incorrect time series and hence an inaccurate analysis on a Cartesian plot. In my Article (pag. 101), I had to consider just average values to have an idea about the methane gas concentrations.

The instruments presented an internal air pump which had almost 2l/min, and could not be modified at all. From the literature, it is well known that the air pump should be around 1l/min. With high temperature

values the devices warmed up so fast and the battery run for no more than 4 hours. The devices were so heavy and difficult to work in the field in many locations. All these issues were considered and improved in my new Prototype device, real time data, continuosly monitoring, data saved with gas concentrations and meteorological data, as well as this Prototype could be modified anytime and reprogrammed again to record soil-atmopshere measurements in the same time and related to the aquifers for the water quality. With one device, one can use it for different environments, the only thing is to choose a good sensor and calibrate it. Further information about it is presented in my Article (on page 95).

I.2 Drilling and Hydraulic fracturing activities in Greeley, Colorado, USA

I.2.1 Problem statement

In Colorado and elsewhere in North America, the oil and gas production industry has been growing alongside and during increasing urban and rural populations. These coinciding trends have resulted in a growing number of people living near petroleum production and processing activities, leading *to potential public health impacts*. Combustion-related emissions from heavy-duty diesel vehicle traffic, generators, compressors, and production stream flaring can potentially lead to locally enhanced levels of nitrogen oxides (NOx), carbon monoxide (CO), and carbon dioxide (CO2). Venting and fugitive emissions of production stream constituents can potentially lead to locally enhanced levels of methane (CH4) and volatile organic compounds (VOCs), some of which (like benzene) are known carcinogens. NOx and VOC emissions can also potentially increase ozone (O3) production. After learning of a large new multiwell pad on the outskirts of Greeley, Colorado, we could quickly mobilize portable air quality monitors outfitted with low-cost gas sensors that respond to CH4, CO2, CO, and O3. The air quality monitors were installed outside homes adjacent to the new multiwell pad several weeks prior to the first spud date. An anemometer was also installed outside one of the homes to monitor wind speed and direction. Measurements continued during drilling, hydraulic fracturing, construction of the pipelines and production phases. The sensors were periodically collocated with reference instruments at a nearby regulatory air quality monitoring site towards calibration via field normalization and validation. As results are presented measurements of CH4ppm and CO2ppm in context with wellpad activities and local meteorology. Since we were using low-cost sensors, several experiments for temperature (T°C) and humidity (H %) were considered. It is well known the sensors are sensitive to atmospheric conditions, so that three experiments were done. First experiment with no T°C and H% control, the second experiment with just the T°C control and the third experiment with the T°C and H% control. During my PhD research I focused on methane and carbon dioxide gas sensors due to the high number of the instruments used, 25 devices divided in several experiments. In the near future we expect to analyze carbon monoxide and ozone, since the data are already available and we could understand the gas concentrations (CO an O3) related to the drilling and hydraulic fracturing activities.

I.2.2 Geology settings of Denver basin, Greeley, Colorado, USA

Drilling and Hydraulic fracturing activities in Greeley are part of the Niobrara formation. The Niobrara formation was deposited beginning nearly 90 million years ago. At that time, an inland seaway submerged all of what is today Colorado in shallow (<100 feet), to moderately deep (>1500 feet), salt water. For the next six to seven million years, calcareous debris from algae and the remains of abundant marine life living

in this seaway slowly accumulated. Additionally, sediment was shed from Utah mountain range growing to the west. When the sea finally withdrew, thick layers of clay, mixed clay and limestone, chalk, and smaller amounts of silt and sand were left behind to form some of the sedimentary rocks (Wrucke and Wilson, 1957; Brandt et al, 2003a; Madole et al. 1998).

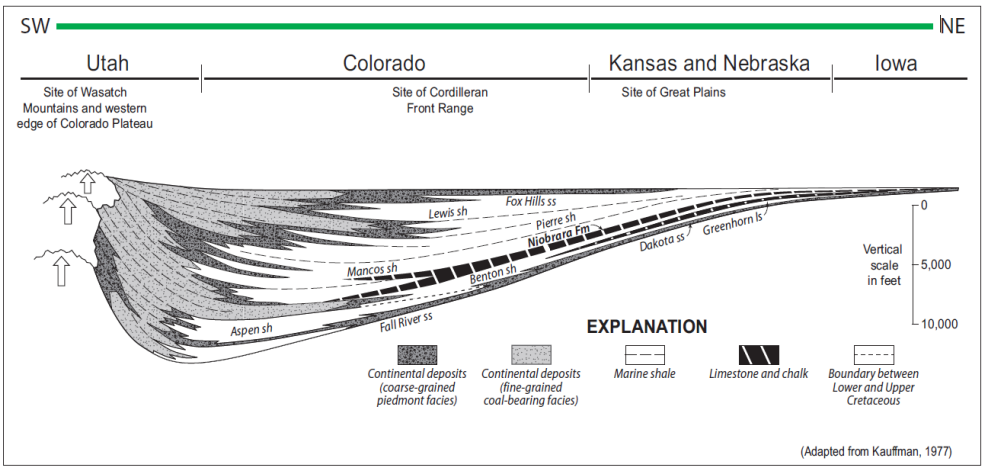

Figure 7. This cross section shows the accumulated sediments at about 60 million years ago in the inland seaway of the late Cretaceous. Toward the west, the Niobrara Formation is part of the Mancos Shale rocks.

Interaction of cooler and warmer waters occurred around the latitude of present day Colorado and Wyoming, so that the alternating layers of shale and chalk generally coincide with the presence of cooler and warmer water respectively at the time of deposition, (Wrucke and Wilson, 1957; Brandt et al, 2003a; Madole et al. 1998).

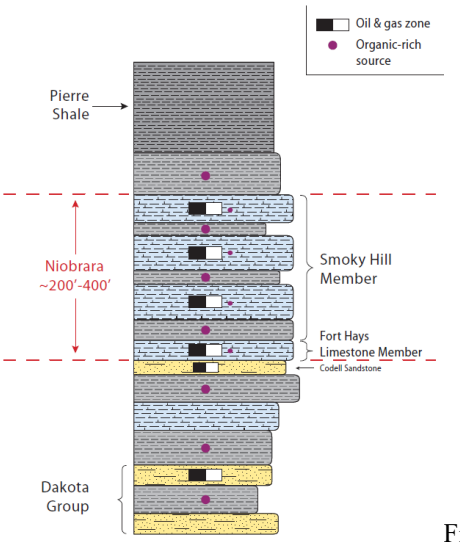

Figure 8. Niobrara Formation stratigraphy for northeastern Colorado. Shales (gray) usually act as source rock and fractured limestones (blue) act as reservoirs. In places, the limestones

can also act as lesser source rocks. In rock units below the Niobrara interval, the sandstones (yellow) can be good hydrocarbon reservoirs as well.

The overall thickness of the Niobrara Formation varies between 200 and 400 feet in northeastern Colorado. In northwestern Colorado, however, thicknesses can be much greater in places more than 1500 feet, (Brandt et al, 2003a). The Niobrara Formation has long been recognized as a hydrocarbon producer in Colorado. The earliest oil production from the Niobrara was in the 1920s in the northwestern part of the state in Rio Blanco, Moffat, and Routt counties. Startingin the mid 1950s through the 1960s, the occasional Niobrara producing wells were drilled in the Denver Basin. As of November 2010, more than 900 wells have at one time produced oil from the Niobrara Formation in the Denver Basin, the overwhelming majority in Weld County. More than 4,000 Colorado wells have produced natural gas from the Niobrara. This is a minimum number, however, as it does not include Niobrara comingled wells (i.e. wells that produce from multiple rock formations). With these wells included, the total Niobrara gas well-count jumps to more than 15,000. In the last decade, 2,738 Niobrara-exclusive gas wells have been completed in Colorado. Horizontal drilling and artificially fracturing the rock have encouraged Niobrara drilling activity in recent years.

I.2.3 Drilling and Hydraulic fracturing activities

In the Denver Basin, the typical Niobrara Formation is approximately 400 feet thick and consequently the potential production zone exposure for a single well will be limited to 400 feet. A horizontal well, however, can increase this reservoir exposure by 10 to 12 times. Wells are often drilled, parallel to the producing layer after the targeted vertical depth is reached. Several newer technologies are used in horizontal drilling. A hydraulic motor just above the drill bit allows the bit to be rotated without rotating the drill pipe. The most recent generation of equipment can allow for a 90 degree turn in just a few feet. A suite of sensors provides the compass direction, the inclination of the drilling assembly, and can even provide the three-dimensional position (x, y, and z location) of the drill bit. Other sensors let drillers know what the conditions are deep in the subsurface including the temperature and some important physical properties of the rocks.

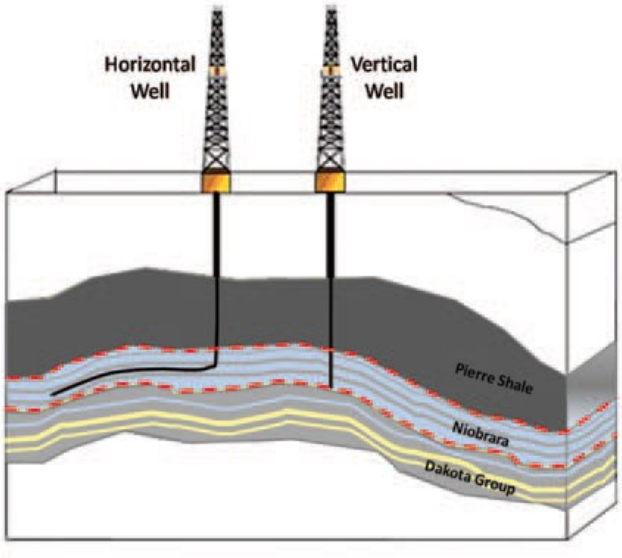

Figure 9. Drilling horizontal versus traditional vertical wells, (Modified from EIA, Office of Oil and Gas, 1993).

A horizontal well also increases the possibility that the wellbore will intersect naturally occurring fractures and positions it for better generation of artificial fractures. Additionally, horizontal wells reduce the surface footprint of wellhead operations as several wells can originate from the same point on the surface. Hydraulic fracturing is a critical technology for the generation of fractures in the Niobrara. Pumping water and other fluids into the formation to raise pressure and force localized cracks to penetrate farther into the reservoir formation is the first stage. Once the fractures are opened, a proppant such as sand is typically used to keep these fluid pathways open. The Colorado Oil and Gas Conservation Commission (COGCC) is responsible for reviewing the design and operation of artificially fractured wells to ensure their safety.

I.2.4 Y-PODs Platform, low-cost sensors

The Y-Pods devices, (fig.10), that I used for the PhD research project, were developed in the Professor Michael Hannigan's Research Group at University of Colorado Boulder, Mechanical Enginering Department, CO, USA. They are low cost (<$1,000) technology that is currently being field tested and refined for air quality research use. Pods can be used indoors or out, and use a wall outlet or car battery for a power source. The sensors that are used in the Pods are a combination of metal oxide semi-conductors, electrochemical, and non-dispersive infrared. Pods measure carbon dioxide, methane, carbon monoxide, total volatile organic compounds, ozone, (fig.11), Temperature, relative humidity, wind speed and direction, and have GPS capabilities. It was developed a web-based data visualization tool (only compatible with Y-Pod data) where one can upload and plot pod data, download simplified excel files, and view other user's data.

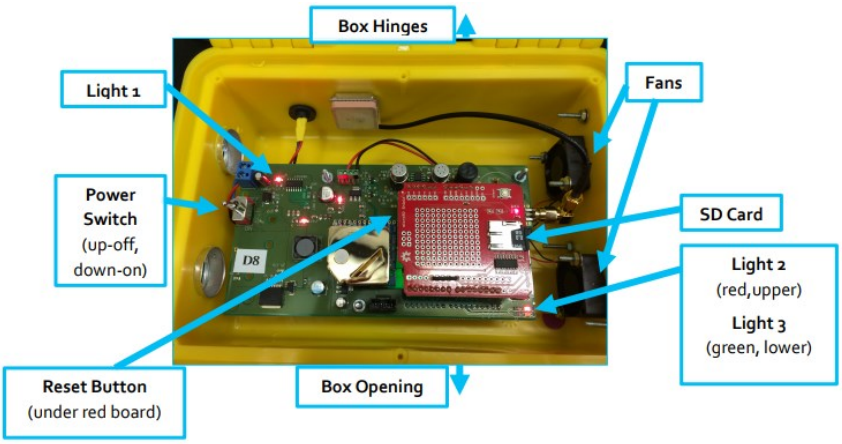

Figure 10. Pod feature diagram.

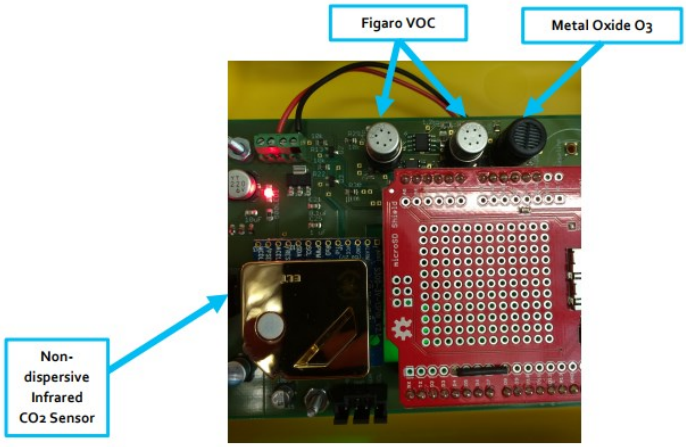

Figure 11. Gas-phase species sensors.

The picture above shows the locations of each sensor on the board. The Figaro VOC sensors have silver caps (not black caps). The ozone sensor has a black plastic cap, and the CO2 sensor is a gold square. The Figaro VOC 2602 is sensitive to heavy hydrocarbons only, whereas the Figaro VOC 2600 is sensitive to both light and heavy hydrocarbons. The ID of Y-PODs are: C1 – C2 – C3, G1 – G10, H1 – H6.

I.2.5 Methodologies

Field deployment and sensor experiments

Y-POD devices were used for several experiments, air and soil monitoring system, that employ low-cost NDIR, metal oxide and electrochemical type gas sensors as well as temperature, pressure, and humidity sensors. The Research Project focused on:

1st: Building 25 instruments (Air – Soil), Real time Data – Xbee; Prepare the cases for the temperature and humidity control; (fig.13)

2nd: Air & Soil Quality Monitoring System in Greeley, Colorado; (fig.12 – 14)

3rd: Field Calibration; (fig.12)

4th: Humidity and Temperature control, Lab and Field experiments; (fig.15-16-17)

Figure 12. Gas survey measurement surrounding drilling and hydraulic fracturing activities, and field calibrations. First the devices were co-located with Picarro reference instrument and other more than 10 devices working for many years. It was deployed around the Drilling and Hydraulic activities three system monitoring.

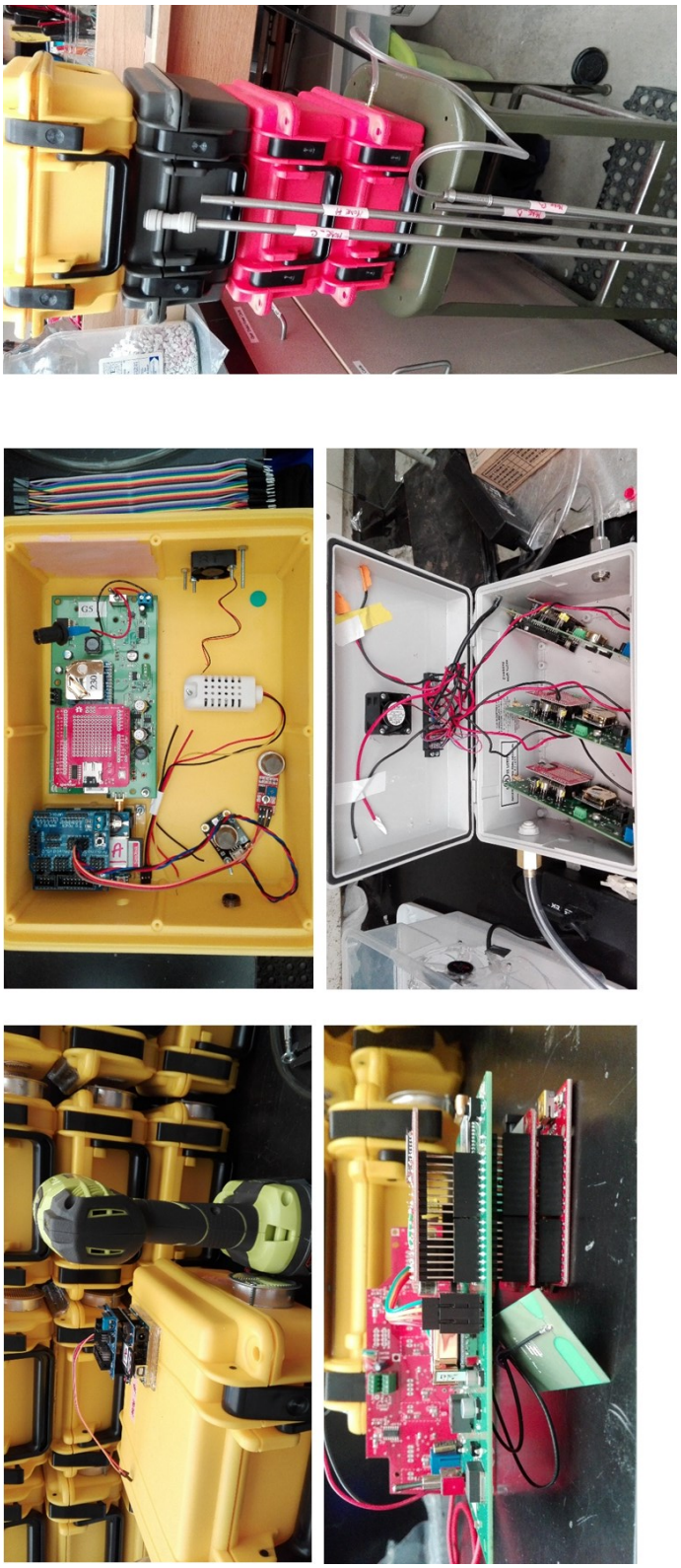

Figure 13. The Y-PODs built for several experiments and for Air - Soil quality monitoring system. In the yellow cases one can notice different microcontrollers and boards with the sensors used. In the white case it can be noticed the location of the 3 boards with CO2 and CH4 sensors for temperature and humidity control experiment.

Soil Monitoring System:

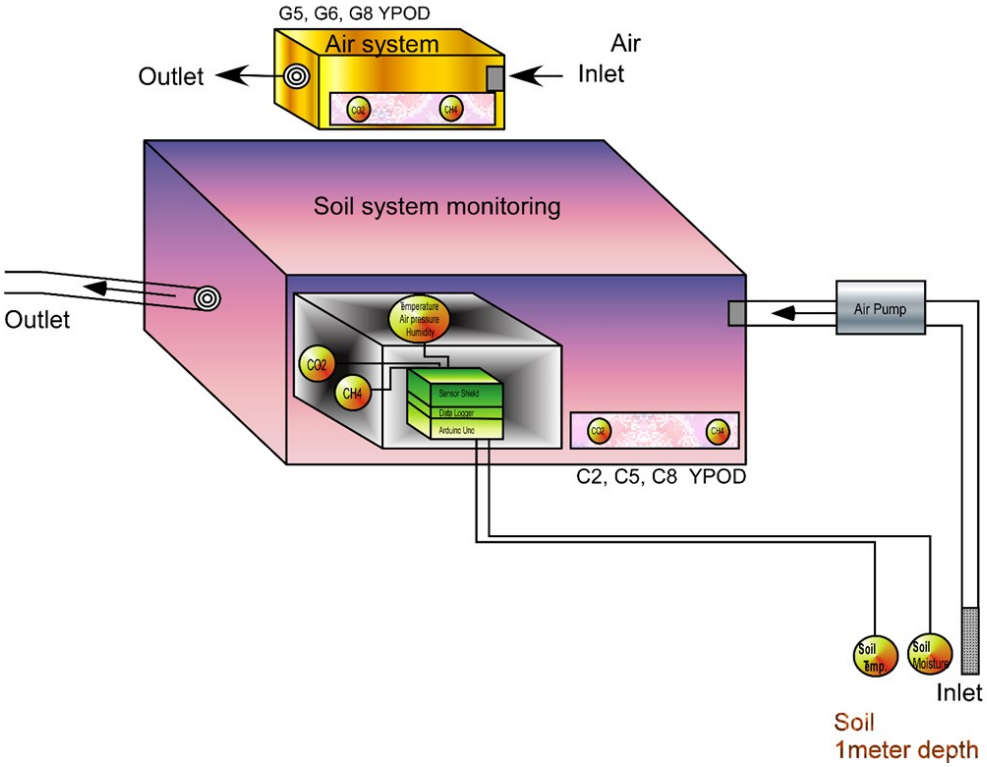

Figure 14. Air&Soil gas monitoring system. This device was built by myself, modifying the real device of University of Colorado in order to collocate the Prototype used in Italy (University of Ferrara, Earth Sciences Department) with their Prototype (CU Boulder, Mechanical Engineering Departmetn, USA). It was used an internal air pump, 1l/min. The measurements were recorded continuously in the atmosphere and into the soil, for more than 3 months.

The soil sampling systems were comprised of a stainless-steel probe, (diameter 1.2 cm), leading to an enclosure with gas sensors. Each probe was installed at 1-meter depth and a pump was used to draw air (1L/min) from the probe to a sensor enclosure. In the box, it was set up the Y-POD and the system used in Italy with an Arduino microcontroller and low-cost gas sensors as MQ-4 for methane and MG8100 for carbon dioxide, as well as temperature, pressure and humidity sensors.

The gas sensors were calibrated in the field in different weather conditions with a reference instrument Picaro of CDPHE Greeley, Colorado. Multiple linear regressions were used for the calibration which correlated the signal of the low-cost sensors with the concentration of the reference instrument in ppm. In the multiple linear regressions were considered the signal of the sensor, temperature, absolute humidity and time against the reference gas concentrations (Cheadle et al, 2017). For each sensor, it was evaluated the performance of the regression fit considering the root mean square error RMSE, coefficient of determination R2 and correlation coefficient.

Figure 15. First experiment. Y-PODs boxes for temperature and humidity control experiment. The red case was used outside without any temperature or humidity control for this experiment, instead the black case was used within a shelter where the temperature was controlled to be about 20°C.

Figure 16. Second experiment. Y-POD box inside the cooler for temperature and humidity control experiment. The previous red case (fig.15) was set up into a cooler with many bottles of a water, trying to have a minimum control on the temperature.

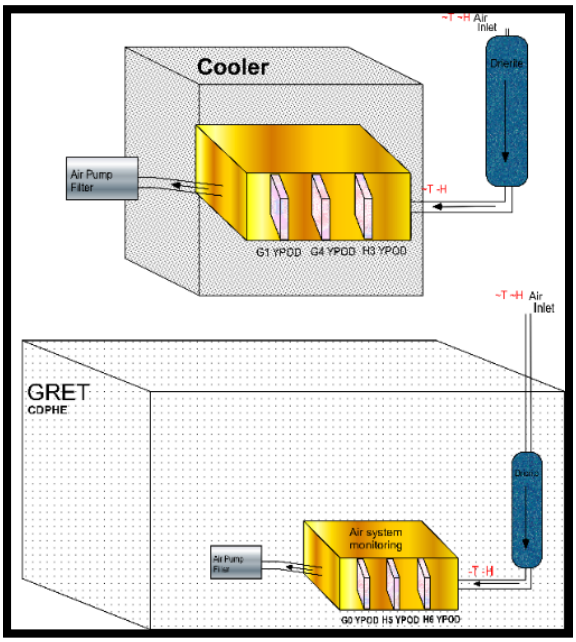

Figure 17. Third experiment. The box within a shelter (GRET CDPHE), had the humidity controlled by using a Drierite as well as for the box outside in the cooler. DRIERITE desiccants are made from the naturally occurring mineral, gypsum (Calcium Sulfate).

I.2.6 Results

Temperature and humidity control

The experiments on temperature and humidity control, with two instruments (three boards with methane, carbon dioxide, ozone gas sensors), gave us interesting results. For those sensors inside a shelter with temperature controlled (air conditioner ~20°C), calibration model was less accurate than those sensors deployed outside in the field (13°C – 45°C), as shown in fig.18.

Multiple linear regression was used to generate a model to convert the raw sensor signal into a concentration (in ppm), (Piedrahita et al., 2015). We found the sensor resistance as a function of the logged voltages then normalized the sensor resistance, Rs, by the sensor signal in clean air at 298 K, Ro. The regression Equations (1)–(4) relate Rs/Ro to the reference instrument concentration (C), temperature (T), and absolute humidity (H); T and RH terms were included to account for the cross-sensitivities of heated metal oxide sensors to those parameters (Piedrahita, R. et al., 2014; Masson, N. et al, 2015). RH was converted to H using methods described by Murphy and Kook and assuming constant atmospheric pressure of 82 kPa Murphy, D.M, 2005). The coefficients p1, p2, p3, p4, and p5 were computed each time a model was generated.

Line 3: $S = p1 + p2*x + p3*T + p4*absHum$

Line 3T: $S = p1 + p2*x + p3*T + p4*absHum + p5*(time-time0)$

Line 4: $S = p1 + x*(p2+p6) + p3*T + p4*absHum + p5*(time-time0)$

Line 4T: $S = p1 + x*(p2+p6*T) + p3*T + p4*absHum + p5*(time-time0) + p6*(time-time0)$

Line 5: $S = p1 + X*(p2 + p6*T) + p3*T + p4*AbsHum + p5*(time-time0) + p6*x(time-time0).$

IN (shelter)	LINE 3	CO2	LINE 3T	CO2	LINE 4	CO2	LINE 4T	CO2	LINE 5	CO2
Y-POD	R2	RMSE	R2	RMSE	R2	RMSE	R2	RMSE	R2	RMSE
G1 25 MAY - 2 JUNE	0.88	4.7	0.88	5.2	0.88	5.1	0.89	5.5	0.89	5.3
G1 2 - 10 JUNE	0.91	5	0.91	5.7	0.91	5.4	0.92	5.8	0.92	5.6
G1 26 JUNE - 3 JULY	0.85	4.7	0.86	5.4	0.86	5.1	0.86	5.8	0.86	5.4
G1 3 - 14 JULY	0.93	4.6	0.94	5.2	0.94	5	0.94	5.5	0.94	5.3
G1 14 - 21 JULY	0.93	4.6	0.92	5	0.92	4.9	0.93	5.2	0.93	5.2
G1 21 - 31 JULY	0.91	4.6	0.91	5.1	0.91	4.9	0.91	5.3	0.91	5.1
G1 14 - 23 AUGUST	0.72	15	0.72	22	0.71	16	0.71	23	0.71	18
OUTside	LINE 3	CO2	LINE 3T	CO2	LINE 4	CO2	LINE 4T	CO2	LINE 5	CO2
Y-POD	R2	RMSE	R2	RMSE	R2	RMSE	R2	RMSE	R2	RMSE
G0 26 MAY - 2 JUNE	0.9	7.7	0.9	9	0.91	9.7	0.91	12	0.92	9.6
G0 2 - 10 JUNE	0.92	6.6	0.92	8.7	0.93	7.6	0.93	11	0.93	8.1
G0 26 JUNE - 3 JULY	0.94	7.8	0.81	9.9	0.83	9.1	0.83	11	0.83	9.7
G0 3 - 14 JULY	0.84	7.6	0.85	8.6	0.87	7.4	0.88	7.8	0.87	7.7
G0 14 - 21 JULY	0.84	7.3	0.85	7.8	0.88	6.8	0.89	7.1	0.89	7
G0 21 - 31 JULY	0.76	8.1	0.78	8.4	0.82	7.9	0.83	8	0.83	8
G0 23 - 31 AUGUST	0.89	5.1	0.89	5.5	0.89	5.5	0.9	5.7	0.9	5.7
IN (shelter)	LINE 3	CH4	LINE 3T	CH4	LINE 4	CH4	LINE 4T	CH4	LINE 5	CH4
Y-POD	R2	RMSE	R2	RMSE	R2	RMSE	R2	RMSE	R2	RMSE
G1 25 MAY - 2 JUNE	0.83	0.078	0.84	0.087	0.91	0.083	0.91	0.093	0.91	0.09
G1 2 - 10 JUNE	0.89	0.12	0.9	0.13	0.89	0.14	0.9	0.14	0.9	0.14
G1 26 JUNE - 3 JULY	0.9	0.089	0.9	0.091	0.91	0.1	0.91	0.11	0.91	0.74
G1 3 - 14 JULY	0.87	0.17	0.87	0.17	0.9	0.18	0.91	0.18	0.91	0.19
G1 14 - 21 JULY	0.87	0.14	0.9	0.14	0.91	0.14	0.93	0.13	0.92	0.15
G1 21 - 31 JULY	0.79	0.14	0.81	0.14	0.86	0.13	0.87	0.13	0.86	0.14
G1 1 -14 AUGUST	0.58	0.12	0.59	0.13	0.65	0.13	0.65	0.14	0.65	0.13
G1 23 - 31 AUGUST	0.67	0.13	0.68	0.13	0.69	0.13	0.69	0.13	0.68	0.14
OUTside	LINE 3	CH4	LINE 3T	CH4	LINE 4	CH4	LINE 4T	CH4	LINE 5	CH4
Y-POD	R2	RMSE	R2	RMSE	R2	RMSE	R2	RMSE	R2	RMSE
G0 26 MAY - 2 JUNE	0.88	0.063	0.89	0.069	0.9	0.075	0.9	0.084	0.9	0.083
G0 2 - 10 JUNE	0.91	0.095	0.91	0.1	0.91	0.11	0.92	0.11	0.91	0.11
G0 26 JUNE - 3 JULY	0.91	0.072	0.91	0.075	0.81	0.063	0.93	0.064	0.93	0.063
G0 3 - 14 JULY	0.91	0.11	0.92	0.12	0.92	0.12	0.93	0.13	0.93	0.13
G0 14 - 21 JULY	0.74	0.22	0.76	0.23	0.78	0.23	0.8	0.25	0.8	0.26
G0 21 - 31 JULY	0.74	0.17	0.76	0.23	0.77	0.19	0.78	0.19	0.78	0.2
G0 4 -15 AUGUST	0.63	0.38	0.63	0.38	0.86	0.11	0.87	0.12	0.87	0.12
G0 14 - 23 AUGUST	0.8	0.16	0.82	0.17	0.85	0.16	0.86	0.17	0.86	0.17

Figure 18. Sensor calibrations results for multiple linear regressions, line3-line3T-line4-line4T-line5.

Results, T°C and H% first experiment

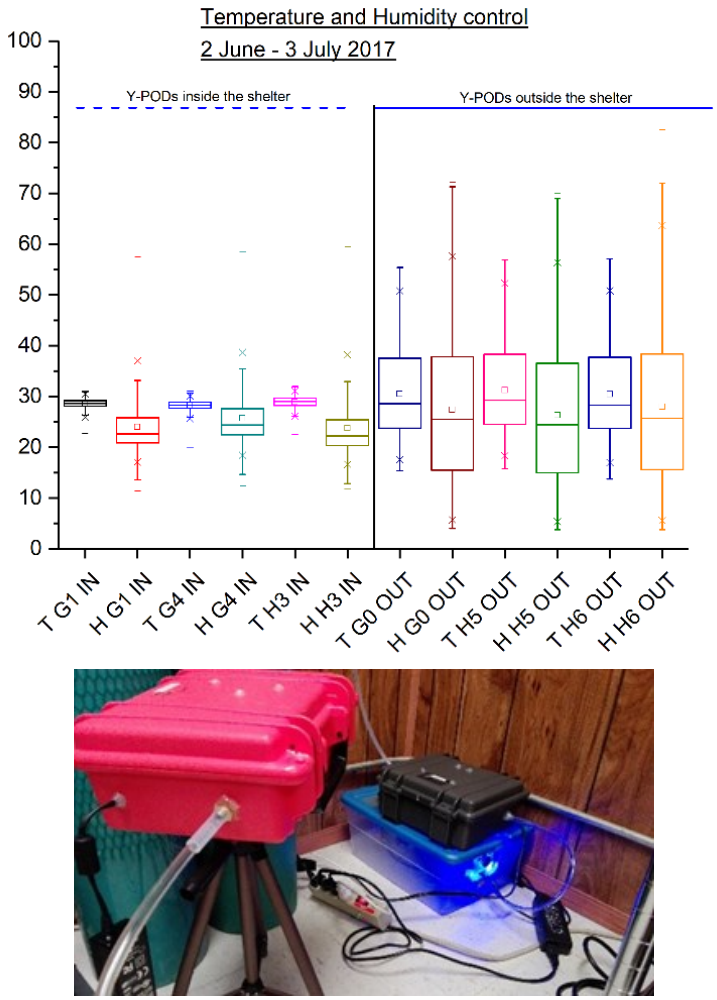

Figure 19. Temperature and humidity control experiment, results.

Legend: ***T or H****, G1, G4, H3* ***IN*** = temperature or humidity for the sensors on the three boards G1, G4, H3, IN – inside the shelter

Legend: ***T or H****, G0, H5, H6* ***OUT*** = temperature or humidity for the sensors on the three boards G0, H5, H6, OUT – outside in the field

Two cases were build, each one had inside with three Y-PODs boards. One case was used to work outside in the field, without any temperature and humidity control, instead the second case was working for all of experiments inside a shelter with the temperature controlled at 22°C. These experiments help us to understand wich linear regression is the best to perform a good calibration, which temperature and humidity is the best for the sensor itself.

In the graph, we can observe the difference of T°C and H% between the sensors used inside the shelter and the sensors used outside. As we expected highest values of T°C, H% amd huge variability on sensors working outside, than for those working inside the shelter. The experiment run for almost one month.

Results, T°C and H% second experiment

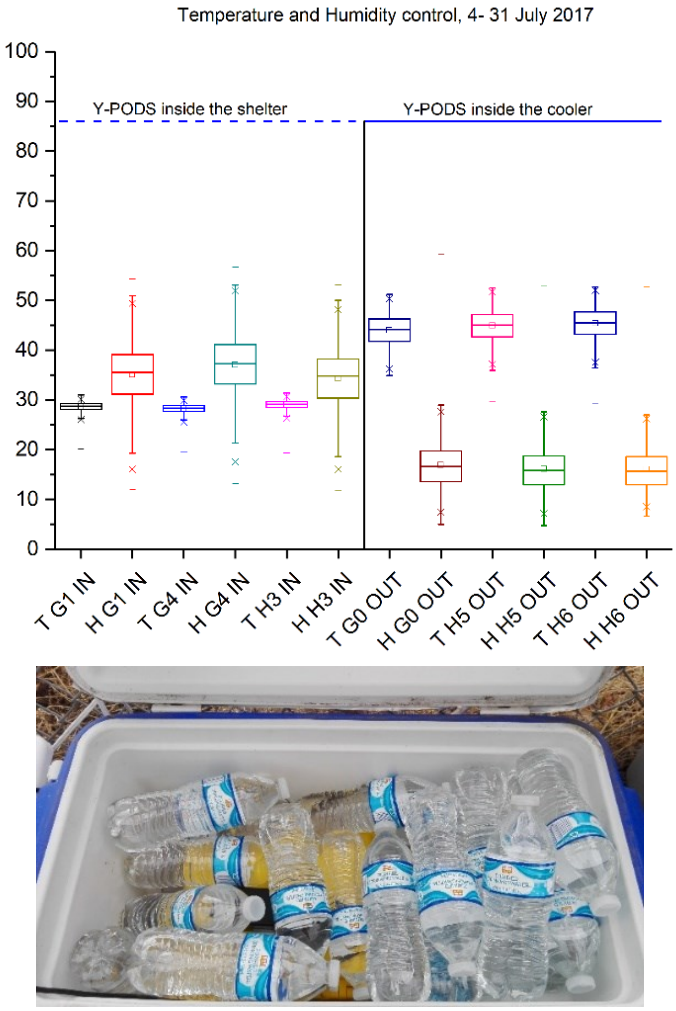

Figure 20. Temperature and humidity control experiment, results.

Legend: ***T or H**, G1, G4, H3 **IN*** = temperature or humidity for the sensors on the three boards G1, G4, H3, **IN** – **inside** the shelter

Legend: ***T or H**, G0, H5, H6 **OUT*** = temperature or humidity for the sensors on the three boards G0, H5, H6, **OUT** – **outside** in the field

One case was used to work outside in the field, with temperature controlled, by seting it up inside a cooler, instead the second case was working for all of experiments inside the shelter with the temperature controlled at 22°C. In the graph, we can observe the difference of T°C and H% between the sensors used inside the

shelter and the sensors used outside in the cooler. As we expected highest values of the T°C for the box used outside in the cooler, and lowest H% values, it meant that the cooler had a good effect on the humidity and not too much on the temperature as we wanted. The experiment run for almost one month.

Results, T°C and H% third experiment

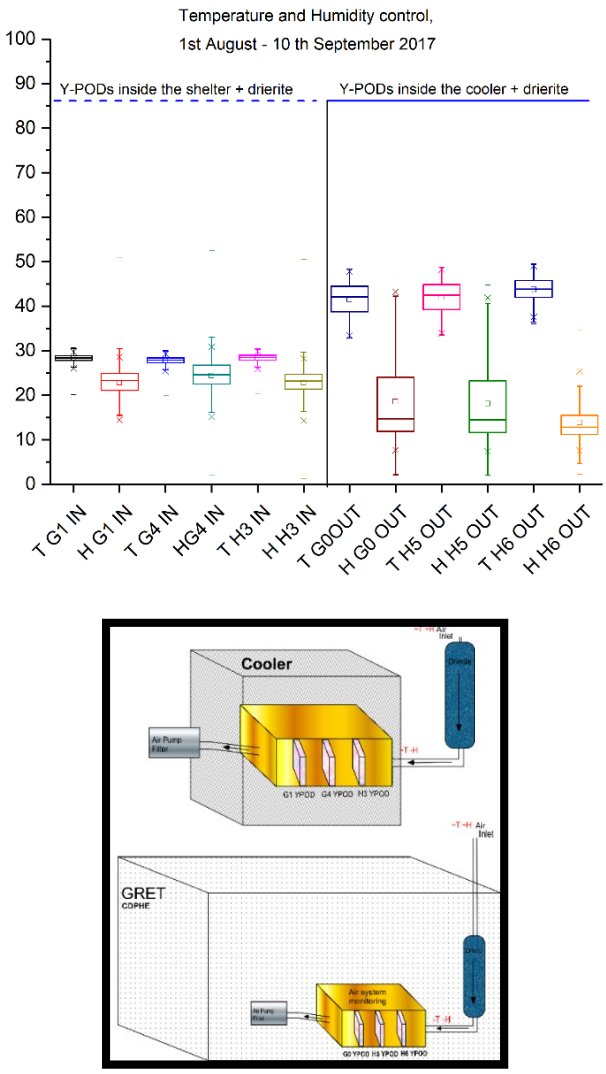

Figure 21. Y-PODs used inside a shelter with temperature and humidity controlled; temperature and humidity control experiment, results.

Legend: ***T or H**, G1, G4, H3* ***IN*** = temperature or humidity for the sensors on the three boards G1, G4, H3, **IN** – **inside** the shelter

Legend: ***T or H**, G0, H5, H6* ***OUT*** = temperature or humidity for the sensors on the three boards G0, H5, H6, **OUT** – **outside** in the field

For this experiment, drierite was used in order to control the humidity. The experiment run for almost one month. As we expected highest values of the T°C for the box used outside in the cooler, and lowest H% values but a huge variability, than the box used inside the shelter. These differences on H% values, due probably to any leaks in the drierite system. Anyway, the humidity outside was about 70%, and our experiement by using the drierite was about 10H% - 20H%.

Soil-atmosphere measurements of CH4 and CO2, surrounding Drilling and Hydraulic fracturing activities in Greeley

- (these results are presented in the Article on page 114, the paper is still in progress, under review, since last measurements finished in November 2017)

Methodologies

The deployment of the six Y-PODs took place around a new multiwell pad in the Denver Julesburg Basin, in west Greeley CO, USA. Three sensor nodes were used for atmospheric measurements and the other three sensor nodes were used to monitor the soil gas concentrations at 1m depths into the soil. Measurements continued through drilling activities, hydraulic fracturing and construction of pipelines. The Y-PODs employed an Arduino microcontroller that acquires the signal from the sensors and saves them to a text file on a microSD card every 12 seconds. We used Figaro TGS 2600 metal oxide sensors to measure methane and elt S-300 NDIR sensors to measure Carbon Dioxide (CO2). The soil sampling systems were comprised of a stainless-steel probe, (diameter 1.2 cm), leading to an enclosure with gas sensors. Each probe was installed at 1-meter depth and a pump was used to draw air (1L/min) from the probe to a sensor enclosure.

The gas sensors were calibrated in the field via field normalization (Piedrahita et al, 2015), by co-locating them with reference measurement collected by a Picarro G2508 cavity ring-down spectrometer operated by Jeffrey Collett and Katherine Benedict of Colorado State University at a Colorado Department of Public Health and Environment (CDPHE) regulatory air quality monitoring site in Greeley, Colorado. Multiple linear regressions were used for the calibration which mapped the signal of the low-cost sensors to concentrations measured by the reference instrument in ppm. The multiple linear regressions were included the signal of the sensor, temperature, absolute humidity, and time (Cheadle, L., et al 2017; Piedrahita et al, 2015). For each sensor, we evaluated the performance of the regression fit using the root mean square error RMSE and the coefficient of determination r^2. Field normalization-type calibration for CH4 and CO2 gas sensor, in all 25 Y-PODs, showed the agreement between the normalized sensor signal and the reference measurements in a time series, scatter plot, and residuals plot, respectively, (fig. 26-31).

Figure 22. Location of test site within Greeley area.

Before and after Y-PODs were deployed at sampling sites around the multiwell pad, they were co-located at the CDPHE reference site with the Picarro reference instrument, as shown in fig.23.

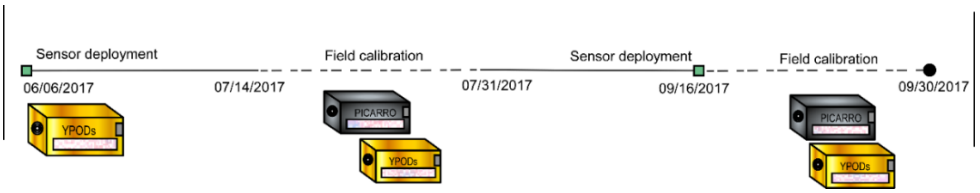

Figure 23. The deployment and co-location of the Y-PODs.

Y-PODs were deployed at sites near the multiwell pad between the 6th of June and the 30th of September in 2017, and we continued the mesurements until November 2017. Two sets of Y-Pods were used so that some were co-located at the CDPHE site while others were at the multiwell pad sampling sites, thus the multiwell sampling sites were active continuously during the hydraulic fracturing activities. For the soil gas monitoring, sampling was interrupted by calibration periods. The data from Picarro instrument, which logged data approximately once per second, were minute averaged. The multiple linear regression used for the calibration:

Line 4T: $S = p1 + Xp6\,(T + p2) + TA\text{bsHum}\;p3p4 + (t - t_0)\;p5$

Line 5: $S = p1 + X*(p2 + p6*T) + p3*T + p4*AbsHum + p5*(time\text{-}time0) + p6*x\;(time\text{-}time0).$

For methane, S is the Figaro 2600 sensor signal in R/Ro, where R is the sensor resistance and Ro is the resistance of the sensor in clean air. X is the pollutant concentration in ppm, T is the temperature in Kelvin, Abs Hum is absolute humidity in mole fraction, and the P1 – Pi are multiple linear regression predictor coefficients. The field calibration of the Y-PODs took place between the 14th-31st of July and the 16th-30th of September in 2017. The Line 4T and Line 5 calibration models were used for CH4 and CO2, respectively.

Considering the ***CH4 calibration***, R2 values ranged from 0.86 - 0.95 and RMSE values ranged from 0.07 - 0.15 ppm. Considering the ***CO2 calibration***, R2 values ranged from 0.64 - 0.95 and RMSE values ranged from 5ppm - 10 ppm. An outlier, just one Y-POD (G3) had an RMSE of 17ppm, as shown in fig. 24.

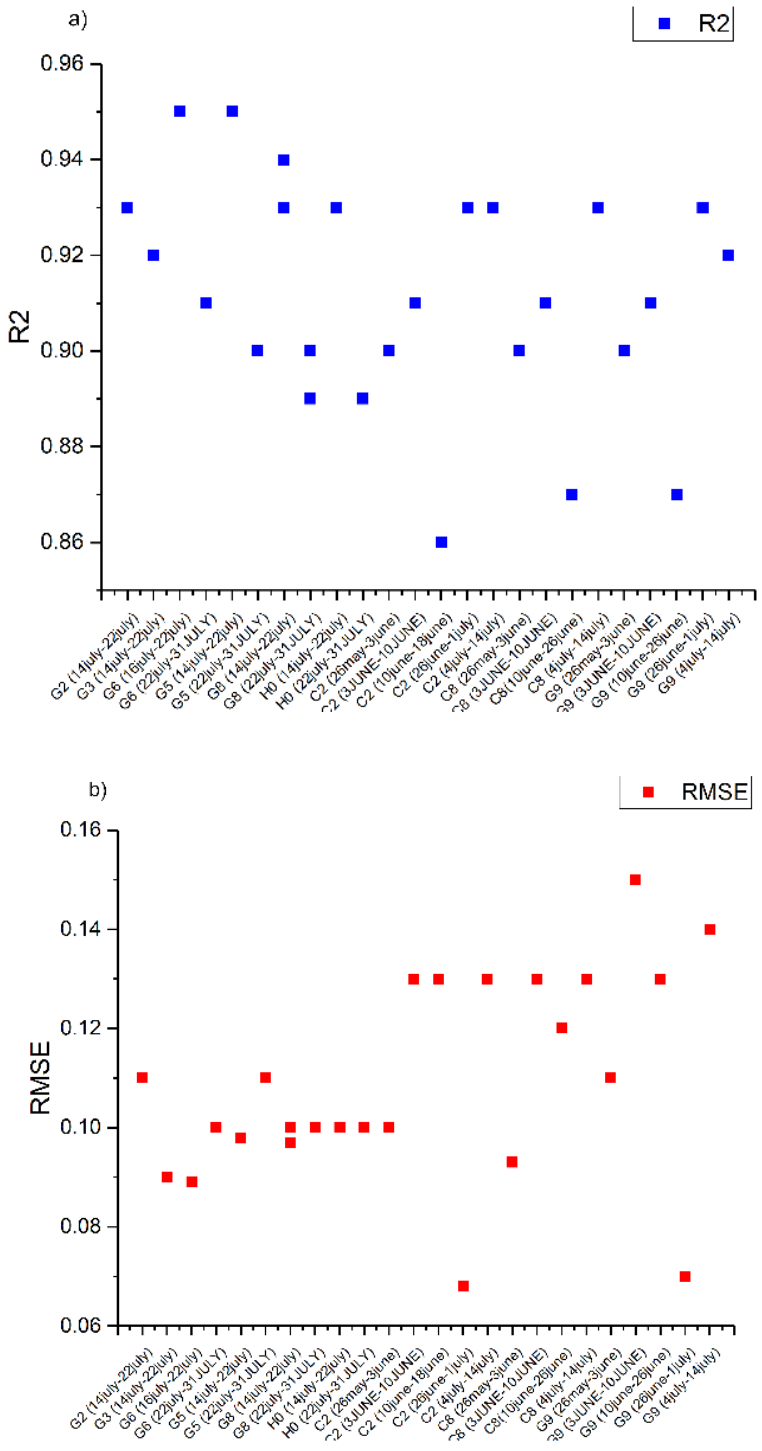

Figure 24. The R2 and RMSE of CH4 gas sensor.

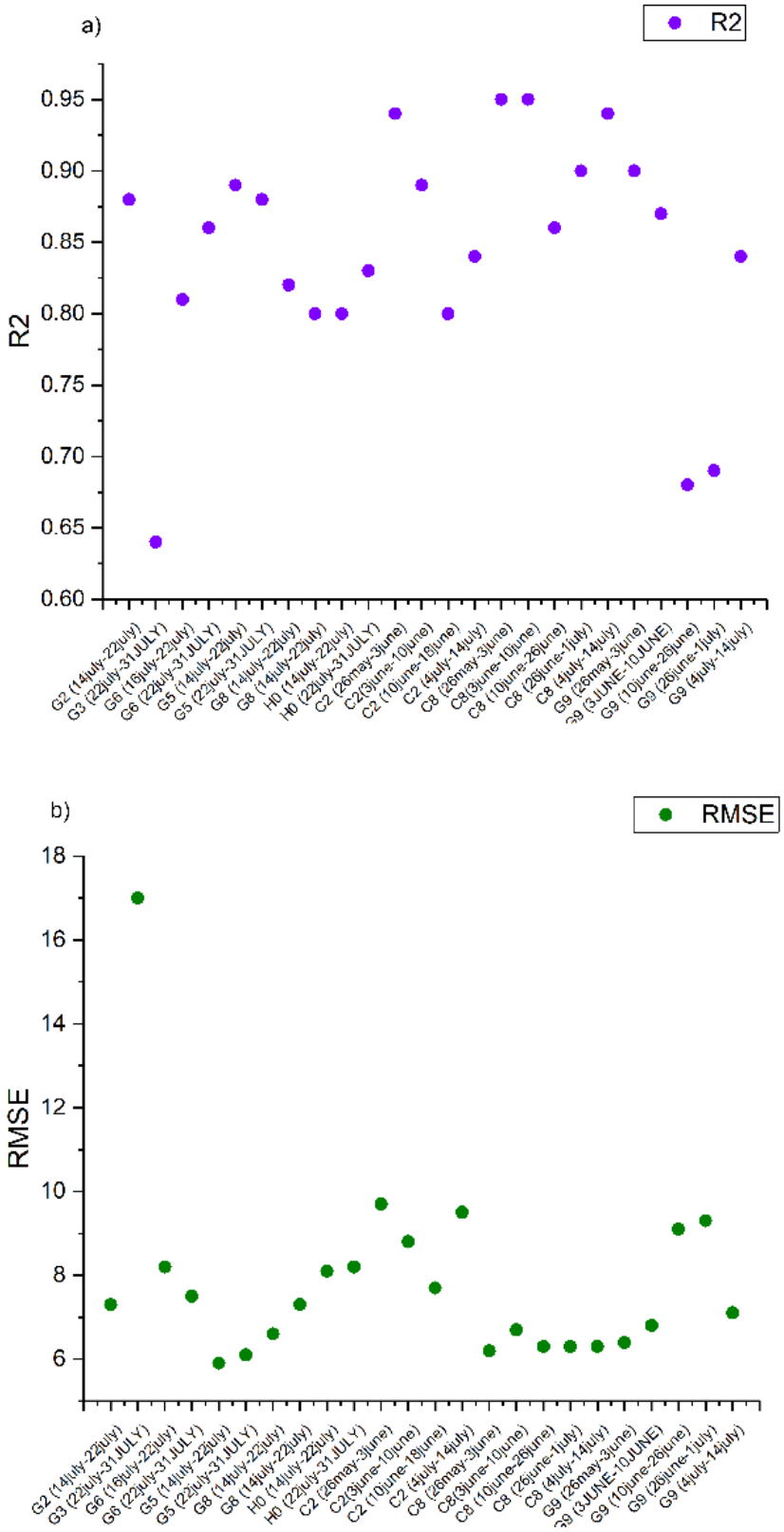

Figure 25. The R2 and RMSE of CO2 gas sensor.

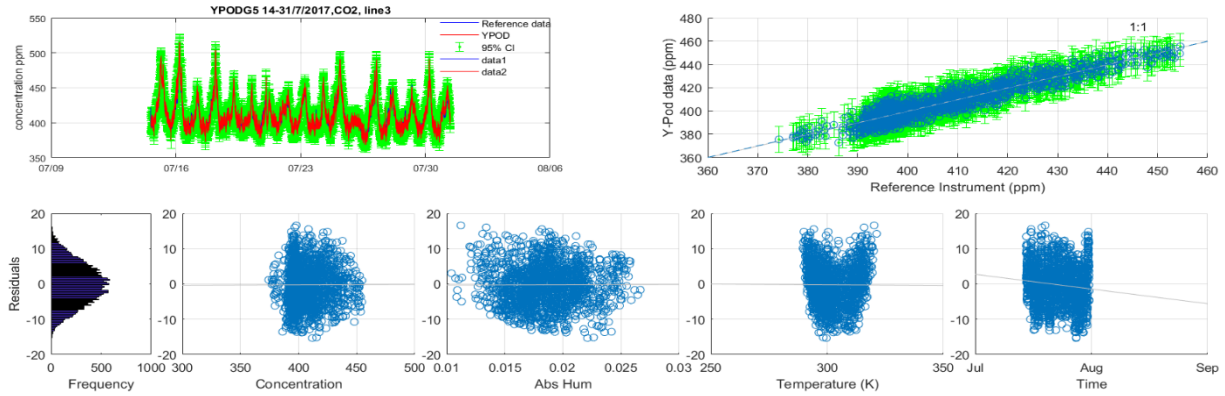

Figure 26. Field normalization-type calibration for CO2 gas sensor, **G5 Y-POD**, it show the agreement between the normalized sensor signal and the reference measurements in a time series, scatter plot, and residuals plot, respectively.

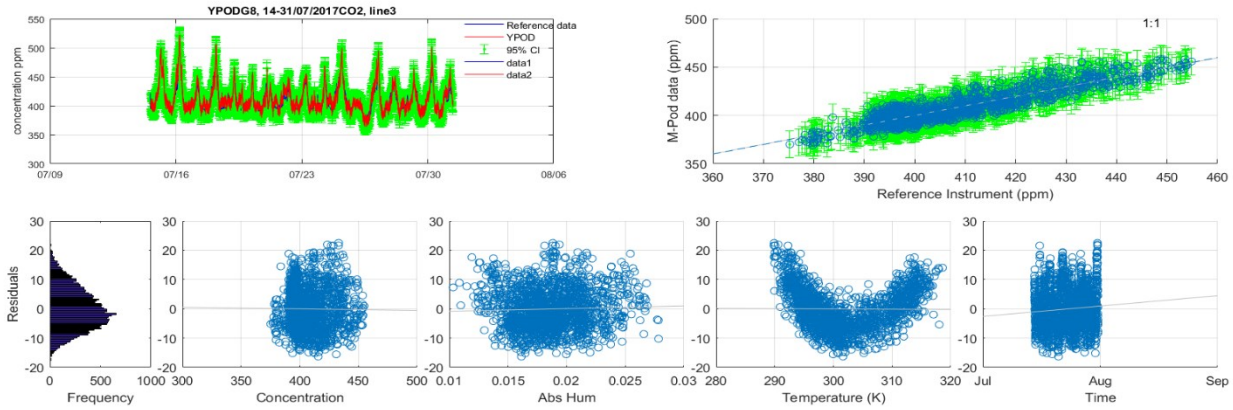

Figure 27. Field normalization-type calibration for CO2 gas sensor, **G8 Y-POD**.

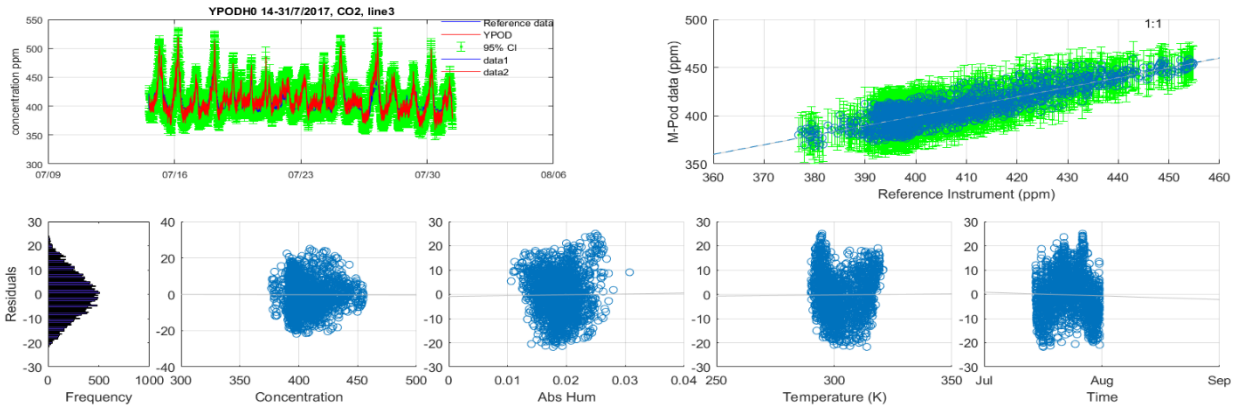

Figure 28 Field normalization-type calibration for CO2 gas sensor, **H0 Y-POD.**

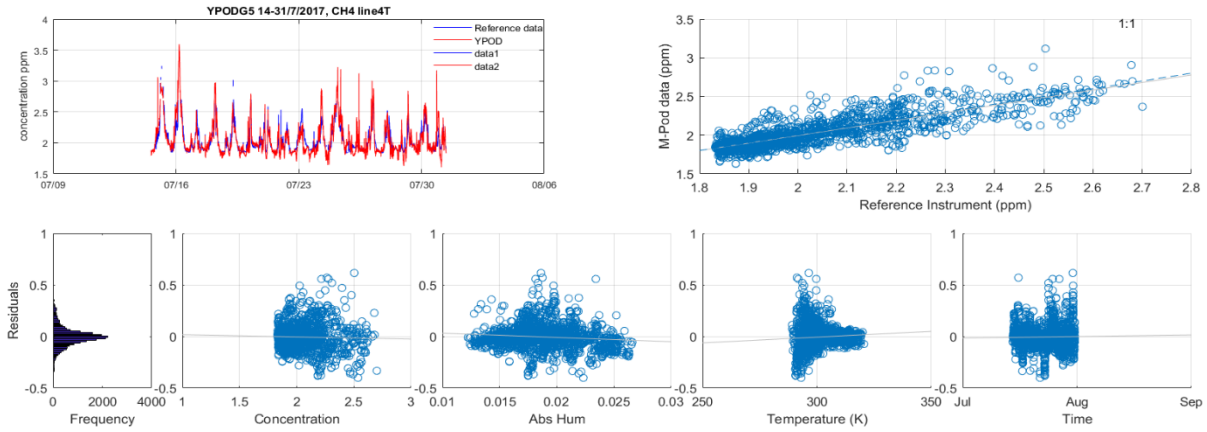

Figure 29. Field normalization-type calibration for CH4 gas sensor, **G5 Y-POD**, it show the agreement between the normalized sensor signal and the reference measurements in a time series, scatter plot, and residuals plot, respectively.

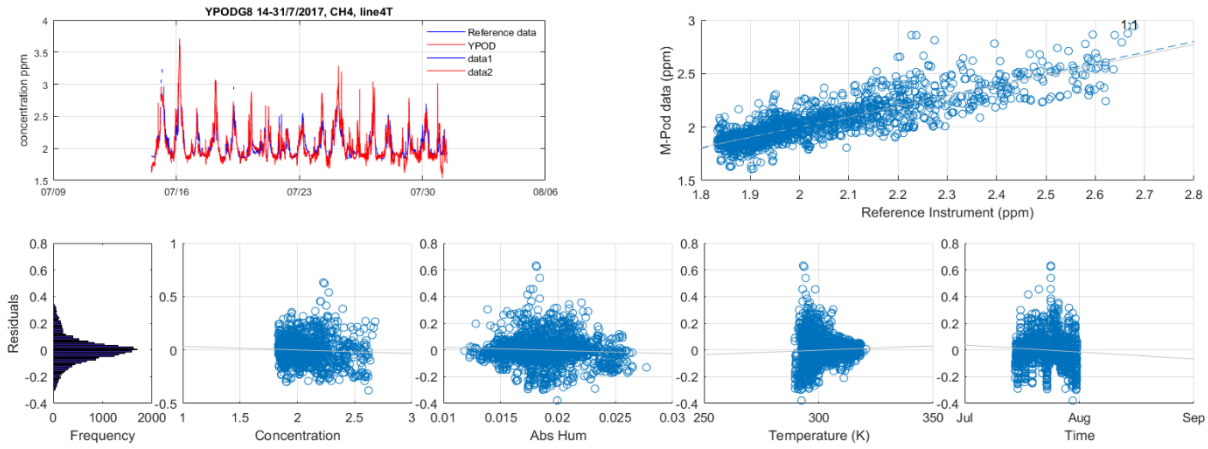

Figure 30. Field normalization-type calibration for CH4 gas sensor, **G8 Y-POD**.

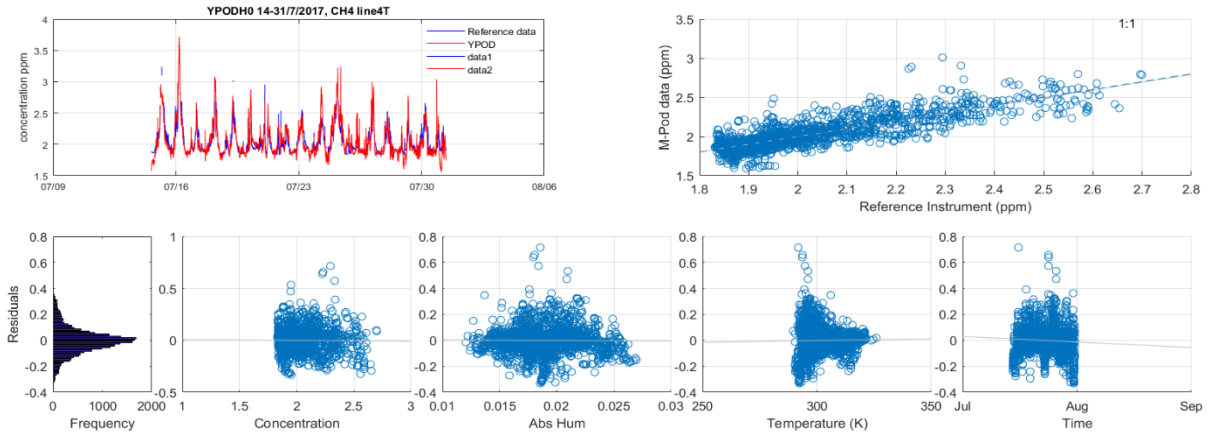

Figure 31. Field normalization-type calibration for CH4 gas sensor, **H0 Y-POD**.

Sensors Validation

During the validation, the YPOD G3 (fig. 32-33) presented RMSE 0.17146, adj R2 0.6302, slope 0.64355, intercept 0.77404. The YPOD G6 (fig. 34-35) presented RMSE 0.17429, adj R2 0.6131, slope 0.64166, intercept 0.77743. The YPOD G2 presented a negative validation, with negative adj R2, we already understood from the previous plots of methane concentration that this Figaro 2600 gas sensor did not worked good, showed most of the time methane concentration less than 1.5ppm.

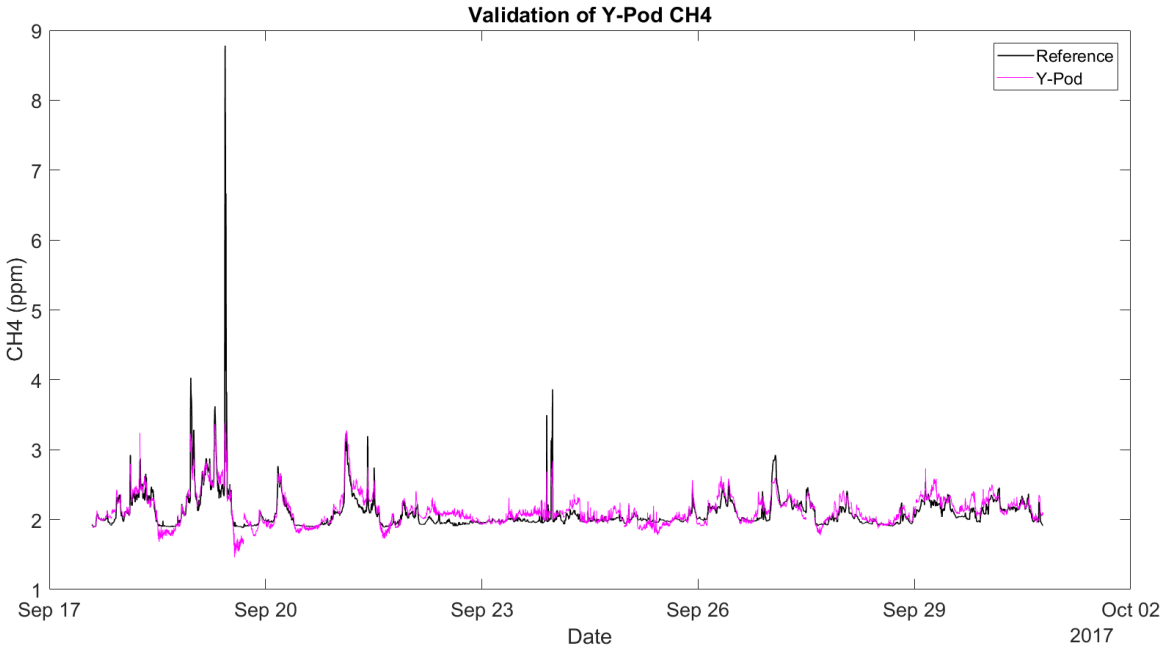

Figure 32. Validation of YPOD G3, temporal variation of the reference data Picarro and methane gas sensor.

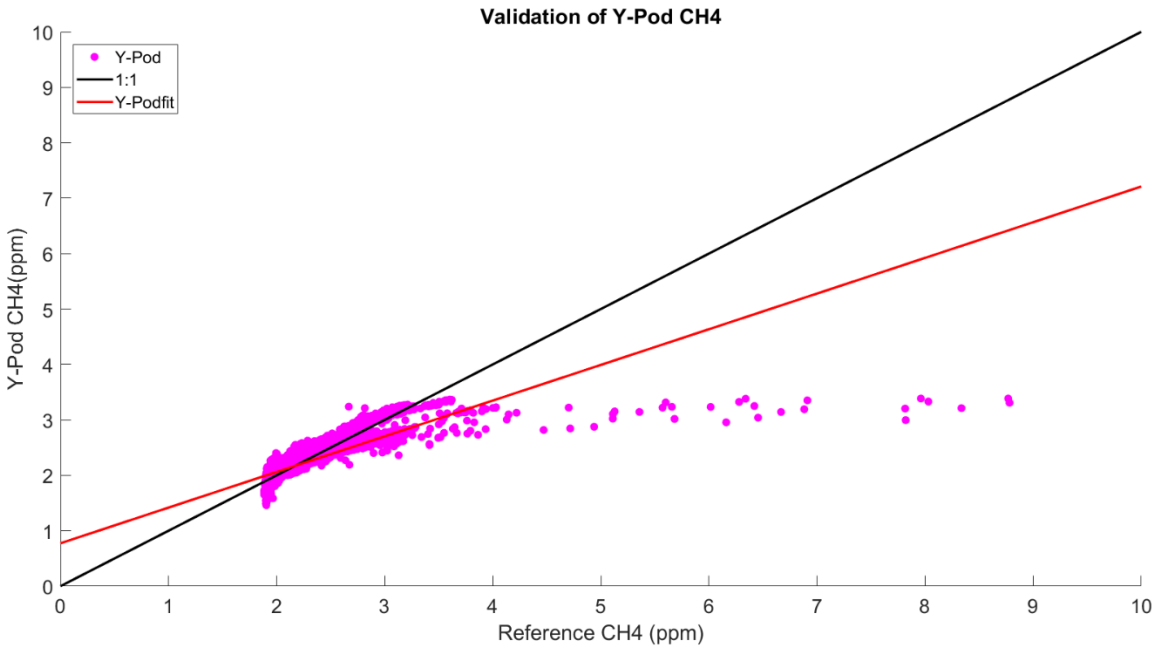

Figure 33. Validation of YPOD G3.

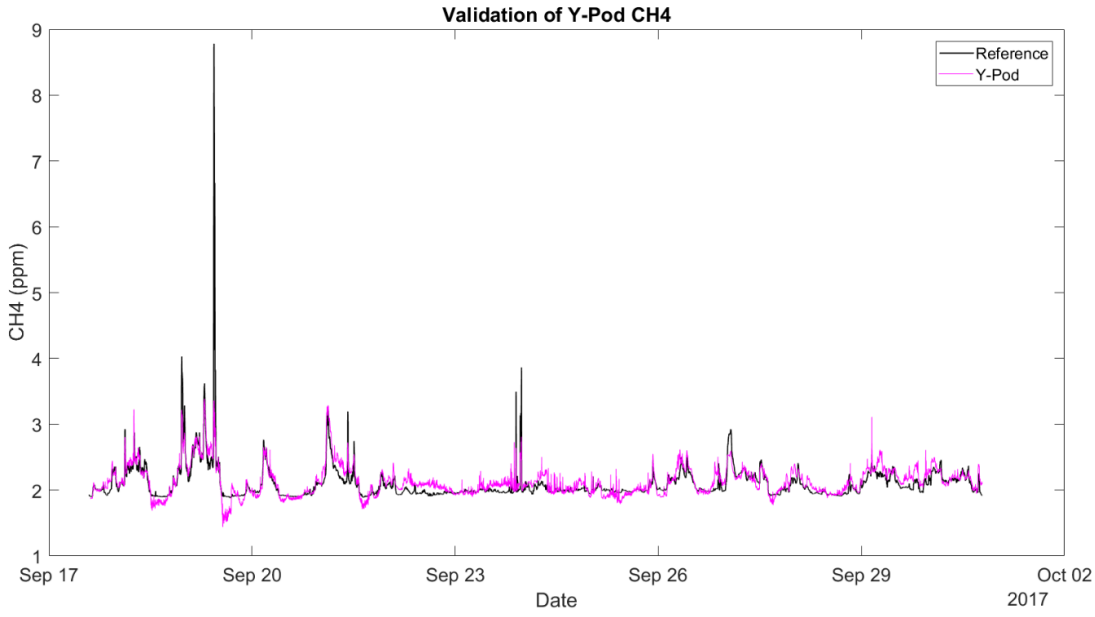

Figure 34. Validation of YPOD G6, temporal variation of the reference data Picarro and methane gas sensor.

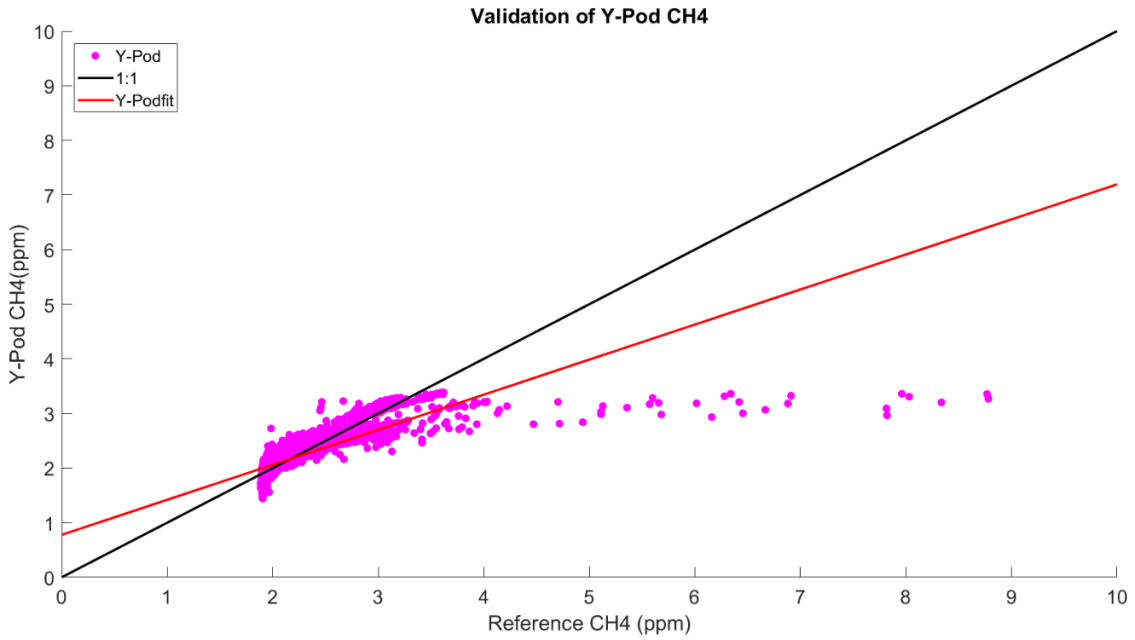

Figure 35. Validation of YPOD G6.

Weather conditions

Figure 36 shows the wind directions during the sampling periods over the course of three months. East winds (E, ESE) were dominant in June, while north winds (N and NNW) were dominant in July and August. Sampling sites were located to the north of the multiwell pad (Greeley 1), to the east side of the multiwell pad (Greeley 2) and to the south of the multiwell pad (Greeley 3).

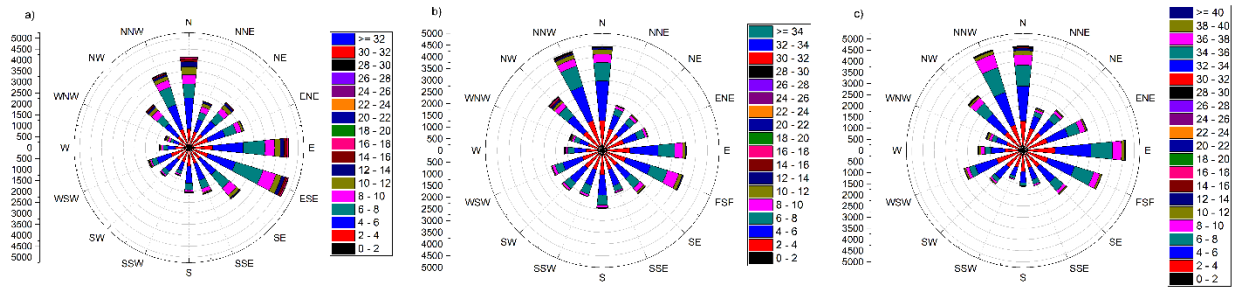

Figure 36. Wind speed and direction measured at the Greeley CDPHE sampling site during June, July and August measurements.

Relative humidity in air quality monitors ranged from 7% to 90% and temperature ranged from 10°C to 45°C, as shown in figure 37-38-39. Relative humidity in soil gas monitors ranged from 10% to 80%, and temperature ranged from 17°C to 58°C. During:

- ***Drilling activities*** (from the 1st of June through the 3rd of July 2017), humidity range was between 20% to 50% and temperature range between 18°C to 30°C;
- ***Hydraulic fracturing activities*** (4th July to 26th August 2017) the humidity range was between 30% to 70% and temperature range between 18°C to 30°C;
- ***Construction of pipelines*** (27th August to 16th September 2017), the humidity range was between 20% to 60% and temperature range between 18°C to 35°C.

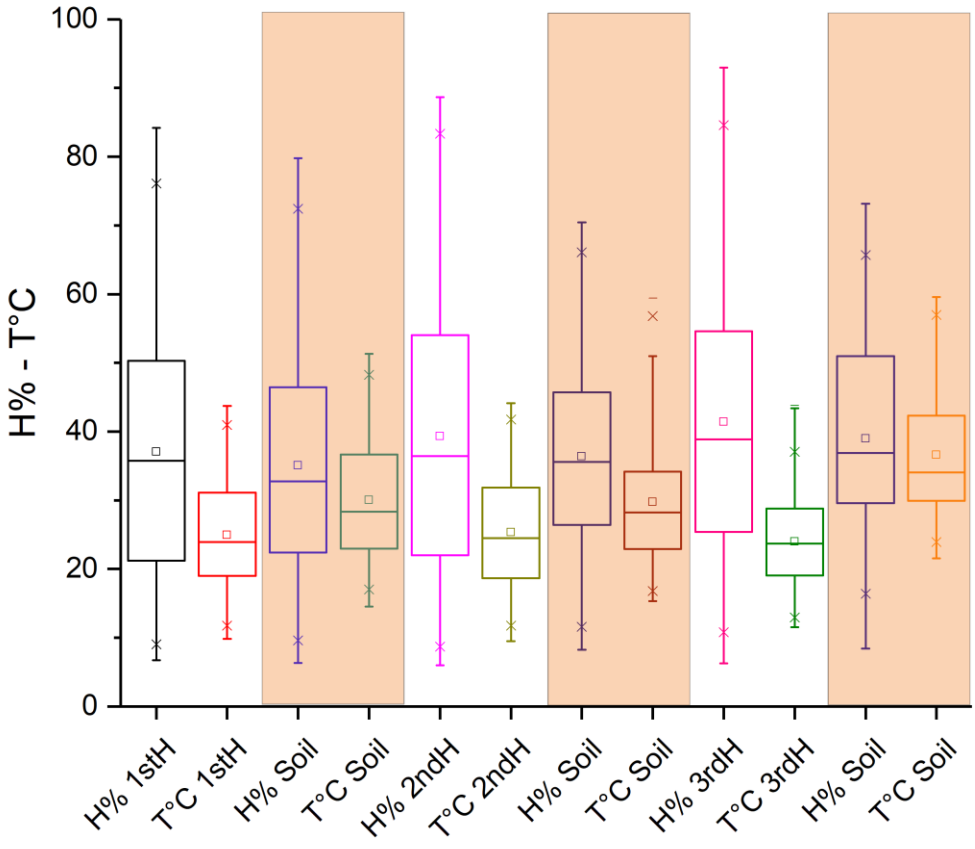

Fig. 37. The humidity and temperature boxplot values during drilling activities. Legend: 1st, 2nd, 3rdH = first, second, third Home where the Y-POD was located; H%, T°C Soil = the H% and T°C values recorded into the soil. In the yellow color soil values are highlighted.

The 3rd house presented small differences in humidity and temperature values since the Y-PODs were covered by trees in the garden, furthermore it was used often irrigation system so we expected highest humidity values. Instead, into the soil it can be observed that humidity and temperature values were different at the 3rd house than the other two places, due to the soil characteristic and chemical reaction into it, we expected highest temperature into an organic matter rich soil, as it is in the 3rd house garden.

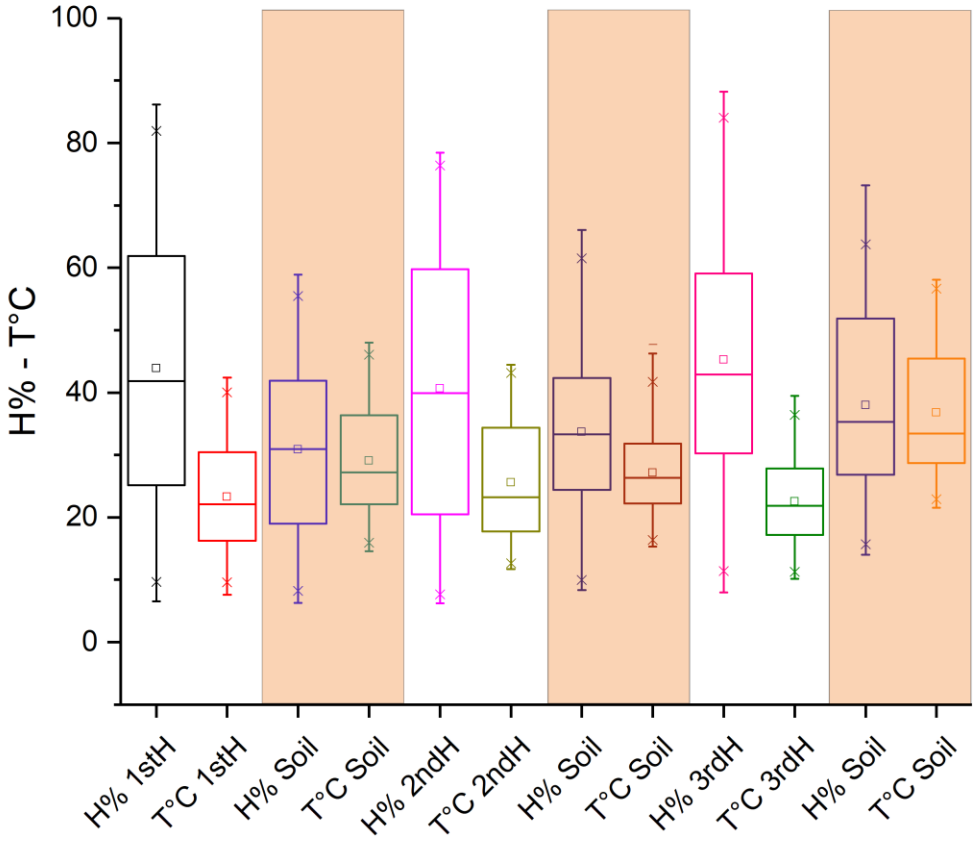

Fig. 38 The humidity and temperature boxplot values during hydraulic fracturing activities. Legend: 1st, 2nd, 3rdH = first, second, third Home where the Y-POD was located; H%, T°C Soil = the H% and T°C values recorded into the soil. In the yellow color soil values are highlighted.

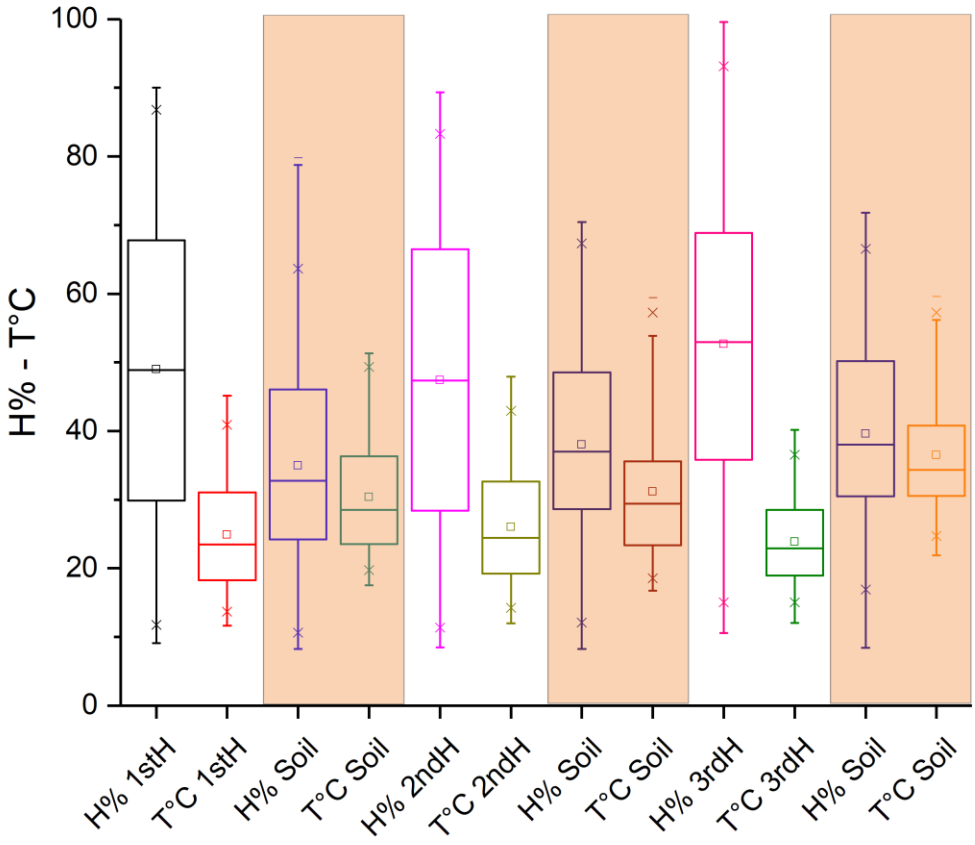

Fig. 39. The humidity and temperature boxplot values during construction of the pipelines. Legend: 1st, 2nd, 3rdH = first, second, third *Home* where the Y-POD was located; H%, T°C Soil = the H% and T°C values recorded into the soil. In the yellow color soil values are highlighted.

Methane gas concentrations

The research focused on understanding the methane and carbon dioxide gas concentrations in atmosphere and into the soil, surrounding a well pad. The measurements were carried out during drilling activities, hydraulic fracturing activities and construction of pipelines, (fig. 40-41-42). The gas measurement survey carried out throughout the Greeley (Colorado, USA) area, presented 350 ppm - 500ppm CO2, and 1,5 ppm - 5,5 ppm CH4 in the atmosphere. Instead into the soil at 1m depth it was obtained almost 4ppm CH4 and 300 ppm – 3000 ppm CO2. The highest value of CO2, 3000 ppm was obtained into a test site with a high concentration of organic matter into the soil as fertilizer.

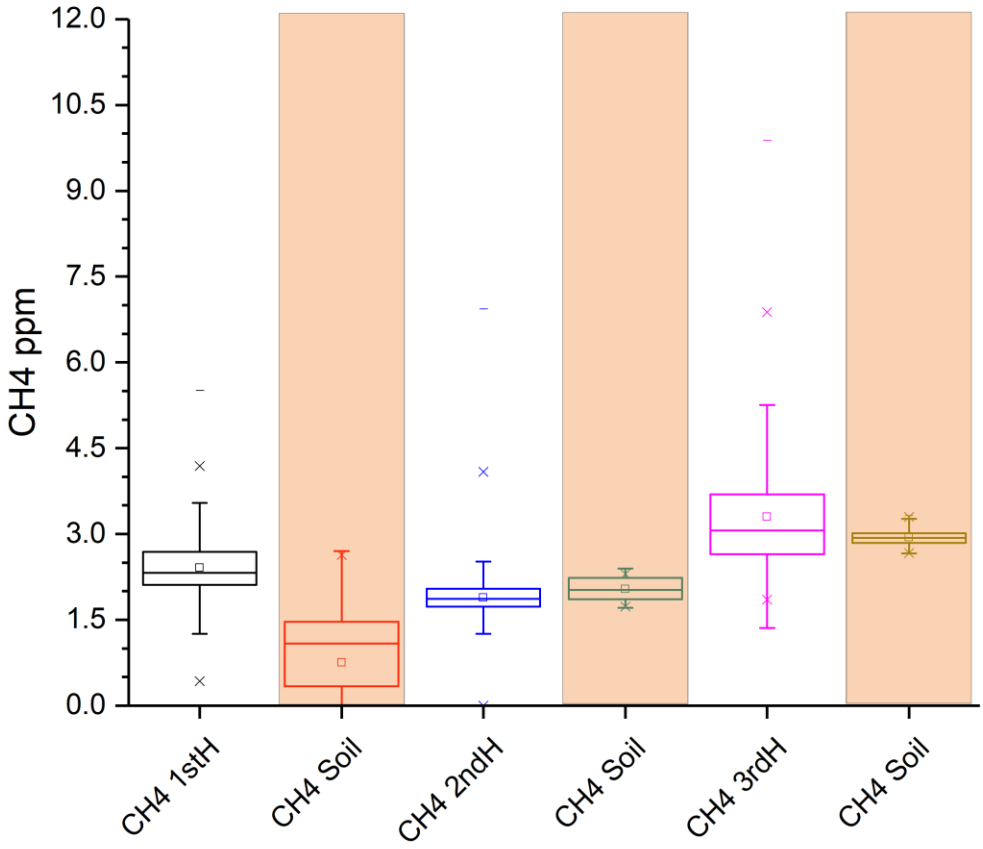

Figure 40. The concentration of methane during drilling activities. Legend: 1st, 2nd, 3rd H = first, second, third Home where the Y-POD was located, CH4 Soil = soil measurements of methane.

During ***drilling activities*** (6th June to 3rd July 2017), atmospheric methane ranged from 1 ppm to 5 ppm, with a range of 2 ppm to 2.5 ppm at the 1st H; 2 ppm at the 2nd H; 2.5 ppm to 4 ppm at the 3rd H. The concentration of methane in soil at 1m depth was lower than 1.5 ppm at the 1st H where there was silty soil with no organic matter; 1.5 ppm to 2 ppm at the 2nd H where there was silty soil with organic matter; 2.7 ppm at the 3rd H, where there was sandy soil, rich in organic matter.

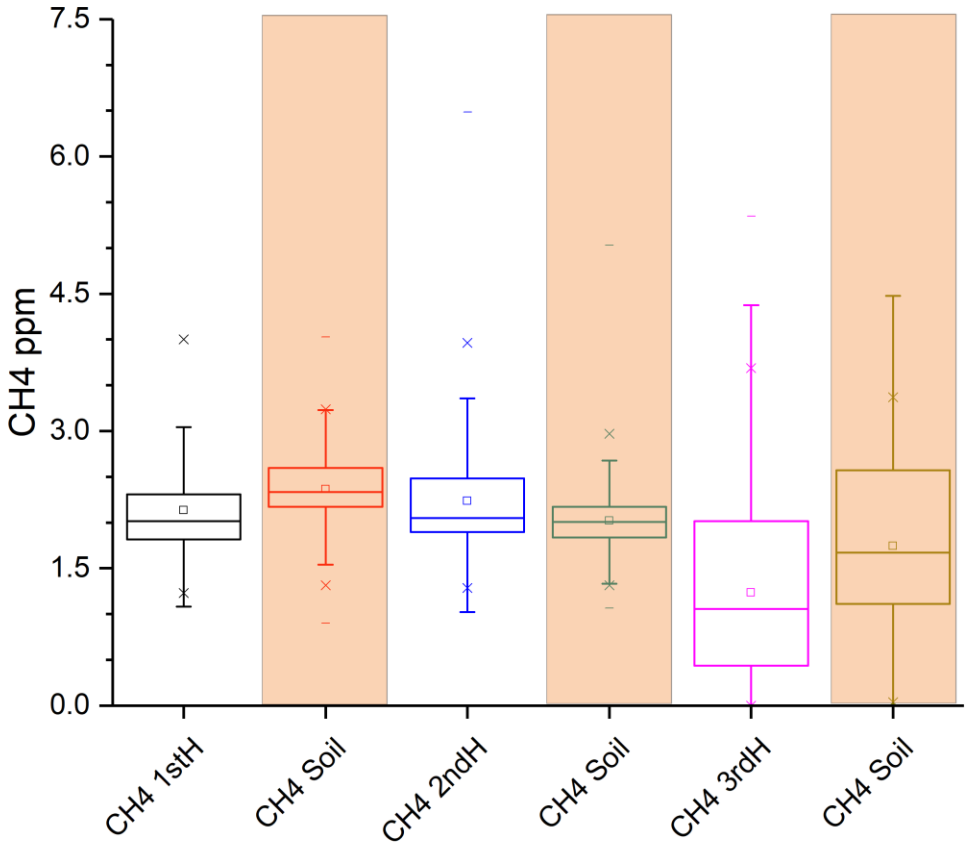

Figure 41. The concentration of methane during hydraulic fracturing activities. Legend: 1st, 2nd, 3rd H = first, second, third Home where the Y-POD was located, CH4 Soil = soil measurements of methane.

During ***hydraulic fracturing activities*** (from the 4th July through the 26th August), the range of methane in the atmosphere ranged from 1 ppm to 4 ppm, with a range of 1 ppm to 3 ppm at the 1st H; 1 ppm to 3.5 ppm at the 2nd H; and 0.05 ppm to 2 ppm at the 3rd H. The concentration of methane into the soil at 1m depth, at the 1st H was between 2ppm to 2.5 ppm; 1.9 ppm to 2.2 ppm at the 2nd H; 1 ppm to 2.5 ppm at the 3rd H.

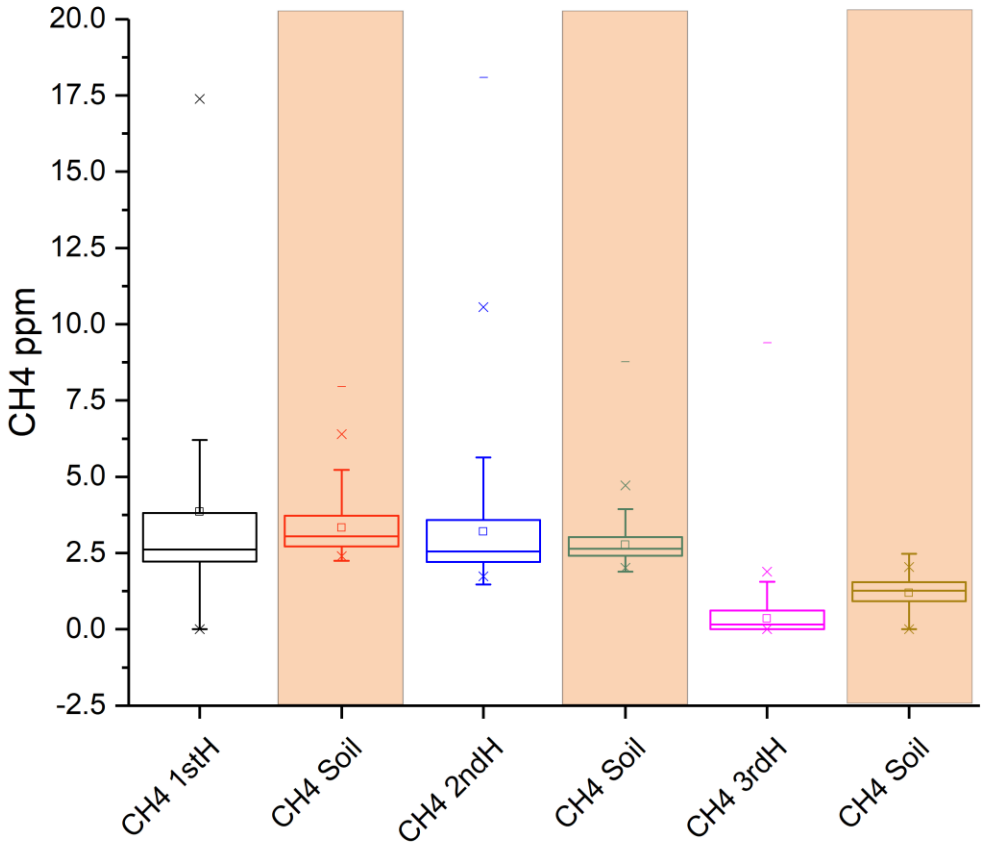

Figure 42. The concentration of methane during construction of pipelines phase. Legend: 1st, 2nd , 3rd H = first, second, third Home where the Y-POD was located, CH4 Soil = soil measurements of methane.

During ***construction of pipelines phase*** (27th August to 16th September), the concentration of methane in the atmosphere ranged from 1.8 ppm as minimum and 5.5 ppm, with a range of 2.4 ppm to 3.5 ppm at the 1st H; 2.5 ppm to 3.5 ppm at the 2nd H; lower than 1.5 ppm at the 3rd H. The concentration of methane into the soil at 1m depth, at the 1st H was between 2.6 ppm to 3.4 ppm; 2.5 ppm to 3ppm at the 2nd H; 1.5ppm to 2.2 ppm at the 3rd H.

It is well known that the concentration of methane in atmosphere is about 1.8ppm, and the gas survey measurements around the well pad showed methane less than 1.5 ppm, it was probably due to the sensor signal response, not working well. Methane levels above the atmospheric background are thought to be plausible and may have been influenced by agricultural activities around the multiwell pad, as well as oil and gas production activities on the multiwell pad and in the surrounding Denver Julesburg Basin.

Carbon dioxide gas concentrations

During drilling, hydraulic fracturing and construction of pipelines phase, the concentration of carbon dioxide in atmosphere ranged from 380 ppm to 450 ppm, as shown in the figure 43-44-45. The concentration of carbon dioxide into the soil present different results and were likely influenced by soil characteristics, temperature, and humidity.

During ***drilling activities*** (June to 3th July), at the 1st Home the CO2 soil gas was 450 ppm, at the 2nd Home the CO2 soil gas was about 4300 ppm silty soil with organic matter, at the 3rd Home the CO2 soil gas was about 2250 ppm organic matter sandy soil.

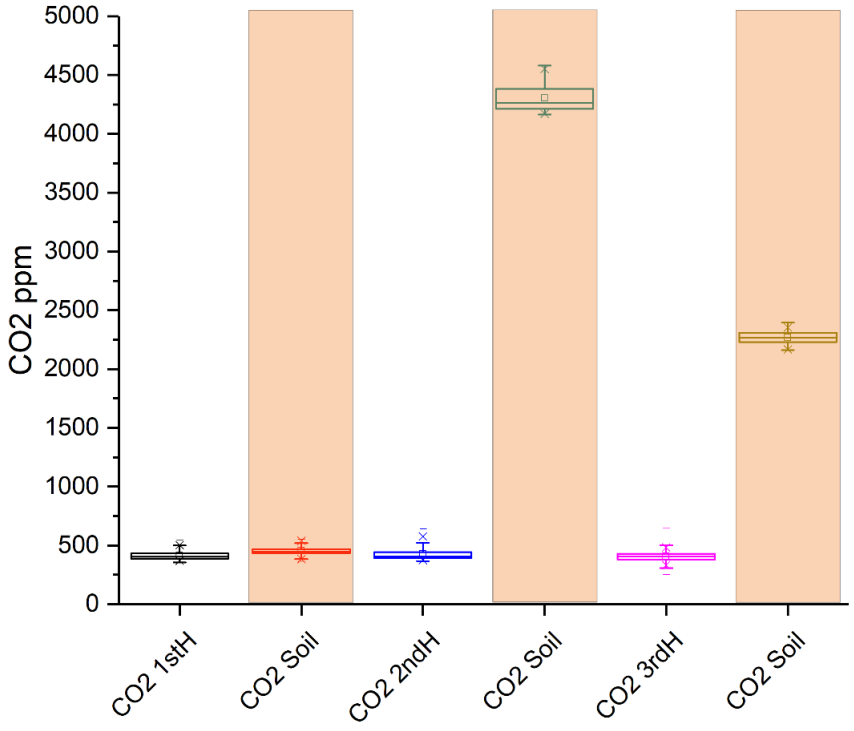

Figure 43. The concentration of carbon dioxide during drilling activities. Legend: 1st, 2nd, 3rd H = first, second, third Home where the Y-POD was located, CO2 Soil = soil measurements of carbon dioxide.

During ***hydraulic fracturing activities*** (4th July to 26th August), at the 1st H the CO2 soil gas was 450ppm, at the 2nd H the CO2 soil gas was between 400 ppm to 3250 ppm, at the 3rd H the CO2 soil gas was between 2750 ppm to 5250 ppm.

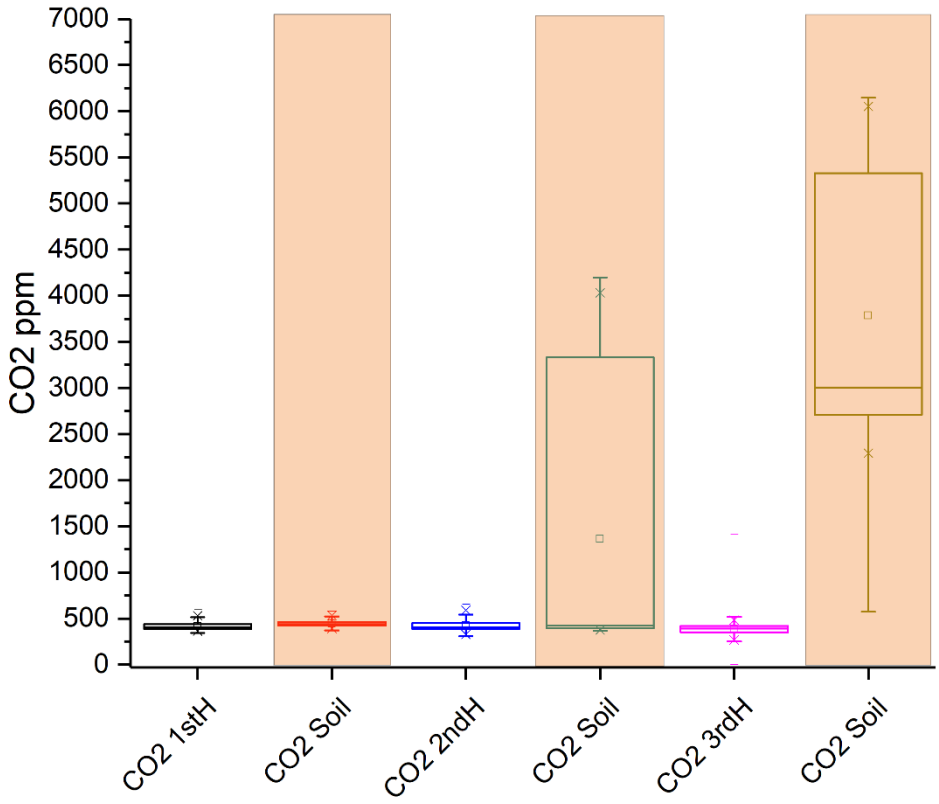

Figure 44. The concentration of carbon dioxide during hydraulic fracturing activities. Legend: 1st, 2nd, 3rd H = first, second, third Home where the Y-POD was located, CO2 Soil = soil measurements of carbon dioxide.

During the ***construction of pipelines phase*** (27th August to 16th September), at the 1st H and 2nd H the CO2 soil gas was 450 ppm, at the 3rd H the CO2 soil gas was between 2400 ppm to 3200ppm.

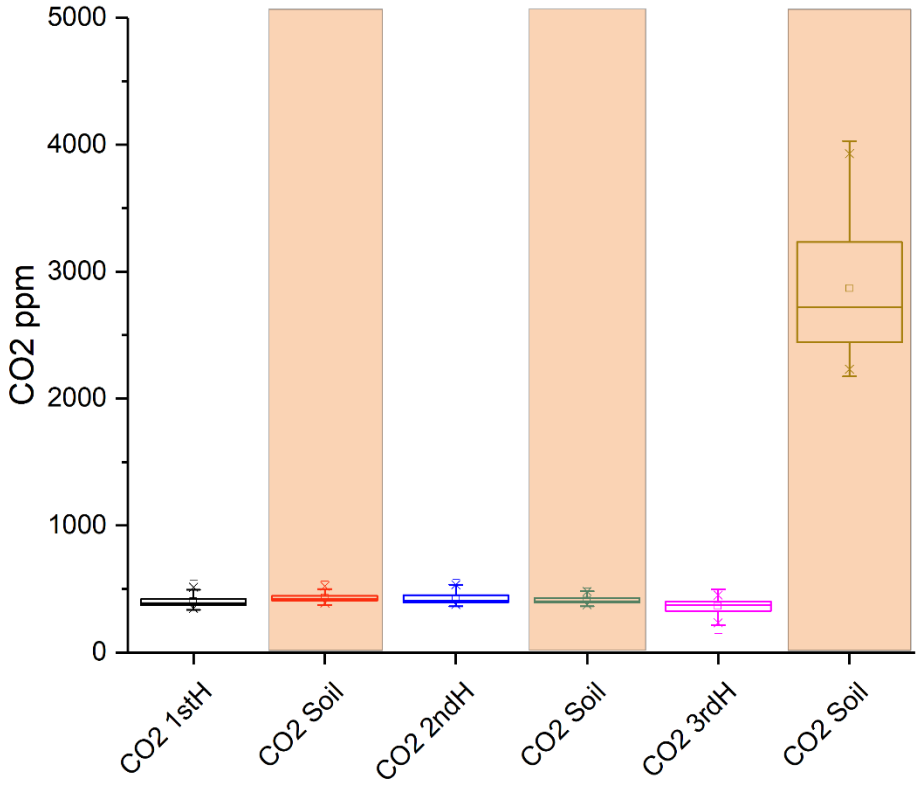

Figure 45. The concentration of carbon dioxide during construction of pipelines phase. Legend: 1st, 2nd, 3rd H = first, second, third Home where the Y-POD was located, CO2 Soil = soil measurements of carbon dioxide.

Diurnal variations of gas concentrations

The average diurnal variations of gas concentrations are shown in fig.46. The diurnal variations for methane and carbon dioxide in atmosphere exhibit generally same shape.

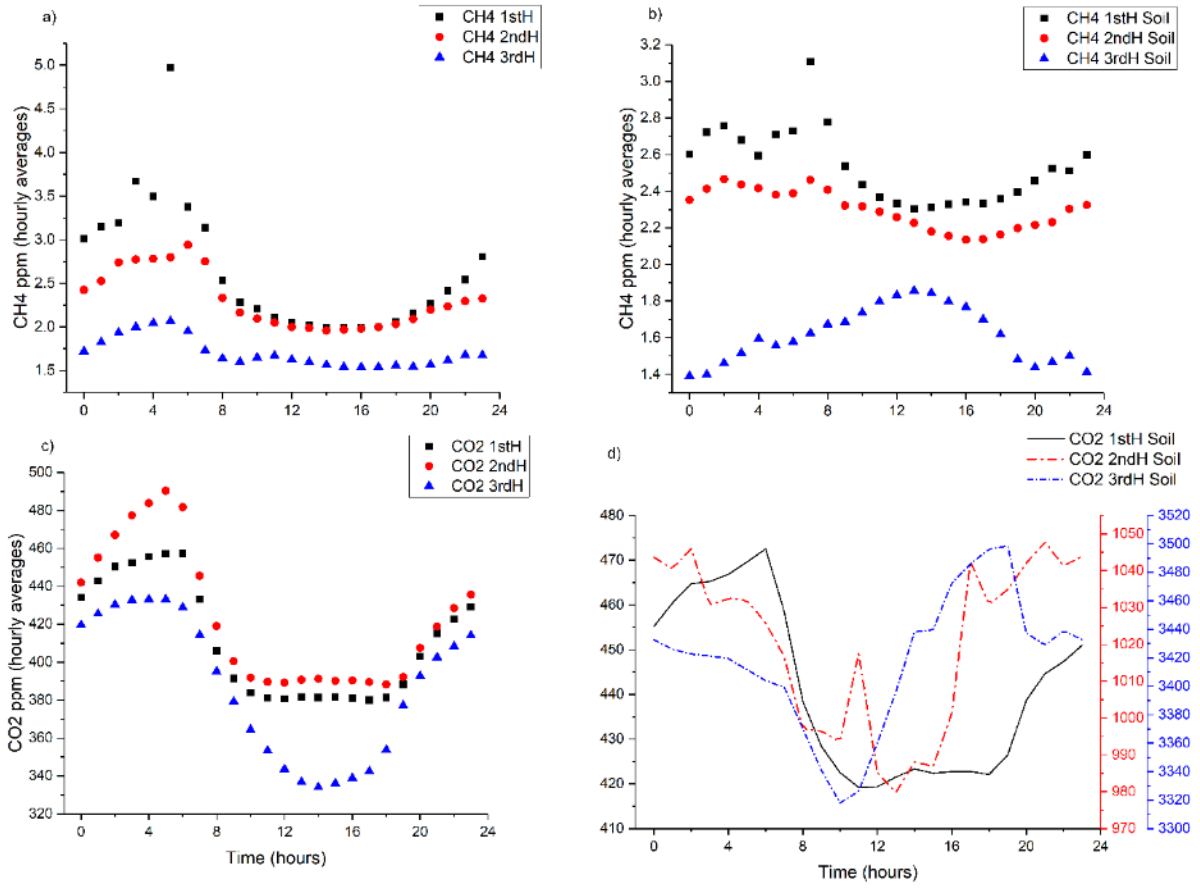

Figure 46. Diurnal variations of methane and carbon dioxide during the three months of measurements.

The methane and carbon dioxide time series shows higher early morning and nighttime concentrations and lower levels from 10:00 to 20:00. Highest concentrations of methane appear during early morning hours (5:00 a.m.) and the same general trend is observed for carbon dioxide. Later, the concentration of gases gradually decreases to the lowest at noon and stays at a low value from 12:00 till 20:00, and then increases gradually to another high value in the night.

The daytime low CH4 and CO2 mixing ratios could be due to the increased planetary boundary layer height in the afternoon, wind circulation, and the development of east and north winds which aid in dilution and ventilation of the pollutants in the area. Furthermore, plant and soil respiration also increases CO2 mixing ratios during the night (Chandra et al., 2016). However, Ganesan et al. (2013) described that the morning

peaks could be due to the radiative heating of the ground in the morning, which breaks the inversion layer formed during night.

The diurnal variations for methane and carbon dioxide in the soil measurements exhibit a different shape. The methane time series (at 1st Home and 2nd Home, silty soil) shows higher early morning and nighttime concentrations and lower levels from 10:00 to 20:00. The highest concentrations of methane appear in the early morning (7:00 a.m.). The methane time series at the 3rd Home shows higher daytime concentrations and lower nighttime concentrations, due to the soil characteristics, organic matter rich sandy soil. The carbon dioxide time series shows different shape for the three sampling sites. At the 1st H, higher nighttime concentrations, instead the lowest concentration was from 12:00 to 20:00. At the 2nd H, two higher concentration peaks are in the early morning at 3:00 and 11:00, instead the lowest concentration from 12:00 to 17:00, to present again highest peaks at 21:00. At the 3rd H, shows higher daytime concentrations, from 12:00 to 19:00.

Gas concentrations related to the temperature and humidity

A relationship is observed between CH4 and temperature (T°C). The highest values of T°C correspond to highest CH4 values, but not with CO2 values. The lower humidity values correspond to higher CH4 and CO2 values. The gas concentrations differ at the three locations, relating to soil characteristics and chemical properties, fig. 47.

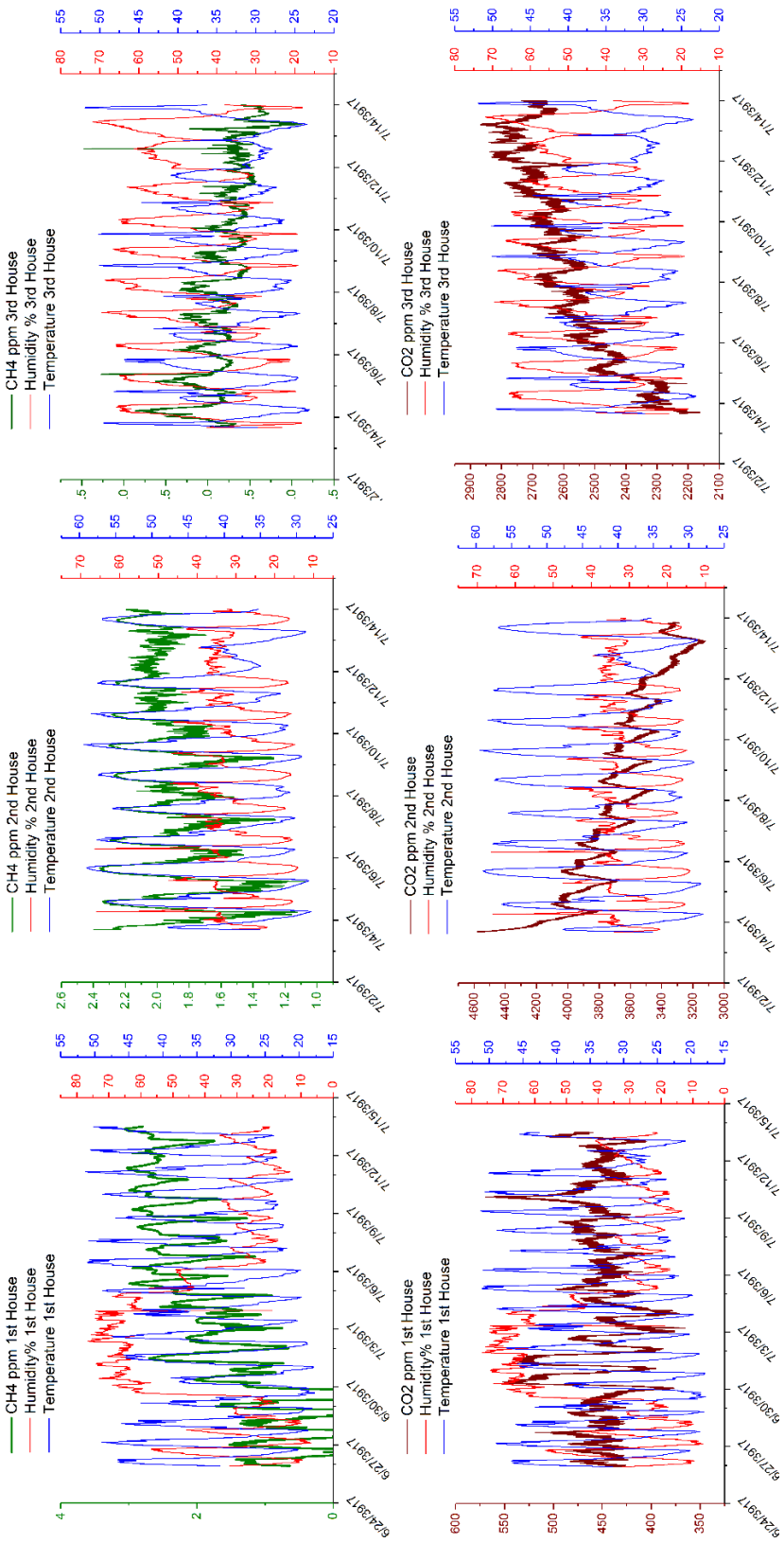

Figure 47. CH4 and CO2 gas concentrations related to the temperature and humidity.

At each home location, average values of methane and T°C, H% were considered, as shown in the fig. 48. The methane concentrations (pink color highlighted) was about 3ppm at the three locations, in the atmposhere and into the soil, instead a difference on T°C and H% was at the third location where the Y-POD air/soil quality monitor was deployed in a garden with tallest trees and irrigation system, as we can observe the humidity was higher and temperature lower than in the other locations.

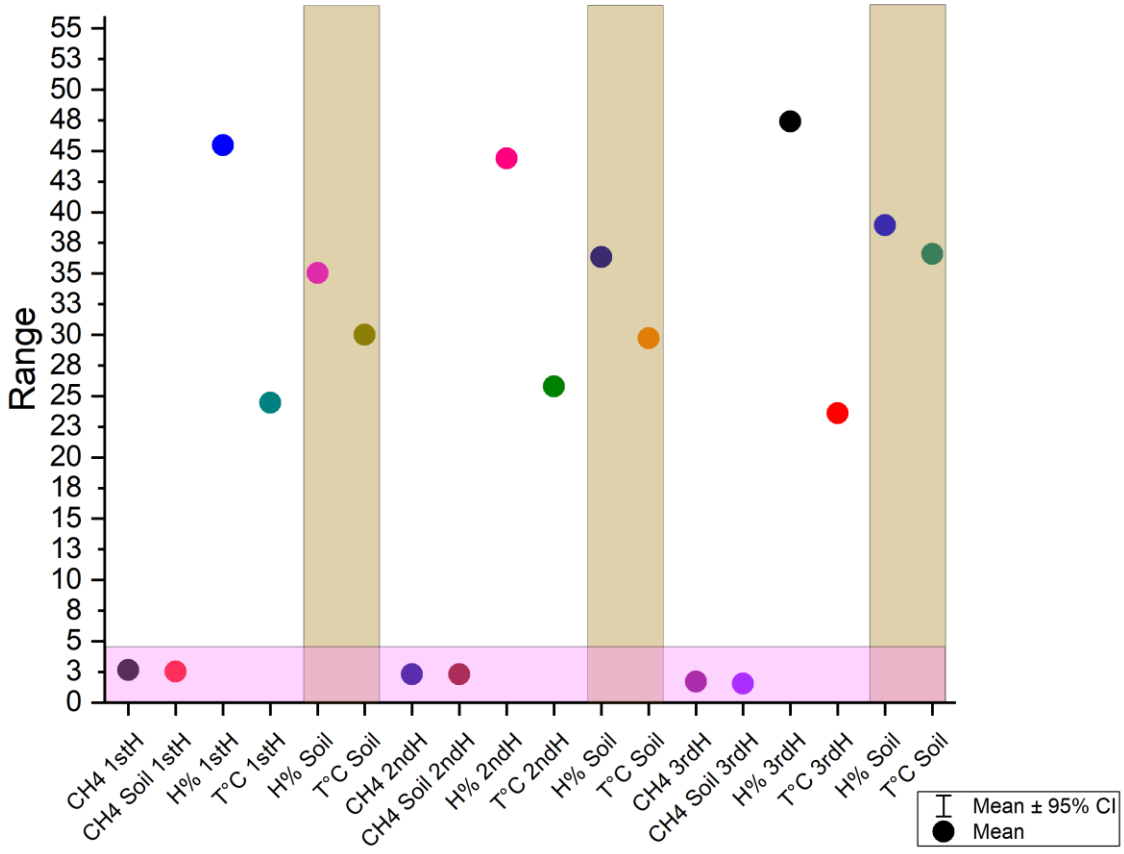

Figure 48. Mean values of Ch4, T°C, H% at the well pad, for almost 3 months of gas survey measurements.

I.2.7 Discussions

Demographic expansion and industrialization are responsible for changes in land use pattern, mainly to produce food and energy, occurring since the beginning of the industrial era. The changes in land use pattern have been the main causes of modifications in sources and sinks of greenhouse gases. According IPCC (2007), however, there is a netincrease in atmospheric GHG concentrations. High atmospheric GHG concentrations are responsible for high strength of green house effect which causes global warming /climate

change. Since the early 20th century, the Earth mean surface temperature has increased by about 0.8ºC, with about two third of the increase occurring since 1980. Consequently, *identification and quantification of sources and sinks of greenhouse gases have become an important environmental/political/public issue*.

With a global warming potential 25 times as high as carbon dioxide (CO2) based on mass on a century time scale (Forster et al. 2007), methane (CH4) is an important greenhouse gas in the climate system. Research effort focuses on identifying the global CH4 sources and sinks to estimate not only their current strength, but also their potential in response to land-use change and global warming (Keppler et al. 2006, Walter et al. 2007, Dlugokencky et al 2009). The atmospheric concentration of CH4 has more than doubled since pre-industrial times (Bousquet et al. 2006) from 715 ppb in the 18th century to 1774 ppb in 2005 (Forster et al. 2007) which gives a radiative forcing of at least 0.48 W m-2 and makes it the second most important greenhouse gas after CO2 (Forster et al. 2007). The increase in atmospheric CH4 concentration is mainly attributed to anthropogenic sources (Etheridge et al. 1992, Lelieveld et al. 1998) which include rice agriculture, livestock, landfills and waste management, biomass burning and energy production and make up 60 to 70 % of the estimated total global source of ~582 Tg CH4 yr-1 for 2000-2004 (Denman et al. 2007, O'Connor et al. 2010). Natural CH4 is emitted from oceans, hydrates, forests, termites, fires, geological sources and wetlands (Denman et al. 2007). CH4 sources can further be divided into biogenic and non-biogenic, the first accounting for more than 70 % (Denman et al. 2007). Since further measurements are needed during the Production phase at the Well Pad Greeley, CO, we cannot try a direct conclusion on the methane concentrations being responsible by drilling and hydraulic acitivities in that area.

I.2.8 Recommendations

Y-POD sensor systems were used to measure ambient CO2ppm, CH4ppm in Greeley (CO, USA) area for more than 4 months. Y-PODs were deployed near a new multiwell pad, to explore air quality impacts associated with hydraulic fracturing activities. Before and after sampling near the multiwell pad, Y-Pods were co-located with reference instruments at a CDHPE air quality monitoring site in Greeley, CO, about 8km away from the multiwell pad. Field calibrations of sensor were performed for methane, resulting in r^2 values that ranged from 0.86 - 0.95 and RMSE values that ranged from 0.07 - 0.15 ppm. Field calibrations of sensors were performed for carbon dioxide also, resulting in r^2 values ranging from 0.64 - 0.95 and RMSE values ranging from 5ppm - 10 ppm. Figaro2600 gas sensors were employed in the quantification of methane, resulting in some observations of atmospheric methane that were lower 1.8 ppm. It is extremely important to calibrate the low-cost sensors as often as possible. As results in calibration, each sensor had a unique response and a unique calibration, so it cannot be considered one calibration for all sensors used in the research. These sensors can be used in the field, without any control in temperature or humidity, but they need calibrations as often as possible and validation data.

The Y-PODs devices can be used in all environments conditions. The only thing it does not have incorporated an internal battery, that can be useful to use it with the GPS sensor, that is incorporated, and so that one can use the device in many locations in a single day, if desired. Some issues came out on SD card and data recorded, due probably to incorrect position of the SDcard into the shield. The Y-POD was prepared for Real Time monitoring, but the raspberry pi3 microcontroller presented some issues on saving the data, due probably to the code programing on the microcontroller. The sensor signal was recorded every 12 seconds but it could have been modified as well. This device need as main microcontroller the Arduino UNO, and the shield for SDcard, as well as need an electronic two boards for the main sensor functions. As mentioned before this device was developed by the Prof. Hannigan research group at the Mechanical Engineering Department, University of Colorado at Boulder, USA. An investigation into the cross sensitivity of the different gases that the sensor will be exposed to, it is extremely important to be done. Cross sensitivity responses will vary from sensor type to sensor type, and suppliers often express the cross sensitivity in percentages while others will specify in actual parts-per-million (ppm) levels. Cross sensitivity is a sensor's reaction to other gases which can "interfere" with how the sensor reacts. Exposing a sensor to a gas that is not the target gas can cause an undesirable effect; this may be a positive response, negative response or inhibition. A positive response means that sensors respond to not just the target gas but to another gas as well. This could give the user the impression that there is target gas present when there isn't, or that there is more target gas present than is really the case. A negative response is when sensors produce a reduced response to the target gas if also exposed to a gas that causes a negative response. If this happens, the user may be exposed to the target gas and not know they are at risk, or it may reduce the level of gas seen on the instrument display as it is been reduced because of this negative effect. Inhibition is similar to a negative response; however what actually happens is the sensor will not respond at all to the target gas if exposed to the inhibitor at the same time, or the sensor may take hours if not days to recover before responding to the target gas again.

Unfortunately, I did not have enough time to analyze the cross sensitivity for all sensors, since it was the last year of my PhD research program. Many issues came out with the codes for the calibration and validaton, so that there was not time enough to analyze the cross sensitivity for all sensors of the 25 instruments used, this is expected to be done in near future since is continuing the collaboration with the University of Colorado.

I.3 Soil Acquifer Treatment – Waste Water Monitoring System, Algarve, Portugal

I.3.1 Problem statement

The Research program developed at National Laboratory for Civil Engineering, LNEC a public institution of scientific and technological research and development in Portugal, present methodologies on improving the water quality in a Wastewater treatment plant, in Algarve south of Portugal. The research was based on soil aquifer treatment, soil column laboratory experiments to obtain the best soil in contaminants retention for the infiltration basins, as a second wastewater treatment process. The wastewater after being treated, it flows directly into a river which is recharging a karstic aquifer. A good water quality of the river, prior to its recharge into the aquifer, was the main objective of this research. Two infiltration basins were built at San Bartolomeo de Messines, and a real-time water monitoring system was used in input and in output, understanding immediately the results from the soil basins and the water parameters as potential of hydrogen, electrical conductivity, temperature and oxidation reduction potential. Further information is presented in the Articles (on page 115, 126, 143). Like CO2 and CH4, the atmospheric concentrations of nitrous oxide were reasonably stable before industrialization (typically quoted as 270 ppb). Since industrialization, nitrous oxide concentrations have increased by about 20 % due to agricultural/land-use practices (for example the use of nitrogenous fertilizers). It continues to rise approximately linearly (Montzka et al., 2011) to reach values as ~323 ppb in 2009. N2O can be produced during both nitrification and denitrification processes. Nitrification is an aerobic microbial process that converts ammonium (NH4+) to nitrate (NO3-) in the presence of oxygen. During denitrification, nitrates are transformed into nitrogen (N2). Denitrification requires anoxic conditions, but denitrifying bacteria are facultative anaerobes (Schlesinger, 1997; Hahn et al., 2000). Higher N2O emissions observed in tropical conditions could reflect the influence of temperature on nitrification and denitrification processes, as well as nitrogen availability, which is greater in tropical than in boreal and temperate forests (Sitaula and Bakken, 1993; Stange et al., 2000; Clein et al., 2002). Production of N2O through nitrification or denitrification will depend on the presence of ammonium or nitrate, and on the soil moisture content. Agricultural and other human activities can increase nitrogen availability in the contributing area leading to significantly higher N2O emissions from agricultural soils. Intense rainfall can contribute to increase labile carbon and nutrients and subsequent N2O emissions.

I.3.3 Geology settings

The study area is in the northern limit of Querença – Silves aquifer system, a Jurassic calcareous formation, situated in the Algarve region, south of Portugal, fig. 49. The Querença – Silves aquifer is a karstic multi-aquifer system, which its formation is due to the tectonic activity and divided in several subsystem aquifers

in hydraulic connections (Almeida *et al.*, 2000, Monteiro *et al.* (2006), Monteiro *et al.* (2007) and Reis *et al.* (2007).

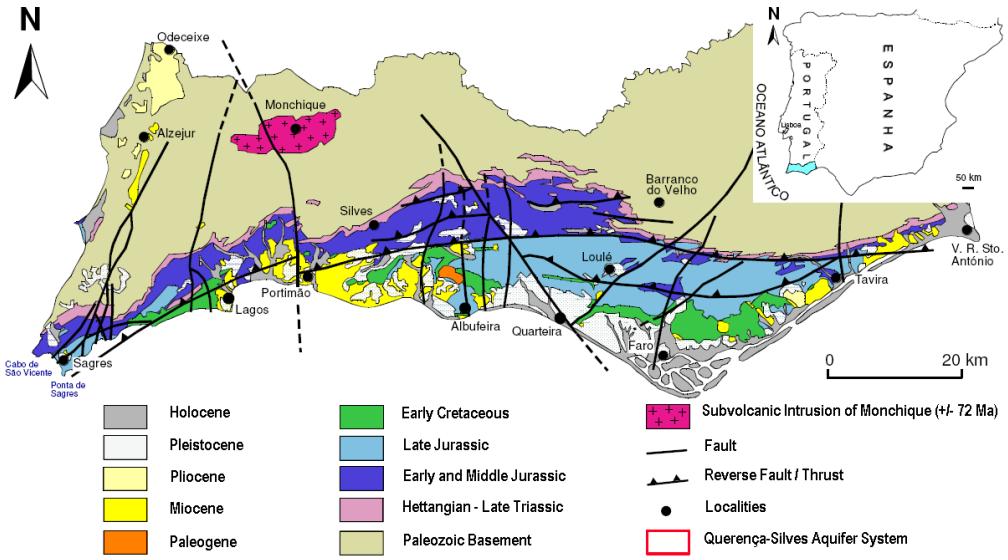

Figure 49. Geologic map of the Algarve.

This karstic multi-aquifer system is researched by surface groundwater, by Ribeiro Meirinho River. This research aimed to focus on soil characteristics of this aquifer, in the laboratory especially and build large infiltration basins, to improve wastewater quality through SAT processes so that to improve aquifer recharge through Ribeiro Meirinho river since São Bartolomeu de Messines Wastewater Treatment Plant (SBM WWTP) treated effluent is directly discharged to Ribeiro Meirinho.

I.3.4 Methodologies

The methodologies are completely presented in the Article (on page 126), and shown in the fig. 50.

I.3.5 Results

As results showed that the soil column, more than one month laboratory experiment, presented almost same average water parameter values as in the field scale infiltration basins, more than three-month field experiment. As contaminants we focused on ammonia, nitrates, nitrites, boron, copper and zinc values, the results showed a good contaminant retention for ammonia and copper. Further information is specified on the Article (on page 126).

Figure 50. Soil column experiments and infiltration basins in Algarve (Portugal) at the Wastewater Treatment Plant.

Results, Softwares used:

For the Soil column experiments & Physical sand box (artificial aquifer), Hydrus and Feflow softwares were used in this research.

Introduction to HYDRUS-1D

HYDRUS-1D is a computer software package which may be used for simulating water, heat, and solutes movement in one-dimensional variably saturated porous media. It can be also used to simulate carbon dioxide and major ion solute movement. Basically, the Richardss equation for variably-saturated water flow and advection-dispersion type equations for heat and solute transport are solved numerically. To account for variability in the soil properties, many modifications are made to the flow equation, such as, a sink term to account for water uptake by plant roots, and dual-porosity type flow or dual-permeability type flow to account for non-equilibrium flow. The program can deal with different water flow and solutes transport boundary conditions (Šimůnek, et al., 2009)**.**

In addition to HYDRUS computer code, the HYDRUS-1D software has an interactive graphics-based user interface module. Basically, the module consists of a project manager and a unit for pre-processing and post-processing.

HYDRUS-1D model development

Input data

Soil hydraulic properties

Investigation of flow water in soli column was done for specific boundary conditions. An one layered soil profiles was used, 30 cm deep, as input data for HYDRUS-1D for 1 sites of interest, Sao Bartolomeu. Soil properties present sand 81.91%, silt 15.96%, clay 2.13% and bulk density 1.46 g/cm3.

Volumetric water content for the soil was calculated according to van Genuchten formula. Van Genuchten hydrodynamic parameters θr and θs were predicted by Hydrus-1D from the particle size distribution and bulk density of the soils.

Geometry information

In HYDRUS-1D geometry of model can be defined. First, the number of soil types, the total depth of soil profile, and length units can be set under the geometry information dialog box. Then, finite element model can be constructed by subdividing each region into linear elements by means of soil profile graphical editor or soil profile summary dialog windows.

In this study, only one of soil profiles was used. The total depth of soil profile is 30cm. The finite element model was constructed by dividing the entire profile into 101 layers.

Time information

Under this section, time units, time discretization, and time-variable boundary conditions can be defined. The unit of time was selected in minutes and the period 26/02/2015 – 23/03/2015 was used for simulation purposes (22928 minutes). In HYDRUS-1D code, the maximum number of time variable records is 10000.

Water flow

Soil hydraulic property model

Within this command window, hydraulic model and hysteresis can be defined. There are various hydraulic models that can be used. In this research, van Genuchten-Mualem single porosity model was selected, without hysteresis.

Soil hydraulic parameters

All the parameters needed for various soil hydraulic models are specified in this section. The parameters needed are residual and saturated water contents, saturated hydraulic conductivity, pore connectivity parameter, and empirical coefficients Alpha and n. To predict the values of these parameters, HYDRUS-1D uses Rosetta DLL (Dynamically Linked Library), by Marcel Schaap (Šimůnek, et al., 2009). The Rosetta model can be used to estimate water retention parameters according to van Genuchten (1980), saturated hydraulic conductivity, and unsaturated hydraulic conductivity parameters according to van Genuchten (1980) and Mualem (1976). To achieve this, the model uses a database of measured water retention and other properties for a wide variety of media. For a given a medium's particle-size distribution and other soil properties the model estimates a retention curve with good statistical comparability to known retention curves of other media with similar physical properties (Nimmo, 2006). As the model uses basic more easily measured data, it is considered as a pedotransfer function model (PTFs) (Schaap, et al., 2001).

Percentage of sand, silt, and clay together with the bulk density for the soil layer were used to get values of all the parameters needed.

Flow boundary conditions

Water flow boundary conditions are selected under this section. The window contains upper and lower boundaries. For 1D modeling purposes, it was assumed to have:

- an atmospheric BC with Surface Layer as an upper boundary condition and

- seepage flux, h=0, at the bottom layer as a lower boundary condition. This type of boundary condition is often applied to laboratory soil columns when the bottom of the soil column is exposed to the atmosphere (gravity drainage of a finite soil column). The condition assumes that the boundary flux will remain zero as long as the pressure head is negative. However, when the lower end of the soil profile becomes saturated, a zero pressure head is imposed at the lower boundary and the outflow calculated accordingly.

In HYDRUS-1D if you select "atmospheric boundary condition with surface layer", the code uses applied flux, calculates the infiltration flux and, if lower than applied flux, allows excess water to accumulate at the soil surface (and infiltrates is after precipitation stops). We can then compare HYDRUS results with our measurement (or use the inverse HYDRUS option to calibrate the code).

Outputs

After HYDRUS-1D models have been prepared, simulations were performed to get the outputs. Generally, the HYDRUS code provides three different groups of output files, which are: T-level information, P-level information, and A-level information. Here, in this research, we made use of different output files from these three groups.

Estimation of water retention was done with statistically calibrated pedotransfer function The Rosetta model. However it predicts water retention for a given soil from database of measured water retention for variety of porous media that is why it difficult to say how good the prediction is. Soil hydraulic parameters obtained from Hydrus-1D, using the single porosity flow model: ɵr 0.0388, ɵs 0.389, alpha 0.044, n 1.9251, Ks 0.128424 and l 0.5.

Legend in graphics:

N1 (top)– N10 (bottom) represent the observation points in soil profile.

T1 – T number of print time in the profile information.

Column5-1stage saturated soil.

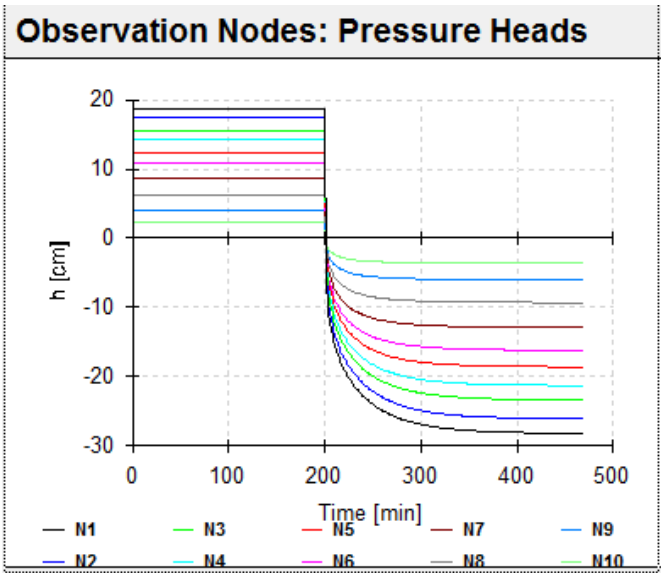

Figure 51. In this figure we can see how is the behaviour of the pressure head after the water was completly infiltrated in the soil, at 230minute. It decreases in the top of the soil and is near to saturation at the bottom of the soil. We can notice, after the water was completely infiltrateted, the pressure head decreased relatively quickly in the top of the soil so a faster propagation of the wetting front.

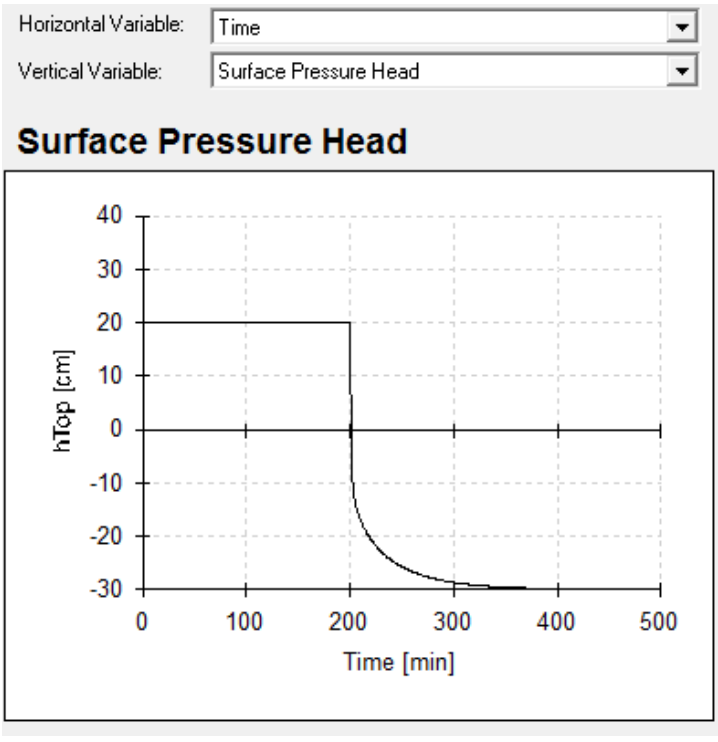

Figure 52. Distribution of the pressure head with time.

In this graph, when the pressure head is zero, saturation at the surface occurs. After 230 minutes approximately, pulse water stops, water drains and pressure head decreases.

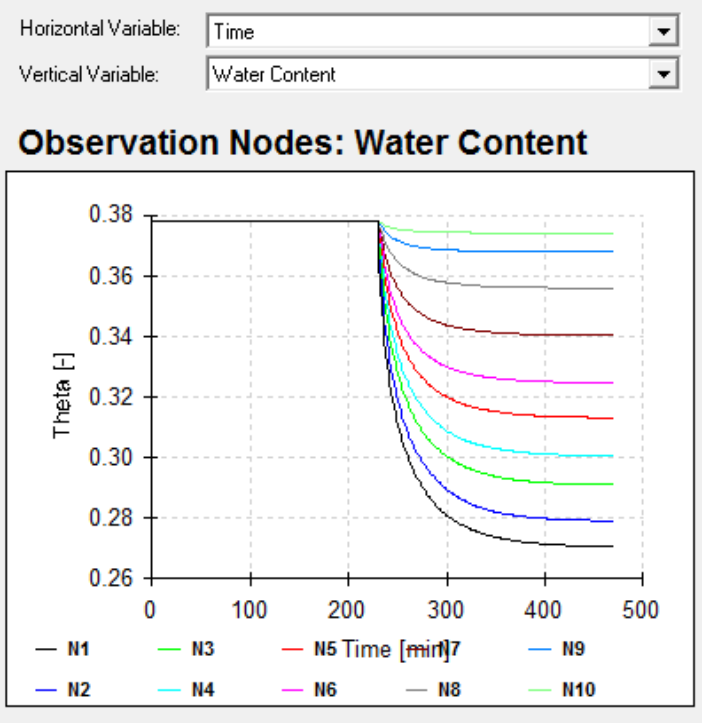

Figure 53. The water retention characteristic curve describes the ability of the soil to release and store water. For the simulations, homogeneous soil with vertical flow was assumed. Hysteresis was not taken into account. After the water was completely infiltrateted, the water content decreased relatively in the top of the soil.

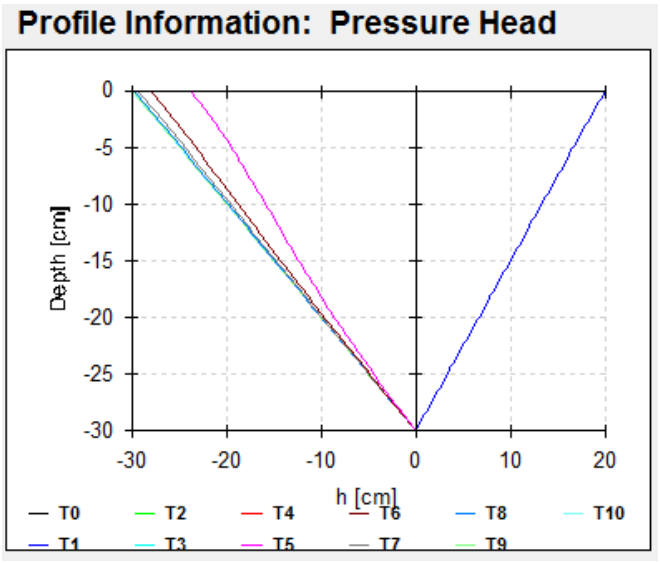

Figure 54. In this graph we can notice that the T1-T4 have positive value of presure head due to the pulse water at the top of the soil. The pressure head at time 230 minute, represented by T5, has a value -14 h (cm) due to the water infiltrated completly in the soil, a negative value also for T6-T10.

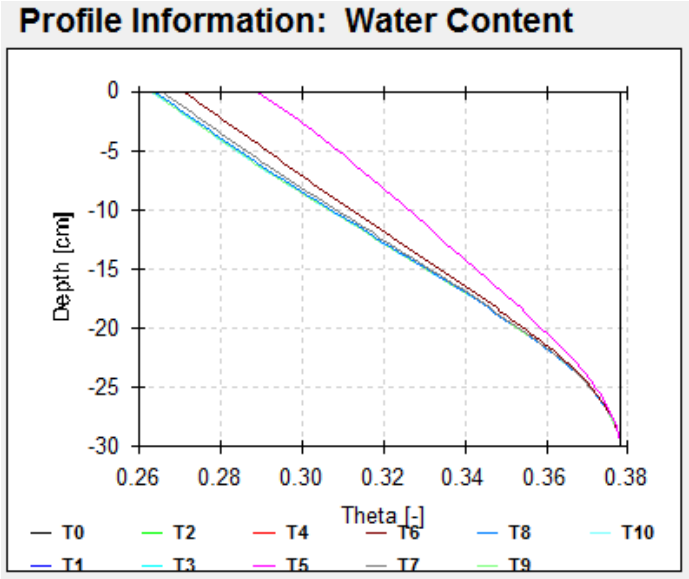

Figure 55. This graph explains the redistribution process of water content in the soil for one pulse injection water, that lasted about 230 minutes. The soil depth for this experiment is 30 meters. Notice that water redistributes in the soil during 6 hours. The water content profile has more water content at the surface T1-T4, with water above the soil, and moved downward with time, T5 – T10 no more water above the soil.

Therefore, water content measurements increased rapidly with water at the soil surface and then gradually decreased when water was infiltrated.

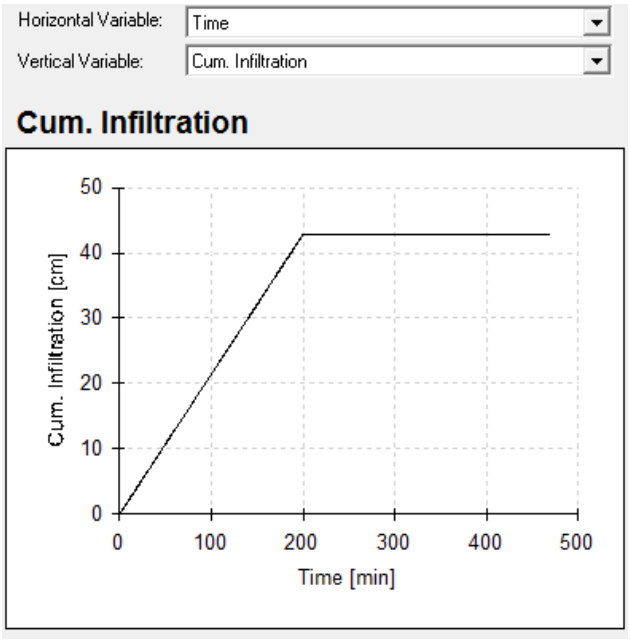

Figure 56. The cumulative infiltration show a gradual increase with time over the whole infiltration process, and a linear relationship with time in the later infiltration stage. It is constant after the water was completly infiltrated at the soil top.

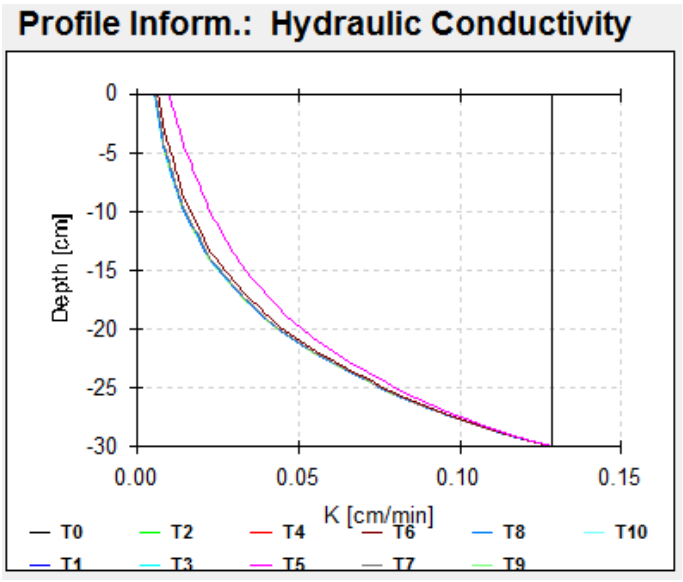

Figure 57. We can notice in this graphs that the K is constant for all the time, with water above the top soil (T0-T4). We can see the decreasing of K(cm/min) at the soil surface after the water was completly infiltrated at the soil top (T5-T10).

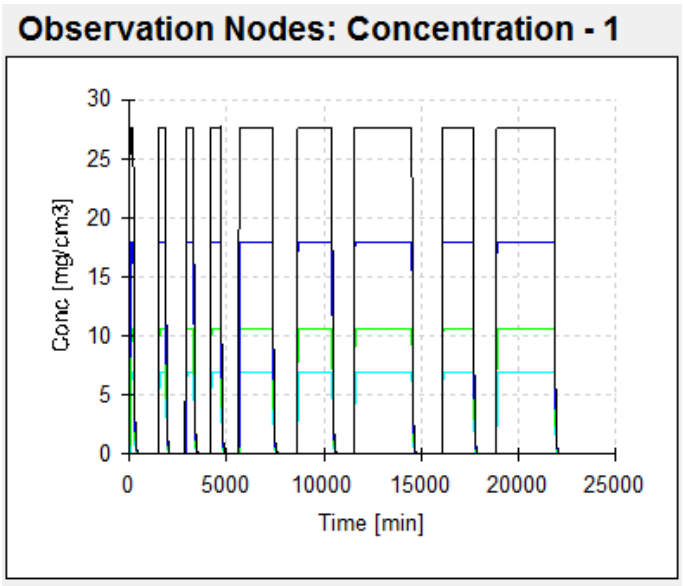

Figure 58. The NH4 concentration during all the experiment.

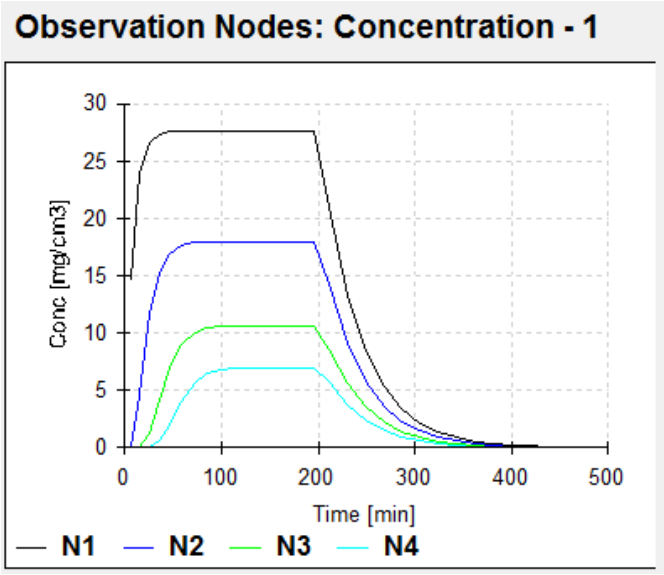

Figure 59. The NH4 concentration when the experiment started and for the first 400 minutes. The N1 is the observation point at first 5cm into the soil and N4 is the last observation point at 25cm depth into the soil. We observe highest NH4 concentration in the upper part of the soil than in the lowest part of the soil.

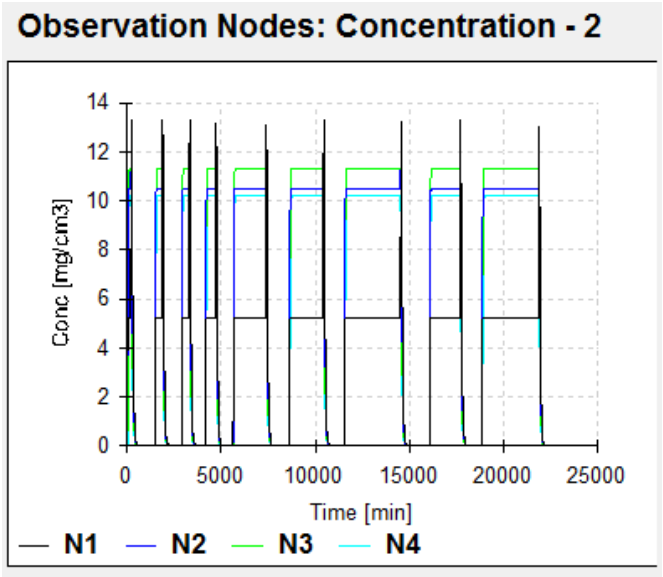

Figure 60. The NO2 concentration during all the experiment.

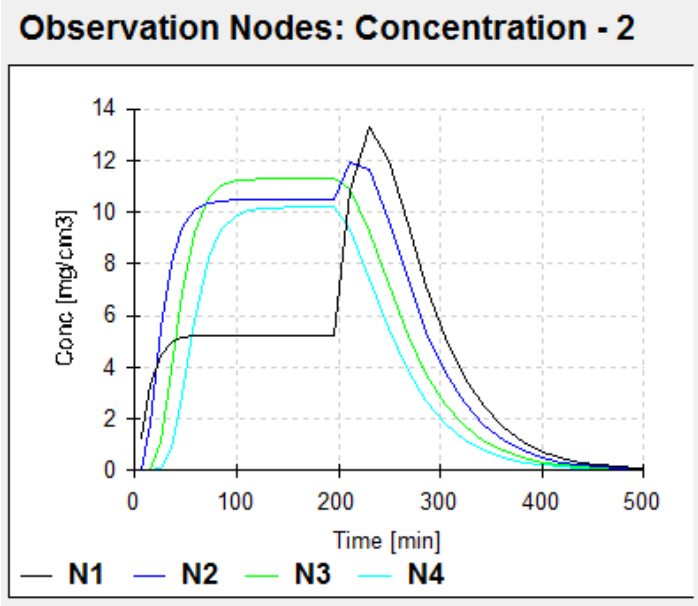

Figure 61. The NO2 concentration when the experiment started and for the first 500 minutes. The N1 at 5cm depth into the soil and N4 at 25cm depth. In the upper part of the soil we notice lower concentration than in the lowest part of the soil. The NO2 is increasing at the lowest part of the soil, about 15cm depth into the soil.

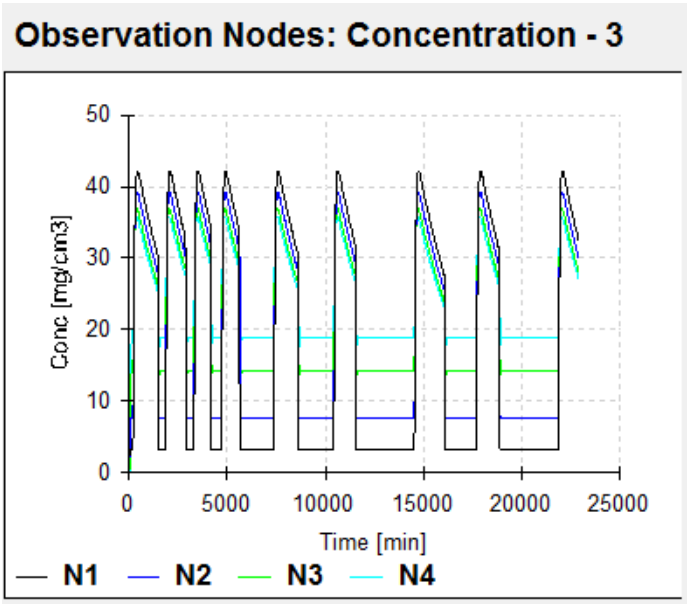

Figure 62. The NO3 concentration during all the experiment.

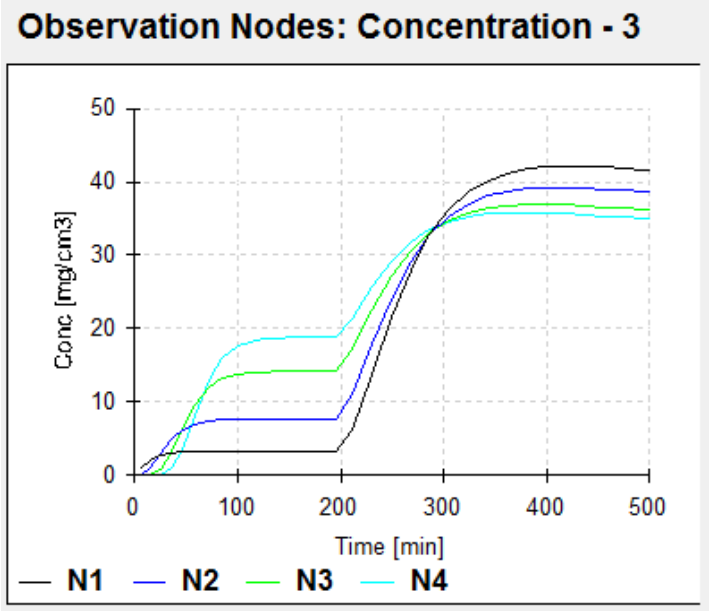

Figure 63. The NO3 concentration when the experiment started. The NO3 is increasing in the powest part of the soil, after that it can be observed an equilibrium at 300minutes with same concentration in all soil column, then the NO3 is increasing in the upper part of the soil.

In the previous figures, it was observed the transformation of ammonium into nitrite and nitrate by nitrification.

NUMERICAL MODELLING FEFLOW 6.2 SOFTWARE

The Feflow 6.2 license at University of Ferrara, Earth Sciences Department (for 6 months).

Modeling of Water Flow and Pollutants Transport in Porous Media, FEFLOW 6.2

This software, in license for 6 months, was important to learn the numerical modeling of groundwater movement and mass transport in soils. The main purpose was to learn the theoretical fundamentals and practical applications of groundwater flow and pollutants transport in soils, both in the saturated and unsaturated zones and the main rules of numerical model development. Definition of required input data, water-transport parameters of soil, initial and boundary conditions, simulation calculations as well as results presentation were conducted with the license and in demo version of FEFLOW 6.2, DHI-WASY.

Problem statement

Numerous authors (e.g. de Wit and Goudriaan, 1978; Heinrich and Pepper, 1999; Grabarczyk, 2000; Karafiat, 2000; Knapik, 2000; Cook, 2002; Kulbik, 2004; Król, 2006; Gromiec, 2007) state that modeling

may be very useful and convenient in irrigation and drainage of agricultural areas planning, designing of building excavations drainage, localization of various objects of water supply or sewage systems, spatial planning of objects potentially hazardous to the natural environment (municipal solid waste landfill sites, petrol stations, fertilizers and pesticides warehouses and reloading points). Modeling may also improve the assessment of agricultural and transport operations effects on water resources condition and characteristics, calculation of required pressure head of pumping devices, selection of disinfectants doses, analysis of water quality onside distribution systems, assessment of thermal isolation efficiency etc. Thus, introduction of modeling may result in reduction of management costs and shortening of designing time, in many cases eliminating the expensive and time-consuming pilot, in-situ tests (M.K. Widomski et al, 2013). FEFLOW was many times positively verified in numerous scientific and engineering applications (e.g. Diersch and Kolditz, 2002; Zhao et al., 2005; Mazzia and Putti, 2006; Trefry and Muffels, 2007; Widomski et al., 2013).

Description of FEFLOW

FEFLOW (Finite Element subsurface FLOW systems) developed by WASY Institute for Water Resources Planning and Systems Research Ltd., nowadays owned by DHI Germany is an interactive, based on graphical user interface (GUI) tool for two (2D) and three-dimensional (3D) modeling of water flow in saturated, partially saturated or unsaturated, isotropic or anisotropic soil domain. FEFLOW allows also the numerical calculations of mass and heat transport in porous media. The model is based on finite elements/volumes method – FEM/FVM (Huebner, 2001; Zienkiewicz et al. 2005a; Zienkiewicz et al., 2005b) and was developed in ANSI C/C++ which allows its application by Windows and Linux OS users.

Mathematical description of water flow in porous media applied to FEFLOW is based on Darcy and Richards equations, also with sink/source term, solved basing on soil media parametrization, applied set of input data, initial and boundary conditions. Parametrization of the modeled porous media may be performed according to the following models: van Genuchten, Brooks-Corey, Haverkamp, exponential and linear Diersch, 2005; Diersch 2005a). It is also possible to reflect the phenomenon of capillary hysteresis in the calculations.

FEFLOW, based on finite elements/volumes method, requires creation of the model in three different stages described below (Diersch, 2005a):

- preprocessor allowing determination of geometric characteristics of modeled domain, generation of finite elements mesh, edition of problem class, method of solution, temporal and control data setting, determination of hydraulic properties of the domain, characteristics of pollutants and models of their propagation, definition of initial and boundary conditions.

- processor allowing the main numerical calculations of water flow, saturation dynamics and mass transport in the studied domain of porous media,
- postprocessor allowing graphical or numerical visualization of calculation results.

The data set required to numerical calculations in FEFLOW's finite elements method covers (e.g. Diersh, 2005a):

- physical and hydraulic parameters of soil: porosity, hydraulic conductivity in saturated conditions, anisotropy ratio, saturated and residual saturation as well as shape parameters of water retention curve and unsaturated hydraulic conductivity model
- initial conditions for water flow: saturation, volumetric moisture content, pressure head and pressure are allowable
- mass transport parameters of soils, including porosity, sorption model, longitudinal and transverse dispersivity, model of dispersion, molecular diffusion coefficient and type and coefficients for decay reaction
- initial condition for mass transport, and characteristics of soil may be prescribed to model area in several ways: to the single nodes, to selected elements of FEM mesh, to the greater area selected by the popular window tool, globally to the whole area and finally data may be imported from data base prepared in ESRI, dBASE or ASCII formats.

Introduction of the boundary conditions to models in FEFLOW is based on selection of one of four offered types of boundary condition, definition of its value (constant of time varied) and assignment of the condition to FEM mesh. Available in FEFLOW types of boundary conditions for water and mass transport are as follows (Diersch, 2005; Diersch, 2005a):

• First type (Dirichlet) describing pressure head (water) and concentration (mass) for the given node.

• Second type (Neuman) determining water flux or mass flux leaving or entering the modeled domain through the selected limit of the model.

• Third type (Couchy) defining reference pressure head (water) and concentration (mass) of the area located outside the modeled domain allowing inflow or outflow.

• Fourth type, a single well allowing water and mass inflow or outflow through a single node.

Objective

It was set up a physical sand box (artificial acquifer) 2D model, and basic FEFLOW operations were practiced. First, the geometry of the model was defined and a finite-element mesh was generated. The model

properties, initial boundary conditions and material properties were applied. The 2D flow model was extended to a 2D mass-transport model.

Model Scenario

The model domain is the physical sand box model with an area of approx. 1000 m^2 for each section A, B, C.

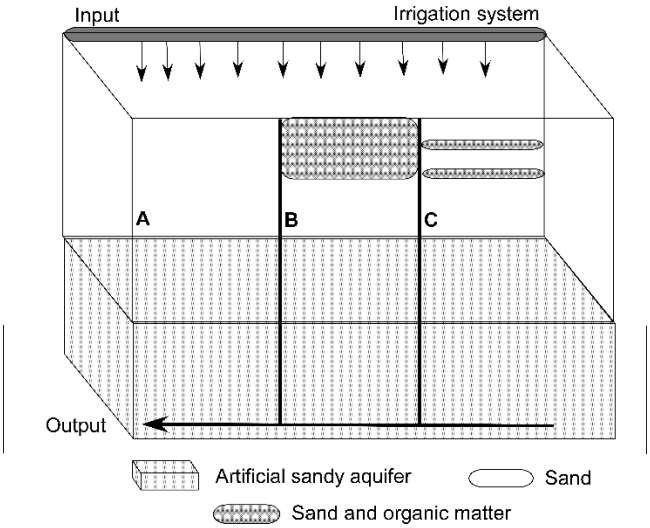

Figure 64. The physical sand box model for Feflow.

The main flow direction follows the hydraulic head gradient vertically. Tap water was applied as a constant value all over the model domain during the experiment (irrigation system) and the contaminant concentrations during the experiments. Figure 1 illustrates the scenario.

The contaminant sources applied during the experiments affected the water quality in the artificial sandy aquifer.

Supermesh

The supermesh defines the geometry of the model. In the simplest case, a supermesh consists of only one polygon that defines the outer boundary. The design of the supermesh also influences the generation of the finite-element mesh. More complex supermeshes contain several polygons and many lines and points. In this experiment, the supermesh consisted of three square polygons with a lateral length of 1000 m as its outer boundary for section A, B, C.

Finite-Element Mesh

The finite-element mesh is the basis of the numerical simulation. FEFLOW can work with quadrilateral as well as with triangular meshes. Triangle can handle very complex geometries and is extremely fast, but yields elements of slightly lower quality. It was entered 500 elements in the total elements field and it was generated the Mesh.

Problem Settings

All general settings of the model were specified, for instance flow only or flow and transport, the temporal domain (steady state or transient) or numerical properties like accuracy settings and the choice of the equation solver.

Problem Class

Both flow and transport simulations, a steady-state or a transient solution, mass solute transport were computed.

Saturated/Unsaturated

The Darcy equation was used for the entire model domain. In unsaturated mode, Richards' equation was applied for the unsaturated parts of the model.

Steady state/Transient

In steady state mode, FEFLOW calculates the state of a model with time-constant boundary conditions and material properties after an infinitely long time, e.g. to simulate average conditions for an aquifer. In transient mode, the simulation is done for a specified time. This time is divided into time steps for which results are computed (temporal discretization). The steady flow/transient transport mode requires a steady state solution of the flow simulation as initial condition.

Model Properties

Physical conditions in the model area were specified, as initial conditions, boundary conditions and material properties. Additional model properties related to the solute transport model were specified.

Conditions for section A, B, C

As boundary conditions, the fluid flux was 8.29 m/d; mass transport HC concentration 7 mg/l; Mg 0.84 mg/l; P2O5 8.32 mg/l.

Material properties, mass transport Cl, porosity 0.372; longitudinal dispersivity 1m; transverse dispersivity 2055m.

Results

The Solute transport, HC, Mg, P2O5 concentration, in section A, B, C, 8 observation points with different color that represent the depth into the physical sand box model, as showed in the fig. 65.

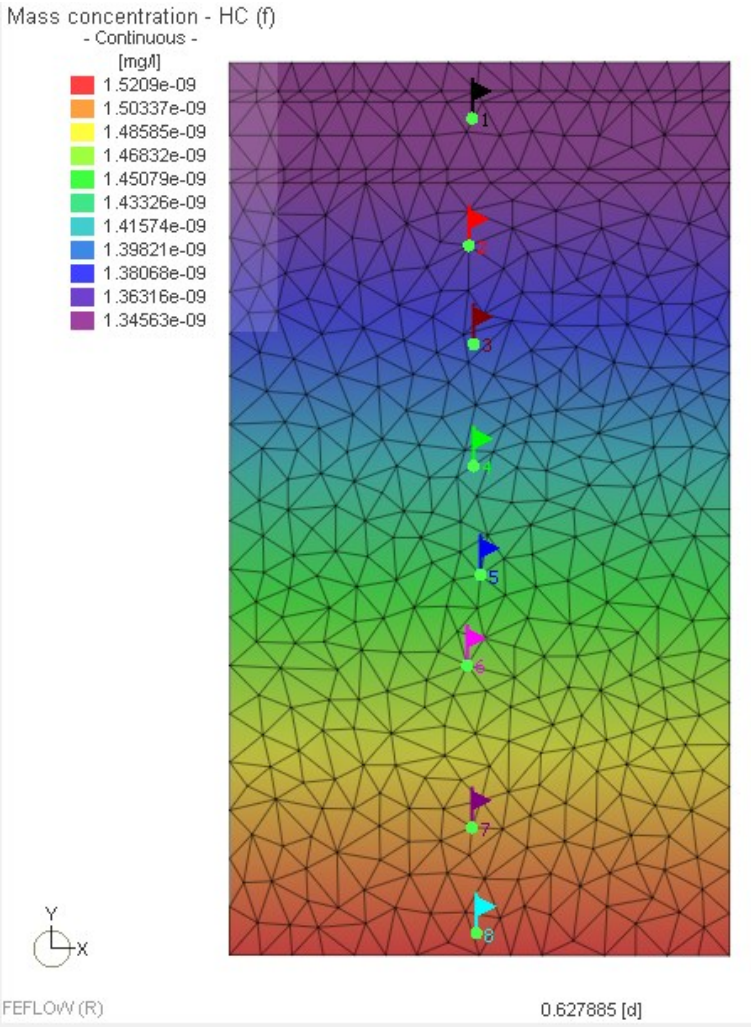

Figure 65. The observation points into the section C, physical sand box model.

The HC, Mg, P2O5 concentration in each section A, B and C has different behavior related to the soil characteristics. The section A is sand-based, section B organic matter-sand based, section C present layers of sand -organic matter – sand.

The HC concentration behavior in section A is increasing immediately in the first 30 cm depth into the soil, observation point 1, and it is not increasing going deep into the soil. In section B, as input of HC was 7 mg/l and one can observe that in upper part of the soil we have highest concentrations than in the lowest part pf the soil, due to chemical reaction of sand and organic matter. In section C, the behavior is so

different, in the lowest part seem to be increasing the HC concentration and after going slowly down. Since this model is not calibrated, we can not consider 100% of these results, just to have an idea about the solute transport into the soil. The research did not focus on calibrating the results of this model.

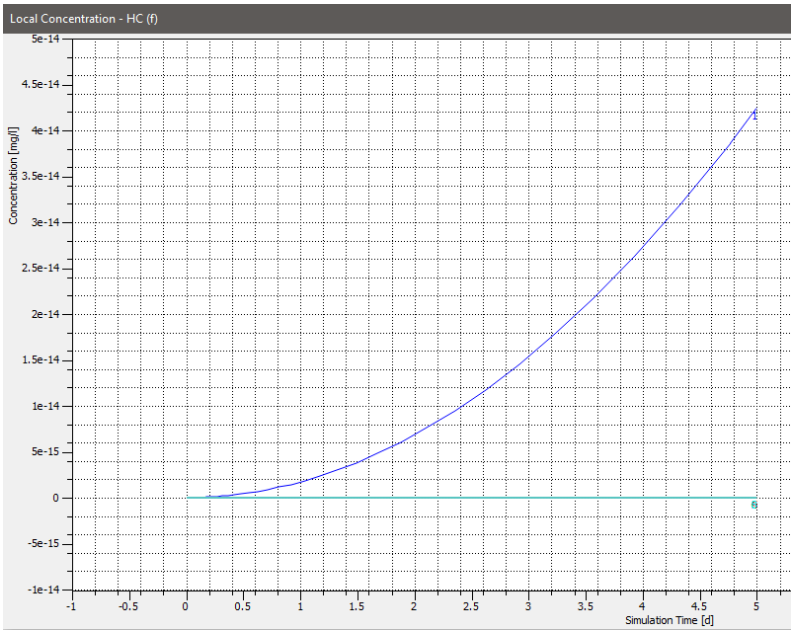

Figure 66. HC concentration and the time simulation of the experiment, in section A.

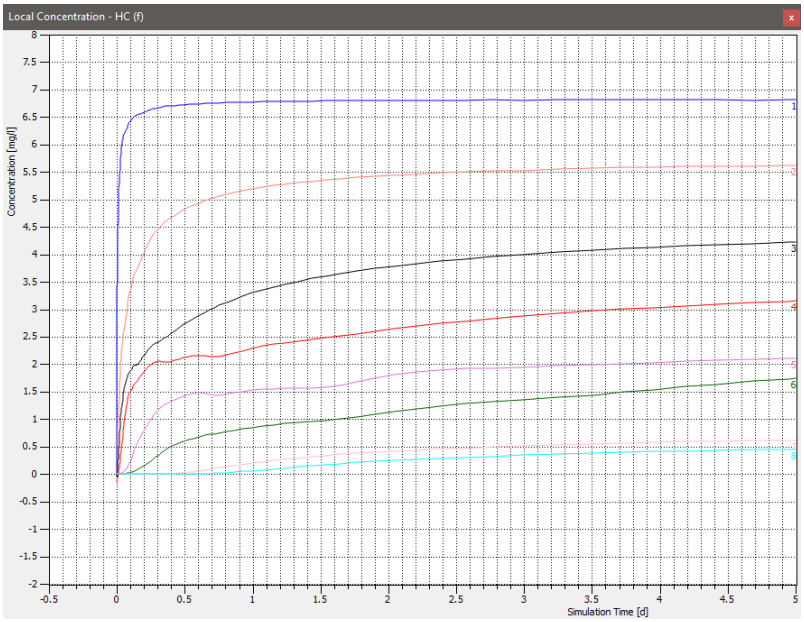

Figure 67. HC concentration and the time simulation of the experiment, in section B.

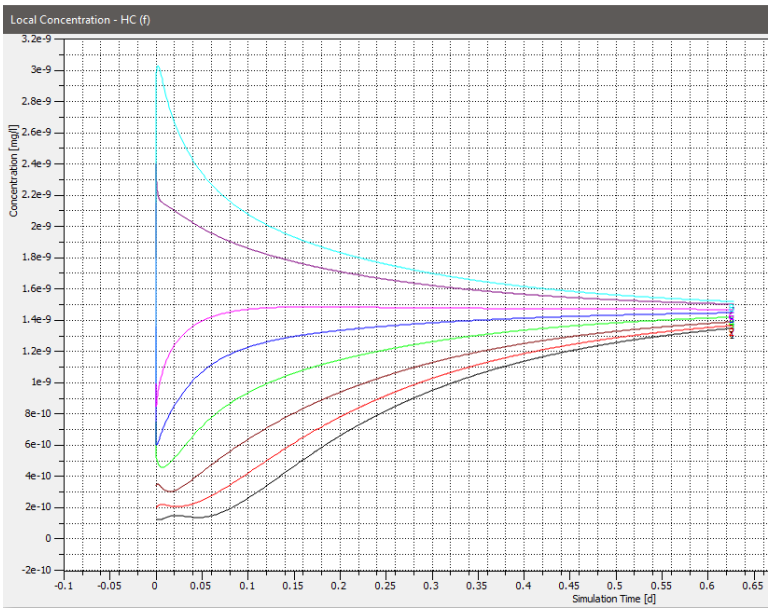

Figure 68. HC concentration and the time simulation of the experiment, in section C.

The Mg concentration behavior in section A is increasing immediately in the first 30 cm depth into the soil, observation point 1, and it is not increasing going deep into the soil, same behavior as HC concentration. In section B, as input of Mg was 0.7 mg/l and one can observe that in upper part of the soil we have highest concentrations than in the lowest part of the soil, due to chemical reaction of sand and organic matter. In section C, we have almost same behavior of the Mg concentration as in section B. The research did not focus on calibrating the results of this model.

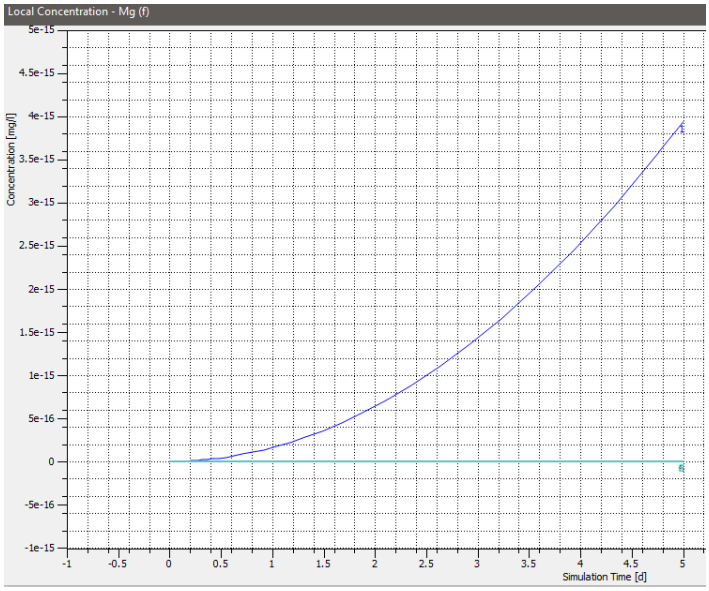

Figure 69. Mg concentration and time simulation of the experiment, in section A.

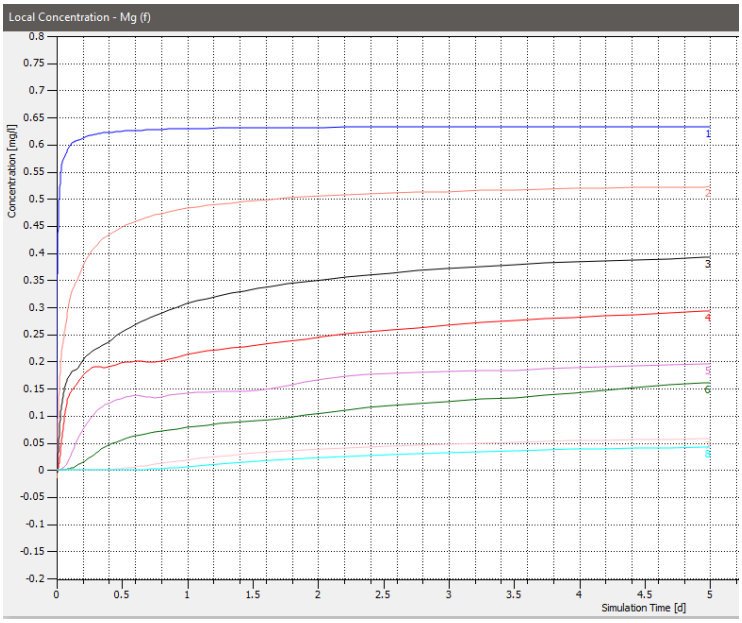

Figure 70. Mg concentration and time simulation of the experiment, in section B.

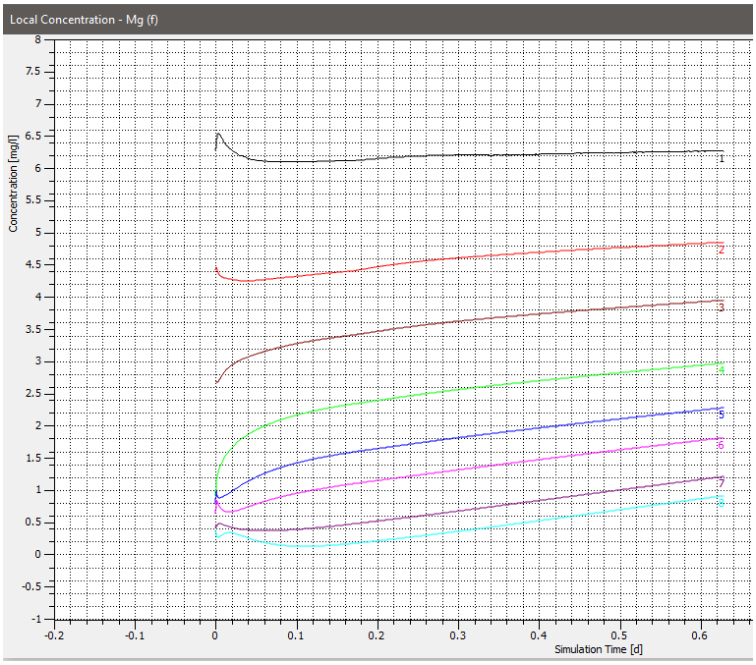

Figure 71. Mg concentration and the time simulation of the experiment, in section C.

The P2O5 concentration behavior in section A is increasing immediately in the first 30 cm depth into the soil, observation point 1, and it is not increasing going deep into the soil, same behavior as HC, Mg concentration. In section B, as input of P2O5 was 7 mg/l and one can observe that in upper part of the soil we have highest concentrations than in the lowest part of the soil, due to chemical reaction of sand and

organic matter. In section C, we have almost same behavior as in section B. The research did not focus on calibrating the results of this model.

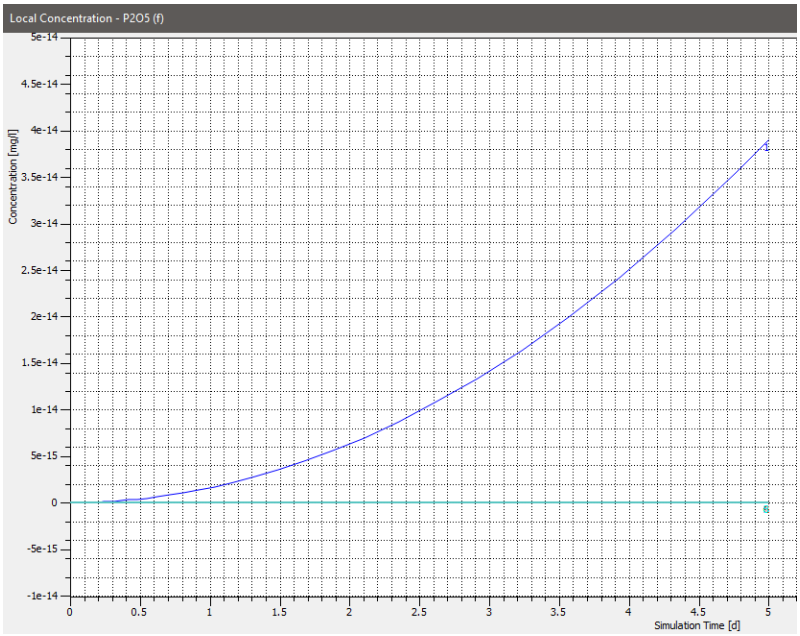

Figure 72. P2O5 concentration and the time simulation of the experiment, in section A.

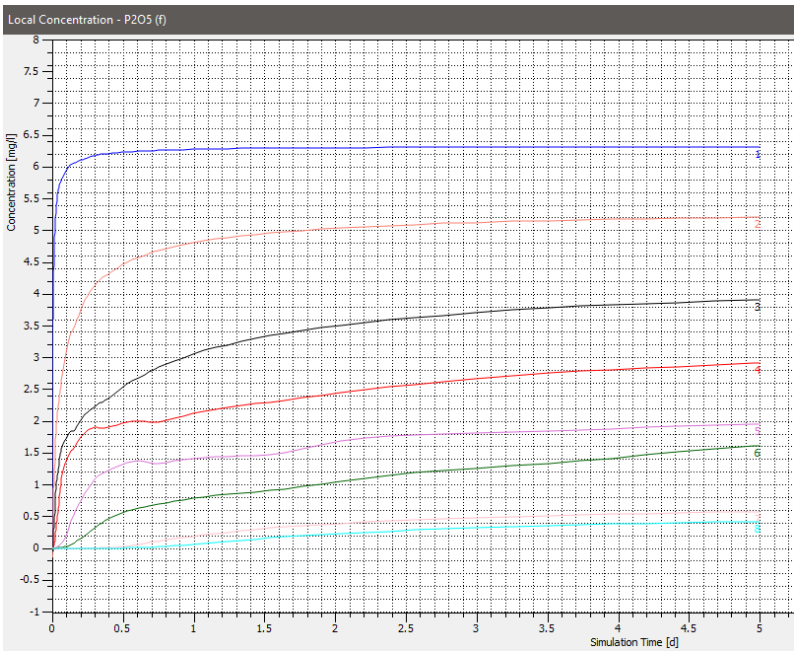

Figure 73. P2O5 concentration and the time simulation of the experiment, in section B.

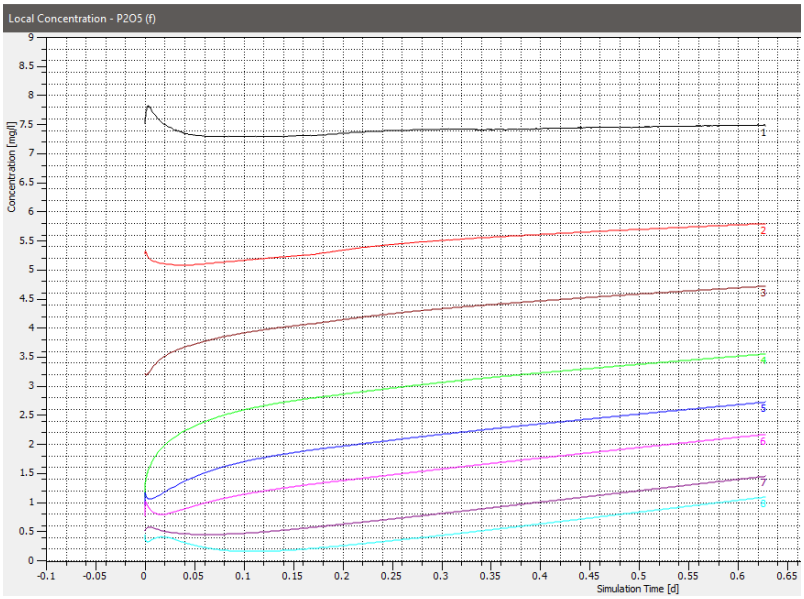

Figure 74 P2O5 concentration and the time simulation of the experiment, in section C.

In section A, B, C as results, presented in the technical report of LNEC (Leitao et al, 2016, Deliverable 12.5), for nitrites, nitrates and ammonia, an increase of concentration was observed immediately in the upper part of the soil, and a decreasing in concentrations right after the experiment stopped.

I.3.6 Recommendations

Soil column experiments in the laboratory gave us good results after caried out different tests. The only issue presented, since these experiments were done in just 30cm of soil, we did not have the opportunity to use smart sensors to obtain more data, especcialy diurnal variations on water parameters. At the infiltration basins, smart sensors were used but I am not sure if the calibration procedure was done precisely, so that pH values would have not presented outliers when the temperature was changing. I would recommend for this research to be used ammonia sensor as well, in order to determine the concentration for a long period of monitoring. In general, the sensors worked well and the system of a sensor node lost data just for 2 weeks in almost 4 months of monitoring. In this research I did not calibrate the input data in the Hydrus and Feflow softwares, so that it is recommended to have a good calibration in order to be sure of results presented. These software were choose to determine the water flow and have an idea about the behavior of the contaminants into the soil.

Chapter 2
II. SMART SENSORS TECHNOLOGY

1. Background and Motivation

A wide range of Smart Sensor Network (SSN) applications have been developed in recent years, in which smart sensor devices are embedded in interconnected devices to sense, monitor, measure, communicate, and exchange information. This enables the collection, processing, analysis, and dissemination of valuable information gathered in various industrial environments. SSN systems offer the ability to perform computations, make intelligent decisions and control industrial equipment to promote the progress of the enterprise or manufacturing unit (Da-Xu L et al, 2014; Echanobe J et al, 2014; Gubbi et al, 2013). Smart sensors must sense, exchange information, transmit useful collected information, and automatically assign roles to manage, deploy, and schedule the behaviors of industrial devices over a network. In an industrial SSN system, different things have different communication functionalities. A gateway must be able to facilitate the communication or interaction of various devices; furthermore, it must connect up to the cloud and down to smart sensors and existing controllers embedded in the network system. Consequently, smart sensors and gateways (Sanislav T et al, 2016; Xia F., 2009) play a crucial role in IoT applications. Perera et al (2014), presented the design of a generalized, low-cost, reconfigurable, and reprogrammable SSN and used a ZigBee with FPGA to develop smart sensor node based on the IEEE1451 family of standards.

Environmental monitoring can be defined as the systematic sampling of air, water, soil, and biota to observe and study the environment, as well as to derive knowledge from this process (Artiola et al., 2004; Wiersma, 2004). Monitoring can be conducted for many purposes, including to establish environmental "baselines, trends, and cumulative effects" (Mitchell, 2002), to test environmental modeling processes, to educate the public about environmental conditions, to inform policy design and decision-making, to ensure compliance with environmental regulations, to assess the effects of anthropogenic influences, or to conduct an inventory of natural resources (Mitchell, 2002). Knowledge-based regulation and benefits of environmental monitoring, as protection of public water supplies weather forecasting, hazardous and non-hazardous and radioactive waste management, natural resources protection and management, global climate change, urban air quality, economic development and land planning, population growth, endangered species and biodiversity. This previous list helps to underscore the importance of monitoring and how its results are ubiquitous in our daily lives (Artiola et al., 2004). Monitoring programs can vary significantly in scope, ranging from community based monitoring on a local scale, to large-scale collaborative global monitoring

programs such as those focused on climate change (Conrad & Daoust, 2008; Lovett et al., 2007). Monitoring need to be conducted under a rigorous application of the scientific method (Artiola et al., 2004) and that it is a "fundamental component of environmental science and policy" (Lovett et al., 2007). There are multiple programs operated by the United Nations that participate in global environmental monitoring activities, such as the World Meteorological Organization (WMO), the Global Atmosphere Watch, and the World Conservation Monitoring Centre (Artiola *et al*., 2004; UNEP, 2011). The WMO, the World Weather Watch, and the World Health Organization collectively manage the Global Environment Monitoring System (GEMS), which is responsible for monitoring and reporting on the "global state of water, air, climate, atmosphere, and food contamination" (Artiola *et al*., 2004). Through the administration of these programs, the United Nations is providing a valuable mechanism for data collection and dissemination on a global scale, making it possible to address global scale issues such as water security and climate change (GEMS, 2011). The sampling of air, water, and soil through environmental monitoring can produce data that can be used to understand the state and composition of the environment and its processes (Artiola et al., 2004; Wiersma, 2004). Despite criticisms that environmental monitoring can be ineffective and costly when programs are poorly planned, well-planned monitoring programs cost little (especially by using the low-cost monitoring system) in comparison to the resources that can be protected and the policy design that can be informed (Lovett *et al*., 2007). Despite the challenges that are faced by environmental monitoring, monitoring remains an important tool in the achievement of major advances in environmental science (Lovett *et al*., 2007).

The most important part of Smart Sensor Network on data transmission is the wireless sensor network. Wireless sensor networks (WSN), C.-Y. Chong et al (2003), are collections of resource constrained sensing and processing devices that have a variety of different successful applications, including environmental monitoring (monitoring of floods, K.S. Chiang Kuang et al (2008) , an active volcano, G. Werner-Allen et al (2006), monitoring of zebra migration, P. Zhang et al (2004), safety and security (monitoring of radioactive materials, F. Ding et al (2009), wildfire A. Somov et al (2011), and buildings E. Jafer et al (2011), assisted living (smart medication system W.-W. Chang et al (2011), control (light control in tunnels L. Mottola et al (2010). Among these, hazardous/combustible gas monitoring, e.g., ethylene A.B.A. Dow et al (2011) and methane V.V. Volkov et al (1997) is particularly promising for WSNs, since it requires capillary sensing capabilities in often difficult or harsh environments, low-maintenance units. There are many reasons why one would like to replace the available wired solutions for gas monitoring in favor of a WSN approach. The principal one is that the major drawbacks of wired monitoring systems are their maintenance cost and their large demandin terms of cables, which constrain the way the system can be deployed. The WSN paradigm, in contrast, enables easy deployment of sensor nodes anywhere they are required and provides high flexibility and easy of maintenance. The use of this technology is possible today

thanks to semiconductor and catalytic sensors with low power consumption on board of a WSN node that can meet the Standard EN 50194 (2000) of gas monitoring and energy aware sensing A. Somov et al (2012) requirements, in terms of accuracy and response time.

2. Methodologies

In this Ph.D. thesis, several prototypes have been proposed for environmental monitoring, which will measure parameters as temperature, humidity, air pressure, gas concentrations present in atmosphere and into the soil, water quality. The data was collected from sensor nodes to Arduino UNO microcontroller and to the Raspberry pi3, ZigBee network and then retransmit the data to smart phones, tabs and PCs using wifi. Sensor node contains analog output sensors.

a. Microcontroller and Sensors

A microcontroller contains all components which allow it to operate standalone, and it has been designed for monitoring and/or control tasks. In consequence, in addition to the processor it includes memory, various interface controllers, one or more timers, an interrupt controller, and last but not least general purpose I/O pins which allow it to directly interface to its environment. Microcontrollers also include bit operations which allow you to change one bit within a byte without touching the other bits [1]. The microcontrollers are integrated into many appliances, like household appliances (microwave, washing machine, coffee machine, telecommunication (mobile phones), automotive industry (fuel injection, ABS), aerospace industry, industrial automation. We need microcontrollers for periodically read the temperature (analog value, is digitized by sensor; uses 4-bit interface), control heating according to the temperature (turn heater on/off; 1 bit), display the current temperature on a simple 3-digit numeric display (8+3 bits), allow the user to adjust temperature thresholds (buttons; 4 bits), and be able to configure/upgrade the system over a serial interface.

The Arduino microcontroller is an easy to use yet powerful single board computer that has gained considerable traction in the hobby and professional market. The Arduino is open-source, which means hardware is reasonably priced and development software is free [2].

The Arduino project was started in Italy to develop low cost hardware for interaction design. The Arduino hardware comes in several flavors. In the United States, Sparkfun (www.sparkfun.com) is a good source for Arduino hardware. With the Arduino board, you can write programs and create interface circuits to read switches and other sensors, and to control motors and lights. The Arduino Uno is a microcontroller board based on the ATmega328 (datasheet). It has 14 digital input/output pins (of which 6 can be used as PWM outputs), 6 analog inputs, a 16 MHz crystal oscillator, a USB connection, a power jack, an ICSP

header, and a reset button. It contains everything needed to support the microcontroller; simply connect it to a computer with a USB cable or power it with a AC-to-DC adapter or battery to get started.

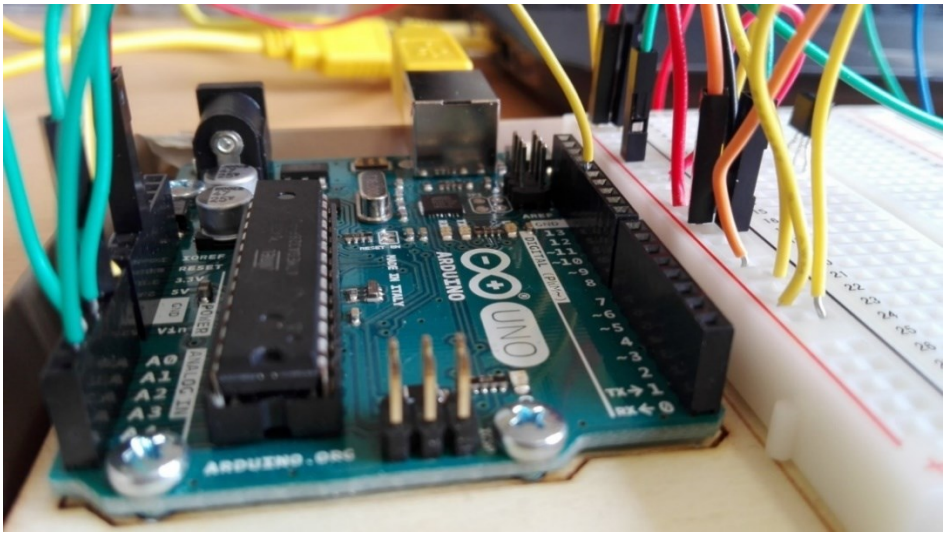

Fig.75 Arduino microcontroller.

The Uno differs from all preceding boards in that it does not use the FTDI USB-to-serial driver chip. Instead, it features the Atmega8U2 programmed as a USB-to-serial converter. "Uno" means one in Italian and is named to mark the upcoming release of Arduino 1.0. The Uno and version 1.0 will be the reference versions of Arduno, moving forward.

The Arduino programming language is a simplified version of C/C++. Programs are created in the Arduino development environment and then downloaded to the Arduino board. Code must be entered in the proper syntax which means using valid command names and a valid grammar for each code line [3].

Based on information in the current technical literature, the committee chose to adopt the following definitions: [4].

- *Sensor element*: The fundamental transduction mechanism (e.g., a material) that converts one form of energy into another. Some sensors may incorporate more than one sensor element (e.g., a compound sensor).
- *Sensor*: A sensor element including its physical packaging and external connections (e.g., electrical or optical).
- *Sensor system*: A sensor and its assorted signal processing hardware (analog or digital) with the processing either in or on the same package or discrete from the sensor itself.

One of the most important advances in sensor technology in the last years has been the focused development of smart sensors, [4]. The definition of "smart" and "intelligent" sensing can be debated. In general, it is difficult to identify any features in a smart sensor that parallel intelligence in natural systems. The basic tenet of smart sensors is that the sensor complexities must be concealed internally and must be transparent

to the host system. Smart sensors are designed to present a simple face to the host structure via a digital interface, such that the complexity is borne by the sensor and not by the central signal processing system. The basic requirement for a smart sensor is that it be a system with dedicated "on-chip" signal processing. Realization of this concept simply means that electronic (or optical) signal processing hardware is dedicated to each sensor and miniaturized to the point that it becomes a part of the sensor package. A smart sensor would include the sensor, interface circuit, signal processing, and power source. The subsystems of a smart sensor include:

- a primary sensing element;
- excitation control;
- amplification (possibly variable gain);
- analog filtering;
- data conversion;
- compensation;
- digital information processing;
- digital communications processing; and
- power supply.

It is clear, however, that the smart-sensing concept creates new opportunities for using novel materials for sensors. The smart-sensing concept makes it possible to avoid the constraint of the paradigm that sensor elements must be linear and noise-free; however, the cost of the added electronics must be considered in the sensor system design analysis.

Potential advantages of the smart-sensor concept include:

- lower maintenance;
- reduced time;
- higher reliability;
- fault tolerant systems;
- adaptability for self-calibration and compensation;
- lower cost;
- lower weight;
- fewer interconnections between multiple sensors and control systems; and
- less complex system architecture.

These advantages of smart sensors are application specific. There is certainly justification for many applications in distributing the signal processing throughout a large sensor system so that each sensor has its own calibration, fault diagnostics, signal processing, and communication, thereby creating a hierarchical system. Innovations in sensor technology have generally allowed a greater number of sensors to be

networked or more-accurate sensors to be developed or on-chip calibration to be included. In general, new technology has contributed to better performance by increasing the efficiency and accuracy of information distribution and reducing overall costs. However, these performance enhancements have been achieved at the expense of increased complexity of individual sensor systems. Currently, the practical utility of smart sensors seems to be limited to applications that require a very large number of sensors. [4].

b. Gas sensors

- TGS 2600 - for the detection of Air Contaminants

The sensing element is comprised of a metal oxide semiconductor layer formed on an alumina substrate of a sensing chip together with an integrated heater. In the presence of a detectable gas, the sensor's conductivity increases depending on the gas concentration in the air. A simple electrical circuit can convert the change in conductivity to an output signal which corresponds to the gas concentration. The TGS 2600 has high sensitivity to low concentrations of gaseous air contaminants such as hydrogen and carbon monoxide which exist in cigarette smoke. The sensor can detect hydrogen at a level of several ppm. Figaro also offers a microprocessor (FIC02667) which contains special software for handling the sensor's signal for appliance control applications.

Due to miniaturization of the sensing chip, TGS 2600 requires a heater current of only 42mA and the device is housed in a standard TO-5 package. The figure to the left side, below represents typical sensitivity characteristics, all data having been gathered at standard test conditions (see reverse side of this sheet). The Y-axis is indicated as sensor resistance ratio (Rs/Ro) which is defined as follows:

Rs = Sensor resistance in displayed gases at various concentrations

Ro = Sensor resistance in fresh air

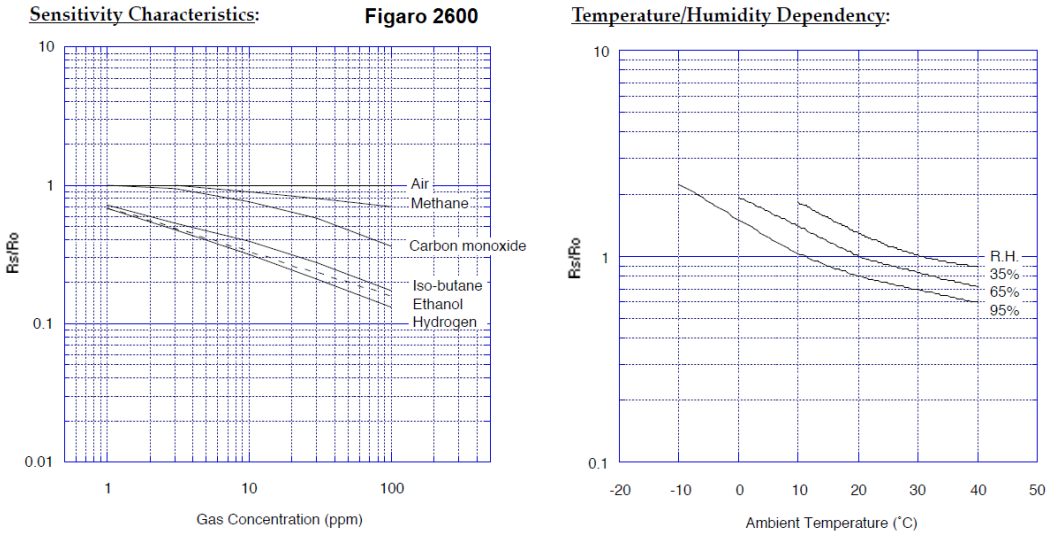

Fig.76 Sensitivity characteristics of Figaro 2600.

The Fig.2 above, to the right side, represents typical temperature and humidity dependency characteristics. Again, the Y-axis is indicated as sensor resistance ratio (Rs/Ro), defined as follows:

Rs = Sensor resistance in fresh air at various temperatures/humidity

Ro = Sensor resistance in fresh air at 20°C and 65% R.H.

The sensor requires two voltage inputs: heater voltage (VH) and circuit voltage (VC). The heater voltage (VH) is applied to the integrated heater to maintain the sensing element at a specific temperature which is optimal for sensing. Circuit voltage (VC) is applied to allow measurement of voltage (Vout) across a load resistor (RL) which is connected in series with the sensor. DC voltage is required for the circuit voltage since the sensor has a polarity. A common power supply circuit can be used for both VC and VH to fulfill the sensor's electrical requirements. The value of the load resistor (RL) should be chosen to optimize the alarm threshold value, keeping power consumption (PS) of the semiconductor below a limit of 15mW. Power consumption (PS) will be highest when the value of Rs is equal to RL on exposure to gas.

Sensor resistance (Rs) is calculated with a measured value of Vout by using the following formula:

RS = ((Vc*RL)/Vout) – RL.

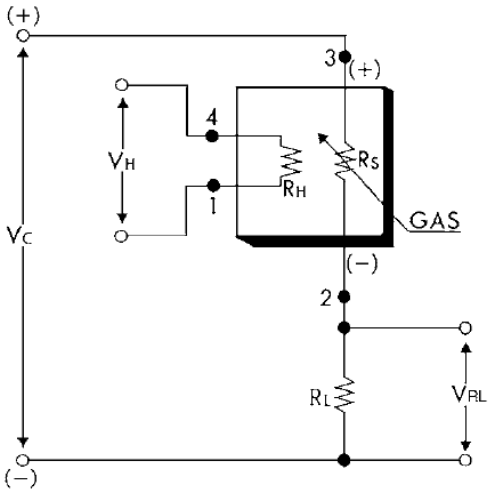

Fig.77 Basic measuring Circuit.

- Carbon Dioxide (CO_2), Module, Model: S-100

S-100 is one of the world's smallest models, of which Persistent stability and Temperature Effect Resistance besides various outputs are much favored by customers in stocks raising, greenhouse, scientific projects, etc. S-100A has Automatic calibration software turned for HVAC customers who want easier monitoring with less management cost, etc. Features like non-Dispersive Infrared (NDIR) technology used to measure CO_2 levels, pre-calibrated, available outputs: Analog Voltage, TTL-UART, I2C, gold-plated sensor

provides long-term calibration stability, installed calibration function, periodic automatic Calibration (ACDL) and non-periodic manual re-calibration(MCDL) are available. Sensing method NDIR (Non-dispersive Infrared), measurement range 0 to 2,000/3,000/5,000/10,000 ppm, 2%, 3% (Optional), accuracy ±30ppm ±5%, response time (90%) 60 seconds, sampling interval 3 seconds.

- MG811 CO2 Sensor

Good sensitivity and selectivity to CO2, low humidity and temperature dependency, long stability and reproducibility. Sensor structure and testing circuit in the Fig.4. It is composed by solid electrolyte layer (1), Gold electrodes (2), Platinum Lead (3), Heater (4), Porcelain Tube (5), 100m double-layer steeless net (6), Nickel and copper plated ring (7), Bakelite (8), Nickel and copper plated pin (9).

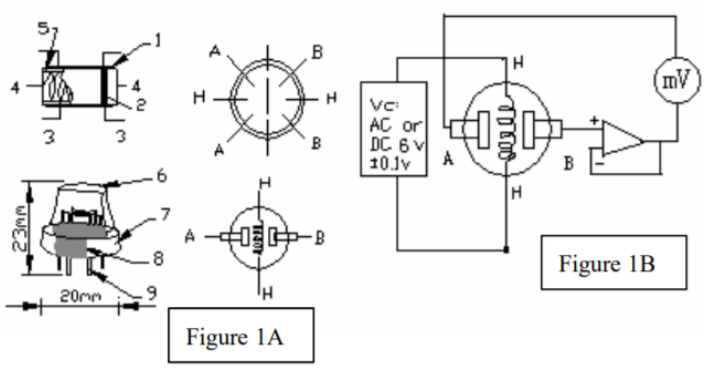

Fig.78 Gas sensors, MG811 CO2 Sensor.

Sensor adopt solid electrolyte cell principle. It is composed by the following solid cells:

Air Au|NASICON|| carbonate|Au, air， CO2.

When the sensor exposed to CO2， the following electrodes reaction occurs：

Cathodic reaction：2Li + + CO2 + 1/2O2 + 2e - = Li2CO3

Anodic reaction：2Na+ + 1/2O2 + 2e- = Na2O

Overall chemical reaction：Li2CO3 + 2Na + = Na2O + 2Li + + CO2

The Electromotive force (EMF) result from the above electrode reaction, accord with according to Nernst's equation:

EMF = Ec - (R x T) / (2F) ln (P(CO2))

P(CO2) - CO2 partial Pressure; Ec - Constant Volume; R - Gas Constant volume; T - Absolute Temperature (K); F - Faraday constant.

Sensor heating voltage supplied from other circuit. When its surface temperature is high enough, the sensor equals to a cell, its two sides would output voltage signal, and its result accord with Nernst's equation. In

sensor testing, the impedance of amplifier should be within 100 - 1000GΩ. Its testing current should be control below 1pA.

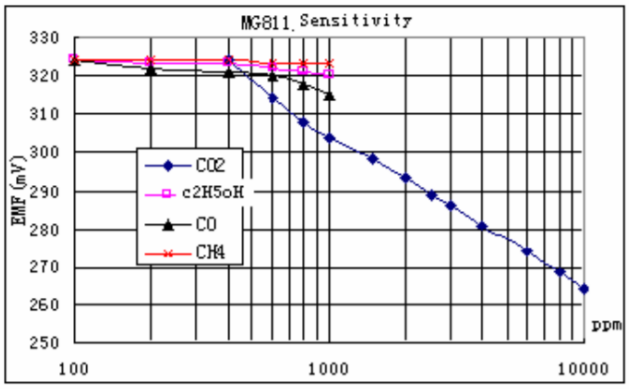

Fig.79 Sensitivity of MG811 CO2 Sensor

Sensitivity in Fig.5 shows gas sensor sensitivity curve. Conditions Temperature 28℃, RH 65%, Oxygen 21%, sensor EMF under different gas and concentration.

- MQ-4 (methane) gas sensors

Sensitive material of MQ-4 gas sensor is SnO2, semiconductor sensor, with lower conductivity in clean air. When the target flammable gas exists, the sensor's conductivity gets higher along with the gas concentration rising. MQ-4 gas sensor has high sensitivity to methane, also has anti-interference to alcohol and other gases. It has good sensitivity to methane in wide range, and has advantages such as long lifespan, low cost and simple drive circuit &etc.

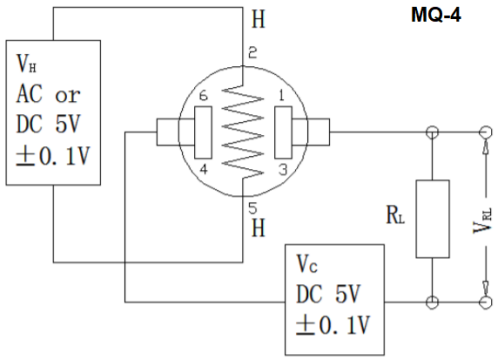

Fig.80 The basic test circuit of MQ-4.

The sensor requires two voltage inputs: heater voltage (VH) and circuit voltage (VC). VH is used to supply standard working temperature to the sensor and it can adopt DC or AC power, while VRL is the voltage of load resistance RL which is in series with sensor. Vc supplies the detect voltage to load resistance RL and it should adopt DC power, Fig.6.

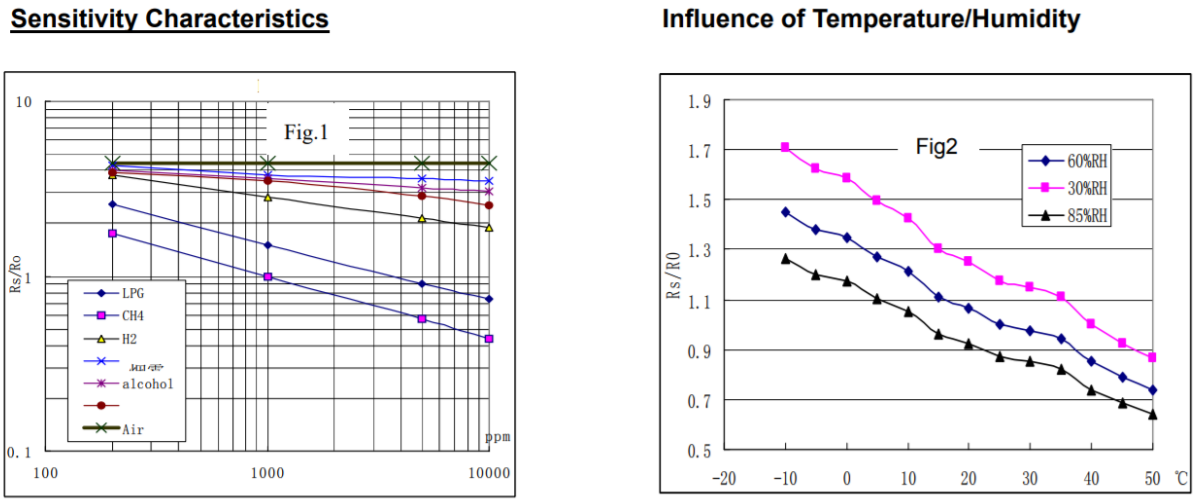

Fig.81 Typical Sensitivity Curve of MQ4.

In the Fig.7, the ordinate is resistance ratio of the sensor (Rs/R0), the abscissa is concentration of gases. Rs means resistance in target gas with different concentration, R0 means resistance of sensor in clean air. Rs means resistance of sensor in 5000ppm methane (CH4) under different tem. and humidity. Rs means resistance of the sensor in 5000ppm methane under 20℃/55%RH.

c. Soil sensors

- Soil moisture

Soil moisture sensor measure the water content in soil. The module uses LM393 comparator to compare the soil moisture level with the preset threshold. When the soil moisture deficit module outputs a high level, and vice versa. The sensor has 3-Pin male header. The pins are as follows VCC (external 3.3V-5V) GND (external GND) and DO-board digital output interface (0 and 1). The pin explanation for each pin is shown below, Fig.8.

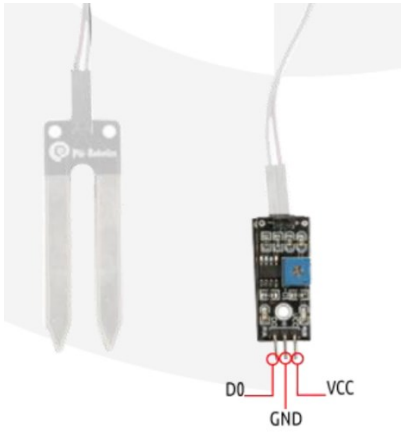

Fig.82 Soil moisture sensor pin layout.

- Soil temperature DS18B20 Digital temperature

The DS18B20 digital thermometer provides 9-bit to 12-bit Celsius temperature measurements and has an alarm function with nonvolatile user programmable upper and lower trigger points. The DS18B20 communicates over a 1-Wire bus that requires only one data line (and ground) for communication with a central microprocessor. It has an operating temperature range of -55°C to +125°C and is accurate to ±0.5°C, over the range of -10°C to +85°C. In addition, the DS18B20 can derive power directly from the data line ("parasite power"), eliminating the need for an external power supply. Each DS18B20 has a unique 64-bit serial code, which allows multiple DS18B20s to function on the same 1-Wire bus.

d. Water sensors

- pH

Sensor type combination electrode, measurement range 0~14pH, temperature of operation: 0~80ºC, zero electric potential: 7±0.25p, response time: <1min. internal resistance: ≤250MΩ. repeatability: 0.017, reader accuracy up to 0.01 (in function of calibration), cable length: < 300 cm. The pH sensor integrated in the Smart Water board is a combination electrode that provides a voltage proportional to the pH of the solution, corresponding the pH 7 with the voltage reference of 2.048V of the circuit, with an uncertainty of ±0.25pH. To get an accurate value from these sensors it is necessary both to carry out a calibration and to compensate the output of the sensor for the temperature variation from that of the calibration moment.

- temperature

Specifications measurement range 0 ~ 100ºC, accuracy: DIN EN 6075, resistance (0ºC) 1000Ω, diameter: 6mm, length: 40mm, cable: 2mm, cable lenght: < 150mm. Measurement process, the PT1000 is a resistive sensor whose conductivity varies in function of the temperature. The temperature sensor is directly powered from the 5 V supply, so is no necessary to switch the sensor ON, but it is advisable to not keep the Smart Water board powered for extended periods and switch it OFF once the measurement process has finished. No calibration is needed.

- electrical conductivity

Sensor type two electrodes sensor, electrode material platinum, conductivity cell constant: 1 ± 0.2 cm-1, cable length: < 500 cm. The conductivity sensor is a two-pole cell whose resistance varies in function of the conductivity of the liquid it is immersed in. That conductivity will be proportional to the conductance of the sensor (the inverse of its resistance), multiplied by the constant cell, in the case of the Libelium sensor

around 1cm-1, leading to a value in Siemens per centimeter (S/cm). To power the conductivity sensor an alternating current circuit has been installed in order to avoid the polarization of the platinum electrodes.

- oxidation reduction potential

Sensor type combination electrode, electric potential: 245~270mV, measurement range 0 ~ ±1999mV, reference impedance: 10kΩ, stability: ±8mV/24h, cable length: < 300 cm. Like the pH sensor, the ORP probe is a combination electrode whose output voltage is equivalent to the potential of the solution. The output of the circuitry to which it is connected is directly read from the analog-to-digital converter of the Smart Water sensor board, being the 2.048V reference subtracted to obtain the actual oxidation-reduction potential in volts (in this case, since this parameter is directly a voltage it is not necessary to call a conversion function).

e. Meteorological sensors

- Barometric pressure

GY-65 BMP085 Barometric digital pressure sensor module board for Arduino is a high precision, ultra-low power consumption pressure sensors. The absolute accuracy of the minimum can reach 0.03hPa, only 3uA low power consumption and the pressure range is 300 - 1100hPa.

- Air temperature/humidity

The DHT11 is a relatively cheap sensor for measuring temperature and humidity, with a calibrated digital signal output. This sensor includes a resistive-type humidity measurement component and connects to a high performance 8-bit microcontroller, offering excellent quality, fast response, anti-interference ability and cost-effectiveness. Its small size, low power consumption and up-to-20-meter signal transmission.

1. Laboratory Calibration

1.1 Gas sensors

The gas sensor is typically calibrated by the manufacturing company and is accompanied by the technical documentation, datasheet, which provides the calibration values. In this case a user should program these values into the memory of the sensor node or microcontroller. Nevertheless, the sensor degrades with time and requires periodical calibration. Calibration consists in measuring the output response voltage for a defined and known methane concentration in the environment and recording the obtained values in the memory of the sensor node. To perform the sensor calibration using the wireless channel we must first wake up the sensor node and set it in calibration mode by a command within 20 s after it is awoken. As soon as the sensor node is in calibration mode, the user can remotely adjust the thresholds for gas detection as well as set other parameters such as the address of the device and the measurement time. To set up the gas detection thresholds we identify two points in the sensor characteristics the sensor response in the air, the sensor response at the gas concentration in the atmosphere. For most of the gas sensors the dependency of the sensor response to concentration in the atmosphere is almost linear. Therefore, the sensor response at the concentration knew in the atmosphere, which we need to set one of the thresholds, is calculated automatically. It is essential to achieve a stable sensor response during the calibration.
Further information about the gas sensors calibraton are in the articles submitted.

1.2 Water sensors calibration

- pH sensor

A periodic calibration is highly recommended for the pH sensors if an accurate measurement is desired. If the sensor is going to be deployed in an environmental with a changing temperature or the calibration is going to be carried out under a different temperature from the operation conditions, it will also be required a temperature compensation to update the sensitivity of the sensor to the actual conditions. The required material for the pH sensor calibration consists of three pH buffer solutions, one of 7.0pH and two of higher and lower values (4.0pH and 10.0pH). It is recommended that the solutions are at the temperature that will be found at the installation environment. Make sure the sensors are completely immersed in the solution. When there is a stable output for the sensors, annotate the value in volts obtained.

- Electrical conductivity (EC)

There are three different Calibration kits for electrical conductivity probe K=0.1, K=1; K=10. The K factor is related to the salinity of the water we want to measure. Each calibration kit takes two solutions: K=0.1 around µS 220 - around µS 3000; K=1 around µS 10500 - around µS 40000; K=10 around µS 62000 -

around µS 90000. We have as the relation between conductivity and dissolved solids is approximately: 2 µS/cm = 1 ppm (which is the same as 1 mg/l). In order to get an accurate measurement, it is recommended to calibrate the conductivity sensor to obtain a precise value of the cell constant. Although a single point calibration should be theoretically enough, a two-point calibration is advisable to compensate for side effects of the circuitry, such as the resistance of the sensor wire or the connector. For a proper calibration two solutions of a conductivity as close as possible to that of the target environment should be used.

- Oxidation reduction potential probe sensor (ORP)

The calibration process will consist in a verification of the proper operation of the sensor with an ORP calibration standard solution, which will lead to the application of a correction offset in the code or in the data processing in the receiver. Libelium provides a standard solution of 225mV at 25ºC. Introduce the sensor into the calibration solution and wait for the output value to stabilize. If the test is being carried out with the solution provided by Libelium at approximately 25ºC, the output should be around the 225mV, with a 10%~15% error.

Chapter 3

III. ENVIRONMENTAL MONITORING APPLICATIONS

PEER REVIEWED PUBLICATIONS

III.1.1 Methane Gas Storage Site in Minerbio (BO), Italy

IEEE XPLORE DIGITAL LIBRARY

978-1-5090-4951-6/17 ©2017 IEEE IGARSS 2017 5954 - 5957

DESIGN OF A SMART GAS DETECTION SYSTEM IN AREAS OF NATURAL GAS STORAGE

Ana M. C. Ilie, Carmela Vaccaro

University of Ferrara, Earth Sciences Department, Italy

Abstract

This paper focus on the development of a new device suitable to detect and measure methane gas in areas of natural gas storage site. This device, the Smart Gas Detection system, can measure the air and water quality, including all the parameters that can have outliers by an eventual gas leak in the aquifer or atmosphere. The air quality parameters measured by low cost sensors, include CH_4 and CO_2 gas, while for water quality parameters measured include temperature, pH and electrical conductivity. The sensor node is based on Arduino UNO microcontroller, receiving the data from the sensors and transmitting to the database on Raspberry pi 3, remotely accessing all the data. It is extremely important to develop devices with the new commercial low-cost sensors to detect and measure gases in atmosphere for monitoring the carbon dioxide and methane due to their role as greenhouse gases and also gas leaks from wellbores can severely affect the health of people and animals too.

Index Terms— carbon dioxide gas sensor, methane gas sensor, microcontroller Arduino, pH sensor, EC sensor, raspberry pi 3, real time monitoring.

1. INTRODUCTION

Greenhouse monitoring system is important to ensure the stabilization of the environment [1]. Greenhouse monitoring system can also be web-based system (remote system) [2] to allow user access, control and monitor of greenhouse laboratory using Internet connection. [2]. Current climate trends augur for considerable increases in atmospheric methane abundance from anthropogenic sources, such as fossil fuel production, and natural sources such as the release of gas sequestered in and below permafrost due to warming trends [3-4]. Although carbon dioxide is significantly more abundant than methane and has a considerably longer atmospheric residence time, the relative potency of methane as a greenhouse agent is

approximately 100 times that of carbon dioxide on decadal timescales [5]. Because of its short lifetime, and the current dominance of anthropogenic sources, methane has greater potential return on investment for regulatory efforts to mitigate greenhouse warming [6]. The use of inexpensive sensor networks and embedded systems are quickly emerging as a key player in the monitoring of local and regional air quality as lower cost monitoring equipment enables new spatial resolution of pollutants [7-8].

2. ARCHITECTURE

The system architecture is based on an Arduino Uno microcontroller-board, programmed in a simple integrated development environment (IDE). The Arduino project development environment, or integrated development environment (IDE) is a free download for Windows system [9]. The microcontroller receives the signal from sensors, save the data on a SD card and transmit the data to the Raspberry pi 3.

2.1. Microcontrollers

Arduino is open-source electronics prototyping platform based on flexible, easy-to-use hardware and software [9]. The heart of the Arduino is a microcontroller board based on the ATmega328. The memory based on ATmega328 has 32 KB (with 0.5 KB used for the bootloader). It also has 2 KB of SRAM and 1 KB of EEPROM (which can be read and written with the EEPROM library). Arduino hardware is programmed using a Wiring-based language (syntax and libraries), similar to C++ with some slight simplifications and modifications, and a Processing-based integrated development environment. This allows the broad to communicate with computer through programming. It receives the input signals from the sensors, and then produces output voltages that are translated into numbers shown by the digital display [9].

The Raspberry pi 3 has a 1.2GHz 64-bit quad-core ARMv8 CPU, 802.11n Wireless LAN, Bluetooth 4.1, Bluetooth Low Energy (BLE), 1GB RAM, 4 USB ports, 40 GPIO pins, full HDMI port, Ethernet port, combined 3.5mm audio jack and composite video, camera interface (CSI), display interface (DSI), Micro SD card (32GB), video Core IV 3D graphics core [10]. The Raspberry pi 3 is used in this project to store the data on MySQL database and check data out through the web server that present web pages to the other computers.

2.2. Arduino-based datalogger

A "datalogger" is defined as a device which will operate independently to store analog data in digital form. The datalogger application may also include programming to do some internal data processing of input, such as averaging multiple values collected over a specified time interval. In general, such a project requires four components microcontroller, analog-to-digital (ADC) converter, clock, data storage device (an SD card). The datalogger shield includes a real-time clock, an essential component of a system for logging data. The coin cell battery will last for several years, so it is simply left in place once installed. Communications with the clock are handled through the widely used "Inter-Integrated Circuit" (I2C) protocol, which allows various devices to communicate with each other [11].

2.3. Arduino Sensor shield

An easy way to connect many input devices and output devices to Arduino, not just sensors, which is called Sensor shield. The Sensor Shield's purpose is make it easy to connect cables and devices to the correct Arduino pins. It is a passive circuit board that simply connects the Arduino pins to many connectors [12].

3. LOW-COST SENSORS

3.1. MQ-4 gas sensor

This sensor is an electrochemical sensor, it has a high sensitivity to CH4, natural gas, small sensitivity to alcohol, smoke, fast response, stable and long life, simple drive circuit. The sensor's output is an analog resistance. Structure and configuration of MQ-4 gas sensor, is composed

of micro AL2O3 ceramic tube, Tin di-oxide (SnO2) sensitive layer, measuring electrode and heater are fixed into a crust made by plastic and stainless steel net. The heater provides necessary work conditions for work of sensitive components. The MQ-4 can detect natural gas concentrations anywhere from 200 to 10000ppm.The Gas Sensor Module is designed to allow a microcontroller to determine when a preset gas level has been reached or exceeded. Interfacing with this sensor is done through a 4-pin SIP header and requires two I/O pins from the host microcontroller [13].

3.2. MG-811 Gas Sensor

This sensor is a metal oxide sensor, which output voltage of the module falls as the concentration of the CO2 increases. The potentiometer onboard is designed to set the threshold of voltage. It has MG-811 sensor module onboard which is highly sensitive to CO2 and less sensitive to alcohol and CO, low humidity & temperature dependency. MG-811 Metal Oxide sensor module manufactured by Sandbox electronics. Onboard heating circuit brings the best temperature for sensor to function. Internal power boosting to 6V for heating sensor best performance [14].

3.3. Analog pH Meter and EC probe Sensors

This industrial pH electrode is made of sensitive glass membrane with low impedance, with fast response and excellent thermal stability. In 0 pH to 14 pH range, the output voltage is linear. The reference system which consist of the Ag/AgCl gel electrolyte salt bridge has a stable half-cell potential and excellent anti-pollution performance. An electrical conductivity (EC) probe sensor meter measures the concentration all soluble salts dissolved in a solution. The passage of an electric current through a solution is measured via the probe with two metal prongs one centimeter apart. Electrical conductivity is measured in millisiemens per centimeter (mS/cm) [15].

3.4. Temperature Sensor

The DHT11 is a relatively cheap sensor for measuring temperature and humidity, with a calibrated digital signal output. This sensor includes a resistive-type humidity measurement component and connects to a high performance 8-bit microcontroller, offering excellent quality, fast response, anti-interference ability and cost-effectiveness. Its small size, low power consumption and up-to-20-meter signal transmission making it the best choice for various applications [16].

3.5. Barometric digital pressure sensor

GY-65 BMP085 Barometric digital pressure sensor module board for Arduino is a high precision, ultra-low power consumption pressure sensors. The absolute accuracy of the minimum can reach 0.03hPa, only 3uA low power consumption and the pressure range is 300 - 1100hPa [17]. The prototype design is shown in the Fig.1 with all the sensors used in this monitoring system.

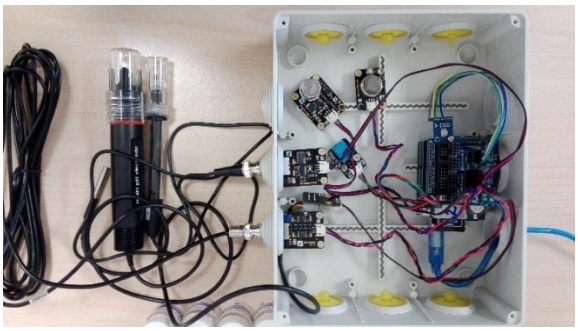

Fig.1 Prototype design monitoring system.

3. Design of the Smart Gas Detection System

This device system, Smart gas detection, as shown in Fig.2, is organized in 3 units the microcontroller board Arduino UNO, the expansion boards with data logging shield and the sensors shield, including the sensors to detect methane and carbon dioxide gas, temperature, humidity and air pressure with the pH and EC probes.

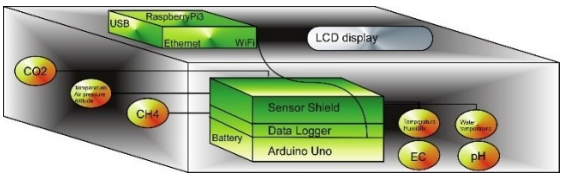

Fig.2 Smart gas detection device.

The prototype put on a waterproof box IP55 allows it to be placed anywhere outdoor. The mechanical dimensions of this box are 240 mm height x 190 mm width x 90 mm thickness, easy to be used in any environment conditions and in any place.

4.1. Gas Sensors Calibration

All sensors must be configured with some parameters before starting the measurements process. The MQ-4 uses the circuit stages, based in voltage divider, which consists in two resistors. One of this resistor, is the sensor resistance (RS), and the other is the load resistance (RL). The RS, changes depending on the concentration of the gas, and the RL resistance can be configured by a digital potentiometer. The value of the RL sensor is minimum 0.45kΩ to 100K, [13]. Once the voltage is measured by the analog-digital converter, the RS can be calculated using the simple formula, Rs=((Vc*RL)/Vout)-RL, where VC its power, Vout is the output voltage measurement, RL the load resistance which has been defined. The RO is the value of the sensor resistance at a known concentration without the presence of other gases or in fresh air [18]. This value must be measured and stored to calculate the concentration of the gas. It was measured the RO resistance at 100 ppm CH4 in the fresh air. Once the Ro resistance is obtained, is necessary to obtain some values to generate an approximation of the response of the sensors. At least is necessary 3 points of calibration with the concentration knew. Once the Rs is calculated for the three points, then is calculated the relation between Rs and Ro (Rs/Ro) of each point, Point1 = Rs(100ppm) / Ro; Point2 = Rs(1000ppm) / Ro; Point3 = Rs(10000ppm) / Ro. These points are the values introduced in the calibration code to obtain the logarithmic approximation and by using a function to obtain directly the conversion from sensor resistance in kilo ohms in ppm. The CO2 don't need a load resistance and the measurement and calibration process is different. The CO2 sensor returns a voltage value, and this value is used to calculate the concentration.

4.2. Analog pH meter and EC probes Calibration

The pH and ORP probe were immersed in reference solutions and the probe readings were assigned to specific variables in the embedded program, where raw electrode voltage values were transformed into values, expressed in proper units (e.g. µS/cm for conductivity) [15]. The conductivity calibration kit includes two reference solutions with nominal values 60µS/cm and 1400µS/cm. The reference solutions are fitting for drinking water values. There are three reference solutions for the pH probe which have nominals values of 4 pH, 7 pH and 10 pH. A periodic recalibration of the sensors is highly advisable in order to maintain an accurate measurement along time, allowing correcting changes owed to a drift output, polarization or wear [18].

4.2. Web Server and PHP

The web server was set up to explore the data collected in the MySQL database, an IP address was fixed for the Raspberry Pi , and it will be browsing within the network. At the same time was set up the database administration tool phpMyAdmin, free software written in PHP to carry out administration of a MySQL database. Thus one insert the IP address/phpmyadmin on the browser it start up the phpMyAdmin interface, as shown in Fig.3. To access to the database remotely occurs by referencing the host computer that the database is on (IP address).

Next step was to connect the Raspberry Pi with Dropbox. We did it through the Dropbox API. After created a new directory on Raspberry it was created the python script that have different functions for uploading files to Dropbox (all the data from the sensors).

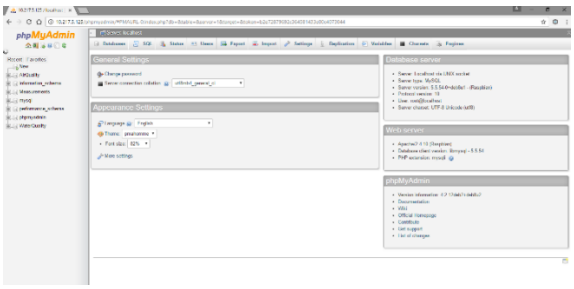

Fig. 3. PHP web interface.

5. RESULTS AND DISCUSSION

In order to have a preliminary study, it was performed a field experiment of this device that can automatically detect gas concentrations and determine the water quality parameter as pH and EC. The device has been tested into a private well, close to the natural gas storage, and it was tested from 09/19/2016 to 10/10/2016, with no outliers identified, as shown in the Fig.4.

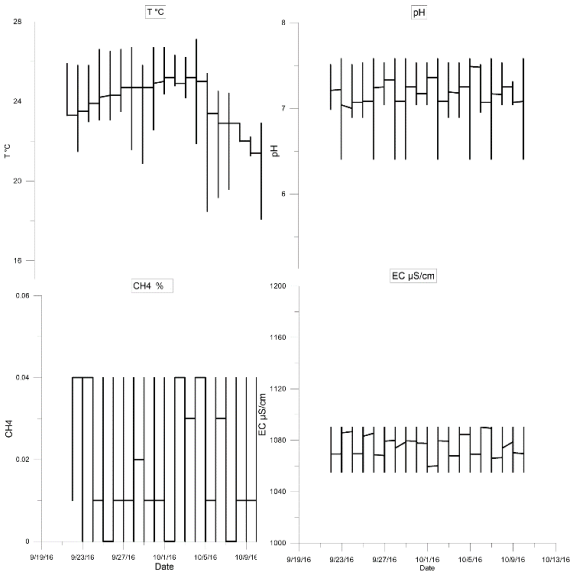

Fig.4 Parameters measured T °C, CH4, pH, EC µS/cm.

The CO2 concentrations were less than 400 ppm, in accordance with the output value of the MG-811 gas sensor. The CH4 concentrations were in the range from 0 ppm to 400 ppm. The pH probe presented values from 6.5 pH to 7.5 pH, and EC probe values from 1050 µS/cm to 1085 µS/cm. Thus, no outliers were detected. We configured, programmed and implemented this Smart gas detection system, to have an idea about the state of the air and of the aquifer. This device is a low-cost monitoring system, as shown in fig.2, a low-power sensor node and WiFi connection by using the phpMyAdmin web interface one can see all the information or by connecting to the drobox. Even if the WiFi is not working, all the data will be stored on the database and in the SD card, no data will be lost. Thus, eventually leaks can be detected and measured. Even though measurements obtained from these low-cost sensors are not so accurate, they can still provide useful information of water and air quality close to oil and gas industry. Nowadays there are many natural gas storage sites, and it is important to develop devices that allow to measure the air and water quality in real time, close to the gas industry. One has to be sure there are not gas leaks, having a high impact on the environment and on health of the people. Since the wellbore actually are so close to the house people, would be important to monitor with many devices in many places and understand the distribution of all of the gases in atmosphere and the distribution of all the water parameter in the aquifer, at different depth levels. These systems can also be used in ex oil extraction areas to identify the location of the abandoned wells very dangerous for urbanization.

ACKNOWLEDGEMENTS

We thank Dott. Paolo Chiarelli electronic technician and Dott. Francesco Droghetti for their support on this research.

6. REFERENCES

[1] R. Gao, “2011 International Conference on Electronics and Optoelectronics (ICEOE 2011) A Wireless Sensor Network Environment Monitoring System Based on TinyOS,” *Electronics*, no. Iceoe, pp. 497-501, 2011.

[2] I. Matijevics, “Wireless Sensors Networks – Theory and Practice,” pp. 405-417, 2009.

[3] Henriet, J. -P., & Mienert, J. (Eds.). (1998). Gas Hydrates: Relevance to World Margin Stability and Climate Change (pp. 137). Geological Society of London Special Publication.

[4] Zhuang, Q., Melillo, J. M.,McGuire, A.D., Kicklighter, D.W., Prinn, R. G., Steudler, P. A., et al. (2007). Net emissions of CH4 and CO2 in Alaska: Implications for the region's greenhouse gas budget. Ecological Applications, 17(1), 203–212.

[5] Solomon, S., Qin, D., Manning, M., Chen, Z., Marquis, M., & Averyt, K. B., et al. (Eds.). (2007). Climate Change 2007: The Physical Science Basis. Contribution of Working Group I to the Fourth Assessment Report of the Intergovernmental Panel on Climate Change. New York: Cambridge Univ. Press

[6] Shindell, D., et al. (2012). Simultaneously mitigating near-term climate change and improving human health and food security. Science, 335(6065), 183–189.

[7] J. Li, B. Faltings, O. Saukh, D. Hasenfratz, J. Beutel, Sensing the air we breathe – the OpenSense Zurich dataset, in: Proceedings of the 26th AAAI on Artificial Intelligence, 2012, pp. 2–4.

[8] V. Jelicic, S. Member, M. Magno, D. Brunelli, G. Paci, L. Benini, Context-adaptive multimodal wireless sensor network for energy-efficient gas monitoring, IEEE Sens. J. 13 (2013) 328–338.

[9] http://www.arduino.it

[10] https://www.raspberrypi.org

[11] https://www.adafruit.com

[12]http://www.epanorama.net/newepa/2016/02/20/arduino sensors-interfacing/

[13] https://www.sparkfun.com/products/9404

[14]http://www.robotdomestici.it/joomla/component/virtuemart/robotica-domotica/sensori/sensori-generici/co2-sensor-arduino-compatible

[15] http://www.robot-domestici.it

[16] www.droboticsonline.com

[17] https://www.sparkfun.com/tutorials/253

[18] https://www.libelium.com

ENVIRONMENTAL MONITORING AND ASSESSMENT JOURNAL, SPRINGER

(submitted)

The Concentration of Methane in Atmosphere and at Different Depths into the Soil surrounding Natural Gas Storage Site

Ana Maria Carmen Ilie , Carmela Vaccaro

University of Ferrara, Earth Sciences Department, Ferrara, Italy

Abstract

Cities are major contributors to greenhouse gas emissions due to high density of urbanization, numerous industrial centers, concentrated breeding of chickens, pigs and intensive agricultural activity. These anthropic GHG sources overlap to the endogenous sources of methane related to peat degradation hosted in the test site, Pliocene and Holocene sediments or to dispersion from buried methane deposits that characterize the outermost, NE-verging fronts of the Northern Apennines. Demonstrative activities were carried out in an area with high density of abandoned wells used before 1962 for the extraction of methane, whose emission contributions are currently unknown. Air quality monitoring and soil gas monitoring system for methane and radon gas, at 10cm and 1m depth was the main purpose of this paper. Measurements have been taken for radon concentrations with an Durridge RAD7 Company, Inc., USA, instrument. It was used for atmosphere and soil gas monitoring system three Biogas ETG (Etg Risorse e Tecnologia, Italy) instruments, with nondispersive infrared sensor (NDIR) CH_4 gas sensor. The measurements started in March 2016 and continued in July-August-September 2016, to determine methane and radon gas concentrations, their distribution and to understand the relationship among gases and atmospheric conditions. What distinguishes this study from those conducted at other gas storage site is the methodology used, the monitoring system was done in the same time in atmosphere and at different depths into the soil (10 cm and 1m depth) to understand the differences of methane gas concentration between atmosphere and soil.

***Keywords*—** greenhouse gas, methane, radon, soil gas monitoring system

INTRODUCTION

Gas migration through wellbore failure, from abandoned wells, is repeatedly identified as the highest risk mechanism (Bachu et al, 2009; Benson et al, 2006). The relative importance of monitoring for wellbore

failure is highlighted by experiences in the natural gas storage industry (Conley et al, 2016; IPCC, 2007), including the recent wellbore blow-out and sustained CH_4 venting of the Aliso Canyon underground gas storage facility in California (Conley et al, 2016). In (Perry, K.F., 2015) review of 600 natural gas storage facilities operating over 90 years it was found that, of ten recorded gas migration incidents, five were associated with well-bore failure, with the rest attributed to poor reservoir selection and cap rock issues. Methane is a greenhouse gas (GHG) and its oxidation produces ozone (O_3) that degrades air quality and adversely impacts human health, agricultural yields, and ecosystem productivity (Mary et al, 2014). Therefore, it is important to understand methane emission sources so that appropriate mitigation strategies can be developed and implemented (Mary et al, 2014). Methane (CH_4) is radiatively important trace gas that is currently increasing in their atmospheric concentration at relative rates of 0.6 and 0.5% year_1 respectively (IPCC, 2007). Increased anthropogenic activity is generally given as the reason for this increase. For methane, the recent growth could be due to a decrease in concentration of the hydroxyl radical which is the largest CH_4 sink or an increase in CH_4 emission rate (Rigby et al, 2008). Methane is 25 times greater relative to the global warming potential of CO_2 for a 100-year time horizon (Rigby et al, 2008; Forster et al, 2007). Most studies have shown greater CH_4 emissions under high CO_2 (Inubushi et al, 2003; Cheng et al, 2006; Lou et al, 2006) and elevated temperature (Inubushi et al, 1984; Ziska et al, 1998; Allen et al, 2003). A temperature rise stimulates microbial activity in submerged soils, which may lead to higher rate of CH_4 production Fey et al, 2000). Increased soil moisture under elevated CO_2 reduces the rate of diffusion and therefore decreases CH_4 oxidation in the soil (Ambus et al, 1999; Phillips et al, 2001a). However, if the rising temperature due to the global climate change makes the soil drier, CH_4 oxidation may be enhanced (Dijkstra et al, 2010). Most experimental designs till date have studied the impact of single climate variable (e.g. increased temperature) on CH_4 cycling. However, for a more accurate explanation it is essential to investigate microbial responses in multi-factorial experimental designs in which several interacting climatic variables could be studied (Singh, 2010). Among the sub-terrestrial gases, helium (He), radon (Rn) and carbon dioxide (CO_2) are the most reliable geochemical signals for fluid circulation, particularly as fault tracers. Since faults and fractures can act as preferential fluid-flow pathways, their locations may be assessed by detecting gases on the surface which use such discontinuities to move upward. The soil-gas method seems to provide good information on gas-bearing faults, even in basins filled with clayey sediments where the mapping of tectonic discontinuities by direct methods is made difficult by the homogeneity and plastic behavior of the clayey cover (Lombardi et al, 1993; Lombardi et al, 1996; Etiope et al, 1995). In this project, it was monitored the Rn with CH_4. ^{222}Rn is a radioactive gas that is produced by the decay of radium (^{226}Ra) within the uranium (^{238}U) decay series. Typical soil air Rn values in Italian sedimentary basins (up to 15 Bq=l; Lombardi et al, 1996) are related to the content of parent radionuclides in the surface rocks (with 1–2 ppm of U). However, some surface radon anomalies can be related to the upward migration of gas along fault zones (Abdoh et al, 1989). The short half-life of ^{222}Rn

(3.85 days) limits its migration distance in the subsoil, and thus, radon measured in the soil air cannot be produced at great depth unless it is lifted upward by a relatively fast-flowing carrier gas, such as CO_2, CH_4, or N_2 (Wilkening et al, 1980; Durrance et al, 1990). Three main factors are known which predispose elevated radon levels. First, the regional and local geochemical and geological characteristics of the soil/rock will establish the in-situ conditions. For example, uranium (^{238}U, ^{235}Th) and radium (^{226}Ra) content will control the amount of radon generated. Uranium and radium occur in all rocks at concentrations from 0.5 to 5 mg/kg, depending on the rock type. Igneous and metamorphic rocks (granites, acid lavas, tuffs, etc.) typically have very high uranium/radium contents and sedimentary rocks generally have lower contents (but high in some types like organic rich rocks, phosphates, reworked igneous or magmatic clastic rocks, etc.) (Drolet et Gregory, 1990). The pre-glacial sediments of the Po plain are rich in uranium, while the post-glacial are poor because the main alpine rivers flow into the large glacial lakes that are anoxic environments where the uranium becomes not soluble for the reduction from hexavalent to tetravalent so it can be trapped in the sediment of the lakes. Second, environmental conditions will control the rate of movement of soil radon toward the surface. The escape of radon atoms at the grain scale is controlled by porosity, water content and grain-size, whereas migration toward the shallow environment is controlled by large scale geological features like rock thickness, permeability, fractures and karst (Castelluccio et al, 2012; Nazaroff, W.W., 1992; Etiope and Martinelli, 2002; Nazaroff et al, 1988; Tanner, A.B., 1980). Meteorological parameters like wind, barometric pressure, relative humidity and rainfall can also affect radon exhalation from the soil to the atmosphere (Piersanti et al, 2015; Szabo et al, 2013; Vasilyev and Zhukovsky, 2013; Zafrir et al, 2012; Baykut et al, 2010; Crockett et al, 2010; Fujiyoshi et al, 2006; Al-Shereideh et al, 2006; Winkler et al, 2001).

Abandoned oil and gas wells provide a potential pathway for subsurface migration and emissions to the atmosphere of methane and other fluids (Nordbotten et al, 2009). Paths of potential methane leakage include point and line sources such as boreholes and faults, area sources caused by diffusion or permeation across the sealing rock formation, or a combination of both (Celia and Bachu, 2003). The risk of leakage from boreholes and faults is of concern as they could provide conduits from the target formation directly or indirectly to the surface (Celia and Bachu, 2003; Bradshaw et al, 2004). Air quality has a tremendous effect on public health and the environment (Künzli et al, 2000). One of the primary tools for assessing air-pollution patterns is continuous monitoring of pollutants' ambient levels. To accomplish that, numerous chemical-physical methods have been developed and standardized Air Quality Monitoring (AQM) station networks have been spread around the world. Air quality and the vadose zone was subject to monitoring system close to the wellbores in Minerbio, nearby methane gas storage site. Measurements taken of the near surface vadose zone are ideal for multiple reasons. Firstly, the vadose zone is quick and easy to sample, as it represents the bounding zone between sub surface storage and the atmosphere (Romanak et al, 2012).

Geology of the experimental site

Minerbio Methane Gas Storage Site

The Minerbio field, discovered in July 1956, lies under the Minerbio village, around 25 Km from Bologna and it is the most important underground gas storage in Italy and Europe. The hydrocarbon bearing zone (seven pools) was discovered in the middle-upper Pliocene sediments at a depth of around 1300 meters, (G. Cau, 1978). The filling of the Pliocene-Pleistocene Apennine foredeep has been estimated to exceed 7,000 meters in the thickest depocenters (Pieri and Groppi, 1981). The main pool, which was conventionally called "C", afterwards used for storage, contained practically all the original reserves. The reservoir is 6 Km x 2 Km; the main axis is in a NW – SE direction. The reservoir has an edge aquifer; the original gas water contact was at 1368 mt below sea level. The maximum thickness of the hydrocarbon bearing reservoir was around 180 mt. The cap rock consists of a shale bank, more than 100 meters thick. The porosity and water saturation are 30% and 20% respectively; permeability is in the range of 60 – 300 Md. Production started in March 1959 and continued until 1972. In the production period around 12.8 billion cubic meters were produced, equal to 90% of the original gas in place. The static pressure declined from the original 153.0 Kg/cmq to 30 Kg/cmq, (G. Cau, 1978). The water table rose to 1260 meters. Gas injection started in April 1975; only three of sixteen existing wells were utilized. The stage of primary production of the field lasted until 1971, with the drilling of 36 wells, including 24 productions. Subsequently, in 1975, four levels, of which the most important are the ones called C1 and C2, were interested in converting storage activities, which currently employs 51 injection / supply wells arranged in clusters and 6 light-wells for monitoring reservoir pressures; all other wells drilled in the primary production were closed. In the field, there is a lateral aquifer of medium intensity which led to an important entrance of water during the primary production period. The ingress of water has continued even during the period of closure of the camp, attenuated gradually until it reaches zero by the middle of 1981, being charged. The entry of water into the reservoir led to a considerable irreversible reduction in the usable volume for storage, equal to approximately 55% of the pore volume occupied by gas in the original conditions. During the storage phase, no major movements of the face of water, but only cyclical variations of the saturation in the gas to a negligible lateral band which surrounds the storage area. The seismic interpretation showed that the Minerbio structure is an anticline asymmetrical affected by fault planes which result in maximum vertical discards up to a hundred meters. The fault planes have a trend sub-parallel to the front of the structure and, to the south-east of the deposit limit, bending towards the south. The traps have been linked to simple elements stratigraphic (lateral variations in porosity of the sediments) and are bounded by faults on the edge of the structures whose seismic activity has been carried out only in the distant geological past, while generating the trap (G. Cau, 1978).

Methods

Field site and measurements

The measurements were carried out surrounding the methane gas storage site in Minerbio (BO), Italy, Fig.1, during March-July-August-September in 2016. All the measurements have been done around the Minerbio city and close to the gas storage wells. Air-Soil samples have been taken at the same daytime on each sampling visit between 9am to 4pm (U.T). Since all the measurements were done in private wells and houses, for their privacy, monitoring points are not showed in this map.

Fig.1 Location of field site within Minerbio area.

Soil Gas monitoring system

Three instruments were used for the gas survey within Minerbio area. A stainless-steel probe, diameter 6.4mm, was used for the soil gas monitoring and the holes were augered to a depth of 1m. In March 2016, the measurements were done in atmosphere and into the soil at 1m depth. Instead, in July-August-September 2016 the measurements were done in atmosphere and into the soil at 10cm – 1m depth, Fig.2. The three instruments, ETG BioGas (www.etgrisorse.com), measures CO_2%, CH_4% concentrations by using an infrared sensor (accuracy 1.5%) and O_2% concentration using an electrochemical O_2 sensor (accuracy of 1%). Each sample was controlled between 10 and 15 minutes. The air pump into the instruments was used to draw the soil gas about 1L/min. In this paper, we focused on methane gas concentrations, since the main objective was to determine eventual gas leaks from the natural gas storage activities within Minerbio city. Before taking each measurement, the four instruments were purged with dry, fresh air for 15 minutes.

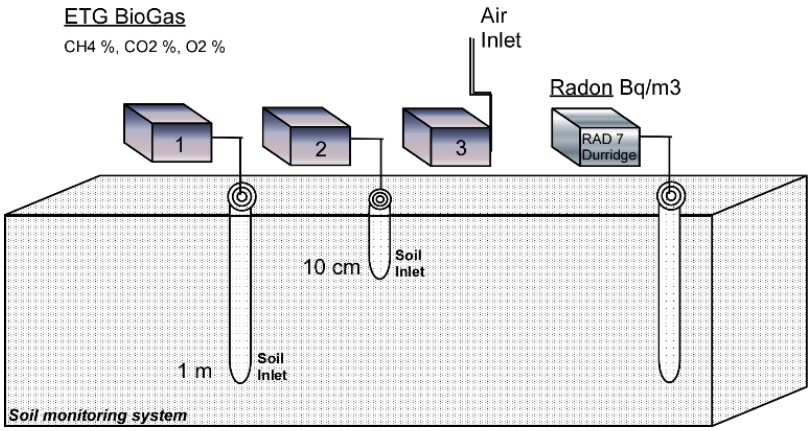

Fig.2 Design of the air and soil gas monitoring system.

Radon gas control

A RAD7 Durridge® alpha spectrometry instrument was used for ^{222}Rn-^{220}Rn soil gas surveys. Soil-gas samples of 60 cm^3 were extracted from soil at a depth of 1m. Soil radon gas measurements were carried out at 8 different places around the gas storage site. The multipurpose electronic radon detector with real-time monitoring and spectral analysis (RAD 7, Durridge Company, Inc., USA) (www.durridge.com), can be considered as a comprehensive system for radon allowing measurements in air, soil and water. During soil gas survey, water samples were collected to measure the radon concentration, in eight private wells.

As for the detection systems used, three modes of soil gas measurement were used, namely: (1) the grab sampling mode, (2) continuous monitoring using standard protocols, and (3) the thoron mode. The soil probe was connected through the desiccant to absorb the moisture. Before taking measurements, RAD7 was purged with dry, fresh air for 20 minutes. Then, the device was set at grab protocol and the measurement started. Radon (^{222}Rn) values were measured every 15 minutes (third cycle reliable for the final reading of the two components) pumping from the steel probe. The ionization chamber of the detector is protected by the > 10% humidity by a “drierite” trap and a “gasoline” type pre-filter. Radon particles generate positive charged ^{218}Po and ^{214}Po ions after entering the chamber and they are collected on the detector by electrical High-Voltage field sources. Radon calculation is based on the sum of ^{218}Po and ^{214}Po peaks.

Soil analysis

A total of thirty-seven shallow soil samples were analyzed in the field, by understanding the humidity and texture of the sediments, and just fifteen samples, in which we found higher gas concentrations, were collected at 10cm and 1m depth, to be analyzed in the Sedimentological Laboratory. The soil texture was analyzed and first procedure was to separate the sandy fraction from the muddy fraction through a wet sieving (net light of 63µm). A further division of the sands was determined by using a mechanical quencher to obtain a fraction of 2.8-3g. It was used an instrumentation based on the principles of Stokes law, an Sedimcol software to obtain the data and elaborate Folk and Ward (Folk and Ward, 1957) textural

parameters, to determine the relative percentages of the granulometric classes per the size scale of Wentworth (Wentworth, C.K., 1922). The X-ray Sedigraph product by Micromeritics (Model 5100) was used to analyze the mud fraction with dimensional range from 0.0884 mm to 0.00049 mm and value standard of density about 2.7 g / cm^3. Shepard's diagram was used to classify the sediments, (Evans, G., 1965; Frey and Basan, 1978).

ICP-MS analysis was done in the Chemical Laboratory to obtain the Uranium and Thorium concentration into the soil samples (at 1m depth). Soil samples were analyzed by inductively coupled plasma-mass spectrometry (ICP-MS) using a Thermo Electron Corporation X series spectrometer (Thermo Fisher Scientific, Waltham, Massachusetts).

Results

Soil analysis

The eight places that showed high methane concentration, soil samples were analyzed for texture analysis (samples at 10cm and 1m depth) and chemical analysis (samples at 1m depth). Through the granulometric data it is possible to calculate the percentages of sand, silt and clay for the construction of the Shepard diagram, in which there are defined the percentage limits of a sediment, M06 sandy soil, M03, M07 and M12 silty sand, and the other samples Loam, as in Fig.3.

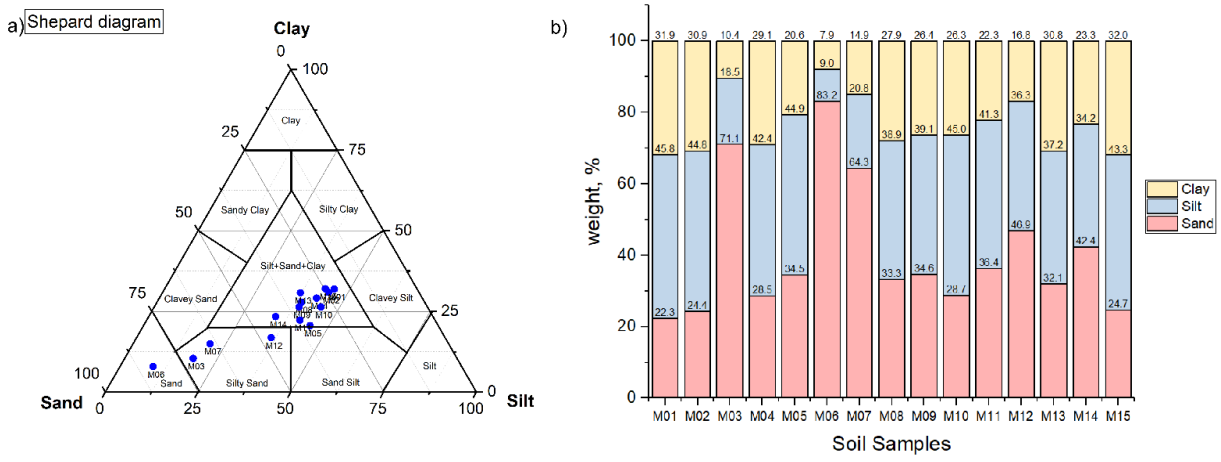

Fig.3 Shepard diagram, the percentage limits of sediment.

Since soil–gas distribution is affected by soil texture were analyzed all the fifteen sample. The samples M03, M06 and M07 are sand-based soils, estimating a highest permeability.

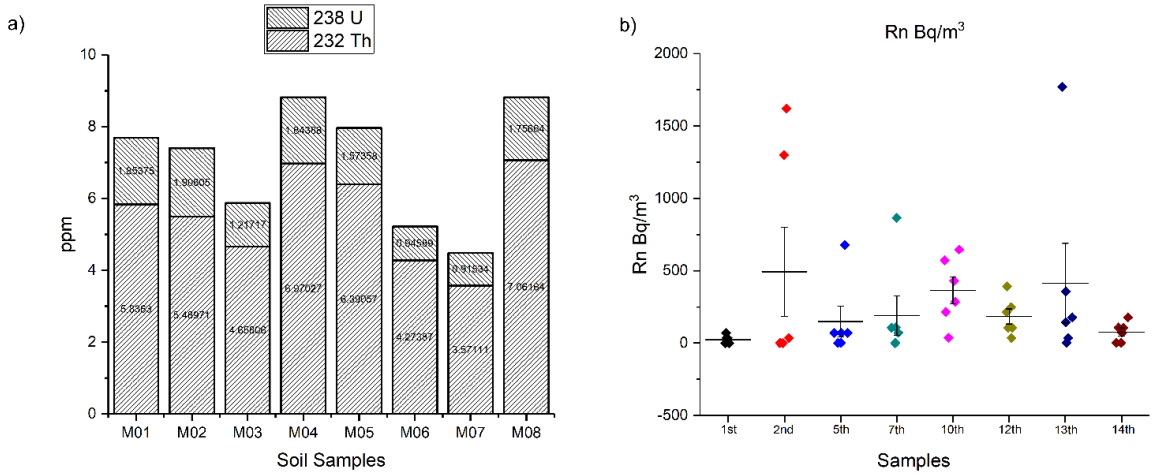

Fig.4 a) Thorium and Uranium in the soil samples, b) Radon gas concentrations.

In the Fig.4 one can observe higher concentrations of thorium and uranium in the soil samples correlated to the fine granulometry as clay-silt, Fig.3. Average values of uranium and thorium concentration in sedimentary rocks (sand stones and shale other than black are reported to be 3.7 ppm and 12 ppm, respectively) (Report No. 094, 1987). On the other hand, the average value of uranium concentration in Earth's crust is reported to be 2.8 ppm. The most common sources of uranium and radium are heavy minerals and iron-oxide coatings on rock and soil grains and organic material in soils and sediments. Less common are phosphate and carbonate complexes and uranium minerals (De Voto, R.H., 1984; Nagda, N.L., 1994). These lithological units may potentially be the cause of soil radon concentrations, Fig.4. Highest radon concentrations were observed in August, as shown in the Fig.4.

Measurements of methane gas concentration were done surrounding gas storage activities to understand which area present highest methane concentrations in atmosphere and into the soil. The data were analyzed by using OriginPRO 2017, to compare atmosphere and soil gas concentration in all places monitored. It can be observed in the Fig.5, atmospheric methane gas concentrations are lower than soil methane gas concentrations. At 1m depth into the soil there are highest concentrations, 0.020 CH_4% - 0.030 CH_4%. It is well known the methane concentration in atmosphere is about 1.85 ppm or 0.0185 %, in this gas survey we did not have outliers.

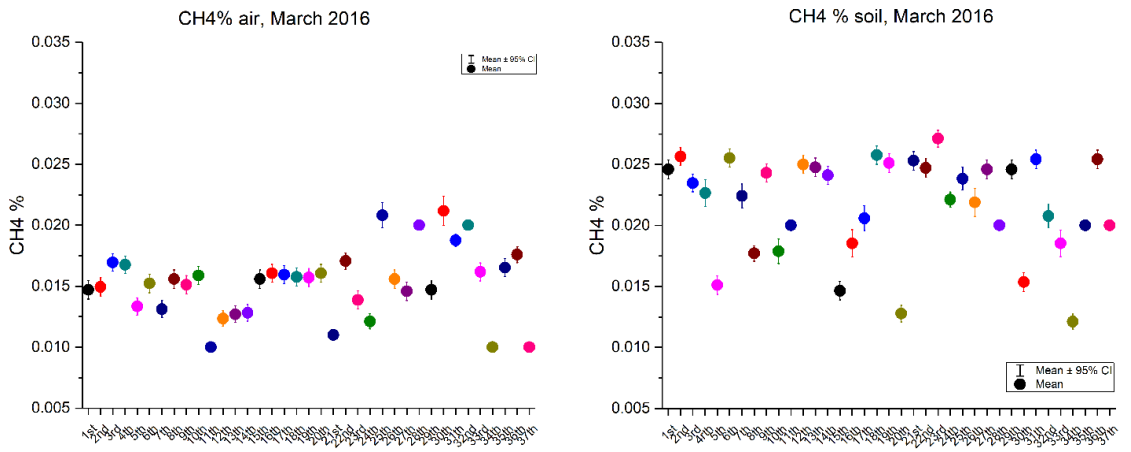

Fig.5 The average concentration of methane in atmosphere and in the soil, at the thirty-seven places within Minerbio area, March 2016.

Gas measurement survey continued in July (07/18/2016 to 07/25/2016), August (08/01/2016 to 08/05/2016) and September (08/28/2016 to 09/01/2016) surrounding gas storage activities in eight places with highest gas concentrations during previous measurements. The measurements were done in the morning since we had afternoons with high temperature values so the instruments warmed up to 44°C and the battery was working for almost 5 hours. For this gas survey, CH_4 concentrations, it was used a different soil gas monitoring system at 10cm and 1m depth and for ^{222}Rn Bq/m^3 at 1m depth. Measurements were taken between 10 and 15 minutes for each sampling, to determine the gas concentration, distribution and the relationship among methane gas and atmospheric conditions. All the data were collected for a week period, after rainy days, by using the same instrument for air and soil gas at 10cm and 1m depth.

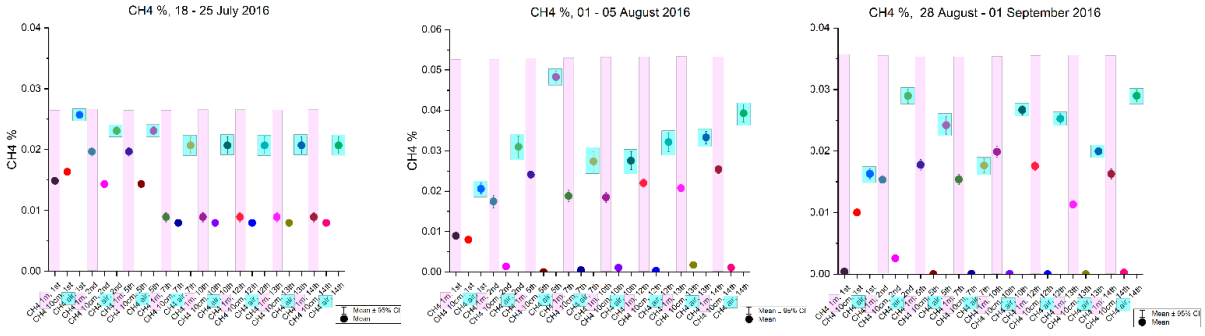

Fig.6. The methane gas concentrations in atmosphere, at 10 cm and 1 m depth into the soil.

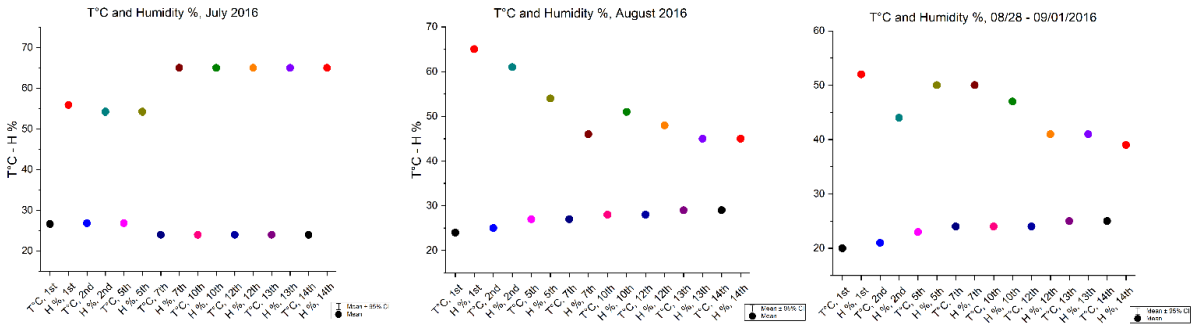

Fig.7 Temperature and humidity values during the gas survey.

In the Fig.6, the corresponding value on the Y-axis is the concentration of CH_4 % v/v and on the X-axis, we have the places monitored during the week, measurements at 1m depth, at 10cm and in the atmosphere. Typically, surface ground methane gas concentration varies between 0.2 and 1.6 ppm (mean concentration in air), with no external source of CH4, the concentration is not expected to exceed 0.1% v/v (Hooker and Bannon, 1993). During the measurements, as shown in Fig.7, temperature and humidity were almost constant. In July, the methane concentration in the soil was higher than in the atmosphere, about 0.03%. In August, the methane concentration was highest in atmosphere, with a maximum concentration about 0.05 %. Methane concentrations were higher into the soil to a depth of 1m than to a depth of 10cm, as one can expect since the 10cm into the soil are influenced by the atmospheric conditions.

Many private water wells, within Minerbio area, were under control during the gas measurement survey. Water samples were collected from domestic wells, aquifer depths from 8m to 100m. Water temperature, potential of hydrogen (pH), electrical conductivity (EC), oxidation reduction potential (ORP) were determined in situ by using Hanna instrument. The pH is defined as the negative logarithm of the hydrogen ion and can be utilized to measure the balance of acids and bases (Trevathan et al, 2012). The oxidation redox potential (ORP) measures the water capability of providing electrons to an oxidizing agent, or of removing electrons from a reducing agent, thus characterizing the oxidation-reduction state in the water. The ORP is usually expressed in mV (Arizaga et al, 2012). Water in its pure state has the capability of solubilizing substances, particularly salts, thus causing some natural waters to having great values of electrical conductivity. This electrical conductivity (EC) depends on the stoichiometry of the dissolved mineral (anions or cations) and on its concentration (Rand et al, 1999).

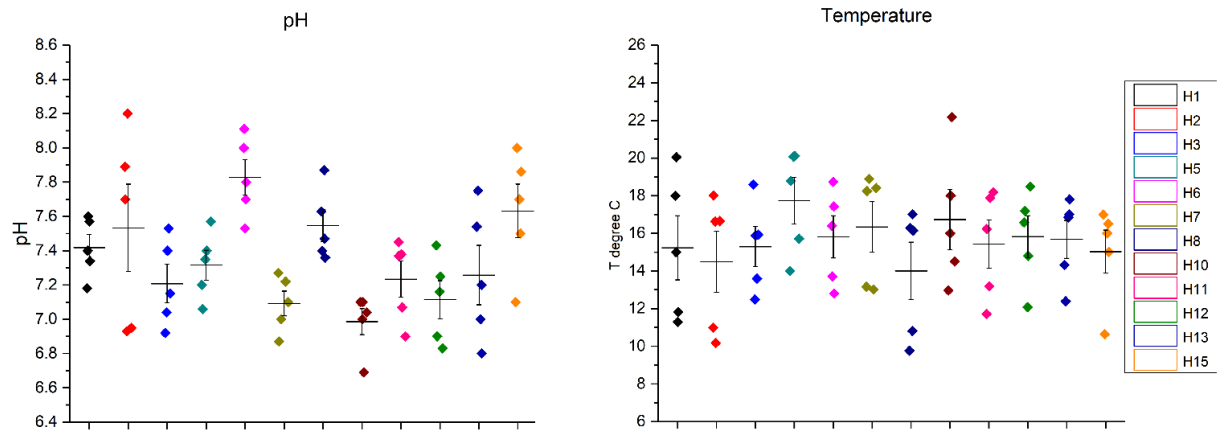

Fig.8 Water parameters in private wells, pH and temperature values.

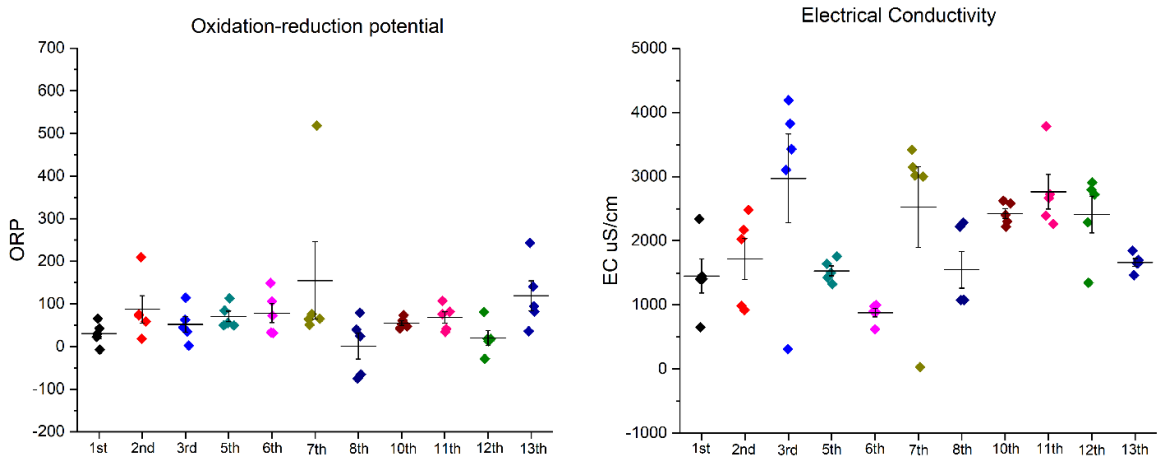

Fig.9 Water parameters in private wells, ORP and EC values.

The pH values, as provided in Fig.8, are in the range of 6.69 to 8.2 pH. The pH of pure water is 7. The normal range for pH in surface water systems is 6.5 to 8.5, and the pH range for groundwater systems is between 6 to 8.5. The temperature ranged between 10° C and 22° C, Fig.8. The electrical conductivity depends on the water temperature and at the 3rd and 7th place monitored we had water samples with high values of EC. In the Fig.9, it can be observed the positive values (oxidation reaction) and negative values (reduction reaction), ORP values measured in millivolts (mv), in most of the water samples. All the measurements presented good values and the highest methane gas concentrations within Minerbio area, were considered relating to agricultural activities.

Discussion and Conclusions

The gas measurement survey within Minerbio area was done to understand if the methane gas concentrations were connected to the gas storage activities or agriculture activities or soil characteristics. It is well known that soil can act as a sink or a source for CH4, with the former occurring primarily in well-drained, oxic, upland soils (methanotrophy) and the latter in water saturated, anoxic, organic rich soils like peats and bogs (methanogenesis) (Jean and Roger, 2001). Methanotrophy depends on both soil moisture content and temperature. It occurs most strongly under optimal moisture conditions, with microbial metabolism being limited under very dry conditions and CH4 and O2 transport to active sites being impeded by very wet ones (Stein and Hettiaratchi, 2001). Methanotrophy has been found to increase with temperature (Stein and Hettiaratchi, 2001) although some authors state that the effect is more pronounced with methanogenesis (Jean and Roger, 2001). Land use also affects methane oxidation. For example, methanotrophy rates decrease in the order forest soil, grasslands and agricultural soils (Hutsch, 2001), with the last having the lowest rates due to the inhibiting effect of fertilizers, tillage, and compaction of the surface soil (Jean and Roger, 2001; Hutsch, 2001). The soil texture, organic matter content and structural features affect the concentration at a specific depth into the soil. It can be observed that the highest methane concentrations were for sand-based soils, with a highest permeability. The Minerbio site is characterized by alluvium sediments that consists of silt, clay, sand and gravel. Eventual gas leaks by the gas storage activities, one should notice increasing concentrations and anomalous concentrations into the atmosphere and into soil with depth (the maximum depth was 1m monitored), the highest methane concentration was only 0.06% v/v in function of processes in the soil. The high concentration of methane into the soil can induce explosions in indoor ambient and it can induce to liquefaction too during earthquakes, that is why it is important to have a continuous monitoring of soil gas concentrations. About the liquefaction, many research were done with the aim to understand the relationship between high concentration of methane into the soil and liquefaction, (Sciarra et al, 2013; Sciarra et al, 2014; Di Giuseppe et al. 2016).

To be precisely, carbon isotopic analysis of atmospheric and soil methane should be done to understand if the methane is biogenic or thermogenic. Since no outliers were identified, in this research, no isotopic analyses were considered. The measurements were carried out in March-July-August-September 2016, almost at the same time in the same place within Minerbio area, values measured almost for fifteen minutes for each sampling. At a depth of 1m, the maximum soil radon gas concentration was about 1770 ±±582 Bq/m3, the soil consisted of 64.31% sand, 20.75% silt and 14.94% clay, and with 0.526 ppm of Uranium. The maximum concentration of methane was about 0.06%, into the soil at a depth of 1m, soil characterized by 83% sand, 8.96% silt and 7.89% clay. The gas measurement survey presented generally values on the range of 0.01% to 0.03% CH4.

Since this gas storage site is the most important in Italy, a continuous monitoring system was done after this field campaign. Several experiments were done for this target by using new low-cost system for water

monitoring, using pH and electrical conductivity sensors, parameters that can be affected having gases dissolved in water (Ilie et al, 2017). It was presented a new device that measured the air and water quality (Ilie and Vaccaro, 2017), it was built in a way to resolve all the issues that we had during the gas measurement survey with the portable gas monitoring devices, no heavy cases, no pump inside the box with the sensors that can induce high temperatures, data saved on SD card each twelve second, so large amount of data by using statistical analysis. This device useful to determine the behavior of methane in atmosphere, into the soil as well as the water parameters for a long period monitoring, so one can determine diurnal and seasonal variations of methane in different environments conditions.

Acknowledgments

We thank Dr. Francesco Droghetti, Dr. Umberto Tessari and Dr. Renzo Tassinari for a field and laboratory technical support. The funding for this project was provided by the Ministry of Universities and Research (MIUR).

References

See all references at the end of this thesis.

Papers in progress

III.1.2 Drilling and Hydraulic fracturing activities in Greeley, Colorado, USA

Several articles are in progress for the PhD Research at University of Colorado Boulder, 3rd year PhD program, 2016/2017.

1) **Ilie, A.M.C.,** Gordon-Casey, J., Coffey, E., Hannigan, M., Vaccaro, C., *Soil-atmosphere measurements of CO2 and CH4, surrounding Drilling and Hydraulic Fracturing activities in Greeley, CO, USA*, Paper in progress.

2) **Ilie A.M.C.,** Gordon-Casey, J., Coffey, E., Hannigan, M., Vaccaro, C., *Temperature and humidity control on low-cost sensors*, Paper in progress

3) Gordon-Casey, J., **Ilie A.M.C.,** Hannigan, M., *Measurements of CH4, CO, O3, and CO2 Outside Homes Adjacent to a Multi-Well Pad During Drilling, Hydraulic Fracturing, and Production Phases, Using Low-Cost Sensors and Artificial Neural Network Quantification Techniques*, Paper in progress

IEEE XPLORE DIGITAL LIBRARY

978-1-5386-0435-9/17 ©2017 IEEE SWC 2017 319 – 326

Configuration, programming and implementation of three Smart Water network wireless sensor nodes for assessing the water quality

Ana M. C. Ilie [1], Carmela Vaccaro [2]
Department of Earth Sciences
University of Ferrara, Unife
Ferrara, Italy
liinrc@unife.it, vcr@unife.it

João Rogeiro [3], Teresa E. Leitão [4], Tiago Martins[5]
Departamento de Hidráulica e Ambiente
Laboratorio Nacional de Engenharia Civil, LNEC
Lisbon, Portugal
jrogeiro@lnec.pt, tleitao@lnec.pt, tmartins@lnec.pt

***Abstract*—** This paper aims to present a Wireless Sensor Network using a Libelium Smart Water kit to allow remote water quality monitoring communication in real time. Equipped with multiple sensors that measure the most relevant water quality parameters, the Smart Water kit can be connected to the internet (using a mobile broadband connection) for real-time water quality control. The water quality parameters measured include pH, oxidation-reduction potential (ORP), electrical conductivity (EC) and temperature. The Smart Water platform includes three ultra-low power sensor nodes designed for use in rugged environments. The sensor nodes communicate through low power radio (802.15.4) sending data to the Meshlium Internet Gateway. This Gateway then sends the data to the Cloud or an external database via 3G or GPRS cellular connections. Sensor data is available in real time, even from sensor nodes situated in remote locations. This specific solution was implemented for three experiments performed in a physical sandbox model or artificial aquifer built in the laboratory.

Keywords— sensors, water quality monitoring, wireless sensor networks

Introduction

Annually, there are approximately 250 million cases of water-related diseases, with roughly five to ten million deaths worldwide. The rapidly increasing environmental pollution problems in recent years raise an urgent need for research and policy-making to conserve the global environment. The increasing water pollution in river areas increases the importance of environmental monitoring systems [1]. In our study, the water quality data such as hydrogen ion exponent (pH), electrical conductivity (EC), oxidation reduction potential (ORP), and temperature are used to monitor the water flowing through the artificial aquifer by using Libelium monitoring system [2].

The used water for human consumption must be free of microorganisms and chemicals that cause risk in human health. Absences of turbidity, color, smell and unpleasant taste are the most important parameters in quality of public drinking water sources [3]. Due to the great importance of water for the planet's life, it has become the focus of discussion in several forums mainly with the goal of finding solutions for the water contamination. It is known that only 3% of

the existing water is appropriate for consuming, thus to be shared between animals and humans. This is not only for drinking, but for all the activities in which clean water is necessary. With the increasing of Earth's population, pollution and contamination of sources of water by human action is another problem that appears. The lack of sanitation and industrial waste dumped into rivers, lakes and the soil yet further decreases the amount of clean water available for drinking. Environmental pollution directly affects the volume of water available for drinking and may destroy the ecosystem if the concentrations of these pollutants reach higher levels. The published experimental studies emphasize the need for continuous water quality monitoring with sufficient spatial and temporal resolution and demonstrate that the state of art sensing technologies fail to satisfy this requirement [4,5,6]. The rapid development of sensor and wireless communication technologies has increased the use of automatic (wireless) sensors in environmental monitoring. The availability of smarter, smaller and cheaper sensors measuring a wider range of environmental parameters has enabled continuous-timed monitoring of environment and real-time applications. Along with developments in sensor and communication technology, complex environmental problems have rapidly increased the need for temporally and spatially accurate data [7]. The intrinsic problems of wireless sensor networks have often been tackled in the literature, for instance in [8,9,10], in [11,12,13] for reliability and energy efficiency or in [14,15,16,17,18,19] for the analysis of environmental condition effects on the WSN. Systems known as RTRM (Real Time Remote Monitoring) are interesting solutions for remote acquisition of data for water quality analysis. Last developments on wireless network communication have enabled substantial advances in this field and it is fundamental in the design and construction of these monitoring systems [20]. In water monitoring sensor networks are used for monitoring water quality and hydrology of rivers, lakes and reservoirs and for flood warning [7,21,22- 25]. The acquisition of remote data from continuous in situ monitoring offers important early warning information to decision-makers, which facilitates quick and adequate management responses. RTRM technologies have lately emerged as economically-viable means of recording key hydrological parameters [26]. The need to continuously protect, regulate and monitor the quality of water in both marine water and freshwater environments is being recognized with the introduction of a growing body of legislation such as the EU Water Framework Directive(http://ec.europa.eu/environment/water/waterframework/info/intro en.htm) issued in 2000. New technologies are emerging to enable remote autonomous sensing of our water systems and subsequently meet the demands for high temporal and spatial monitoring. Advances in communication and sensor technology have provided a catalyst for progress in remote monitoring of our water systems [27]. Wireless sensor networks have the potential to be very powerful tools to address several operational issues, including pollution monitoring [35,36], emergency response during catastrophic events [37] or environmental monitoring [38]. To function properly, sensor networks for water monitoring normally require a relatively dense deployment of sensors [39]. In MARSOL project (http://www.marsol.eu/), a Libelium Smart Water kit have been used, which included low-cost sensors, waterproofed, capable of monitoring water physical parameters (i.e., pH, EC, ORP and temperature) in water environments. The objective of this work has been the configuration, programming and implementation of a WSN using three Libelium Smart Water sensor nodes, recording and wirelessly transmitting the data on water content at different depths, in the artificial aquifer built at LNEC, Lisbon (Portugal). Monitoring water quality in real time is the best method to use it and understanding the eventual contaminations in different aquifers with different soil characteristics.

Materials and methods

Architecture

The Libelium Smart Water kit [2], a commercial platform, was selected to build a wireless sensor network (WSN) used in this project. Several tests to evaluate the performance of the system have been conducted. Monitoring the parameters of the tap water flowing through the physical sandbox model was the main focus, collecting measurements from sensors in real-time. The real-time remote monitoring network comprised three different stations or Waspmote, node A-B-C, which provides water quality information. The term "Waspmote" encompasses both the Waspmote device itself and its modules and sensor boards, in Fig. 1. The Waspmote consists of the sensor probes, the box where the electronic components (including the battery) are enclosed and an external solar panel.

Hardware

The Libelium Smart Water kits allow to build a small and simple Wireless Sensor Network, offering a complete range of features, which make them very useful and practical systems. The used kit, Smart Water, includes three sensor nodes, also known as Waspmotes, and a Gateway, called Meshlium, as shown in Fig. 2. These two components have very different roles, while the waspmotes are in charge of the sampling process, having the sensor probes attached, the meshlium's goal is to capture all waspmotes sample data and their local archiving, optionally uploading them to some external place. Waspmotes consume very low power, they are equipped with a 6600mAh battery and a 2W solar panel, which can make them autonomous and very easily deployed in the sampling site. The waspmotes also include an Arduino-like microcontroller (Atmega 1281 running at 14Mhz with 32Kb of RAM), the device's brain, connecting the sensor probes and an 802.15.4 low-power radio used to send sampled data to the meshlium. The meshlium, on the other hand, is a far more capable and powerful device, a small computer running Linux Operating System, OLSR Mesh communication protocol, and comprising a bunch of network interfaces, 802.15.4 radio to receive waspmote sample data, and RJ45 Ethernet, WiFi and GPRS/3G modem for LAN and WAN networking. Acting as a logger and gateway, the meshlium doesn't give the same degree of autonomy as a waspmote, lacking the battery and the solar panel power source, with a maximum power consumption of about 5W (18V). It still offers Power Over Ethernet (POE) as a way of ease the installation. The meshlium's x86 CPU runs at 500MHz it has 256MB of memory RAM, and 8GB of flash memory for internal storage (including the operation system). Another big difference between the two is the storage, where meshlium has internal storage, waspmotes are completely volatile and limited to sample and send data. Wospmotes can withstand harsh environments, being water and dust proof, allowing them to be placed outdoor.

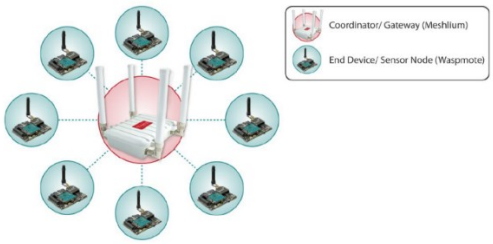

Fig 2: The Gateway and Sensor nodes.

Wireless Sensor Networks with Waspmote and Meshlium

The Smart Water kit includes everything to build a Wireless Sensor Network, from the hardware radio to the software infrastructure. Both the Waspmotes and the Meshlium come with low-powered radio 802.15.4 hardware installed, needing only a minor software setup to be ready to communicate. The low-power radio covers a radius of a few hundred meters (line of sight) with a low rate transmission, up to 250Kbps, but plenty enough for the purpose. The connection between the waspmotes and the meshlium is encrypted using AES128 with a pre-shared key

[2], to ensure that only somebody who is authorized to access data will be able to connect to the network and on a best-effort delivery basis, which means the network does not provide any guarantees that data is delivered. Since waspmotes don't store sample data, every sample the meshlium doesn't receive is lost. As long as the sample data reach the meshlium they are stored internally, and in case of having an active WAN connection, typically a GPRS/3G, and an external database or a cloud service, properly configured, sample data are also exported, as shown in Fig. 3. Either RJ45 ethernet, WiFi or the GPRS/3G interfaces can also be used to connect to the meshlium web interface, called Meshlium Manager System, for configuration and access internal stored sample data.

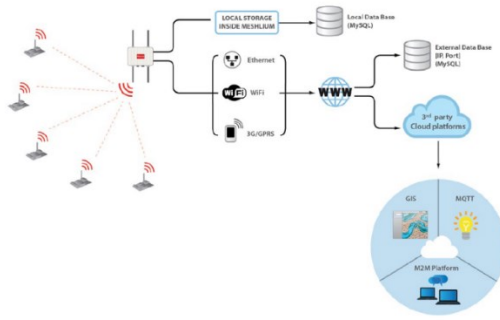

Fig 3: Meshlium Sensor Parser receives data frames from WiFi modules and sends to the Cloud.

Frame Structure

The data are ordered in a frame having the structure as shown in Fig. There are two kind of frames ASCII and Binary. These frames facilitate the comprehension of the data to be sent. As the frame is composed by ASCII characters is easier to understand all the fields included within the payload.

HEADER									PAYLOAD						
<=>	Frame Type	Num Fields	#	Serial ID	#	Waspmote ID	#	Sequence	#	Sensor_1	#	Sensor_2	#	...	Sensor_n	#

Fig 4: ASCII Frame structure.

It is recommended to use the official Data Frame format of Libelium, because Meshlium parses frames in an automatic way thanks to a feature called “Sensor Parser”. That is, as long as the frame format is familiar to the meshlium, received frames are parsed and stored in its internal database without any kind of setup or configuration, independently of the radio technology being used. These frames formats are used by the waspmote firmware APIs to achieve an easy way of sending data to the meshlium. Inside the frame structure one can identify two different parts. The first one corresponds to the header and the second part corresponds to the payload and is where data values are included. In the structure fields as shown in the Fig. 4, the *start delimiter* is composed by three characters “<=>”, it is a 3-Byte field and it is necessary to identify each frame starting. The *Frame Type Byte [1 Byte]* field is used to determine the frame type (ASCII or Binary) and the aim of the frame (event frames or alarm frames). The *Number of Fields Bytes [1 Byte]* is used to specifies the number of the sensors fields sent in the frame and to determine the frame length. The *Separator [1 Byte]* with the “#” character defines a separator. The *Serial ID [10 Byte]* field which identifies each Waspmote device. *Waspmote ID* is a string defined by the user which may identify each Waspmote inside the user’s network. The field size is variable [0Byte-16Bytes]. The *Frame Sequence* [1Byte-3Bytes], field indicates the number of sequence frame and it is used to detect loss of frames [2]. The frame payload is composed by several sensor data. All data sent in this field correspond to a predefined sensor data type in the sensor table. This sensor table is stored in Meshlium and it will be used to interact with the database.

The Web Interface and storage of sensor data

All the networking options can be controlled from the Manager System, a web interface which is available in Meshlium [2], as shown in Fig. 5. It allows to control all the interfaces and system options in a secure and easy way the WiFi, 802.15.4 and 3G/GPRS radio interface configurations along with the storage options of the sensor data received. The Waspmotes come configured to send frames to the Gateway. The configuration where to store the sensor data captured need to be added, in an automatic way with any type of frame thanks to the new Sensor Parser. In just one minute we can get an external data base being updated with the data coming

from the Waspmote network. Later, once the code was developed for transmitting to the Gateway, it can be switched to transmit to the Meshlium. Meshlium will receive the sensor data sent by Waspmote using the radio module and it will store the frames in the Local Data Base. Sensor Parser, which is a new software system able to receive frames from XBee, GPRS, 3G or WiFi (with the Data Frame format), parse these frames, stores the data in a local Database, (MySQL), and synchronizes the local Database with an external Database, (MySQL). All mysql databases were managed in Meshlium using "phpmyadmin". All data sent using the Waspmote Frame to Meshlium is stored in the Meshlium's database using the Frame Parser. Therefore, it is possible to access to this database or synchronize it to an external Cloud Partner. The sendFrameToMeshlium() function sends the HTTP GET request to the specified host and port.

Fig 5: Meshlium Manager System.

Sensor probes

The Waspmote equipment installed used 4 sensing probes: a) the *temperature probe*, a resistive sensor whose conductivity varies in function of the temperature, this probe is directly powered from the 5V supply with a range from 0 ºC to 100ºC and 3.5 mA consumption; b) the *electrical conductivity probe*, a two-pole cell whose resistance varies in function of the conductivity of the liquid in which is immersed, this probe is powered by an alternating current circuit to avoid the polarization of its platinum electrodes and with a range from µS/cm 220 to µS/cm 90000 and 2.5 mA consumption; c) the *potential-of-hydrogen* (pH) probe, a combination electrode that provides a voltage proportional to the pH of the solution corresponding the pH 7 with the voltage reference of 2.048 V of the circuit with a range from 0 to 14 and 170 uA consumption; d) the *oxidation-reduction potential* (ORP), a combination electrode whose output voltage is equivalent to the potential of the solution and with a range from 0 to ± 1999 mV and with a 170 uA consumption. The consumption of the sensors shown corresponds to the maximum current measured when the sensors relate to the board and its circuit on. It is possible to completely disconnect the Smart Water board, thus reducing its consumption to zero. To get accurate measurements from these probes it is necessary to perform a calibration taking into consideration the temperature variation from that of the calibration moment.

Calibrating Sensors

For each sensor node, it was done the calibration for each probe as shown in Fig. 6. The pH, EC and ORP probes have been immersed in reference solutions and the probe values were inserted in the embedded program. For the conductivity calibration were used two reference solutions with nominal values 84µS/cm and 1413µS/cm, values for tap water. There are three different calibration kits for conductivity: K=0.1, K=1; K=10. The K factor is related to the salinity of the water to be measured. Each calibration kit takes two solutions: K=0.1 around µS 220 - µS 3000; K=1 around µS 10500 - µS 40000; K=10 around µS 62000 - µS 90000. To get an accurate measurement, it is recommended to calibrate the conductivity sensor to obtain a precise value of the cell constant. Although a single point calibration should be theoretically enough, a two-point calibration is advisable to compensate for side effects of the circuitry, such as the resistance of the sensor wire or the connector.

Fig 6: Calibration sensors EC, pH, ORP, and Waspmote node with the Meshlium (Gateway).

For a proper calibration, two solutions with an electrical conductivity range as close as possible to that of the target environment should be used. The ORP probe calibration, was used the reference solution with value 0.225V at the temperature of 25 degree Celsius. The precision of the ORP probes is in the range of 10% and 15%. In the pH probe calibration kit one should use three reference solutions with values of 4 pH, 7 pH and 10 pH. The accuracy of the calibration can be understand immerging each probe in the reference solutions and figure out if the values are correct.

Sensors deployment

The main problems regarding the setup of the sensors concern both the way and the place they are deployed in. First, they must be installed in a way in which there is no interference between the sensor and near objects, making sure that the sensing parts (the bulb of the pH and ORP sensors and the electrodes of the electrical conductivity sensor) are not in touch with the objects nearby. In the case of the electrical conductivity sensor, it will have to be placed at certain distance from other objects in order to not interfere with the sensor magnetic field. Secondly, it must be made sure that the sensors are completely submerged in the liquid all the time or the sensors may give an incorrect output [2]. The sensors were deployed in the artificial aquifer facility (or physical sandbox model) used to conduct laboratory large scale infiltration and tracer tests [40]. This facility is approximately 3.5 m long, 1 m wide and 2 m high, as shown in Fig. 7, and can be filled with the porous medium soil to be studied (soil from Melides in South Portugal). The area can be divided in up to three different compartments to perform simultaneous experiments. The facility was equipped with three piezometers and monitoring devices such as multiparametric probes (pH, temperature, electrical conductivity and oxidation reduction potential).

- Section A – Melides soil in all the vertical profile;
- Section B – 30 cm top layer of a mixture of Melides soil (60%) and vegetal compost (40% with 65% organic matter), followed by Melides soil in the remaining depth;
- Section C – two layers of the same vegetal compost about 3 cm separated by 17 cm of Melides soil, followed by Melides soil in the remaining depth.

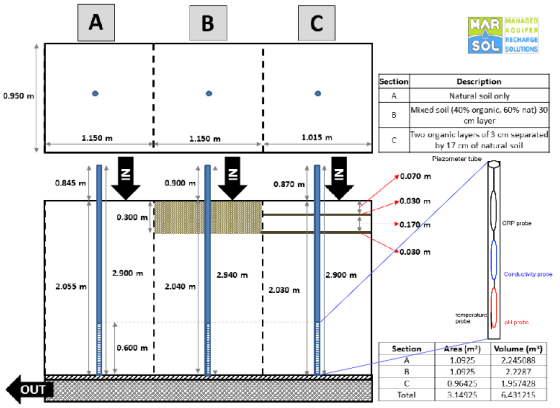

Fig 7. Schematic diagram of the physical (sandbox) model dimensions and soil mixtures used in MARSOL SAT experiments [40].

The sensors were deployed in a large scale, after the laboratory experiment, in São Bartolomeu de Messines (South Portugal) with two SAT (Soil Aquifer Treatment) basins Fig. 8, constructed under MARSOL project.

Fig 8. MARSOL SAT basins at São Bartolomeu de Messines waste water treatment plant (South Portugal) [41].

This project is focused on building these basins with a precise soil characteristic to retain contaminants and to improve the waste water treatment plant (WWTP) effluent quality, prior to its discharge into Ribeiro Meirinho, a stream which naturally recharges the karstic aquifer in part of its river bed. The SAT system design, built in June 2016, consists of two SAT basins 15 m x 7 m designed to work continuously with gravitational water flow, without any pumping requirements and to work either in parallel (simultaneously) or in series, in case a second round in the treatment is proved to be necessary. The monitoring boxes were built to collocate the sensors inside and to collect water samples. In each box, one for inflow and two for outflow, was used a Smart Water quality monitoring system in real time. Each Smart Water node was connected to several sensors, as electrical conductivity, temperature, pH and redox potential [41].

Results

To understand the functionality of the three Waspmote or Smart Water sensor nodes A-B-C, an experiment with salt tracer was tested in a physical sand box, created in laboratory [39]. For that, the quality of the tap water flowing through the artificial aquifer was assessed for different kinds of soils. Water quality was measured in the piezometer tube by the sensor nodes. The probes remained immersed in each piezometer tube from 4 June to 18 June 2016, with one exception in 7 June, to understand the time response of the sensors. The depth of the sensor probes was fixed at approximately 0.600 m in the saturated zone. Nodes A-B-C worked continuously with a constant sampling interval of 10 seconds and an upload interval of 5 minute to the external database MySQL. Each monitoring node was related to four sensors (water temperature sensor, pH probe, ORP probe and EC probe) as mentioned. In the Fig. 9, Fig. 10 and Fig. 11 it can be observed the behavior of each parameter measured by the node. During the test the water level was flowing up and down in the piezometer tube. When the water level is below the sensor, one figures out the fast response time of it giving negative values. The node A and node B present the same behavior in the water system monitoring.

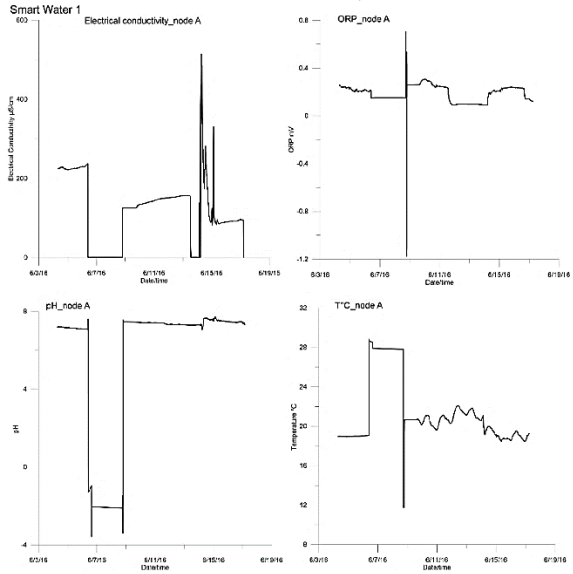

Fig 9. Sensor node A monitoring system.

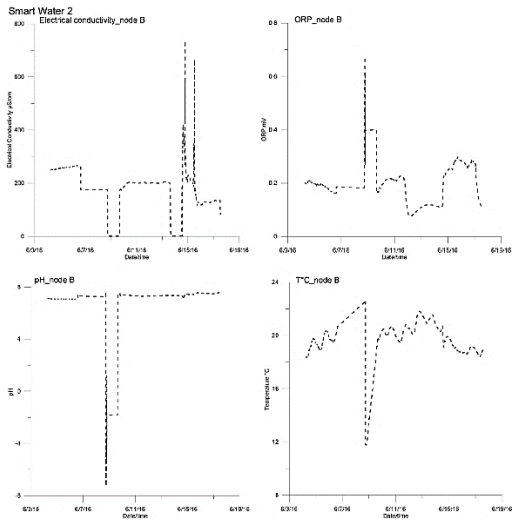

Fig 10. Sensor node B monitoring system.

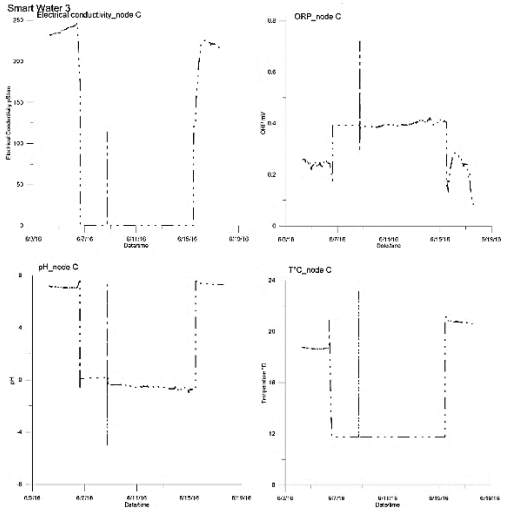

Fig 11. Sensor node C monitoring system.

The node C, as shown in Fig. 11, one observe distorted values. For example, the pH level is almost negative for a long time. Also, a decrease in the temperature and conductivity values has taken place. The biggest variation has occurred in this node C, maybe it could not stabilize, more attention should be considered when the sensors are going to be deployed in the piezometer.

The pH is defined as the negative logarithm of the hydrogen ion and can be utilized to measure the balance of acids and bases [28]. The pH range is from 0 to 14, and as we can see in graphs, there are negative values, which are related directly with the flowing down of water level. When the water level is flowing up in the piezometer tube, there is a fast response of the sensors, there are positive values about 7 pH typical tap water value. The water flowing direction influences the Ph values. This system could be configured to cope with these variations by pushing the sensors deeper in a piezometer, the sensor must remain inside the water.

The oxidation redox potential (ORP) measures the water capability of providing electrons to an oxidizing agent, or of removing electrons from a reducing agent, thus characterizing the oxidation-reduction state in the water. The redox potential is usually expressed in mV [33]. Moreover, from the ORP values, it is possible to analyze the existence and state of metals such as iron and manganese [34]. In our experiment the ORP shows a subtle variation, because of water level beneath of the sensors. The ORP values are about 250 mV.

Temperature affects the measurement, and the effects of it can diminish the accuracy and speed of response of the electrode and the temperature coefficient of variation effects on the material being measured by the sensor [29]. The water can be classified as cold when the average annual temperature is 19 ºC or lower. Brazilian laws do not establish a maximum temperature for water. Canadian and American standards stipulate a maximum value of 15 ºC [31]. In the experiment the temperature is stable about 20 ºC is related also to the flowing up and down of water level, since the temperature of the water is colder than the soil temperature. The temperature graphics vary considerably.

Water in its pure state has the capability of solubilizing substances, particularly salts, thus causing some natural waters to having great values of electrical conductivity. This electrical conductivity (EC) somewhat depends on the stoichiometry of the dissolved mineral (anions or cations) and on its concentration [30]. EC also increases with temperature [31]. It is expressed in micro Siemens per centimeter (µS/cm) presenting similar characteristics to the dissolved total solids. In natural waters, they can be present values below 100 µS/cm, and reaching up to 1000 µS/cm [32,31]. The electrical conductivity in our experiment present values related to the salt tracer testing placed on the surface soil, to be flushed by the water flowing down into the aquifer through the soil. From this we figured out

a different values of EC probes in the node A-B-C, because of different chemical properties of soil used. In the node A the EC probe had a fast response when the salt tracer has reached the aquifer, we had 2 peaks values from 500 µS/cm to 350 µS/cm. In the node B the EC probe had a fast response to the salt tracer with values from 650 µS/cm to 630 µS/cm, consider that in this compartment there is an organic soil layer about 30 cm. In the node_C, we had problems with the stabilization of the probe. In general, during the all experiment, the parameters in the nodes present a range of values as the level standards, confirming a tap water quality.

Discussion and Conclusion

In this paper was configured a Wireless Sensor Network using a Libelium Smart Water kit to allow remote water quality monitoring communication in real time. The Libelium Smart Water kit was used in the laboratory for a real-time monitoring system including temperature sensor, pH probe, ORP probe and EC probe, with low power consumption. A periodic recalibration of the sensors is highly advisable to maintain an accurate measurement along time, allowing correcting changes owed to a drift output, polarization or wear. This experiment came out with several issues, by using the pH probe and ORP probes that present a glass bulb with a liquid inside it. Due to the shaking while fitting the probes in the piezometer, bubbles were formed inside the bulb and the sensors from node_C reported wrong values. Once the experiment finished the sensors were shacked, downward quickly to break these bubbles, and after that the probe presented acceptable values. The EC and pH sensors should be used at least at 5 cm distance between them, to avoid interference. In a piezometer, there is not enough space available to collocate the sensors in parallel at 5 cm distance, that is why these sensors were fixed one above the other, Fig. 6. Sensors collocated at different depths in the aquifer, it can be obtained results a little bit different than collocate them in parallel at the same depth in the water. The sensors should be collocated one above the other, if the purpose of the research is to determine the water quality at different depths in an aquifer, therefore should be used a piezometer large enough to allow it.

This monitoring system was deployed in a real scale test to validate the applicability of the proposed method. After the test in the laboratory, the 3 node sensors were deployed in São Bartolomeu de Messines (South Portugal) with two SAT (Soil Aquifer Treatment) basins. Since only 3 nodes were working and transmitting the data every 10 minutes, no interference was noticed with each other. Most of our communication problems came from the fact that we did not have line of sight between the waspmotes and the meshlium. The distance between the Meslium and Waspmote 1 is about 65m and the distance between Meslium and Waspmote 2 and 3 is about 125m. This experiment came out with some problems too, for instances one of the Waspmote started to take measurements every 4 seconds instead of 10 minutes, without sleeping between samples. In this condition, the battery ran out much quicker and the database was filled with unwanted data. This situation was fixed by re-flashing the firmware and the sensors were re-calibrated. Secondly there were some problems with the pH data collected with high oscillation in the values in certain periods that were not coherent with *in situ* measurements taken from water samples. Another issue was presented by Meshlium, after one day or so after turning it on/rebooting, the broadband (3G) connection was lost. That was due to SIM card problems, per the system manager web portal, probably because the device was outside without proper conditions. Once it was moved from the roof into the interior of the shed, the SIM card problems never happened again. Currently the system is still working in S. Bartolomeu de Messines, SAT, receiving data every 5 minutes, and will continue to work for the near future. An interesting fact about the waspmotes power consumption, sampling every 10 minutes give us almost a whole year of autonomy without any kind of power source, and

because of that we are still not using the solar panels. Libelium Smart Water kit by analyzing the experiment and results, one concludes that the system can be used in many environmental conditions, getting an idea about the state of the water in real time.

ACKNOWLEDGMENT

We thank our colleague Nuno Charneca who provided expertise. Águas do Algarve, SA is also kindly acknowledged for all support given during this project.

References

[1] Grinning Planet, http://www.grinningplanet.com

[2] http://www.libelium.com/

[3] Martins, A.; Malaquias, I.; Martins, D.; Campos, A.; Lopes, J.; Fiúza, E.; Silva, M.; Neves, M.; Soares, R. O Livro branco da Física e da Química. Available online: http://www.spq.pt/magazines/BSPQ/610/article/30001061/pdf (accessed on 31 July 2016).

[4] Vreeburg, J. H. G., 2007. Discoloration in drinking water systems: a particular approach. PhD thesis, Technische Universiteit Delft, The Netherlands.

[5] Yang, Y.J., Haugh, R., Goodrich, J., 2009. Real-time contaminant detection and classification in a drinking water pipe using conventional water quality sensors: techniques and experimental results. Journal of Environmental Management 90 (8), 2494-2506.

[6] Panguluri, S., Meiners, G., Hall, J., Szabo, J.G., 2009. Distribution System Water Quality Monitoring: Sensor Technology Evaluation Methodology and Results. U.S. Environmental Protection Agency, Washington, DC. EPA/600/R-09/076, 2009.

[7] Hart, J.K.; Martinez, K. Environmental sensor networks: A revolution the earth system science? Earth-Science Reviews 2006, 78, 177-191.

[8] N. Baccour, A. Koubaa, L. Mottola, M.A. Zuniga, H. Youssef, C.A. Boano, M. Alves, Radio link quality estimation in wireless sensor networks: a survey, ACM Trans. Sensor Netw. (TOSN) 8 (4) (2012) 34.

[9] P. Tarrío, M. Cesana, A. Redondi, Energy-accuracy trade-offs for hybrid localization using rss and inertial measurements in wireless sensor networks, Ad Hoc Netw. (2013).

[10] F. Wang, J. Liu, Networked wireless sensor data collection: issues, challenges, and approaches, Commun. Surveys Tutorials, IEEE 13 (4) (2011) 673–687.

[11] Moscetta, P.; Sanfilippo, L.; Savino, E.; Allabashi, R.; Gunatilaka, A. Instrumentation for Continuous Monitoring in Marine Environments. In Proceedings of the MTS/IEEE Biloxi—Marine Technology for Our Future: Global and Local Challenges (OCEANS '09), Biloxi, MS, USA, 26–29 October 2009.

[12] D.J. Vergados, N.A. Pantazis, D.D. Vergados, Energy-efficient route selection strategies for wireless sensor networks, Mobile Netw. Appl. 13 (3–4) (2008) 285–296.

[13] F. Stajano, N. Hoult, I. Wassell, P. Bennett, C. Middleton, K. Soga, Smart bridges, smart tunnels: transforming wireless sensor networks from research prototypes into robust engineering infrastructure, Ad Hoc Netw. 8 (8) (2010) 872–888.

[14] C.A. Boano, J. Brown, Z. He, U. Roedig, T. Voigt, Low-power radio communication in industrial outdoor deployments: the impact of weather conditions and atex-compliance, in: Sensor Applications, Experimentation, and Logistics, Springer, 2010, pp. 159–176.

[15] K. Bannister, G. Giorgetti, S.K. Gupta, Wireless sensor networking for hot applications: effects of temperature on signal strength, data collection and localization, in: Proceedings of the 5th Workshop on Embedded Networked Sensors (HotEmNetsn++ 08), Citeseer, 2008.

[16] H. Wennerström, F. Hermans, O. Rensfelt, C. Rohner, L.-Å. Norden, A long-term study of correlations between meteorological conditions and 802.15. 4 link performance, in: SECON, 2013, pp. 221–229.

[17] P. Corke, T. Wark, R. Jurdak, W. Hu, P. Valencia, D. Moore, Environmental wireless sensor networks, Proc. IEEE 98 (11) (2010) 1903–1917.

[18] C. Alippi, R. Camplani, C. Galperti, M. Roveri, A robust, adaptive, solar-powered wsn framework for aquatic environmental monitoring, Sens. J. IEEE 11 (1) (2011) 45–55.

[19] Niina Kotamäki, Sirpa Thessler, Jari Koskiaho, Asko O. Hannukkala, Hanna Huitu, Timo Huttula, Jukka Havento and Markku Järvenpää. Wireless *in-situ* Sensor Network for Agriculture and Water Monitoring on a River Basin Scale in Southern Finland: Evaluation from a Data User's Perspective. Sensors (Basel), 2009; 9(4): 2862–2883.

[20] Glasgow, H.B.; Burkholder, J.M.; Reed, R.E.; Lewitus, A.J.; Kleinman, J.E. Real-time remote monitoring of water quality: A review of current applications, and advancements in sensor, telemetry, and computing technologies. J. Exp. Mar. Biol. Ecol. 2009, 300, 409–448.

[21] Delin, K.A.; Jackson, S.P.; Johnson, D.W.; Burleigh, S.C.; Woodrow, R.R.; McAuley,

M.; Britton, J.T.; Dohm, J.M.; Ferré, T.P.A.; Ip, F.; Rucker, D.F.; Baker, V.R. Sensor web for spatiotemporal monitoring of a hydrological environment. In Proceedings of the 35th Lunar and planetary science conference, League City, Texas, USA, March 2004.

[22] Glasgow, H.B.; Burkholder, J.M.; Reed, R.E.; Lewitus, A.J.; Kleinm, J.E. Real-time remote monitoring of water quality: A review of current applications, and advancements in sensor, telemetry, and computing technologies. J. Exp. Mar. Biol. Ecol. 2004, 300, 409–448.

[23] Busquets, J.; Busquets, J.V.; Tudela, D.; Perez, F.; Busquets-Carbonell, J.; Barbera, A.; Rodriguez, C.; Garcia, A.; Gilabert, J. Low-cost AUV based on Arduino open source microcontroller board for oceanographic research applications in a collaborative long term deployment missions and suitable for combining with a USV as an autonomous automatic recharging platform. In Proceedings of the IEEE/OES Conference on Autonomous Underwater Vehicles (AUV), Southampton, UK, 24–27 September 2012; pp. 1–10.

[24] Gandra, M.; Seabra, R.; Lima, F.P. A low-cost, versatile data logging system for ecological applications. Limnol. Oceanogr. Methods 2015, 13, 115–126. [CrossRef]

[25] Floodnet. Available online: http://envisense.org/floodnet/floodnet.htm (accessed on Oct 28-29, 2008).

[26] Singh, R.; Singh, S.P. Development of a low cost wireless temperature monitoring system of industrial and research application. Int. J. Curr. Eng. Technol. 2015, 5, 355–361.

[27] Diamond, D.; Coyle, S.; Scarmagnani, S.; Hayes, J. Wireless sensor networks and chemo-/biosensing. Chem. Rev. 2008, 108, 652–679.

[28] Trevathan, T.; Johnstone, R.; Chiffings, T.; Atkinson, I.; Bergman, N.; Read, W.; Theiss, S.; Stevens, T. SEMAT—The next generation of inexpensive marine environmental measurement and monitoring Systems. Sensors 2012, 12, 9711–9748. [CrossRef] [PubMed].

[29] Wickert, A. The Alog: Inexpensive, open-source, automated data collection in the field. Bull. Ecol. Soc. Am. 2014, 95, 166–176. [CrossRef].

[30] Rand, M.C.; Greenberg, A.E.; Taras, M.J. Standard Methods for the Examination ofWater andWastewater, 16th ed.; Joint published by American Public Health Association: Washington, DC, USA; American Water Works Association: Denver, CO, USA;Water Environment Federation: Washington, DC, USA, 1999.

[31] Libânio, M. Fundamentos de Qualidade e Tratamento de Agua, 3rd ed.; Atomo: Campinas, Brazil, 2010.

[32] Gastaldini, M.C.C.; Mendonça, A.S.F.; Paiva, J.B.D.; Paiva, E.M.C.D. Conceitos para a avaliação da qualidade da água. In Hidrologia Aplicada à Gestão de Pequenas Bacias HidrográFicas; ABRH: Porto Alegre, Brazil, 2001; pp. 428–451.

[33] Arizaga, J.; de la Calleja, J.; Hernandez, R.; Benitez, A. Automatic Control for Laboratory Sterilization Process based on Arduino Hardware. In Proceedings of the 22nd International Conference on Electrical Communications and Computers (CONIELECOMP), Cholula, Puebla, 27–29 February 2012; pp. 130–133.

[34] Fuchs, C.R. Classification of Water Quality of the Lanoso River, Uberaba. Ph.D. Thesis, Faculdade de Ciências Agrárias e Veterinárias de Jaboticabal, Universidade Estadual Paulista Júlio de Mesquita Filho, São Paulo, Brazil, 2012. (In Portuguese)

[35] K.K. Khedo, R. Perseedoss, A. Mungur, et al., A wireless sensor network air pollution monitoring system, arXiv preprint arXiv:1005. 1737, 2010.

[36] E.A. Basha, S. Ravela, D. Rus, Model-based monitoring for early warning flood detection, in: Proceedings of the 6th ACM Conference on Embedded Network Sensor Systems, ACM, 2008, pp. 295–308.

[37] G. Barrenetxea, F. Ingelrest, G. Schaefer, M. Vetterli, The hitchhiker's guide to successful wireless sensor network deployments, in: Proceedings of the 6th ACM Conference on Embedded Network Sensor Systems, ACM, 2008, pp. 43–56.

[38] Marcelli, M.; Piermattei, V.; Madonia, A.; Marcelli, U. Design and Application of New Low-Cost Instruments for Marine Environmental Research. Sensors 2014, 14, 23348–23364. [CrossRef] [PubMed].

[39] http://www.lnec.pt/en/research/research-infrastructures/fluvial-hydraulics-experimental-facility/.

[40] Leitão, T.E., Martins, T., Henrinques, M.J., Lobo Ferreira, J.P., Rogeiro, J. and Ilie, A.M.C., 2016 - Deliverable 12.5 Physical (Sandbox) Modelling of Melides Demo Site. Projeto UE MARSOL - Demonstrating Managed Aquifer Recharge as a Solution to Water Scarcity and Drought, outubro, 50 pp. [CrossRef] [PubMed], http://www.marsol.eu/files/marsol_d12-5_physical-model_20161011.pdf .

[41] Leitão T. E., Lobo Ferreira J.P., Martins T., Oliveira M. M., Henriques M. J., Carvalho T., Carvalho J M., Agostinho R., Carvalho R., Sousa R., Monteiro J.P., Costa L.R.D., Hugman R., Mota R., Mesquita E., Rogeiro J., Rosa M. J., 2016, Deliverable 4.5 Demonstrating Managed Aquifer Recharge as a Solution to Water Scarcity and Drought MAR to Improve the Groundwater Status in South Portugal. http://www.marsol.eu/files/marsol_d4-5_mar-south-portugal_final-report.pdf

JOURNAL OF HYDROLOGY, ELSEVIER

(Submitted)

Managed Artificial Recharge into a Karstic Aquifer, Soil Treatment Studies from Small-Scale Laboratory to Field Scale Basin Infiltrations

Ana M. C. Ilie [1], Tiago Martins [3], Carmela Vaccaro [2], Teresa E. Leitão[5], João Rogeiro [4]

[1,2] Department of Earth Sciences, University of Ferrara, Via Saragat 1, Ferrara, Italy

[3,4,5] Departamento de Hidráulica e Ambiente, Laboratorio Nacional de Engenharia Civil, LNEC, Lisbon, Portugal

Abstract

This paper aims to present methodologies on improving the water quality in a Wastewater treatment plant, in Algarve south of Portugal. The research was based on soil aquifer treatment, soil column laboratory experiments to obtain the best soil in contaminants retention for the infiltration basins, as a second wastewater treatment process. The water from the wastewater treatment plant after being treated flows directly into a river that is recharging a karstic aquifer. A good water quality of the river, prior to its recharge into the aquifer, was the main objective of this research. Two infiltration basins were built at San Bartolomeo de Messines, and a real-time water monitoring system was used in input and in output, understanding immediately the results from the soil basins and the water parameters as potential of hydrogen, electrical conductivity, temperature and oxidation reduction potential. As results showed that the soil column, more than one month laboratory experiment, presented almost same average water parameter values as in the field scale basin infiltrations, more than two-month field experiment. As contaminants we focused on ammonia, nitrates, nitrites, boron, copper and zinc values, the results showed a good contaminant retention for ammonia and copper.

Keywords: Soil-column experiments; Soil-aquifer Treatment; Contaminant retention; Wastewater

1. Introduction

Reuse of treated municipal wastewaters is increasingly becoming popular in arid and semiarid regions of the world (Akberet al. 2008; Candela et al. 2007; Drewes et al. 2003; Nadav et al. 2012; Quanrud et al.

1996; Viswanathan et al. 1999; Yu et al. 2006). Managed Artificial Recharge (MAR) techniques are of substantial interest for karst aquifers, particularly in Mediterranean coastal regions where this is generally the most common type of aquifer. Karst aquifers are the most exploitable existing groundwater resources in these areas (Margat, 2008), but they are highly sensitive to overexploitation and seawater intrusion, even under natural conditions (Fleury et al., 2007). Improvements to water quality using infiltration have been demonstrated to reduce organic matter (Quanrud et al., 2003; Vanderzalm et al., 2010), trace organic compounds (Montgomery-Brown et al., 2003), nitrogen (Zhang et al., 2005) and bacteria (Schafer et al., 1998; Toze et al., 2004). A soil aquifer treatment (SAT) system is primarily based on the infiltration of treated wastewater from large-scale recharge basins through the vadose (unsaturated) zone. The percolated wastewater finally reaches the native groundwater (saturated zone) and is stored in the unconfined aquifer. During this percolation and storage, nitrogen, phosphorus, dissolved organics, heavy metals, and pathogens are significantly removed. SAT systems are used in many countries around the world to reuse treated wastewater (Candela et al. 2007; Cha et al. 2004; Fox et al. 2001; Idelovitch et al. 2003; Nadav et al. 2012; Quanrud et al. 1996; Viswanathan et al. 1999). Filtration, adsorption, ion exchange, precipitation, and microbial degradation are the most effective treatment mechanisms in an SAT system (Amy and Drewes 2007; Essandoh et al. 2011; Lee et al. 2004; Quanrud et al. 1996, 2003b; Shuang et al. 2007; Viswanathan et al. 1999; Yun-zheng and Jian-long 2006). While suspended organic matter is removed by filtration, dissolved organic matter is primarily removed by biodegradation and adsorption. Filtration and biodegradation mechanisms are considered to last forever, whereas adsorption mechanism is limited by adsorption capacity of soil (Idelovitch 2003; Viswanathan et al. 1999). During SAT, the dominant mechanism is biodegradation (Drewes et al. 2003; Ernst et al. 2000; Quanrud et al. 2003a; Rauch and Drewes 2004, 2005, 2006; Xue et al. 2009). Biodegradation can occur under aerobic, anaerobic, or anoxic conditions (Drewes and Jekel 1998; Westerhoff and Pinney 2000). In the framework of EU MARSOL project, several soil-column experiments were conducted at LNEC, Lisbon using a soil collected in Sao Bartolomeo de Messines, one of the Algarve demo sites. This paper presents the soil characteristics suitable to be used in the infiltration basins, as well as the results from the small-scale laboratory to field-scale basin infiltrations.

2. Geological settings

The study area is in the northern limit of Querença – Silves aquifer system, a Jurassic calcareous formation, situated in the Algarve region, south of Portugal. The Querença – Silves aquifer is a karstic multi-aquifer system, which its formation is due to the tectonic activity and divided in several subsystem aquifers in hydraulic connections (Almeida *et al.*, 2000, Monteiro *et al.* (2006), Monteiro *et al.* (2007) and Reis *et al.*

(2007). This karstic multi-aquifer system is researched by surface groundwater, by Ribeiro Meirinho river. This paper aimed to study the soil characteristics of this aquifer in the laboratory and build large infiltration basins, to improve wastewater quality through SAT processes so that to improve aquifer recharge through Ribeiro Meirinho river since São Bartolomeu de Messines Wastewater Treatment Plant (SBM WWTP) treated effluent is directly discharged to Ribeiro Meirinho.

3. Materials and methods

Soil samples had been taking from the SBM site. Before preparing each soil column, the soil was dried at 40°C, cleaned and removed the roots, leaves. In the laboratory was determined soil texture and organic matter percentage. First soil texture procedure, was to separate the sandy fraction from the muddy fraction through a wet sieving (net light of 63μm). A further division of the sands was determined by using sieves tower with a diameter from 4mm to 0.063mm, and each sandy fraction was weighted, as well as the muddy fraction was dried, weighted and used a laser diffraction instrument to determine the size of the particles. To determine the organic matter in the soil sample, the material was weighted and after that it was left in the oven at 600ºC, and weighted again, to obtain the percentage. To determine the soil porosity the following equation was used:

$$n = \frac{Vw}{Vt} * 100(\%)$$

where Vw is the volume of water in the soil sample (cm3); Vt is the total volume of the sample (cm3).

Soil bulk density (ρb) (g/cm3) was determined by the following equation:

$$\rho b = \frac{Wd}{Vt}$$

where Wd is the weight of the dried soil sample (g).

Soil thickness cm	30	30	30	30
saturation	saturated	saturated	saturated	saturated
injection	continuous	continuous	pulse	pulse
natural soil %	60	40	40	40
vegetal commercial soil %	40	30	20	20
artificial commercial soil	N	30	40	40
water	deionized	deionized	wastewater	wastewater

Table2. Soil characteristic.

In Sao Bartolomeo de Messines were built two infiltration basins, as dimensions 15 m x 7 m and three boxes were built for the sensor. It was used just one sensor node for the input monitoring wastewater parameters and two sensor nodes as well for the output monitoring. The wastewater was flowing down within the basin through the soil, previously studied in the laboratory, composed of 40% natural soil, 40% industrial sand and 20% vegetal compost. The soil thickness is about 60cm, as shown in the Fig.1.

The monitoring system was deployed relating to the environmental conditions in this area and the deployment of the sensors were in function of eventual interference between them. In fact, 5cm distance was considered for each sensor. The distance between the Meshlium and Waspmote 1 was about 65m and the distance between Meshlium and Waspmote 2 and 3 was about 125m. In this site was used a Wireless Sensor Network using a Libelium Smart Water kit to allow remote water quality monitoring communication in real time. Equipped with multiple sensors that measure the most relevant water quality parameters, the Smart Water kit was connected to the internet (using a mobile broadband connection) for real-time water quality control. The water quality parameters measured include pH, oxidation-reduction potential (ORP), electrical conductivity (EC) and temperature. The Smart Water platform included three ultra-low power sensor nodes designed for use in rugged environments. The sensor nodes communicate through low power radio (802.15.4) sending data to the Meshlium Internet Gateway. This Gateway then sent the data to the Cloud and to external database via 3G or GPRS cellular connections. Sensor data was available in real time, even from sensor nodes situated in remote locations (Ilie et al, 2017).

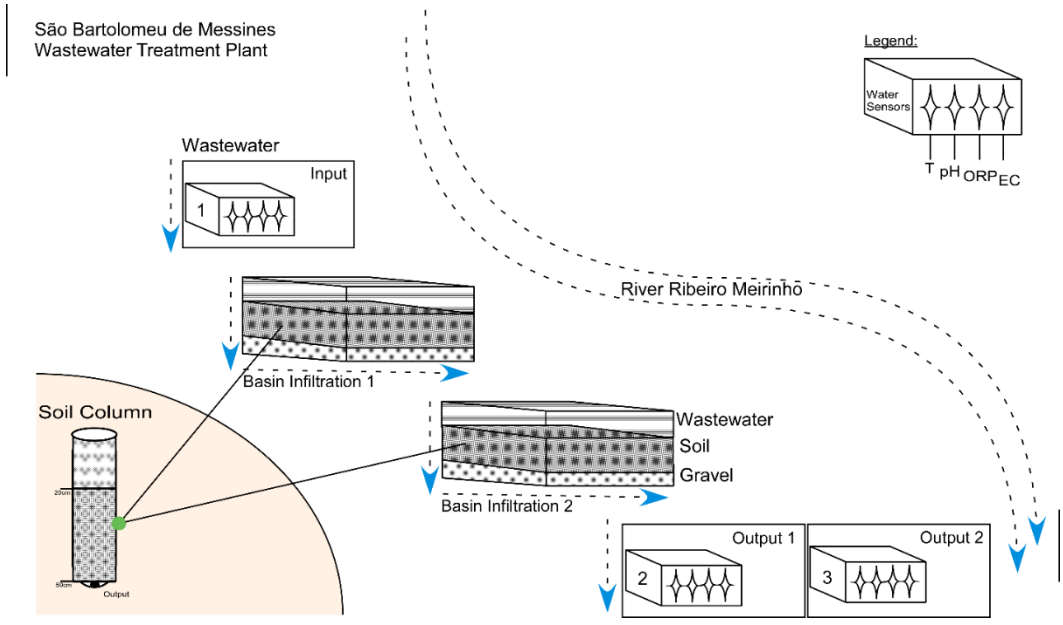

Fig.1 Design of S. Bartolomeu de Messines soil aquifer treatment plant basins and monitoring devices, one sensor node in input and two sensor nodes in output.

Calibrating sensors

The pH, EC and ORP probes have been immersed in reference solutions and the probe values were inserted in the embedded program. For the conductivity calibration, reference solutions were used with nominal values: K=0.1, K=1; K=10. The K factor is related to the salinity of the water to be measured. Each calibration kit takes two solutions: K=0.1 around µS 220 - µS 3000; K=1 around µS 10500 - µS 40000; K=10 around µS 62000 - µS 90000. The ORP probe calibration, was used the reference solution with value 0.225V at the temperature of 25 degree Celsius. The precision of the ORP probes is in the range of 10% and 15%. In the pH probe calibration kit, one should use three reference solutions with values of 4 pH, 7 pH and 10 pH. The accuracy of the calibration can be understood immerging each probe in the reference solutions and figure out if the values are correct, (Ilie et al, 2017).

Sensor deployment

The main problems regarding the setup of the sensors concern both the way and the place they are deployed in. First, they must be installed so that there is no interference between the sensors and nearby objects, making sure that the sensing parts (the bulb of the pH and ORP sensors and the electrodes of the electrical conductivity sensor) are not in touch with the objects. As electrical conductivity sensor, it will have to be placed at certain distance from other objects to not interfere with the sensor magnetic field. Secondly, it must be made sure that the sensors are completely submerged in the liquid all the time or the sensors may give an incorrect output. The sensors were fixed in parallel, in a plastic container at the bottom of the box monitoring.

4. Soil Column experiments

Soil-column experiments were conducted to determine the hydraulic characteristics of the soil. Previous experiments (Martins T. et al., 2016, 2017; Lobo Ferreira et al., 2016) on soil columns were presented. As inflow were used both deionized water and wastewater from São Bartolomeo de Messines (SBM) wastewater treatment plant (WWTP). These experiments were carried out to determine the soil infiltration capacity as well as its capacity to retain the wastewater contaminants, so that can be suitable to use it in the infiltration basins. The soil samples and the wastewater for these experiments have been taken in SBM since the SAT-MAR basins were constructed in that place using treated wastewater. In the soil columns was used as input this wastewater and flowing through the soil column, as output one had the water samples to be analyzed the physical and chemical parameters, as metals, nitrogen cycle components. It was used a peristaltic pump for continuous injection of water/wastewater. In the Fig.2 is shown the design of the soil-column experiment, as well as some pictures of the experiment. The column is made by an acrylic transparent column (as specified in the DEMEAU2 project specifications), characterized by 5cm diameter

and 50cm height. At the bottom of the column an inert Teflon membrane filter was fixed in a way that the fine particles should not have gone into the water samples. Before starting the experiment, the wastewater physical parameters, as electrical conductivity (EC), Eh, pH and temperature were measured, as well as during the experiment for all the samples collected in the output column. Bottles, 0.5L polyethylene, were used to store all the water samples and being analyzed for boron, zinc, copper, ammonia, nitrites and nitrates. The data was analyzed using statistical analysis, such as minimum, maximum, mean, median and deviation standard and scatter (box) plot to identify differences in water samples.

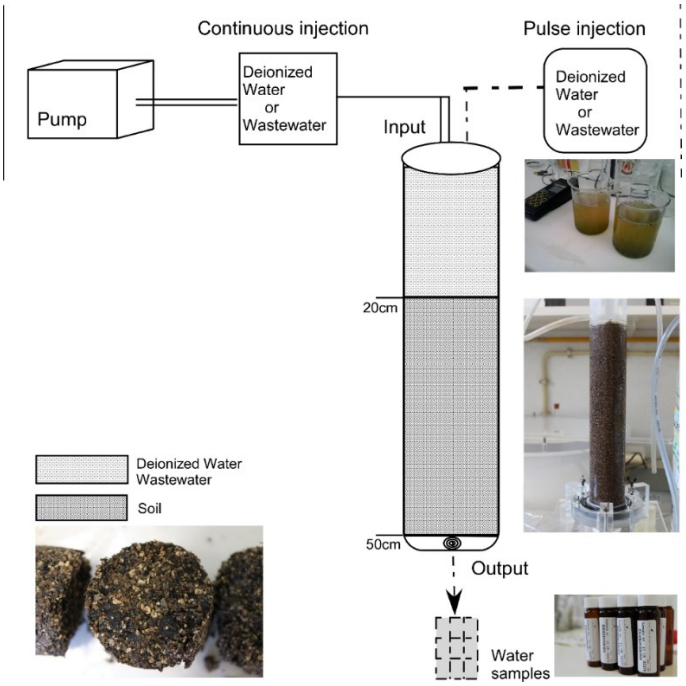

Fig. 2 –Soil-column experiment design.

The soil-column was filled following the CEN/Technical Specification 14405 (2004). A layer composed by Fontainebleau quartz sand product was used above the soil in the column, about 0.5 thickness, to ensure during the water injection a minimum soil surface disturbance and prevention in early stage of clogging process. In the four soil-column experiments (6^{th} – 7^{th} – 8^{th} – 9^{th} column) the soil was weighted and then completely saturated by using deionized water from bottom to top. The experiment in 6^{th} and 7^{th} column started with continuous water flow using an automatic peristaltic pump. In the 8^{th} and 9^{th} column the experiment started with pulse injection, about 378ml deionized water, 20cm above the soil column. In the Table1 are shown the soil-column characteristics. In these experiments, it was used an industrial sand (limestone) 98.1% sand and 1.49% clay, natural sand and commercial organic matter. The industrial sand was used to increase the permeability and to facilitates retention and cationic exchange processes; the organic matter (70% humus, 25% peat and 5% sand) was used to contribute to a high biological activity,

biodegradation processes and good soil oxygenation. In the laboratory, the columns were built by using this soil mixture and after all just one soil column, was suitable to be part of soil reactive layer in the SAT soil treatment plant, in San Bartolomeo de Messines, Algarve. The characteristic of the soil used at the SAT, had 40% natural soil, 40% artificial sand and 20% organic matter. The reason that we selected this type of soil and not the other ones, it was because of using too much organic matter in the other soil columns, observing that fine sediments were removed by washing inducing compaction, in fact the 6th and 7th soil column experiments were stopped due to the clogging too.

5. Results

5.1 Soil column experiments

The 6th soil column was built with 60% natural soil - 40% organic soil; the 7th soil column was built with 40% natural soil - 30% organic soil - 30% industrial sand, soil thickness 30 cm. For these experiments, deionized water was used as input, continuous injection and starting as a saturated soil. The 8th column and 9th column built with 40% natural soil – 20% organic matter – 40% industrial sand (limestone), soil thickness 30 cm, wastewater was used as input pulse injections and saturated soil. The porosity was highest in 8th - 9th columns, as shown in Table 2, due to the industrial sand (limestone) present in high percentage in these columns.

The soil composition in each column influenced the physical and chemical data results. The first two columns presented highest permeability, flow rate but lower porosity and apparent density, as shown in the Table.2 It was observed also that even the two columns, 8th and 9th, had the same soil composition, they presented small differences in the results, as permeability, flow rate, porosity and apparent density.

Soil column	**6th column**	**7th column**	**8th column**	**9th column**
porosity %	53.1	45	74.8	69.8
apparent density g/cm3	0.93	1.09	1.23	1.19
flow rate (mean) cm3/min	1.789	4.931	0.948	1.515
permeability cm/min	0.091	0.251	0.048	0.077

Table 2 - Soil-column characteristics on the experiments.

In the Fig. 3, it can be observed the 8th column and 9th column had a good behavior in the flow rate. In the 8th soil column the flow rate showed a range between 0.05 - 1 ml/min with a maximum value 7ml/min; in the 9th soil column the flow rate presented a range between 0.05 - 2 ml/min. The 6th and 7th soil column showed a different shape in the flow rate, with a range between 0.8 - 1.2 mil/min and 1 – 8.5mil/min respectively.

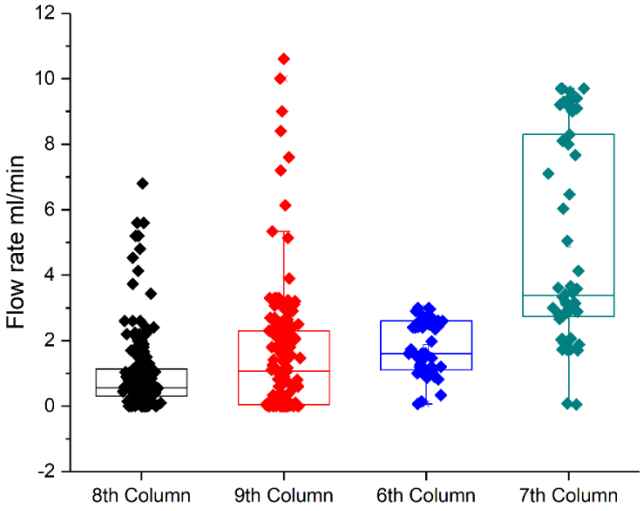

Figure 3. Flow rate boxplot of soil column experiments.

The reason we tried a new soil mixture in the 8th column was because of the high permeability in the 6th – 7th column as well as the soil compaction was too evident and low porosity. Both soil columns, 6th and 7th, formed cavities and air pockets due to the fine particles washing out, so that in the 8th – 9th column it was reduced the organic soil percentage and increasing the industrial sand percentage, giving much resistance to washing out effects. Increasing the industrial sand, we were expected to obtain good results in contaminant retention reaction, due to the high percentage in limestone. The 8th – 9th columns were working at the same time, same soil characteristics, with the only difference that the water samples in output from 8th column were analyzed for metals and nitrogen cycle, instead the water samples in output from 9th column were analyzed for pharmaceuticals analysis. The physical parameters as shown in Fig.4., of water samples were determined by using an HANNA instrument.

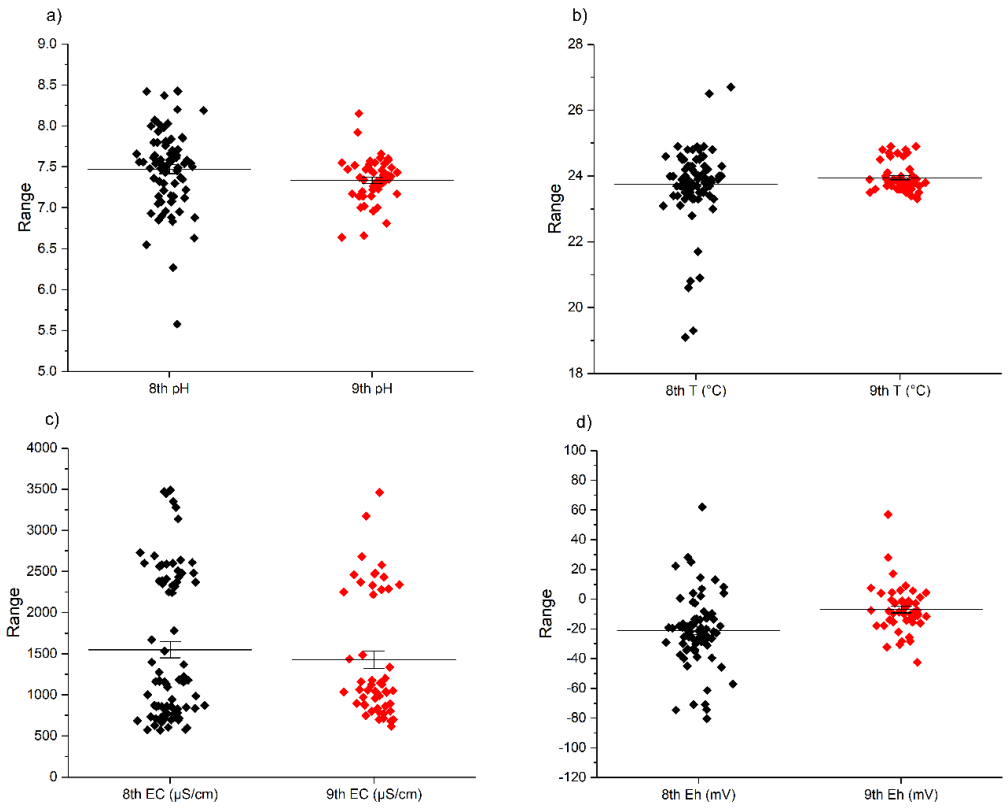

Fig.4 Water physical parameters determined in 8th – 9th soil column output.

As shown in the Fig.4 one can observe a regular behavior of the pH, temperature and electrical conductivity (EC) in both soil columns. As input wastewater was used for both soil columns. The pH, T°C, EC and Eh values of the 8th column seemed to be more spread than the ones in 9th column. Instead the EC values presented similar minimum and maximum values in both soil columns.

The inflow water pH was about 7.28. In the experiment, there were used several stages of wastewater input. Usually the wastewater input started in the morning and it completely infiltrated after more than 5 hours. During the weekend the experiment was stopped, since the LNEC Laboratory had to be closed. The highest pH values where when wastewater was infiltrating at the beginning of the experiment in the soil column, and lower pH values related to no chemical reaction for retention contaminants. The inflow water of Eh was about 90 mV, and its value in output was lower than in input, the behavior was almost constant. Electrical conductivity EC in output was higher than the input values, it increases significantly when the experiment started and decreased again when the soil had no more wastewater input.

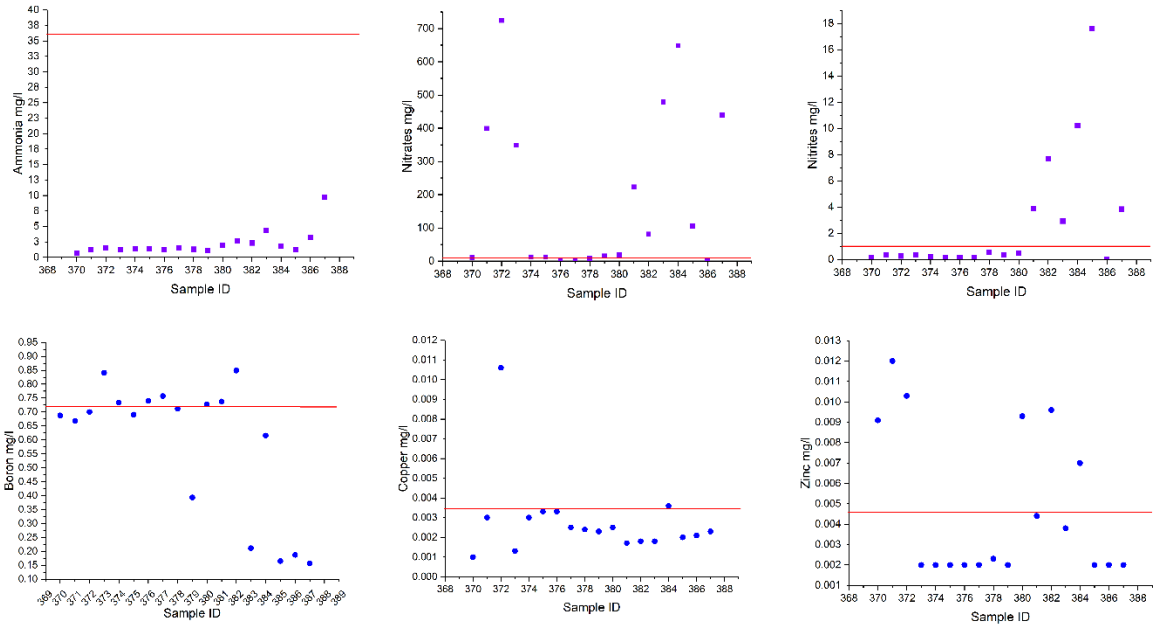

Fig.5 Ammonia, nitrates, nitrites, boron, copper and zinc values, with their input values in red line, sample ID or water samples in output 8th soil column.

In the Fig.5, good soil retention contaminants were for copper and ammonia. For boron and zinc, we obtained good retention but with high values too. The lower values obtained in output in this experiment because of highest concentration in organic matter in the 8th column. The nitrites and nitrates presented lower values in input than in output due to the transformation of ammonia in nitrites and nitrites into nitrates, known as the nitrogen cycle.

5.1 Algarve basins

After all the laboratory experiments, the 8th soil characteristic was suitable to be part of the infiltration basins in Sao Bartolomeo de Messines, Wastewater treatment plant. In input and output, as shown in the fig 1, the wastewater was controlled for almost three months, and the basins were controlled, by using the three sensor node monitoring systems, (Ilie et al, 2017). The main water parameters measured were pH, temperature (°C), electrical conductivity EC (uS/cm), oxidation reduction potential ORP (V).

In the Fig.6, it can be observed the temperature values related to the wastewater physical parameters in the three basins, one in input before second treatment *basin_in* and two in output after the soil treatment *basin1_out* and *basin2_out.* The pH values in the *basin2_out* and *basin1_out* presented values about 7ph to 8ph until first week of November, then lower values 7ph to 3pH to the end of November. Instead, in the *basin_in* the pH values had a constant behavior about 7.5ph to 9pH. The EC of *basin2_out* presented higher

values during the first week of October about 1500uS/cm, then it presented lower values about 800uS/cm, to the end of November with 700uS/cm. In the *basin1_out* the EC presented values from 800uS/cm to 1300uS/cm going to stabilize about 1000uS/cm to the end of October, where after that the sensor node did not saved data for two weeks anymore. At the end of November in the two basins in output, we observed same behavior of EC with lower values, about 700uS/cm. The basins in input, *basin_in,* the EC had lower values at the beginning about 1100uS/cm to 800uS/cm and the values went down to 600uS/cm to the end of November. The temperature values in the three basins varied between 20°C to 24°C in the first period of October, and it was going down to the end of November about 14°C, as we were expected for winter season. The temperature values in the two basins in output were generally related to the temperature of the wastewater in input, but in some periods the values were totally different during daytime, as shown in fig 11 -13. The ORP in the *basin2_out* presented positive values about 0.3V the first week of October and continued with negative values to the end of November about -0.4V. In the *basin1_out* the ORP was about 0.1V to -0.1V in the first period of October continuing to be negative to the end of November. In the *basin_in* the ORP values were positive 0.4V to 0.1V until first week of November, and it continued to be negative about -0.3V. It can be observed generally that in November the water parameters presented lower values with lower temperature values.

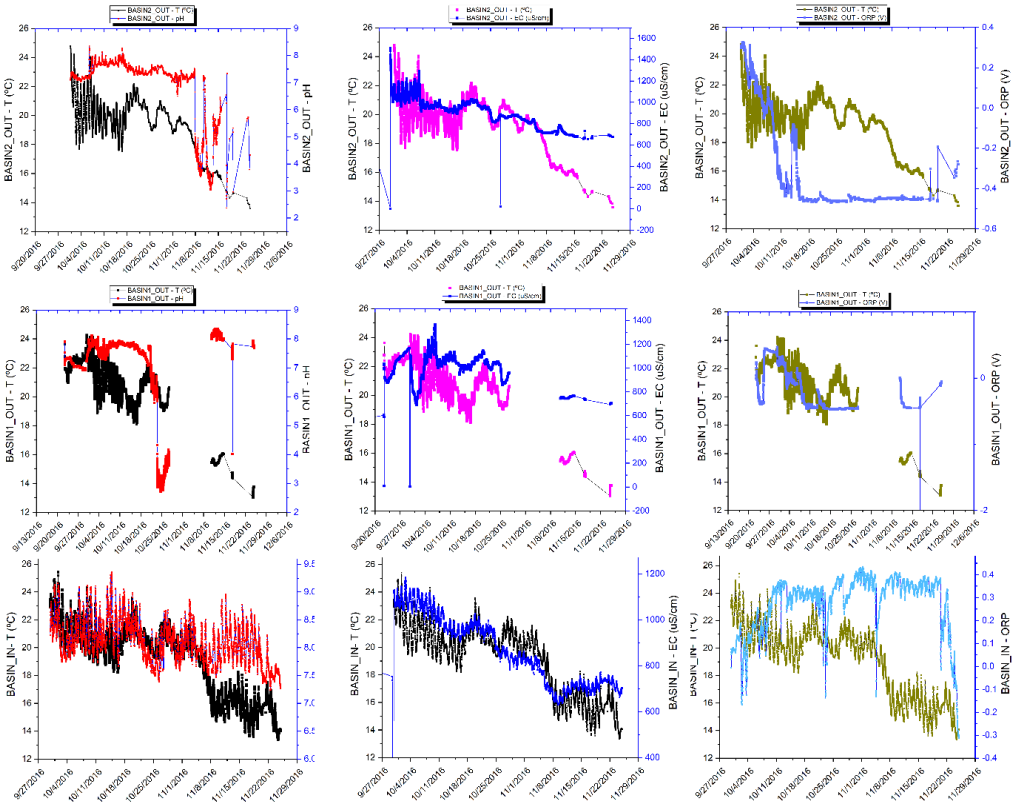

Fig.6 Basin infiltrations at SBM, water parameters in relationship with temperature.

6. Discussion

This paper focused on determining a good soil permeability and good soil contaminant retention, by caring out several experiments at a lab scale simulating infiltration basin conditions. The best soil characteristic was applied as a reactive layer in the infiltration basin so that able to improve the water quality in the wastewater treatment plant in Sao Bartolomeo de Messines. The soil characteristics of 6th, 7th, 8th and 9th columns were different and we could figure out from the results, those columns with more organic matter showed a higher soil compaction due to the washout of the particles, while those columns as 8th and 9th, composed by higher percentage in sand, presented a good permeability for more than 1 month working. During soil column experiments, different conditions were considered as using cycles of saturation and non-saturation, so that the soil column in unsaturated conditions would have had better soil oxygenation and thus oxidation of ammonia process. The 8th and 9th column were considered suitable to be used in a real scale, as a layer infiltration for the infiltration basins, even though we would never have been able to obtain same results as in the lab scale with all the environment conditions controlled. Thus, we were expecting different soil behavior in the infiltration basins, but not too much, as it can be observed in the Fig.7 the pH, EC, Eh (ORP) and temperature mean values. It can be observed that the soil column, for more than one month laboratory experiment, presented almost same mean values as in the field scale basin infiltrations, more than two-month field experiment. In the basin infiltrations, we had same mean values but there were small differences as shown in Fig.8-9.

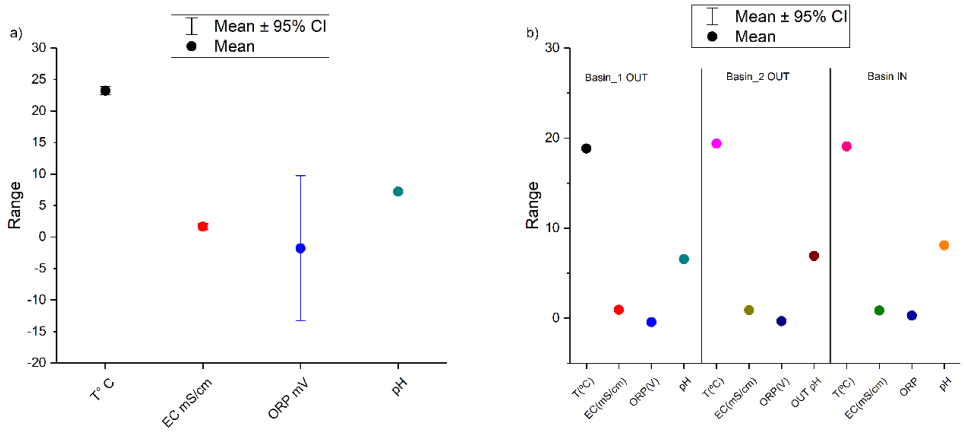

Fig.7 The mean values of water parameters, a) in the soil column, b) in the three basin infiltrations.

In the Fig. 8 – 9, it can be observed differences between the input basin and output basins, as pH values we had variability in the second basin than the first one and input basin. Instead for the ORP higher values were showed and positive values in input than in output, with small differences between the two output basins. The temperature and EC mS/cm values, presented almost same behavior in the three basins, as

mentioned for two weeks in the *basin2_out* we did not have any data, so that the box plot of temperature values is different than the other ones. Thus, there are highest pH values in input than the output in the two basins, and EC and ORP present similar mean values during the two months of measurements, in input and in output basins.

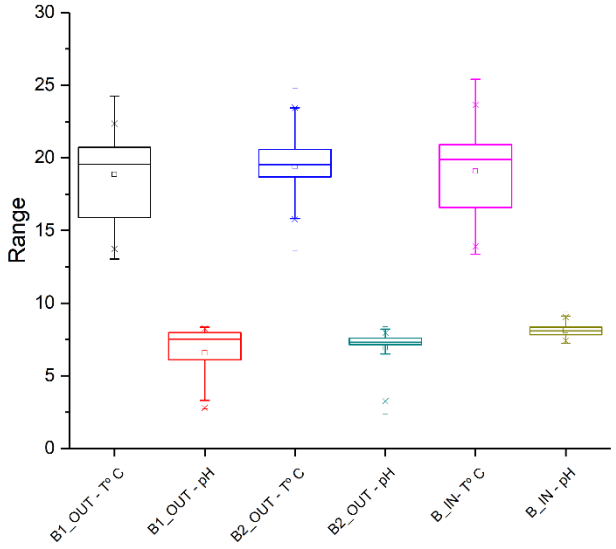

Fig.8 The mean values of water parameters, a) in the soil column, b) in the three basin infiltrations.

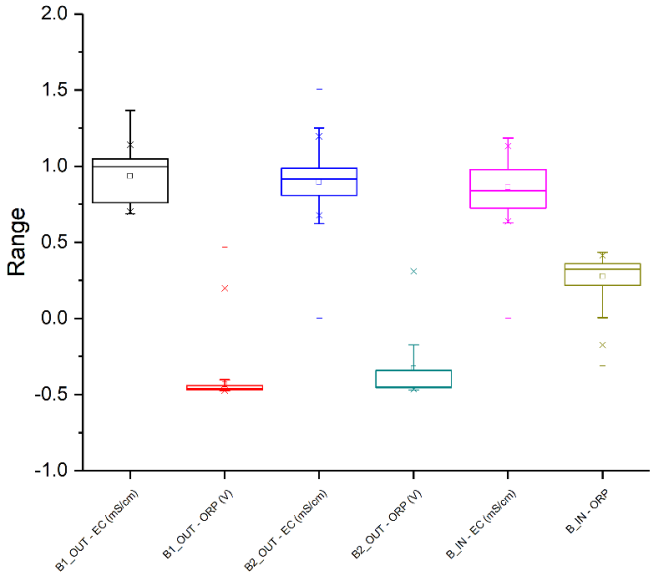

Fig.9 The boxplot of water parameters in the three basin infiltrations, a) pH and temperature, b) EC and ORP values during the two months monitored.

It is well known that the wastewater parameters could present data that can be affected due to the precipitation, in the Fig.10, one can observe that we did not have so many rainy days, and in that case, it can be observed a decrease in all the parameter values, as expected due to the dilution reaction.

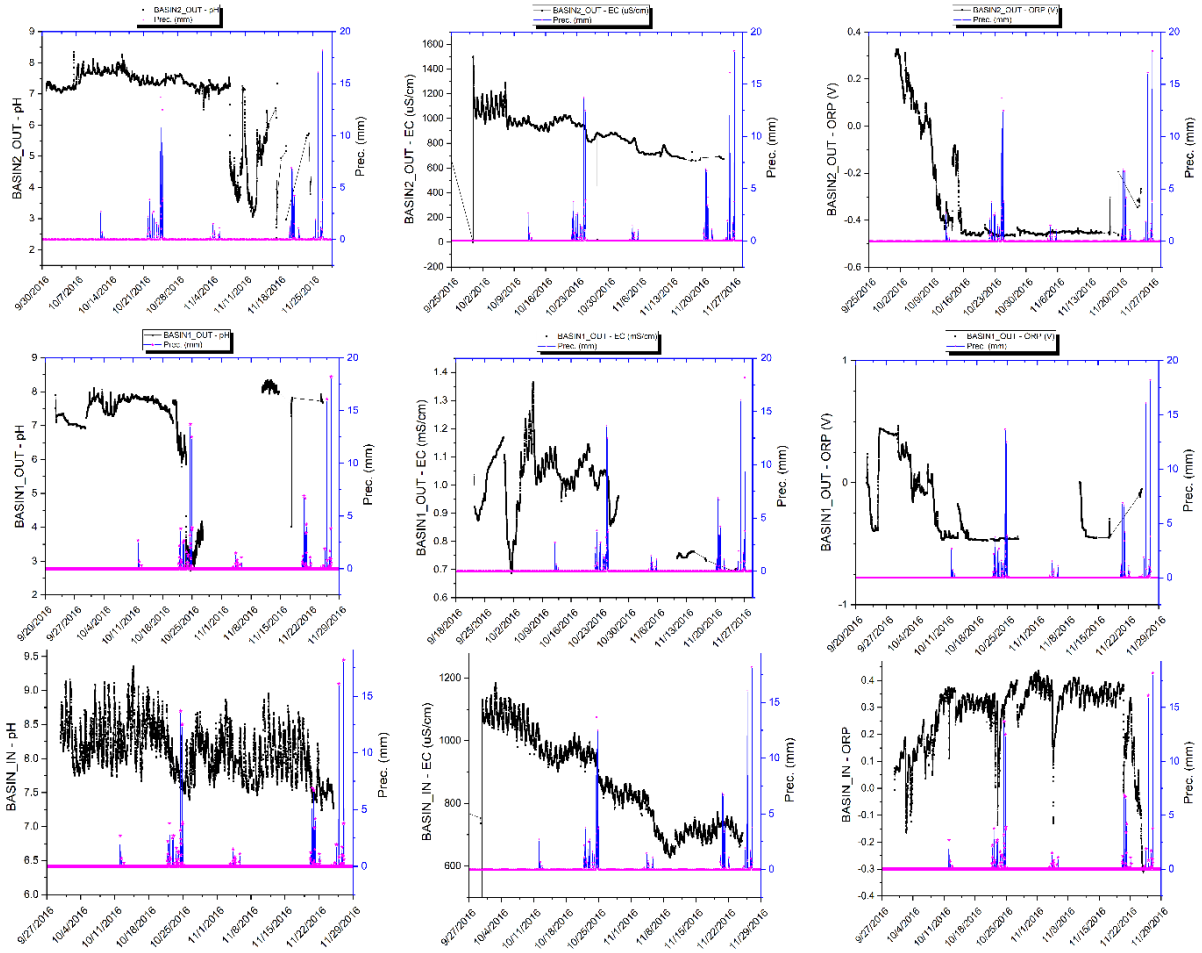

Fig.10 Relationship between water parameters and precipitation. Basin 1 sensor had a problem during a 2-week period, during which no data was therefore obtained.

We considered diurnal variations in the wastewater parameters to understand better how the temperature conditions affected the other parameters. In the Fig.11, it can be observed during daytime, an increasing on temperature *basin_in* values with the other parameters. We need to consider the activity in the Wastewater Treatment Plant of Sao Bartolomeo de Messines, first treatment of the wastewater at a certain temperature so that bacteria can be eliminated. The temperature need to be controlled in input as well as in output, since it affects the pH and EC sensors. We observed that pH in the two output basins presented lower values about 3 pH, it could be affected by temperature values as showed in the fig 12-13, it was decreasing from 24°C to 14°C and probably affected the signal of the pH sensors. The pH probe need to have a good calibration with reference solutions at the same temperatures as in the output basins. The calibration need

to be organized related to the temperature values, it is required by the sensor manufacture, it is for that also it is important to have a real-time monitoring system to decide immediately when the sensor calibrations should be done.

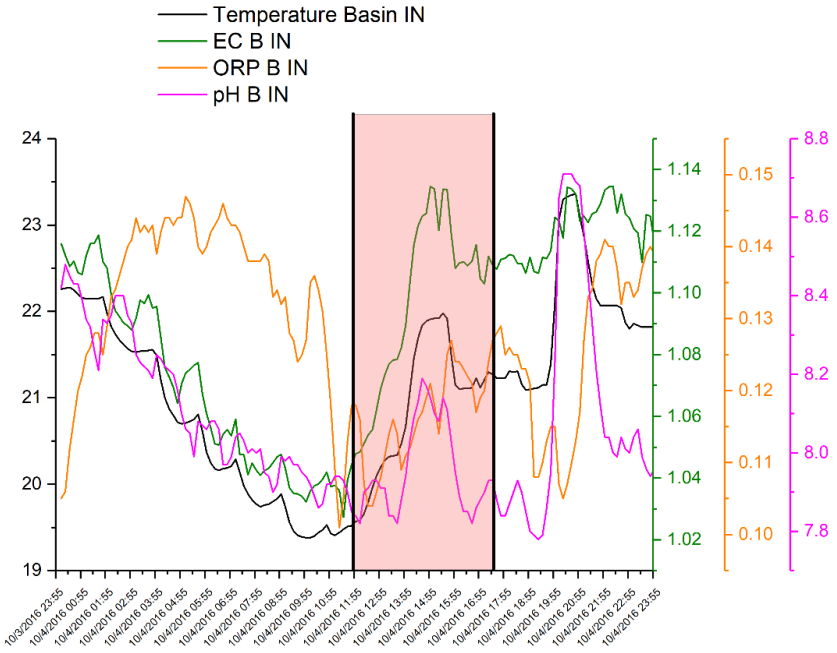

Fig.11 The mean values of water parameters in the three basin infiltrations at SBM.

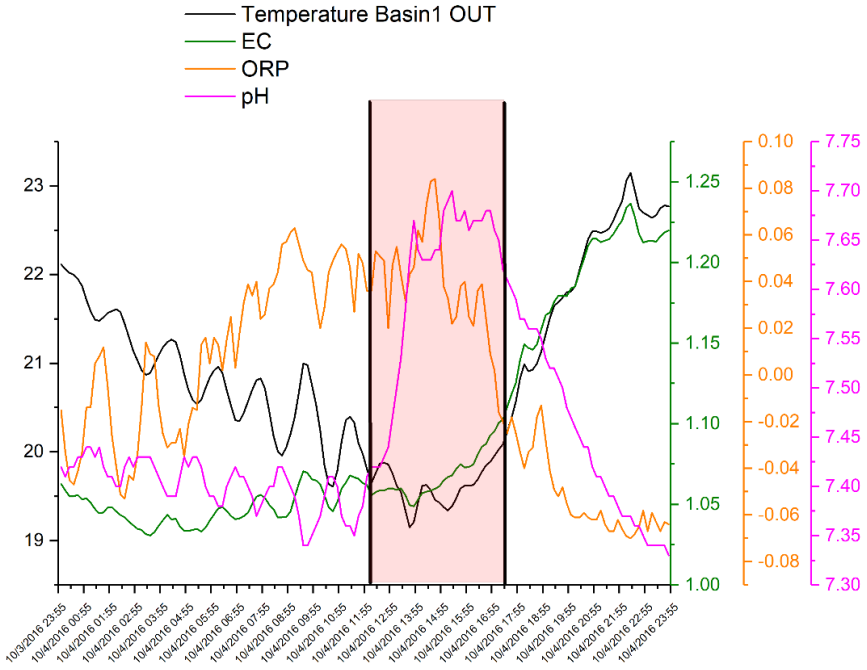

Fig.12 The mean values of water parameters in the three basin infiltrations at SBM.

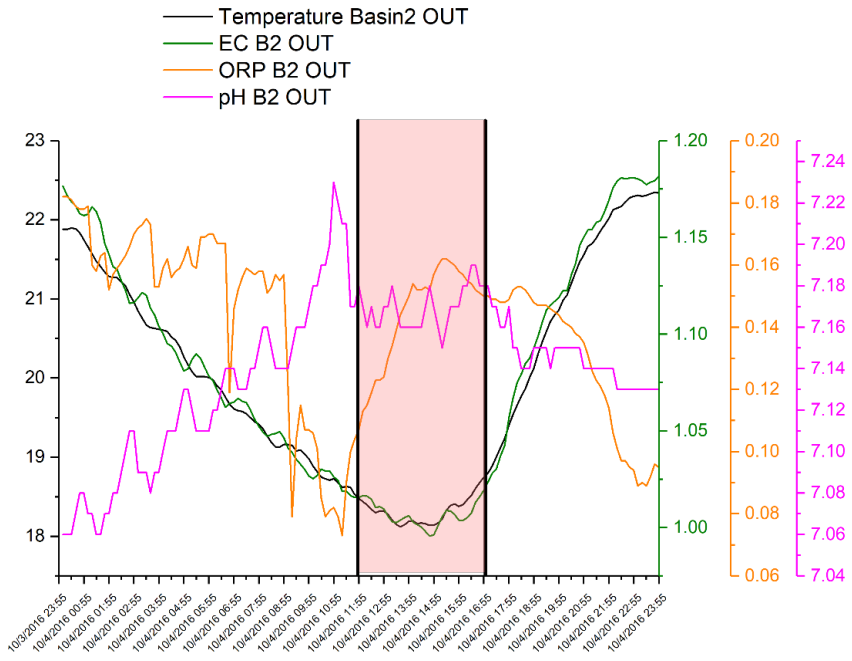

Fig.13 The mean values of water parameters in the three basin infiltrations at SBM.

7. Conclusions

All the results presented at the lab scale experiment were a little bit different than in the real scale or field experiment since we had many environment conditions not in our control. In the soil column experiment we had diminished the nitrogenous compounds and metal concentrations. The water parameters values were related to the biodegradation, chemical reactions, physical characteristic, mineralogy and organic matter into the soil. Unfortunately, in the soil column experiments we did not have the opportunity to use the new low-cost sensors and having a continuous monitoring system as it was used in the field experiment. It is recommended that the sensors must be calibrated before and during the experiment, especially if the temperature values are changing that can affect the pH sensor.

Acknowledgments

LNEC is kindly acknowledged for all support given during this project.

The research project was made possible by funding from MARSOL project, funding from the European Union's Seventh Framework Programme for Research, Technological Development and Demonstration under grant agreement no 619120, and funding from "*5 per mille*" contribution assigned to the University of Ferrara income tax return year 2013.

References All references are specified at the end of this thesis.

MEASUREMENT JOURNAL – ELSEVIER
(submitted)

Statistical Analysis of Low-Cost Water Sensors for Measuring the Electrical Conductivity

Ana M. C. Ilie [1] , João Rogeiro [2] , Carmela Vaccaro [3]
[1,3] Department of Earth Sciences, University of Ferrara, Via Saragat 1, Ferrara, Italy
[2] Departamento de Hidráulica e Ambiente, Laboratorio Nacional de Engenharia Civil, LNEC, Lisbon, Portugal

Abstract

An electrical conductivity low-cost sensor was used in a physical sandbox model that was built in LNEC's modelling facilities under MARSOL project. The artificial aquifer facility or physical sandbox model was built to conduct laboratory large scale infiltration and tracer tests, aiming to determine the soil infiltration rate and the contaminants retention and/or degradation capacity, namely to simulate Soil-Aquifer Treatment (SAT) in a Managed Aquifer Recharge (MAR) basin. Calibration and validation of the low-cost sensors was carried out before and after the experiments, by using as reference instrument a CDT diver multi-parameter groundwater datalogger. In this paper, we focused on sodium chloride tracer, to determine the concentration of electrical conductivity into the aquifer. Validation data of low-cost sensors presented an R^2 correlation coefficient of 0.77 – 0.96 and Pearson's r coefficient of 0.87 – 0.98, that confirmed the linear relationship between the two variables.

Keywords: electrical conductivity sensor, low-cost sensor, real-time data, tracer experiments, sensor validation

1. Introduction

Electrical conductivity (EC), or conductivity, is the ability of a substance to conduct an electric current. Specific electrical conductivity is the conductivity of a body of unit length and unit cross section at a specified temperature (Hem, 1989). Due to its importance, measurements of EC have become frequent in water quality related research (Laxen, 1977; Pawlowicz, 2008; Visconti et al., 2010; Siosemarde et al., 2010; McNeil and Cox, 2000; McCleskey, 2011). The dependence of electrical conductivity on concentration of solutes has been extensively investigated for aqueous solutions. A limiting law for

conductivity was developed by Onsager (1926) by using the Debye–Hückel (1924) equilibrium distribution functions. After that several studies dealt with relationship between conductivity and chemical composition of natural waters (Logan, 1961; Rossum, 1975; Hem, 1989; Hughes et al., 1994; McNeil and Cox, 2000). Most of the aforementioned research concentrates on finding the statistical correlation between the concentration of solutes and electrical conductivity in order to calculate conductivity based on the chemical composition of natural waters. The goal of developing such a method has been to provide as precise quality control method for checking water analyses as possible. There is often a strong correlation between some of the major anions and cations in natural waters (Hem, 1989; Appelo and Postma,1993), due to the presence of soluble minerals with fixed stoichiometry, such as calcite, gypsum or halite. Electrical conductivity (EC) has become a proven and effective indicator for detection of dissolved CO2 in a vadose zone (Strazisar et al., 2009; Zhou et al., 2012) or in a shallow aquifer (Denchik et al., 2014; Trautz et al., 2013; Lamert et al.,2012; Auken et al., 2014). The geochemical processes following a CO2 leakage into a shallow aquifer include reduced pH due to the formation of carbonic acid and elevated EC due to dissolved CO2 and mineral dissolution in the ground-water (Dethlefsen et al., 2013; Cahill and Jakobsen, 2013). New technologies are emerging to enable remote autonomous sensing of our water systems and subsequently meet the demands for high temporal and spatial monitoring. Advances in communication and sensor technology have provided a catalyst for progress in remote monitoring of our water systems (Diamond et al., 2008). Wireless sensor networks have the potential to be very powerful tools to address several operational issues, including pollution monitoring (Khedo et al., 2010; Basha et al., 2008), emergency response during catastrophic events (Barrenetxea et al., 2008) or environmental monitoring (Marcelli et al., 2014).

2. Materials and methods

The artificial aquifer facility (or physical sandbox model) was built under MARSOL project and used to conduct laboratory large scale infiltration and tracer tests, both for saturated and non-saturated conditions. This facility was used to study Soil-Aquifer Treatment (SAT) simulating a Managed Aquifer Recharge (MAR) infiltration basin. It can be used to simulate other situations such as risk of contaminants leaching from a spill; reactive barriers for groundwater rehabilitation; contaminants release from a contaminated porous material. The physical sand box is approx. 3.5 m long, 1 m wide and 2 m high and was filled with sandy soil. The area was divided in up to three different compartments to perform simultaneous experiments and was equipped with three piezometers and monitoring devices (Leitao et al., 2016).

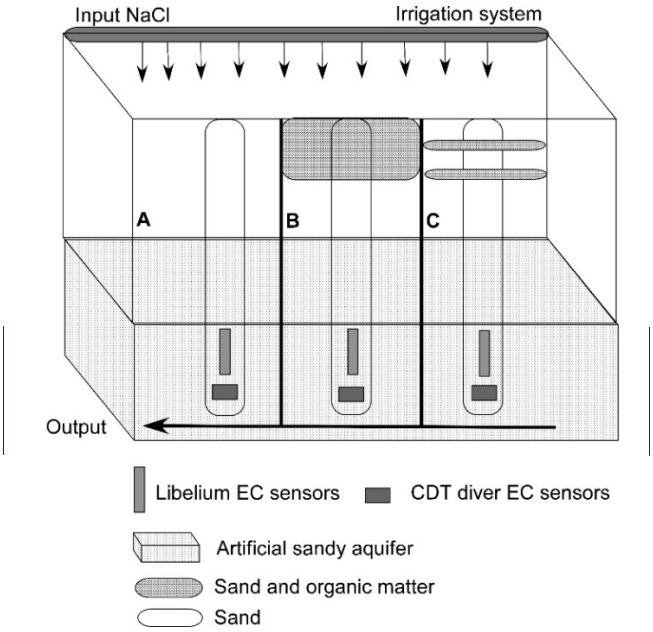

Figure 1. Design of the physical sandbox model and deployment of the Libelium low-cost sensors and CDT divers inside the piezometers.

In the section A it was used a sandy soil; in section B it was used a mixed soil, natural soil (60%) with organic matter (40%), and the sandy soil; in section C it was used sandy soil, with two layers of mixed soil (Leitao et al, 2016). The Libelium sensor nodes and CDT divers were installed in each section A, B, C at a distance of 5 cm between them. Real time data was used in both of experiments.

In each section (A, B and C), two NaCl tracer experiments were performed to analyze the concentration of the electrical conductivity (EC) into the aquifer. The 1st experiment was performed by flooding the soil surface with 0.5 m^3 of water. This experiment was done May 31st to June 1st, 2016. The NaCl tracer was about 500 mg/L used in the experiment as well as hydrocarbons were used 21 mg/L.

The 2nd experiment was performed with the tracer applied in powder and with irrigation system working on. This experiment was done from June 1st to June 3rd 2016.

The sensors used in the experiments are the Libelium low-cost sensors, conductivity sensors. The conductivity sensor is a two-pole cell whose resistance varies in function of the conductivity of the liquid it is immersed in. That conductivity will be proportional to the conductance of the sensor (the inverse of its resistance), multiplied by the constant cell, in the case of the Libelium sensor around 1cm-1, leading to a value in Siemens per centimeter (S/cm). To power the conductivity sensor an alternating current circuit has been installed to avoid the polarization of the platinum electrodes, the sensor consumption is 2.5mA. The magnetic field between the two electrodes of the conductivity sensor may be affected by objects close to the probe, so it will be necessary to maintain the sensor at least five centimeters apart from the surroundings.

In the case of the conductivity sensor the readConductivity() function will return the resistance of the sensor in ohms. In order to convert this value into a useful conductivity unit (uS/cm) function conductivityConversion() will have to be invoked with the calibration parameters of the sensor. To get an accurate measurement it is recommended to calibrate the conductivity sensor to obtain a precise value of the cell constant. Although a single point calibration should be theoretically enough, a two-point calibration is advisable to compensate for side effects of the circuitry, such as the resistance of the sensor wire or the connector. For a proper calibration two solutions of a conductivity as close as possible to that of the target environment should be used. There are three different Calibration kits for Conductivity: K=0.1, K=1; K=10. The K factor is related to the salinity of the water we want to measure. Each calibration kit takes two solutions, K=0.1 - around µS 220 - around µS 3000; K=1 - around µS 10500 - around µS 40000; K=10 - around µS 62000 - around µS 90000. Once the probe is immersed in the solution and the output is steady, the value of the conductivity resistance is obtained, (www.libelium.com). A periodic recalibration of the sensors is highly advisable to maintain an accurate measurement along time to correct changes owed to a drift output, polarization or wear. These sensors were used for other experiments, to determine their fast response in dry and wet conditions, as it is known the sensors need to be fixed all the time in the water, (Ilie et al, 2017).

As reference instrument was used CDT diver, that measures the water's electrical conductivity in millisiemens per centimetre (mS/cm). Conductivity range of 0 to 120 mS/cm, accuracy ±1% of reading with a minimum of 10 µS/cm, resolution 0.1% of reading with a minimum of 1 µS/cm for 30 mS/cm range and 10 µS/cm for 120 mS/cm range. The conductivity is measured using a 4-electrode measuring cell. Each CTD-Diver is calibrated for pressure, temperature and conductivity. First the CTD-Diver is calibrated for pressure and temperature. Then the factory calibration of the conductivity sensor is performed. The CTD-Diver immersed in a 6 ascending conductivity values. The exact value of the conductivity of the liquid is determined with a calibrated reference sensor. During the calibration check of the conductivity sensor, the CTD-Diver is immersed in 6 conductivity fluids: (0.15, 0.9, 3.0, 12, 35 and 75) mS/cm. The values measured by the CTD Diver are compared to the reference values, this determines whether the deviation is within the limits of the specifications. The factory calibration is stored permanently in the CTD-Diver.

3. Results

This paper aimed to understand the accuracy of the low-cost sensors, by using them for many experiments. The 1st experiment was carried out for 24 hours, between 11 a.m. of May 31st to 11 a.m. of June 1st, using salt tracer. In the fig. 2, one can see the behavior of EC at the three sections. In the fig.2 datetime values on

x-axis and the electrical conductivity (EC) response from CDT divers and Libelium sensors on the y-axis. When the experiment started with the tracers, it took time to arrive into the aquifer.

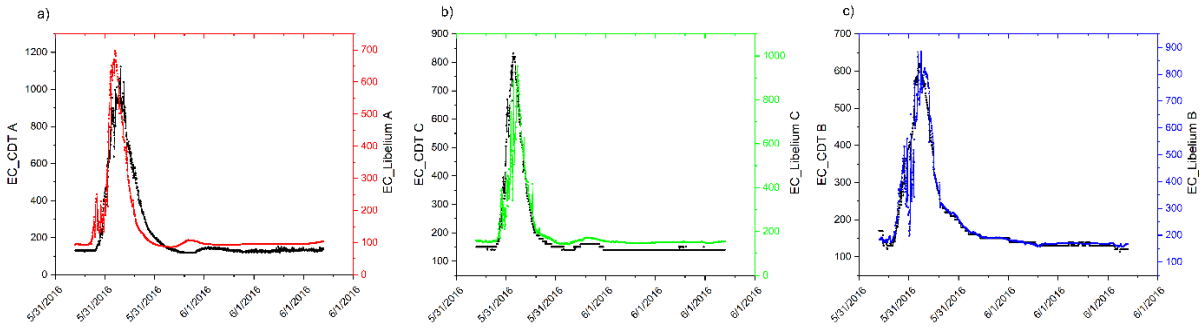

Figure 2. Temporal variation of EC at the 1st experiment, CDT and Libelium sensors.

In the fig. 3, EC measurements from CDT divers can be observed in each section. The 1st experiment started at 11 a.m., and as we can see in the section B after one hour and a half the tracer reached the aquifer, instead for the other sections the tracer reached the aquifer after 2 hours. The behavior of EC in the section B was different than section A and section C. The EC peak was after 4 hours when started the experiment in section B. Instead for section A the peak of EC was after 5 hours, and after 3 hours in section C. The EC values turn at the tap water quality after 5 hours in the section C, instead in the section A and B it took 7 hours to have same water quality.

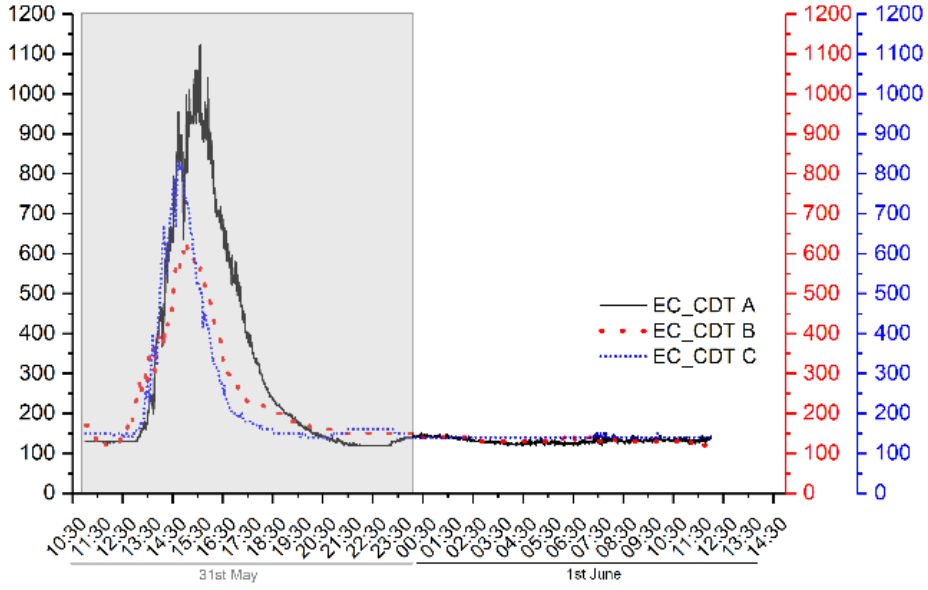

Figure 3. The 1st experiment, EC measurements with CDT divers in each section.

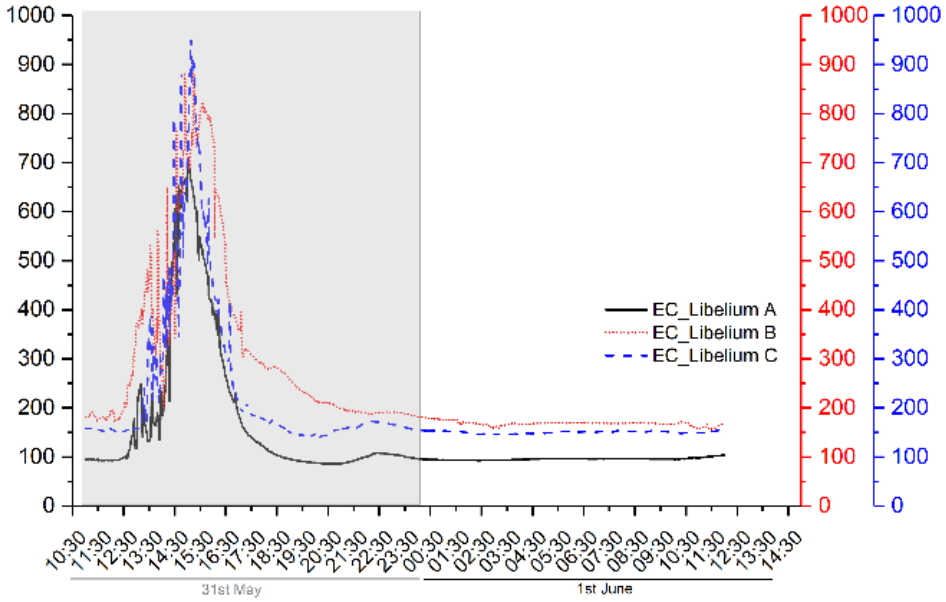

Figure 4. The 1st experiment, EC measurements with Libelium low-cost sensors in each section.

In the fig. 4, the behavior of EC from Libelium sensors is a little bit different, seems to be noisier in the sensor response. The first EC measurements do not have same values, the lowest EC values is in section A, and the highest in the section B. The values from these sensor, started to go up at the same time after the tracer was used. In the section B, we noticed a certain up and down of the EC values, than the other sections. After the experiment end, the EC measurements presented same values before the experiment started. To know the accuracy of these sensors, statistical analysis was carried out, using OriginPRO software.

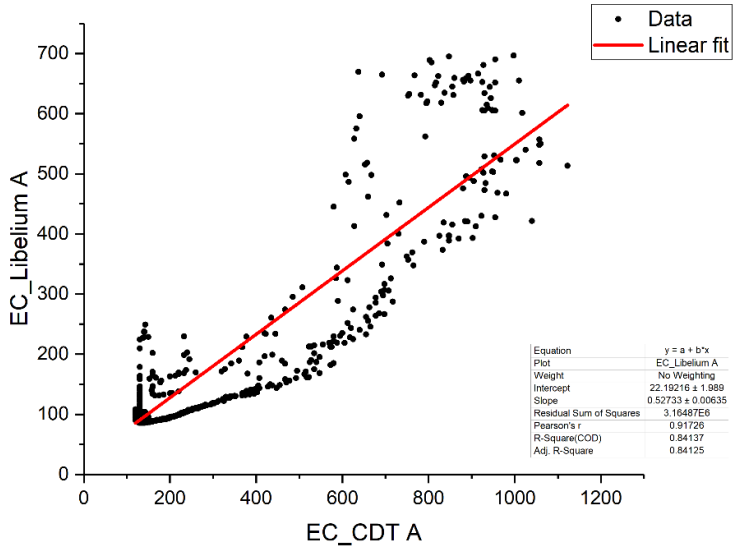

Figure 5. Linear fit between Libelium sensor node A against CDT diver (reference instrument), 1st experiment.

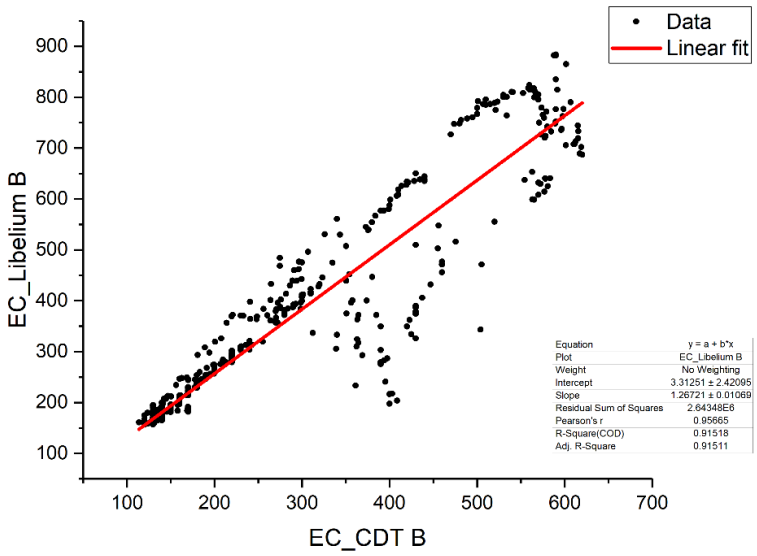

Figure 6. Linear fit between Libelium sensor node B against CDT diver (reference instrument), 1st experiment.

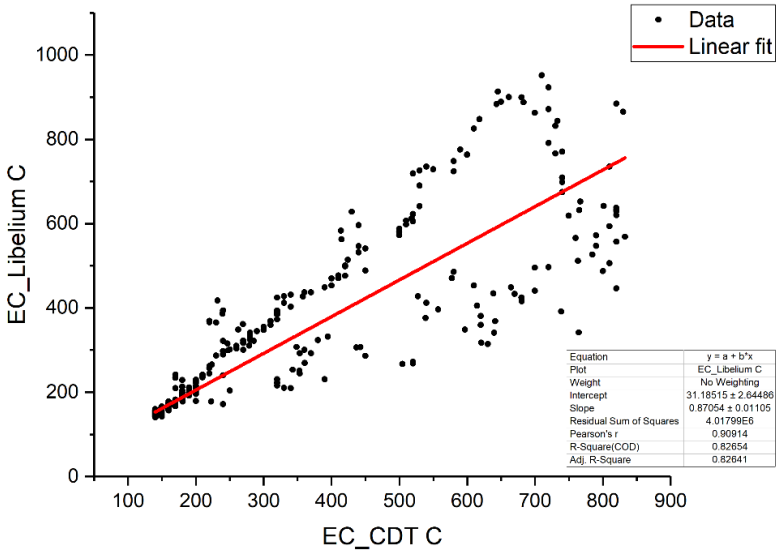

Figure 7. Linear fit between Libelium sensor node C against CDT diver (reference instrument), 1st experiment.

Based on the descriptive statistical analysis a conclusion could me made about the relationship between the low-cost sensor and the reference instrument CDT diver, in section A, fig. 5. An R^2 correlation coefficient of 0.84 and Pearson's r coefficient of 0.91 confirmed the linear relationship between the two variables. In section B, fig.5., An R^2 correlation coefficient of 0.82 and Pearson's r coefficient of 0.90 confirmed the

linear relationship between the two variables. In section C. An R^2 correlation coefficient of 0.82 and Pearson's r coefficient of 0.90 confirmed the linear relationship between the two variables.

Since no pattern could be found on the residual plots, fig. 8., between low-cost sensor and reference instrument CDT diver, a relationship is affirmed. Based on the regular residual plot with the count, a log normal distribution for the variance can be observed. Most of the points lie around the residual value of 0 and hence verifies the regression model. The normal probability plot of the residual shows that the errors are linear in the beginning and deviate from the straight line later.

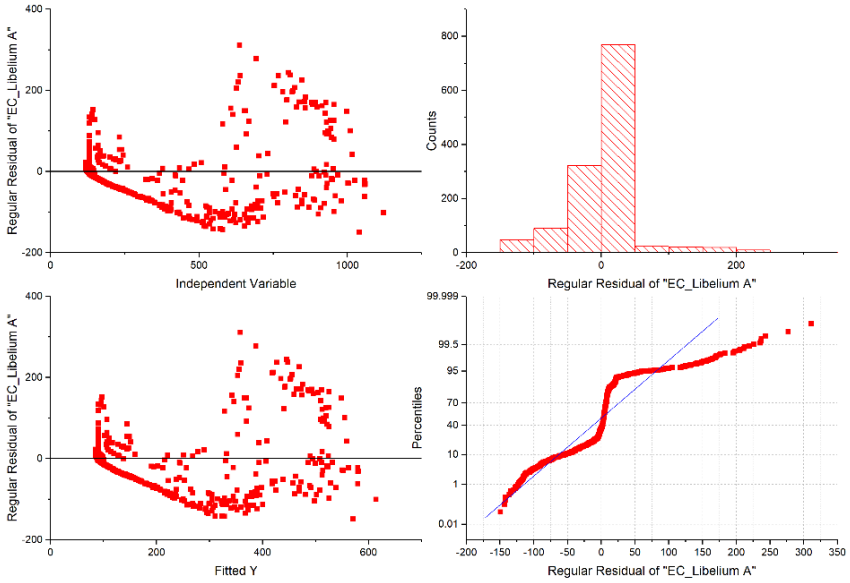

Figure 8. Residual plot of Libelium node A, 1st experiment.

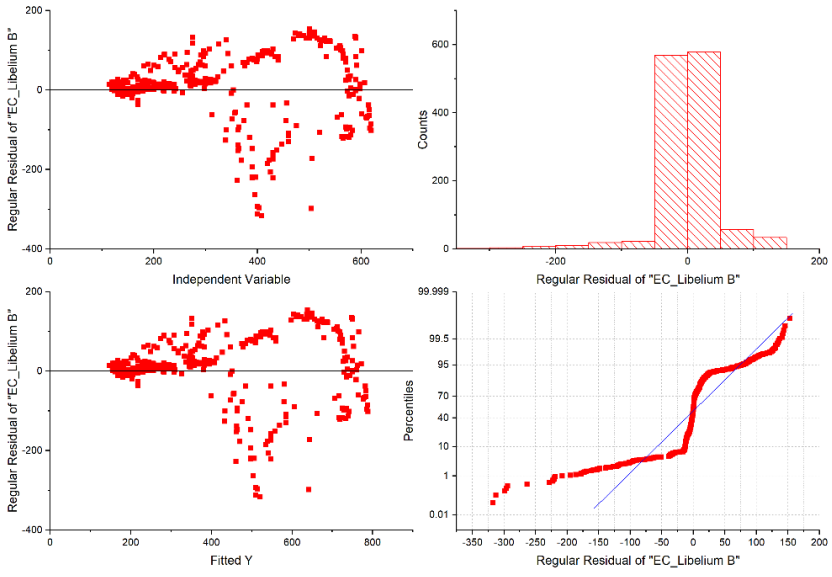

Figure 9. Residual plot of Libelium node B, 1st experiment.

No clear pattern could be found on the residual plots, fig. 9, between low-cost sensor and reference instrument which signifies the random error variance. Based on the regular residual plot with the count, a normal distribution is observed. In this case too, most of the data points lie around 0, which verified the regression model. The normal probability plot of the residual shows that the errors are close to the straight line which confirms the deduction made above.

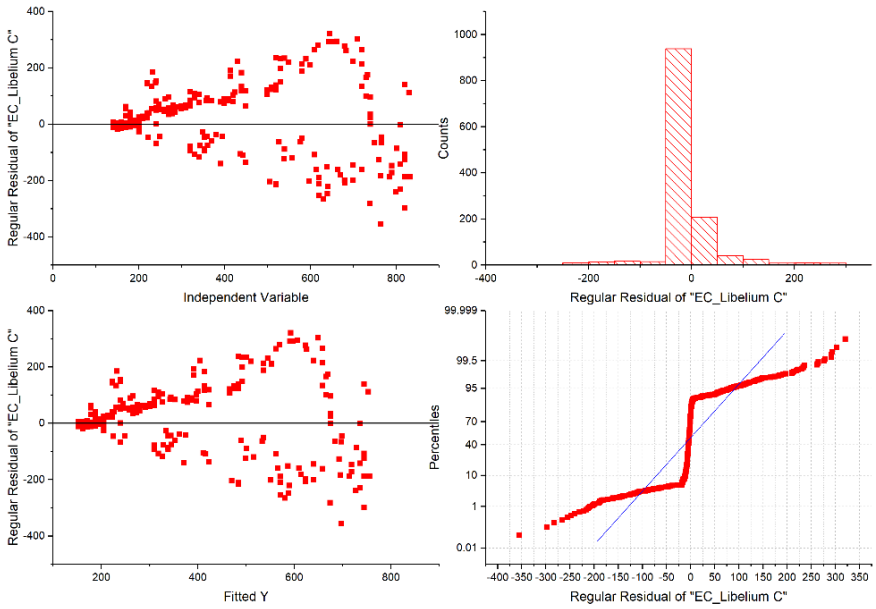

Figure 10. Residual plot of Libelium node C, 1st experiment.

A similar trend as node B is observed in this case, fig.10. There is no clear pattern on the residual plots between low-cost sensor – node C and reference instrument which signifies the random error variance. A normal distribution for the regular residual plot is observed here as well, however major part of the variance with error lies on the negative side. This could be verified with the data points lying around the straight line in the probability plot.

The 2nd experiment was carried out for 48 hours, between 12 p.m. June 1st to 12 p.m. June 3rd. In this experiment, the same tracer (fertilizer and NaCl) and concentrations were used, but no hydrocarbons (TH). The tracer was placed as powder on soil surface and it was slowly washed down by the irrigation system.

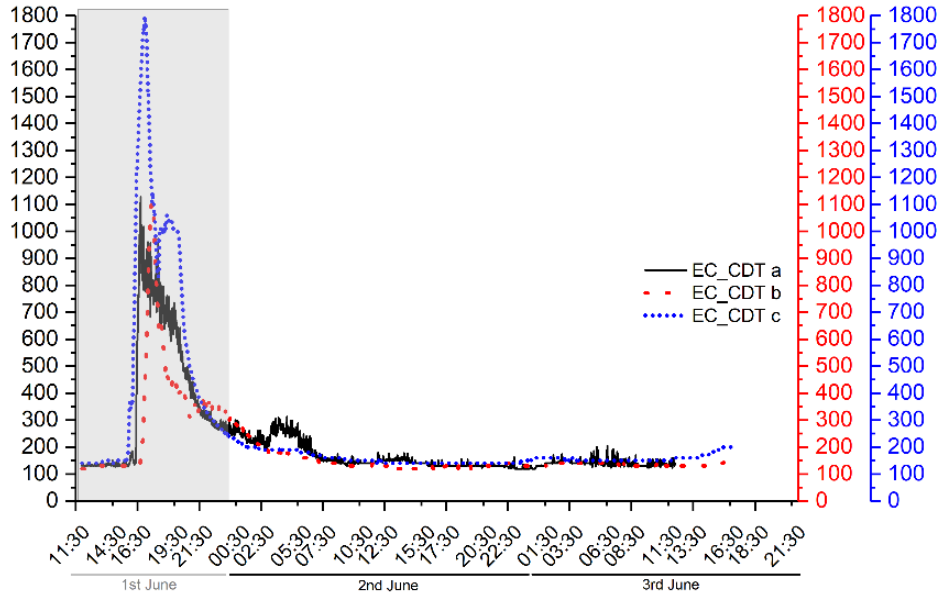

Figure 11. The 2nd experiment, EC measurements with CDT divers in each section.

The 2nd experiment started at 12 p.m. The tracer arrived into the aquifer after almost 3 hours, first in C section with a highest EC value. The behavior of EC was different in each section related to the soil characteristic, fig.11. After almost 18 hours the EC behavior presented same values for a tap water quality. In this experiment, the tracer was used as a powder so the tracer infiltration was slower than previous experiment.

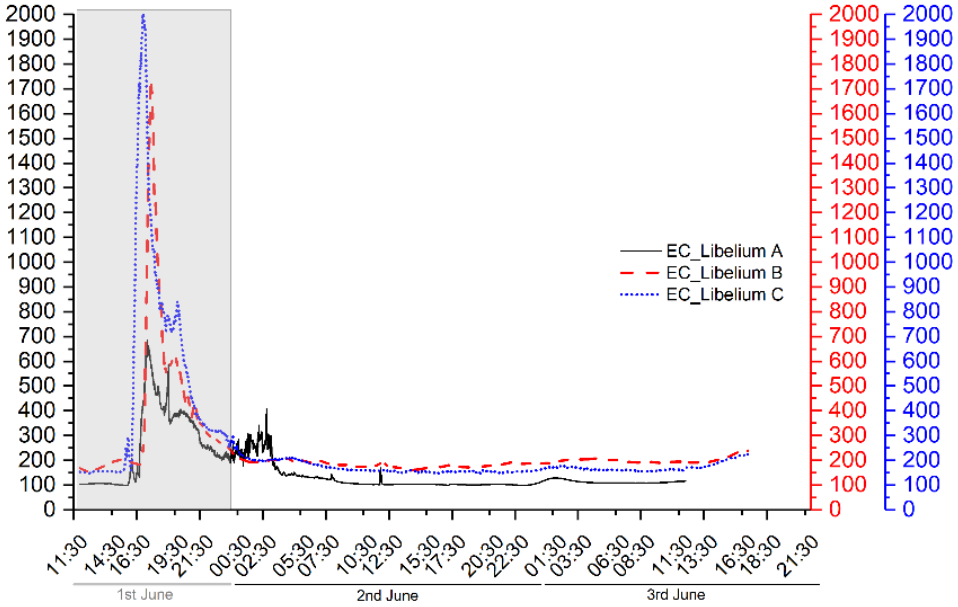

Figure 12. The 2nd experiment, EC measurements with Libelium sensors in each section.

In the fig.12 the behavior of EC from Libelium sensors is a little bit different. The first EC measurements did not have same values, the lowest EC values is in section A, and the highest in the section B. The values from these sensor, started to go up almost at the same time after the tracer was used. The node B presented highest EC values than the CDT diver, and lower EC values in Libelium node A.

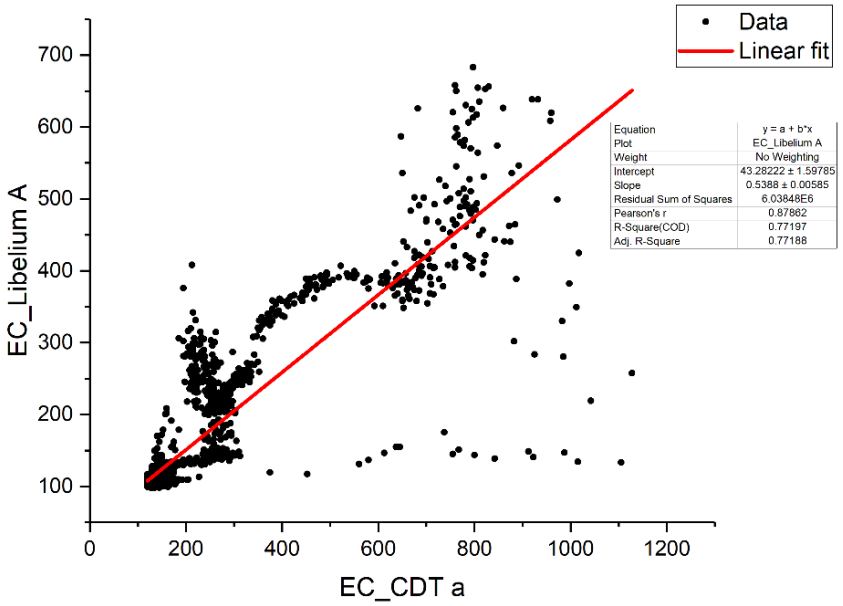

Figure 13. Statistical analysis and linear fit of Libelium node A, 2nd experiment.

Based on the descriptive statistical analysis a conclusion could me made about the relationship between the low-cost sensor and the reference instrument CDT diver, in section A, fig.13. An R^2 correlation coefficient of 0.77 and Pearson's r coefficient of 0.87 confirmed the linear relationship between the two variables.

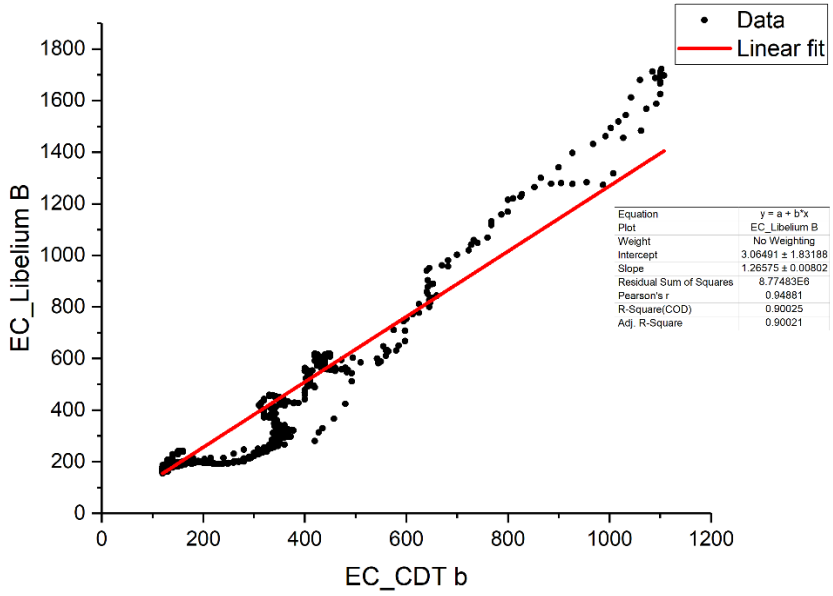

Figure 14. Statistical analysis and linear fit of Libelium node B, 2nd experiment.

Based on the descriptive statistical analysis a conclusion could me made about the relationship between the low-cost sensor and the reference instrument CDT diver, in section B, fig.14. An R^2 correlation coefficient of 0.90 and Pearson's r coefficient of 0.94 confirmed the linear relationship between the two variables.

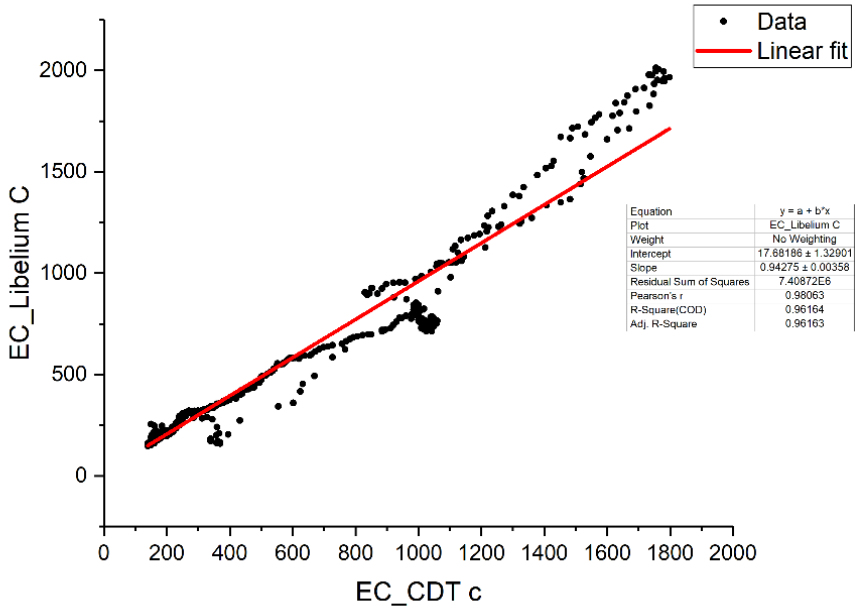

Figure 15. Statistical analysis and linear fit of Libelium node C, 2nd experiment.

Based on the descriptive statistical analysis a conclusion could me made about the relationship between the low-cost sensor and the reference instrument CDT diver, in section C, fig.15. An R^2 correlation coefficient of 0.96 and Pearson's r coefficient of 0.98 confirmed the linear relationship between the two variables.

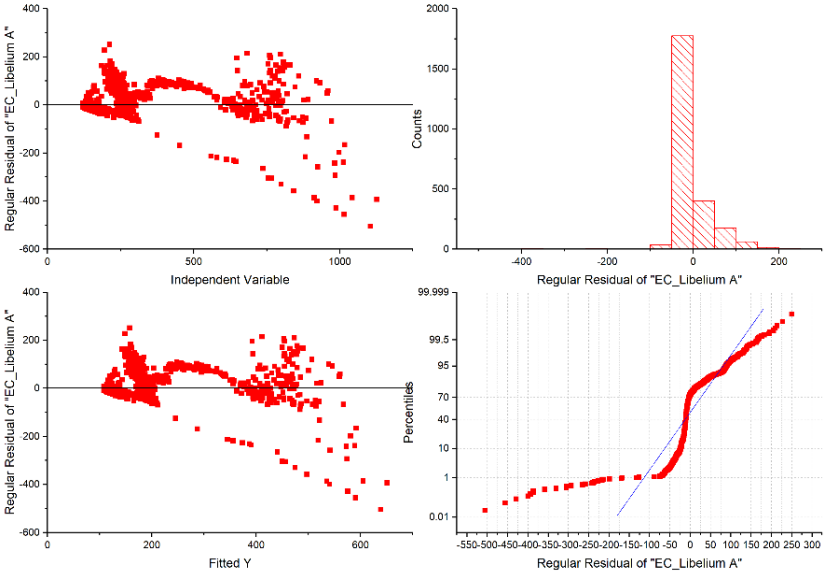

Figure 16. Residual plot of Libelium node A, 2nd experiment.

There is no clear pattern on the residual plots between low-cost sensor – node A and reference instrument which signifies the random error variance, fig.16. A normal distribution for the regular residual plot is observed here as well, however major part of the variance with error lies on the negative side. This could be verified with the data points lying around the straight line in the probability plot.

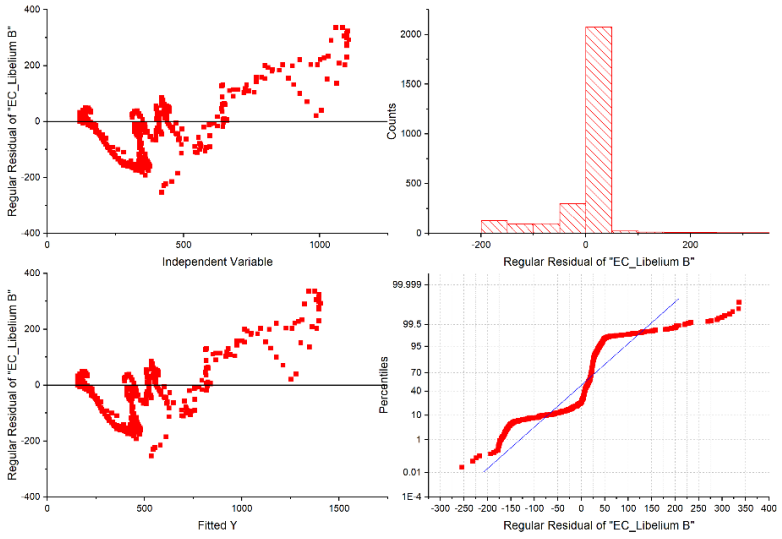

Figure 17. Residual plot of Libelium node B, 2nd experiment.

There is no clear pattern on the residual plots between low-cost sensor – node B and reference instrument which signifies the random error variance, fig.17. A normal distribution for the regular residual plot is observed here as well, however major part of the variance with error lies on the positive side. This could be verified with the data points lying around the straight line in the probability plot.

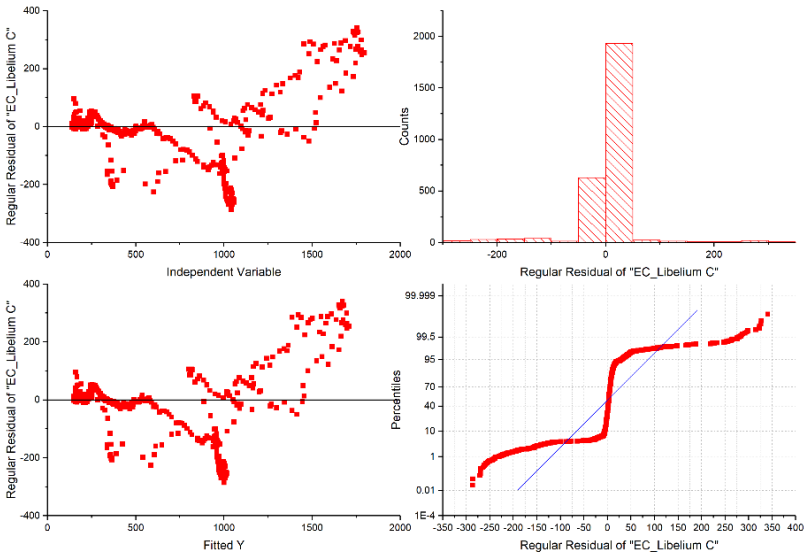

Figure 18. Residual plot of Libelium node C, 2nd experiment.

There is no clear pattern on the residual plots between low-cost sensor – node C and reference instrument which signifies the random error variance, fig.18. A normal distribution for the regular residual plot is observed here as well, however major part of the variance with error lies on the negative side as well as on the positive side. This could be verified with the data points lying around the straight line in the probability plot.

4. Conclusions

Low-cost sensors were used in the experiments for measuring electrical conductivity sensor and to determine their accuracy. The conductivity sensors are important to determine increase of salinization and pollution in groundwater systems. The benefits of these sensors EC-Logger components could typically be acquired for about $200 USD, easily powered the system runs on two 9-volt (V) and 5- volt (V) batteries, lightweight as designed making it easily transported and operable by a single person, one person can easily operate EC-Logger and record measurements. Real time data also is an important factor to be considered, so that one can immediately understand if pollutants are released to the ground and make their way down into groundwater systems. With low-cost sensors can be designed several nodes to be used in a groundwater

system, lakes, rivers and get an idea about diurnal and temporal variations, spatial distribution of water parameters.

Acknowledgments

LNEC is kindly acknowledged for all support given during this project.

The research project was made possible by funding from MARSOL project, funding from the European Union's Seventh Framework Programme for Research, Technological Development and Demonstration under grant agreement no 619120, and funding from "*5 per mille*" contribution assigned to the University of Ferrara income tax return year 2013.

References

All references are specified at the end of this thesis.

Chapter 4

IV. DISCUSSIONS, CONCLUSIONS AND RECOMMENDATIONS

Smart Sensor Technology for Environmental Monitoring Applications

The new monitoring system technology give us a huge opportunity to monitor for a long period in real time different environments (Air – Soil -Water). Nowadays is extremely important to understand the behaviour of contaminants, pollutants as well the accuracy of low-cost sensors used in the devices. Since the environments are so vulnerable to industrial activities, as Oil and Gas production or Natural Gas Storage, it is extremely important to consider the possibility of using so many devices with new low-cost gas sensors, since the comercial instruments for gas measurements cost more than 10000$, as Picarro or Licor. This consideration is useful as well for the Water Sensors, the Hanna Instruments cost too much, than the low-cost sensors. Obviously, we need to consider not just the price of the new sensors but their accuracy too. This PhD research project aimed to understand the characteristics of the new sensors, how do they work in differents environment conditions and which are the parameters that affect the sensor signal (response). So that, new instruments were built for Air – Soil - Water quality monitoring system, after the comercial instruments were used in the field and were carried out all of the issues found during several field measurments campaign. Most of the new low-cost sensors came out with a calibration by the company itself, and this does not allow us to use them without a right calibration in the laboratory and in the field since the meteorological parameters could affect the sensor signal. I tried also to use the sensors without a further calibration by using the sensor information from the datasheet itself, making several linear regressions and understand the sensor accuracy. Obviously, as the temperature and humdity behaviour was changing, the accuracy was too low. Furthermore, laboratory and field calibrations were done and the results presented the required qualities so far, good accuracy with a R^2 (0.70 – 0.94) in connection with temperature and humidity behaviour, and RMSE (0.01 ppm – 11 ppm), although the low price of these sensors. The electrochemical sensors, of 5$ price, have presented a bad correlation with the reference instruments, low accuracy and for this reason, they were not used anymore. The price of low-cost sensors goes from 5$ to 100$ each, and it was found that the good sensor signal was figured out by those who price was about 100$. Each instrument that I built at University of Ferrara and University of Colorado Boulder, employed low-cost NDIR, metal oxide and electrochemical type gas sensors as well as temperature, pressure, and humidity sensors, for Air – Soil Quality monitoring system, trying to figure out the concentration of CH4 and CO2, as well as CO, O2, O3, Voc. Since the sensors are so sensitive to

temperature and humidity, several experiments were done, especialy for CO2 and CH4 gas sensors. Issues came out when the temperature was too low, in the lab calibration process, I used less than 5°C for methane Figaro gas sensors, and I obtained just noise on signal sensor. Instead in the field calibration process, the Figaro gas sensor gave good correlation and good R^2 – RMSE (0.93, 0.01 ppm). The experiments that I have done on temperature and humidity control, with 2 instruments gave us interesting results. For those sensors inside a shelter with temperature controlled (air conditioner ~20°C), calibration model was less accurate than those sensors deployed outside in the field (13°C – 45°C). The new low-cost sensors can be used in diferent environments conditions, and it is extremely recomended to calibrate them as often as possible. These instruments were built by using real time data, GPS and wind speed and direction. The waterproof cases are light, easily to be transported and small dimensions.

The water sensors are different than the gas sensors, I did not find issues on calibration process, and they presented good results in correlation with reference instruments (HANNA). The water sensors cost about 40$ to 300$. In connection with the environment conditions one should use a specific water sensor. If we do have water parameter measurements (pH, EC, ORP, DO, T°C) in rivers, so high energy, one need to make sure the sensors will not be affected by the fast stream of water or by the sediments. If we do have water parameter measurements in lakes, the sensors need to be protected by special filters so that the fine sediments will not get dirty the sensors. Water sensors calibration as well is recommended as often as possible, and the solution used for the water sensors as calibration model, need to be at the same temperature as the environment under control. All codes used to program the microcontrollers and perform the multiple linear regression are not included, it will requiere so much time to explain all the program languages C++, python and matlab code functions used as well as raw data are not included because they cannot be interpreted in concentrations without the regression model codes.

A.B.A. Dow, A. Sklorz, W. Lang, A microfluidic preconcentrator for enhancedmonitoring of ethylene gas, Sensors and Actuators A: Physical 167 (2011)226–230.

Abdoh, A., Pilkington, M., 1989. Radon emanation studies of the Ile Bizard Fault, Montreal. Geoexploration 25, 341–354.

Abel, C. D. T. (2014) Soil Aquifer Treatment - Assessment and Applicability of Primary Effluent Reuse in Developing Countries. Submitted in fulfilment of the requirements of the Board for Doctorates of Delft University of Technology and of the Academic Board of the UNESCO-IHE Institute for Water Education for the Degree of Doctor. CRC Press/Balkema. 187pp.

Allen Jr., L.H., Albrecht, S.L., Colon-Guasp, W., Covell, W.S.A., Baker, J.T., Pan, D., Boote, K.J., 2003. Methane emissions of rice increased by elevated carbon dioxide and temperature. Journal of Environmental Quality 32, 1978e1991.

Al-Shereideh, S.A., Bataina, B.A., Ershaidat, N.M., 2006. Seasonal variations and depth dependence of soil radon concentration levels in different geological formations in DeirAbu-Said district, Irbid e Jordan. Radiat. Meas. 41, 703e707

Almeida, C.; Mendonça, J.L.; Jesus, M.R.; Gomes, A.J. (2000) – Sistemas Aquíferos de Portugal Continental, Relatório. INAG, Instituto da Água. Lisboa. Doc. Electr. CD-ROM.

Ambus, P., Robertson, G.P., 1999. Fluxes of CH4 and N2O in aspen stands grown under ambient and twice-ambient CO2. Plant and Soil 209, 1e8.

Amy, G., & Drewes, J. (2007). Soil aquifer treatment (SAT) as a natural and sustainable wastewater reclamation/reuse technology: Fate of wastewater effluent organic matter (EfOM) and trace organic compounds. Environmental Monitoring and Assessment, 129(1–3), 19–26.

Amorosi A., Colalongo M.L., Fiorini F., Fusco F., Pasini G., Vaiani S.C. & Ssrti G. (2004) - Palaeogeographic and palaeoclimatic evolution of the Po Plain from 150-ky core records. Global and Planetary Change, 40, 55-78.

Appelo, C.A.J., Postma, D., 1993. Geochemistry, Groundwater and Pollution. A.A. Balkema Publishers, Rotterdam.

Arizaga, J.; de la Calleja, J.; Hernandez, R.; Benitez, A. Automatic Control for Laboratory Sterilization Process based on Arduino Hardware. In Proceedings of the 22nd International Conference on Electrical Communications and Computers (CONIELECOMP), Cholula, Puebla, 27–29 February 2012; pp. 130–133.

Artiola, J.F., Pepper, I.L., Brusseau, M. (Eds.). (2004). *Environmental Monitoring and Characterization*. Burlington, MA: Elsevier Academic Press.

Auken, E., Doetsch, J., Fiandaca, G., Christiansen, A.V., Gazoty, A., Cahill, A.G.,Jakobsen, R., 2014. Imaging subsurface migration of dissolved CO2in a shallowaquifer using 3D time lapse electrical resistivity tomography. J. Appl. Gerontol.101, 31–41.

Azzolina NA, Small MJ, Nakles DV, Bromhal GS. Effectiveness of subsurface pressure monitoring for brine leakage detection in an uncertain CO2 sequestration system. Stoch Env Res Risk A. 2014;28(4):895-909.

Bachu, S., Celia, M.A., 2009. Assessing the Potential for CO2Leakage, ParticularlyThrough Wells, from Geological Storage Sites, Carbon Sequestration and ItsRole in the Global Carbon Cycle. AGU Monograph, pp. 203–216.

Basha E.A., Ravela S., Rus D., Model-based monitoring for early warning flood detection, in: Proceedings of the 6th ACM Conference on Embedded Network Sensor Systems, ACM, 2008, pp. 295–308.

Barrenetxea G., Ingelrest F., Schaefer G., Vetterli M., The hitchhiker's guide to successful wireless sensor network deployments, in: Proceedings of the 6th ACM Conference on Embedded Network Sensor Systems, ACM, 2008, pp. 43–56.

Baykut, S., Akgül, T., Inan, S., Seyis, C., 2010. Observation and removal of daily quasiperiodic components in soil radon data. Radiat. Meas. 45, 872e879.

Basili R., Valensise G., Vannoli P., Burrato P., Fracassi U., Mariano S., Tiberti M.M. & Boschi E. (2008) - The Database of Individual Seismogenic Sources (DISS), version 3: summarizing 20 years of research on Italy's earthquake geology. Tectonophysics, doi:10.1016/j.tecto.2007.04.014.

Benson, S., 2006. Carbon Dioxide Capture and Storage: Assessment of Risks from Storage of Carbon Dioxide in Deep Underground Geological Formations. Lawrence Berkeley National Laboratory.

Bdour, A., Hamdi, M. and Tarawneh, Z. (2009). Perspectives on sustainable wastewater treatment technologies and reuse options in the urban areas of the Mediterranean region. Desalination, 237(1-3), 162-174pp.

Bode F, Nowak W, Loschko M. Optimization for Early-Warning Monitoring Networks in Well Catchments Should Be Multi-objective, Risk- Prioritized and Robust Against Uncertainty. Transp Porous Media. 2015;114(2):1-21.

Bousquet, P., P. Ciais, J. B. Miller, E. J. Dlugokencky, D. A. Hauglustaine, C. Prigent, G. R. Van der Werf, P. Peylin, E. G. Brunke, C. Carouge, R. L. Langenfelds, J. Lathiere, F. Papa, M. Ramonet, M. Schmidt, L. P. Steele, S. C. Tyler, and J. White. 2006. Contributionof anthropogenic and natural sources to atmospheric methane variability. Nature 443:439-443.

Busquets, J.; Busquets, J.V.; Tudela, D.; Perez, F.; Busquets-Carbonell, J.; Barbera, A.; Rodriguez, C.; Garcia, A.; Gilabert, J. Low-cost AUV based on Arduino open source microcontroller board for oceanographic research applications in a collaborative long term deployment missions and suitable for combining with a USV as an autonomous automatic recharging platform. In Proceedings of the IEEE/OES Conference on Autonomous Underwater Vehicles (AUV), Southampton, UK, 24–27 September 2012; pp. 1–10.

Bradshaw, J., Boreham, C., La Pedalina, F., 2004. Storage retention time of CO2 in sedimentary basins; examples from petroleum systems. In: Proceedings of the Seventh International Conference on Greenhouse Gas Control Technologies (GHGT-7), September 5–9, 2004, Vancouver, 9 pp. http://uregina.ca/ghgt7/PDF/papers/peer/427.pdf (Electronic preprint papers).

Brandt, T.R., Moore, D.W., Murray, K.E., and Colton, R.B., 2003a, A spatial database of of bedding attitudes to accompany geologic map of Boulder- Fort Collins, Greeley area, Colorado: U.S. Geological Survey, Open-File Report OF-2003 -24, scale 1:100000.

C. Alippi, R. Camplani, C. Galperti, M. Roveri, A robust, adaptive, solar-powered wsn framework for aquatic environmental monitoring, Sens. J. IEEE 11 (1) (2011) 45–55.

C.A. Boano, J. Brown, Z. He, U. Roedig, T. Voigt, Low-power radio communication in industrial outdoor deployments: the impact of weather conditions and atex-compliance, in: Sensor Applications, Experimentation, and Logistics, Springer, 2010, pp. 159–176.

Cahill, A.G., Jakobsen, R., 2013. Hydro-geochemical impact of CO2leakage fromgeological storage on shallow potable aquifers: a field scale pilot experiment.Int. J. Greenh. Gas Control 19, 678–688.

Candela, L., Fabregat, S., Josa, A., Suriol, J., Vigues, N., Mas, J. (2007). Assessment of soil and groundwater impacts by treated urban wastewater reuse. A case study: Application in a golf course (Girona, Spain). Science of the Total Environment, 374, 26–35.

Castelluccio, M., Giannella, G., Lucchetti, C., Moroni, M., Tuccimei, P., 2012. La classificazione della pericolosit_a radon nella pianificazione territoriale finalizzata alla gestione del rischio. Classification of radon hazard in urban planning focused to risk management. Ital. J. Eng. Geol. Environ. 2, 5e16. http:// dx.doi.org/10.4408/IJEGE.2012-02. O-01.

Celia, M.A., Bachu, S., 2003. Geological sequestration of CO2: is leakage unavoidable and acceptable? In: Gale, J., Kaya, Y. (Eds.), Proceedings of the Sixth International Greenhouse Gas Technologies Conference (GHGT-6), vol. VI. Kyoto, October 1–4, 2002. Pergamon, pp. 477–482

Cha, W., Choi, H., Kim, J., & Kim, I. S. (2004). Evaluation of wastewater effluents for soil aquifer treatment in South Korea. Water Science and Technology, 50(2), 315–322.

Cheng, W., Yagi, K., Sakai, H., Kobayashi, K., 2006. Effects of elevated atmospheric CO2 concentrations on CH4 and N2O emission from rice soil: an experiment in controlled-environment chambers. Biogeochemistry 77, 351e373.

Cheadle, L., Lauren Deanes, Kira Sadighi, Joanna Gordon Casey, Ashley Collier-Oxandale and Michael Hannigan, 2017. Quantifying Neighborhood-Scale Spatial Variation of Ozone at Open Space and Urban Sites in Boulder Colorado Using Low-Cost Sensor Technology. Sensors 2017, 17, 2072.

Clein, J. S., A. D. McGuire, and X. Zhang. 2002. Historical and projected carbon balance of mature black spruce ecosystems across North America: the role of carbon-nitrogen interactions. Plant and Soil 242:15 32.

Cook R.D.: Concepts and applications of finite element analysis. John Wiley& Sons, New York 2002. de Wit C.T., Goudriaan J.: Simulation of ecological processes. PUDOC, Wageningen 1978

Conrad, C. and Daoust, T. (2008). "Community-Based Monitoring Frameworks: Increasing the Effectiveness of Environmental Stewardship" *Environmental Management 41*(3): 358-388

Conley, S., Franco, G., Faloona, I., Blake, D., Peischl, J., Ryerson, T., 2016. Methane emissions from the 2015 Aliso Canyon blowout in Los Angeles, CA. Science 351(6279), 1317–1320.

Crockett, R.G.M., Perrier, F., Richon, P., 2010. Spectral-decomposition techniques for the identification of periodic and anomalous phenomena in radon time-series. Nat. Hazard. Earth Sys. 10, 559e564.

C.-Y. Chong, S.P. Kumar, Sensor networks: evolution, opportunities, and chal-lenges, Proceedings of the IEEE 91 (8) (2003) 1247–1256.

Curry, C. L. 2009. The consumption of atmospheric methane by soil in a simulated future climate. Biogeosciences 6:2355-2367.

Dai Z, Keating E, Bacon D, et al. Probabilistic evaluation of shallow groundwater resources at a hypothetical carbon sequestration site. Sci Rep. 2014;4:4006.

Da-Xu L, He W., Li S . Internet of things in industries: a survey. IEEE Trans Ind Informat 2014; 10:2233–43.

Denchik, N., Pezard, P.A., Neyens, D., Lofi, J., Frederick, G., Girard, J., Levannier, A.,2014. Near-surface CO2leak detection monitoring from downhole electricalresistivity at the CO2Field Laboratory, Svelvik Ridge (Norway). Int. J. Greenh.Gas Control 28, 275–282.

Dethlefsen, F., Kober, R., Schafer, D., al Hagrey, S.A., Hornbruch, G., Ebert, M., Beyer,M., Grobmann, J., Dahmke, A., 2013. Monitoring approaches for detecting andevaluating CO2and formation water leakages into near-surface aquifers.Energy Procedia 37, 4886–4893.

Debye, P., Hückel, E., 1924. Theory of electrolytes. I. Lowering of freezing point and related phenomena. Phys. Z. 24, 185.

De Voto, R. H., Uranium Exploration, Uranium Geochemistry, Mineralogy, Geology, Exploration and Resources (Eds. B. Devivo, F. Ippolito, G. Capaldi, P. R.Simpson), The Institution of Mining and Metallurgy, London, 1984, pp. 101-108

Delin, K.A.; Jackson, S.P.; Johnson, D.W.; Burleigh, S.C.; Woodrow, R.R.; McAuley, M.; Britton, J.T.; Dohm, J.M.; Ferré, T.P.A.; Ip, F.; Rucker, D.F.; Baker, V.R. Sensor web for spatiotemporal monitoring of a hydrological environment. In Proceedings of the 35th Lunar and planetary science conference, League City, Texas, USA, March 2004.

Denman, K. L., G. Brasseur, Chidthaisong, A. P. Ciais, P. M. Cox, R. E. Dickinson, D. Hauglustaine, C. Heinze, E. Holland, D. Jacob, U. Lohmann, S. Ramachandran, P. L.da Silva Dias, S. C. Wofsy, and X. Zhang. 2007. Couplings Between Changes in the Climate System and Biogeochemistry. In: Climate Change 2007: The Physical Science Basis. Contribution of Working Group I to the Fourth Assessment Report of the Intergovernmental Panel on Climate Change [Solomon, S., D. Qin, M. Manning, Z. Chen, M. Marquis, K.B. Averyt, M.Tignor and H.L. Miller (eds.)]. Cambridge, United Kingdom and New York, NY, USA.

Diamond, D.; Coyle, S.; Scarmagnani, S.; Hayes, J. Wireless sensor networks and chemo-/biosensing. Chem. Rev. 2008, 108, 652–679.

Diersch H.J.G., Kolditz O.: Variable-density flow and transport in porous media: approaches and challenges. Advances in Water Resources, 25(8–12), 899–944, 2002.

Diersch H.J.G.: FEFLOW 5.2 Finite Element Subsurface Flow and Transport Simulation System, Reference Manual. WASY Ltd., Berlin 2005.

Diersch H.J.G.: FEFLOW 5.2 Finite Element Subsurface Flow and Transport Simulation System, User's Manual. WASY Ltd., Berlin 2005a.

Dillon, P., Pavelic, P., Page, D., Beringen, H., Ward, J. (2009) – Managed Aquifer Recharge, An Introduction. Waterlines. CSIRO, National Water Commission, 77pp.

Di Giuseppe, D., Tessari, U., Faccini, B., Coltorti, M., Vaccaro, C., Marin, E.2016 Multiple X-ray approaches to discriminate the origin of liquefied sand erupted during the 2012 Emilia Romagna earthquake(2016) X-Ray Spectrometry, 45 (1), pp. 19-27 https://www.scopus.com/inward/record.uri?eid=2-s2.0-84955741081&partnerID=40&md5=e1d25a2bde9e266d2fcf5b71ca59f14d DOI: 10.1002/xrs.2632

Dijkstra, F.A., Morgan, J.A., LeCain, D.R., Follett, R.F., 2010. Microbially mediated CH4 consumption and N2O emission is affected by elevated CO2, soil water content, and composition of semi-arid grassland species. Plant and Soil 329, 269e281.

Diss working group (2007) - Database of Individual Seismogenic Sources (version 3.0.4): A compilation of potential sources for earthquakes larger than M 5.5 in Italy and surrounding areas. Available at: http://www.ingv.it/DISS.

D.J. Vergados, N.A. Pantazis, D.D. Vergados, Energy-efficient route selection strategies for wireless sensor networks, Mobile Netw. Appl. 13 (3–4) (2008) 285–296.

Dlugokencky, E. J., K. A. Masarie, P. M. Lang, and P. P. Tans. 1998. Continuing decline in the growth rate of the atmospheric methane burden, Nature, 393, 447-450.

Dlugokencky, E. J., S. Houweling, L. Bruhwiler, K. A. Masarie, P. M. Lang, J. B. Miller, and P. P. Tans. 2003. Atmospheric methane levels off: Temporary pause or a new steady-state?, Geophys. Res. Lett., 19,

doi:10.1029/2003GL018126.

Dlugokencky, E. J., L. Bruhwiler, J. W. C. White, L. K. Emmons, P. C. Novelli, S. A. Montzka, K. A. Masarie, P. M. Lang, A. M. Crotwell, J. B. Miller, and L. V. Gatti. 2009. Observational constraints on recent increases in the atmospheric CH4 burden. Geophysical Research Letters 36:5.

Drewes, J. E., Reinhard, M., & Fox, P. (2003). Comparing microfiltration-reverse osmosis and soil-aquifer treatment for indirect potable reuse of water. Water Research, 37(15), 3612–3621.

Drewes, J. E., & Jekel, M. (1998). Behavior of DOC and AOX using advanced treated wastewater for groundwater recharge. Water Research, 32, 3125–3133.

Drolet, J.P., Martel, R., Poulin, P., Dessau, J.C., Lavoie, D., Parent, M., Levesquem, B., 2013. An approach to define potential radon emission level maps using indoor radon concentration measurements and radiogeochemical data positive proportion relationships. J. Environ. Radioact. 124, 57e67.

Dueñas, C., M. C. Fernández, J. Carretero, M. Pérez, and E. Liger. 1994. Consumption of methane by soils. Environmental Monitoring and Assessment 31:125-130-130.

Durrance, E.M., Gregory, R.G., 1990. Helium and radon transport mechanisms in hydrothermal circulation systems of Southwest England. In: Geochemistry of Gaseous Elements and Compounds. Theophrastus Publ., Athens, pp. 337–352.

E.A. Basha, S. Ravela, D. Rus, Model-based monitoring for early warning flood detection, in: Proceedings of the 6th ACM Conference on Embedded Network Sensor Systems, ACM, 2008, pp. 295–308.

Echanobe J, delCampo I , Basterretxea K , Martinez M , Doctor F . An FPGA-based multiprocessor-architecture for intelligent environments. Microproc Microsyst 2014; 38:730–40.

E. Jafer, R. Spinar, P. Stack, C. O'Mathuna, D. Pesch, Design and deployment ofa new wireless sensor node platform for building environmental monitoringand control, ICST Transactions on Ambient Systems 11 (2011), e3 1–12.

Essandoh, H. M. K., Tizaoui, C., Mohamed, M. H. A., Amyc, G., & Brdjanovic, D. (2011). Soil aquifer treatment of artificial wastewater under saturated conditions. Water Research, 45(14), 4211–4226.

Ernst, M., Sachse, A., Steinberg, C. E. W., & Jekel, M. (2000). Characterization of the DOC in nanofiltration permeates of a tertiary effluent. Water Research, 34(11), 2879–2886.

Etheridge, D. M., G. I. Pearman, and P. J. Fraser. 1992. Changes in tropospheric methane between 1841 and 1978 from a high accumulation-rate Antarctic ice core Tellus Series B-Chemical and Physical Meteorology 44:282-294.

Etiope, G., Martinelli, G., 2002. Migration of carrier and trace gases in the geosphere: an overview. Phys. Earth Planet. Inter 129, 185e204.

Etiope, G., 1995. Migrazione e comportamento del 'Geogas' in bacini argillosi. Ph.D. Thesis, Dept. of Earth Sciences, Univ. La Sapienza, Rome.

Evans, G. (1965) Intertidal flat sediments and their environment of deposition in the Wash, U.K. Quart. Jour. Geol. Soc. London 121, 209 - 245.

F. Stajano, N. Hoult, I. Wassell, P. Bennett, C. Middleton, K. Soga, Smart bridges, smart tunnels: transforming wireless sensor networks from research prototypes into robust engineering infrastructure, Ad Hoc Netw. 8 (8) (2010) 872–888.

F. Wang, J. Liu, Networked wireless sensor data collection: issues, challenges, and approaches, Commun. Surveys Tutorials, IEEE 13 (4) (2011) 673–687.

Fey, A., Conrad, R., 2000. Effect of temperature on carbon and electron flow and on the archaeal community in methanogenic rice field soil. Applied and Environmental Microbiology 66, 4790e4797.

F. Ding, G. Song, K. Yin, J. Li, A. Song, A GPS-enabled wireless sensor network formonitoring radioactive materials, Sensors and Actuators A: Physical 155 (2009)210–215.

Fleury, P., Bakalowicz, M., de Marsily, G., 2007. Submarine springs and coastal karst aquifers: a review. Journal of Hydrology 339, 79–92.

Floodnet. Available online: http://envisense.org/floodnet/floodnet.htm (accessed on Oct 28-29, 2008).

Folk, R.L. and Ward, W. (1957) "Brazos river bar: A study in the significance of grains-size parameters". Journal of Sedimentary Petrology, Volume 27, pp.3- 26.

Forster, P., V. Ramaswamy, P. Artaxo, T. Berntsen, R. Betts, D. W. Fahey, J. Haywood, J. Lean, D. C. Lowe, G. Myhre, J. Nganga, R. Prinn, G. Raga, M. Schulz, and R. Van Dorland. 2007. Changes in Atmospheric Constituents and in Radiative Forcing. In: Climate Change 2007: The Physical Science Basis. Contribution of Working Group I to the Fourth Assessment Report of the Intergovernmental Panel on Climate Change [Solomon, S., D. Qin, M. Manning, Z. Chen, M. Marquis, K.B. Averyt, M.Tignor and H.L. Miller (eds.)]. Cambridge, United Kingdom and New York, NY, USA.

Fox, P., Narayanaswamy, K., Genz, A., & Drewes, J. E. (2001). Water quality transformations during soil aquifer treatment at the Mesa Northwest Water Reclamation Plant, USA. Water Science and Technology, 43(10), 343–350.

Freitas, M.C., Andrade, C., Cruces, A., 2002a. The geological record of environmental changes in southwestern Portuguese coastal lagoons since the Lateglacial. Quaternary International 93–94, 161–170.

Freitas, M.C., Andrade, C., Cruces, A., Amorim, A., Cearreta, A., Ramalho, M.J., 2002b. Coastal environmental changes at different time-scales: the case of the Melides barrier-lagoon system (SW Portugal). Proceedings, Littoral 2002—The Changing Coast, Eurocoast–Portugal, Porto, vol. 3, pp. 397–402.

Frey, R.W. & Basan, P.B. (1978) Coastal salt marshes. In: Davis, R.A. Jr. (Ed.) Coastal Sedimentary Environments. New York Springer-Verlag. 101 - 169.

Fuchs, C.R. Classification of Water Quality of the Lanoso River, Uberaba. Ph.D. Thesis, Faculdade de Ciências Agrárias e Veterinárias de Jaboticabal, Universidade Estadual Paulista Júlio de Mesquita Filho, São Paulo, Brazil, 2012. (In Portuguese)

Fujiyoshi, R., Sakamoto, K., Imanishi, T., Sumiyoshi, T., Sawamura, S., Vaupotic, J., Kobal, I., 2006. Meteorological parameters contributing to variability in 222Rn activity concentrations in soil-gas at a site in Sapporo. Jpn. Sci. Total Environ. 370, 224e234.

G. Barrenetxea, F. Ingelrest, G. Schaefer, M. Vetterli, The hitchhiker's guide to successful wireless sensor network deployments, in: Proceedings of the 6th ACM Conference on Embedded Network Sensor Systems, ACM, 2008, pp. 43–56.

G.-Cau-1978, Underground-storage-of-natural-gas-in-Italy. G.-Cau-1978.pdf

G. Lollino, A. Manconi, F. Guzzetti, M. Culshaw, P. Bobrowsky and F. Luino (eds), Proc. IAEG XII Congress, Torino, Italy, September 15-19.

Gale, I. (ed.) (2005) Strategies for Managed Aquifer Recharge (MAR) in semi-arid areas. International Hydrological Programme (IHP), International Association of Hydrogeologists commission on Management of Aquifer Recharge IAH – MAR. 30pp.

Gandra, M.; Seabra, R.; Lima, F.P. A low-cost, versatile data logging system for ecological applications. Limnol. Oceanogr. Methods 2015, 13, 115–126. [CrossRef]

Gastaldini, M.C.C.; Mendonça, A.S.F.; Paiva, J.B.D.; Paiva, E.M.C.D. Conceitos para a avaliação da qualidade da água. In Hidrologia Aplicada à Gestão de Pequenas Bacias HidrográFicas; ABRH: Porto Alegre, Brazil, 2001; pp. 428–451.

GEMS, Global Environment Monitoring System, (2011). The world of water quality. Retrieved from http://www.gemswater.org/index.html

Glasgow, H.B.; Burkholder, J.M.; Reed, R.E.; Lewitus, A.J.; Kleinm, J.E. Real-time remote monitoring of water quality: A review of current applications, and advancements in sensor, telemetry, and computing technologies. J. Exp. Mar. Biol. Ecol. 2004, 300, 409–448.

Glasgow, H.B.; Burkholder, J.M.; Reed, R.E.; Lewitus, A.J.; Kleinman, J.E. Real-time remote monitoring of water quality: A review of current applications, and advancements in sensor, telemetry, and computing technologies. J. Exp. Mar. Biol. Ecol. 2009, 300, 409–448.

Grabarczyk Cz.: Modele w naukach technicznych. W: Problemy inżynierii środowiska u progu nowego tysiąclecia. Oficyna Wydawnicza Politechniki Wrocławskiej, Wrocław 2000.

Gromiec J. (red.): Modelowanie matematyczne wód podziemnych – przykłady zastosowań. Biblioteka Jakości Polskiego Komitetu IWA, tom 23, Europejskie Centrum Ekologiczne, Polski Komitet IWA, Warszawa 2007.

Grinning Planet, http://www.grinningplanet.com

Gubbi J , Buyya R , Marusic S , Palaniswami M . Internet of Things (IoT): a vision, architectural elements, and future directions. Future Gen Comput Syst 2013; 29:1645–60.

G. Werner-Allen, K. Lorincz, M. Ruiz, O. Marcillo, J. Johnson, J. Lees, M. Welsh,Deploying a wireless sensor network on an active volcano, Journal of InternetComputing 10 (2006) 18–25.

H. Wennerström, F. Hermans, O. Rensfelt, C. Rohner, L.-Å. Norden, A long-term study of correlations between meteorological conditions and 802.15. 4 link performance, in: SECON, 2013, pp. 221–229.

Hahn, M., K. Gartner, and S. Zechmeister-Boltenstern. 2000. Greenhouse gas emission (N2O, CO2, CH4) from three different soils near Vienna (Austria) with different water and nitrogen regimes. Die Bodenkultur 51(2):115-125.

Hart, J.K.; Martinez, K. Environmental sensor networks: A revolution the earth system science? Earth-Science Reviews 2006, 78, 177-191.

Heinrich J.C., Pepper D.W.: Intermediate finite element method: fluid flow and heat transfer applications / Series in Computational and Physical Processes in Mechanics and Thermal Sciences. Taylor & Francis, Philadelphia 1999.

Hem, J.D., 1989. The Study and Interpretation of the Chemical Characteristics of Natural Water, third ed. U.S. Geol. Surv. Water Supply Paper 2254.

Henriet, J. -P., & Mienert, J. (Eds.). (1998). Gas Hydrates: Relevance to World Margin Stability and Climate Change (pp. 137). Geological Society of London Special Publication.

Hooker, P. J.; Bannon, P. Methane: Its Occurrence and Hazards in Construction; Construction Industry Research & Information Association (CIRIA); London, UK, 1993; p 137

Hovorka SD. In quest of robust and commercial CO2 monitoring. Greenh Gases Sci Technol. 2012;2(3):145-147.

Hughes, S.G., Taylor, E.L., Wentzell, P.D., 1994. Models for conductance measurements in quality assurance of water analysis. Anal. Chem. 66, 830–835.

Huebner K.H.: The finite element method for engineers. John Wiley & Sons, New York 2001.

Hutsch, B.W., 2001. Methane oxidation in non-flooded soils as affected by crop production – invited paper. European Journal of Agronomy 14, 237–260

IEA Greenhouse Gas R&D Programme (IEAGHG). 2009 A review of the international state of the art in risk assessment guidelines and proposed terminology for use in CO2 geological storage, Technical Study, 2009/TR7, December 2009.

Ilie, A. M. C., Vaccaro, C., Rogeiro, J., Leitão, T.E., Martins, T., Configuration, programming and implementation of 3 Smart Water network wireless sensor nodes for assessing the water quality, in the Proceedings of the 2017 IEEE Smart World Congress, San Francisco, USA, 319-326.

Ilie, A. M. C. and Vaccaro, C., Design of a smart gas detection system in areas of natural gas storage, in Proceedings of the 2017 IEEE International Geoscience and Remote Sensing Symposium, Fort Worth, Texas, USA, 5954-5957.

Idelovitch, E., Icekson-Tal, N., Avraham, O., & Michail, M. (2003). The long-term performance of soil aquifer treatment (SAT) for effluent reuse. Water Science and Technology: Water Supply, 3(4), 239–246.

Idelovitch, E. (2003). SAT (soil aquifer treatment)—The long-term performance of the Dan Region reclamation project. Washington, DC: The World Bank Water Week.

Inubushi, K., Cheng,W., Aonuma, S., Hoque, M.M., Kobayashi, K., Miura, S., Kim, H.Y., Okada, M., 2003. Effects of free-air CO2 enrichment (FACE) on CH4 emission from a rice paddy field. Global Change Biology 9 (10), 1458e1464.

Inubushi, K., Wada, H., Takai, Y., 1984. Easily decomposable organic matter in paddy soil: IV. Relationship between reduction process and organic matter decomposition. Soil Science and Plant Nutrition 30, 189e198.

IPCC, 2007. Summary for policymakers. In: Solomon, S., Qin, D., Manning, M., Chen, Z., Marquis, M., Averyt, K.B., Tignor, M., Miller, H.L. (Eds.), Climate Change 2007: The Physical Science Basis. Contribution ofWorking Group I to the Fourth Assessment Report of the Intergovernmental Panel on Climate Change. Cambridge University Press, Cambridge, United Kingdom and New York, USA, pp. 1e18

I. Matijevics, "Wireless Sensors Networks – Theory and Practice," pp. 405-417, 2009.

Intergovernmental Panel on Climate Change IPCC. 2007. In: Solomon, S., et al. Eds., Climate Change 2007: The Physical Science Basis: Working Group I Contribution to the Fourth Assessment Report of the IPCC. Cambridge Univ. Press, New York.

J. Li, B. Faltings, O. Saukh, D. Hasenfratz, J. Beutel, Sensing the air we breathe – the OpenSense Zurich dataset, in: Proceedings of the 26th AAAI on Artificial Intelligence, 2012, pp. 2–4.

Jean Le Mer, Pierre Roger, Production, oxidation, emissions and consumption of methane by soils: A review, Eur. J. Soil Biol. 37 (2001) 25-50.

K. Bannister, G. Giorgetti, S.K. Gupta, Wireless sensor networking for hot applications: effects of temperature on signal strength, data collection and localization, in: Proceedings of the 5th Workshop on Embedded Networked Sensors (HotEmNetsn++ 08), Citeseer, 2008.

Karafiat A. (red.): Adaptive finite element method in fluid mechanics problems/ Seria Monografia – Politechnika Krakowska im. Tadeusza Kościuszki, Podstawowe Nauki Techniczne CUT, Kraków 2000.

Keating E, Dai Z, Dempsey D, Pawar R. Effective detection of CO2 leakage: A comparison of groundwater sampling and pressure monitoring. Energy Procedia. 2014;63:4163-4171.

Keppler, F., J. T. G. Hamilton, M. Brass, and T. Rockmann. 2006. Methane emissions from terrestrial plants under aerobic conditions. Nature 439:187-191.

K.K. Khedo, R. Perseedoss, A. Mungur, et al., A wireless sensor network air pollution monitoring system, arXiv preprint arXiv:1005. 1737, 2010

Knapik K.: Dynamiczne modele w badaniach sieci wodociągowych. Politechnika Krakowska, Kraków 2000.

Król K.: Metoda elementów skończonych w obliczeniach konstrukcji. Wydawnictwo Politechniki Radomskiej, Radom 2006.

K.S. Chiang Kuang, S.T. Quek, M. Maalej, Remote flood monitoring system basedon plastic optical fibres and wireless motes, Sensors and Actuators A: Physical147 (2008) 449–455.

Kulbik M.: Komputerowa symulacja i badania terenowe miejskich systemów wodociągowych. Politechnika Gdańska 2004.

Künzli, N., Kaiser, R., Medina, S., Studnicka, M., Chanel, O., Filliger, P., et al. (2000). Publichealth impact of outdoor and traffic-related air pollution: a european assessment. The Lancet, 356(9232), 795–801.

Lamert, H., Geistlinger, H., Werban, U., Schütze, C., Peter, A., Hornbruch, G., Schulz,A., Pohlert, M., Kalia, S., Beyer, M., Großmann, J., Dahmke, A., Dietrich, P., 2012.Feasibility of geoelectrical monitoring and multiphase modeling for processunderstanding of gaseous CO2injection into a shallow aquifer. Environ. EarthSci. 67 (2), 447–462.
Laxen, D.P.H., 1977. A specific conductance method for quality control in water analysis. Water Res. 11, 91–94.

Lee, S. Y., Lee, J. U., Choi, H., & Kim, K. W. (2004). Sorption behaviors of heavy metals in SAT (soil aquifer treatment) system. Water Science and Technology, 50(2), 263–268.

Leitão T. E., Lobo Ferreira J.P., Martins T., Oliveira M. M., Henriques M. J., Carvalho T., Carvalho J M., Agostinho R., Carvalho R., Sousa R., Monteiro J.P., Costa L.R.D., Hugman R., Mota R., Mesquita E., Rogeiro J., Rosa M. J., 2016, Deliverable 4.5 Demonstrating Managed Aquifer Recharge as a Solution to Water Scarcity and Drought MAR to Improve the Groundwater Status in South Portugal. http://www.marsol.eu/files/marsol_d4-5_mar-south-portugal_final-report.pdf

Leitão, T.E., Martins, T., Henrinques, M.J., Lobo Ferreira, J.P., Rogeiro, J. and **Ilie, A.M.C.,** 2016 - Deliverable 12.5 Physical (Sandbox) Modelling of Melides Demo Site. Projeto UE MARSOL - Demonstrating Managed Aquifer Recharge as a Solution to Water Scarcity and Drought, outubro, 50 pp. [CrossRef] [PubMed], http://www.marsol.eu/files/marsol_d12-5_physical-model_20161011.pdf

Lelieveld, J. O. S., P. J. Crutzen, and F. J. Dentener. 1998. Changing concentration, lifetime and climate forcing of atmospheric methane. Tellus B 50:128-150.

Libânio, M. Fundamentos de Qualidade e Tratamento de Água, 3rd ed.; Átomo: Campinas, Brazil, 2010.

Lions, J., Devau, N., de Lary, L., Dupraz, S., Parmentier, M., Gombert, P., Dictor, M., 2014. Potential impacts of leakage from CO2geological storage on geochemicalprocesses controlling fresh groundwater quality: a review. Int. J. Greenh. GasControl 22, 165–175.

Logan, J., 1961. Estimation of electrical conductivity from chemical analyses of natural waters. J. Geophys. Res. 66, 2479–2483.

Lobo Ferreira J.P., Leitão T. E., Oliveira M. M., Martins T., Mota R., Ilie A.M.C., Monteiro J.P., Luís R.D. Costa, Rui Hugman (UAlg) Tiago Carvalho, Rita Carvalho, Raquel Sousa (TARH), 2016. D4.4, Demonstrating Managed Aquifer Recharge as a Solution to Water Scarcity and Drought. (http://www.marsol.eu/files/marsol_d4-4_modelling-south-portugal-sites_20160726-compr.pdf)

Lombardi, S., Benvegni, F., Brondi, A., Polizzano, C., 1993. Field investigation with regard to the impermeability of clay formations: helium-4 soil gas surveys in sedimentary basins as a tentative study of secondary permeability in clayey sequences. Final Report. Work carried out under contract with the European Atomic Energy Community in the framework of its shared cost R&D programme 'Management and Storage of Radioactive Waste' (1985–1989) Part A, Task 4: 'Geological disposal studies'. EUR 14585 EN.

Lombardi, S., Etiope, G., Guerra, M., Ciotoli, G., Grainger, P., Duddridge, G.A., Gera, F., Chiantore, V., Pensieri, R.,Grindrod, P., Impey, M., 1996. The refinement of soil gas analysis as a geological investigative technique. Final Report. Work carried out under a cost-sharing contract with the European Atomic Energy Community in the framework of its 4th R&D programme on 'Management and Storage of Radioactive Waste' (1990–1994) Part A, Task 4: 'Disposal of Radioactive Waste'. EUR 16929 EN.

Lou, Y., Mizuno, T., Kobayashi, K., Okada, M., Hasegawa, T., Hoque, M., Inubushi, K., 2006. CH4 production potential in a paddy soil exposed to atmospheric CO2 enrichment. Soil Science and Plant Nutrition 52, 769e773.

Lovett, G.M., Burns, D.A., Driscoll, C.T., Jenkins, J.C., Mitchells, M.J., Rustad, L., Shanley, J.B., Likens, G.E., Haeuber, R. (2007). Who needs environmental monitoring? *Frontiers in Ecology and the Environment, 5*(5), 253-260.

L. Mottola, G.P. Picco, M. Ceriotti, S. Guna, A.L. Murphy, Not all wireless sensornetworks are created equal: a comparative study on tunnels, ACM Transactionson Sensor Networks 7 (2010) 1–33.

Madole, R.F, Braddock, W.A., and Colton, R.B., 1998, Geologic map of the Hygiene quadrangle, Boulder County, Colorado: US Geological Survey Geologic Quadrangle Map GQ-1772, scale 1:24,000.

Malolo, Y. (2011) Effect of Temperature and Redox Conditions on Removal of Contaminants during Soil Aquifer Treatment. UNESCO-IHE Institute for Water Education. MSc Thesis MWI-2011/09. 123p.

Marcelli, M.; Piermattei, V.; Madonia, A.; Marcelli, U. Design and Application of New Low-Cost Instruments for Marine Environmental Research. Sensors 2014, 14, 23348–23364. [CrossRef] [PubMed].

McCleskey, R.B., Nordstrom, D.K., Ryan, J.N., Ball, J.W., 2012. A new method of calculating electrical conductivity with applications to natural waters. Geochim. Cosmochim. Acta 77, 369–382.

McNeil, V.H., Cox, M.E., 2000. Relationship between conductivity and analyzed composition in a large set of natural surface-water samples, Queensland, Australia. Environ. Geol. 39, 1325–1333.

Margat, J., 2008. Les eaux souterraines dans le monde. BRGM Editions, 187 p.

Martins, A.; Malaquias, I.; Martins, D.; Campos, A.; Lopes, J.; Fiúza, E.; Silva, M.; Neves, M.; Soares, R. O Livro branco da Física e da Química. Available online: http://www.spq.pt/magazines/BSPQ/610/ article/30001061/pdf (accessed on 31 July 2016).

Martins, T. Contaminants retention in soils as a complementary water treatment method. Application in soil-aquifer treatment processes. Master Thesis. Faculty of Sciences. University of Lisbon, 2016.

Martins, T., Leitão T.E., Carvalho M.R., 2016. Assessment of wastewater contaminants retention for a Soil-Aquifer Treatment system using soil-column experiments, 15th Water-Rock Interaction International Symposium, WRI-15, Procedia Earth and Planetary Science 17 (2017) 332 – 335.

Mary Kanga, Cynthia M. Kannoa, Matthew C. Reida, Xin Zhangb, Denise L. Mauzeralla, Michael A. Celiaa, Yuheng Chenc, and Tullis C. Onstott, Direct measurements of methane emissions from abandoned oil and gas wells in Pennsylvania. In: Proceedings of the National Academy of Sciences of the United States of America, PNAS December 23, 2014, vol. 111, no. 51, 18173-18177.

Masson, N.; Piedrahita, R.; Hannigan, M. Approach for Quantification of Metal Oxide Type Semiconductor Gas Sensors Used for Ambient Air Quality Monitoring. Sens. Actuators B Chem. **2015**, 208, 339–345.

Mazzia A., Putti M.: Three-dimensional mixed finite element – finite volume approach for the solution of density-dependent flow in porous media. Journal of Computational and Applied Mathematics, 185, 347–359, 2006.

Methane Gas in Well Water, Practical information for Alberta's Agriculture Industry, June 2006, Agdex 716(D63). http://www1.agric.gov.ab.ca/$department/deptdocs.nsf/all/agdex10840/$file/716D63_web.pdf?OpenElement

Mengis, M., R. Gachter, and B. Wehrli. 1997. Sources and sinks of nitrous oxide N2O in deep lakes. Biogeochemistry 38, 281-301.

Meyer PD, Valocchi AJ, Eheart JW. Monitoring network design to provide initial detection of groundwater contamination. Water Resour Res. 1994;30(9):2647-2659.

Miotliński, K., Barry, K., Dillon, P. (2010) Alice Springs SAT Project Hydrological and Water Quality Monitoring Report 2008-2009. CSIRO: Water for a Healthy Country National Research Flagship, 85p.

Mitchell, B. (2002). *Resource and Environmental Management* (2nd ed.). Harlow: Pearson 7.

Montgomery-Brown, J., Drewes, J., Fox, P., Reinhard, M., 2003. Behavior of alkylphenol polyethoxylate metabolites during soil aquifer treatment. Water Research 37 (15), 3672e3681.

Montzka, S. A., E. J. Dlugokencky, and J. H. Butler. 2011. Non-CO2 greenhouse gases and climate change, Nature, 476, 43-50.

Moscetta, P.; Sanfilippo, L.; Savino, E.; Allabashi, R.; Gunatilaka, A. Instrumentation for Continuous Monitoring in Marine Environments. In Proceedings of the MTS/IEEE Biloxi—Marine Technology for Our Future: Global and Local Challenges (OCEANS '09), Biloxi, MS, USA, 26–29 October 2009.

Mualem, Y. 1976. A new model predicting the hydraulic conductivity of unsaturated porous media. Water Resour. Res. 12:513–522.

Murphy, D.M.; Koop, T. Review of the vapour pressures of supercooled water for atmospheric applications. Q. J. R. Meteorol. Soc. **2005**, 131, 1539–1565.

N. Baccour, A. Koubaa, L. Mottola, M.A. Zuniga, H. Youssef, C.A. Boano, M. Alves, Radio link quality estimation in wireless sensor networks: a survey, ACM Trans. Sensor Netw. (TOSN) 8 (4) (2012) 34.

Nadav, I., Arye, G., Tarchitzky, J., & Chen, Y. (2012). Enhanced infiltration regime for treated-wastewater purification in soil aquifer treatment (SAT). Journal of Hydrology, 420– 421, 275–283.

Nagda, N. L., Radon Prevalence Measurements, Health Risks and Control., ASTM Manual Series: MNL 15 ASTM Publication Code Number (PCN) 28-015094-17. 1994, ISBN 0-8031-2057-5

National Research Council NRC (1994) Ground Water Recharge Using Waters of Impaired Quality, National Academy Press. Washington D.C., 282pp.
Nazaroff, W.W., 1992. Radon transport from soil to air. Rev. Geophys. 30 (2), 137e160.

Nazaroff, W.W., Moed, B.A., Sextro, R.G., 1988. Soil as a source of indoor radon: generation, migration, and entry, in radon and its decay products in indoor air. In: Nazaroff, W.W., Nero Jr., A.V. (Eds.). John Wiley, New York, pp. 57e112.

Niina Kotamäki, Sirpa Thessler, Jari Koskiaho, Asko O. Hannukkala, Hanna Huitu, Timo Huttula, Jukka Havento and Markku Järvenpää. Wireless in-situ Sensor Network for Agriculture and Water Monitoring on a River Basin Scale in Southern Finland: Evaluation from a Data User's Perspective. Sensors (Basel), 2009; 9(4): 2862–2883.

Nordbotten JM, Kavetski D, Celia MA, Bachu S (2009) Model for CO2 leakage including multiple geological layers and multiple leaky wells. Environ Sci Technol 43(3):743–749.

O'Connor, F. M., O. Boucher, N. Gedney, C. D. Jones, G. A. Folberth, R. Coppell, P. Friedlingstein, W. J. Collins, J. Chappellaz, J. Ridley, and C. E. Johnson. 2010. Possible role of wetlands, permafrost, and methane hydrates in the methane cycle under future climate change: a review. Reviews of Geophysics 48.

Perera MDR, Meegama RGN, Jayananda MK. FPGA based single chip solution with 1-wire protocol for the design of smart sensor nodes. J Sensors 2014;2014. http://dx.doi.org/10.1155/2014/125874 .

Oliveira, J.T., 1984. Carta Geológica de Portugal 1:200 000 e Notícia Explicativa. Serviços Geológicos de Portugal, Lisbon.

Onsager, L., 1926. The theory of electrolytes. Phys. Z. 27, 388.

P. Corke, T. Wark, R. Jurdak, W. Hu, P. Valencia, D. Moore, Environmental wireless sensor networks, Proc. IEEE 98 (11) (2010) 1903–1917.

P. Tarrío, M. Cesana, A. Redondi, Energy-accuracy trade-offs for hybrid localization using rss and inertial measurements in wireless sensor networks, Ad Hoc Netw. (2013).

Panguluri, S., Meiners, G., Hall, J., Szabo, J.G., 2009. Distribution System Water Quality Monitoring: Sensor Technology Evaluation Methodology and Results. U.S. Environmental Protection Agency, Washington, DC. EPA/600/R-09/076, 2009.

Paula Galego Fernandes, Paula Carreira, Manuel Oliveira da Silva, 2008. Anthropogenic sources of contamination recognition — Sines coastal aquifer (SW Portugal). Journal of Geochemical Exploration 98 (2008) 1–14.

Pawlowicz, R., 2008. Calculating the conductivity of natural waters. Limnol. Oceanogr. Methods 4, 489–501.

Piedrahita, R.; Xiang, Y.; Masson, N.; Ortega, J.; Collier, A.; Jiang, Y.; Li, K.; Dick, R.P.; Lv, Q.; Hannigan, M.; et al. The next Generation of Low-cost Personal Air Quality Sensors for Quantitative Exposure Monitoring. Atmos. Meas. Tech. 2014, 7, 3325–3336.

Perry, K.F., 2015. Natural gas storage industry experience and technology:potential application to CO2geological storage. In: Thomas, D.C., Benson, S.M.(Eds.), Carbon Dioxide Capture for Storage in Deep Geologic Formations-Results From the CO2Capture Project: Volume 2: Geologic Storage Of Carbon Dioxide With Monitoring And Verification. Elsevier.

Phillips, R.L., Whalen, S.C., Schlesinger, W.H., 2001a. Response of soil methanotrophic activity to CO2 enrichment in a North Carolina coniferous forest. Soil Biology and Biochemistry 33, 793e800.

Pieri, M., Groppi, G. 1981. Subsurface geological structure of the Po Plain, Italy. In: Progetto finalizzato alla geodinamica 414, Pieri, M., Groppi, G. (eds.). C.N.R: Roma, 1-23.

Piersanti, A., Cannelli, V., Galli, G., 2015. Long term continuous radon monitoring in a seismically active area. Ann. Geophys. 58 (4), S0437. http://dx.doi.org/10.4401/ag-6735.

Pinault J.-L. and J.-C. Baubron, Signal processing of soil gas radon, atmospheric pressure, moisture, and soil temperature data: A new approach for radon concentration modeling, J. Geophys. Res., 101, 3157-3171, 1996.

P. Zhang, C.M. Sadler, S.A. Lyon, M. Martonosi, Hardware design experience inZebraNet, in: Proceedings of the 2nd International Conference on EmbeddedNetworked Sensor Systems, Baltimore, USA, November 3–5, 2004, pp. 227–238.

Quanrud, D. M., Hafer, J., Karpiscak, M. M., Zhang, J., Lansey, K. E., & Arnold, R. G. (2003b). Fate of organics during soil-aquifer treatment: Sustainability of removals in the field. Water Research, 37, 3401–3411.

Quanrud, D. M., Arnold, R. G., Lansey, K. E., Begay, C., Ela, W., & Gandolfi, A. J. (2003a). Fate of effluent organic matter during soil aquifer treatment: Biodegradability, chlorine reactivity and genotoxicity. Journal of Water and Health, 01(1), 33–44.

Quanrud, D., Hafer, J., Karpiscak, M., Zhang, H., Lansey, K., Arnold, R., 2003. Fate of organics during soil-aquifer treatment: sustainability of removals in the field. Water Research 37 (14), 3401e3411.

Quanrud, D. M., Arnold, R. G.,Wilson, L. G., & Conklin, M. H. (1996). Effect of soil type on water quality improvement during soil aquifer treatment. Water Science and Technology, 33(10–11), 419–431.

R. Gao, “2011 International Conference on Electronics and Optoelectronics (ICEOE 2011) A Wireless Sensor Network Environment Monitoring System Based on TinyOS,” Electronics, no. Iceoe, pp. 497-501, 2011.

Rand, M.C.; Greenberg, A.E.; Taras, M.J. Standard Methods for the Examination ofWater andWastewater, 16th ed.; Joint published by American Public Health Association: Washington, DC, USA; American Water Works Association: Denver, CO, USA;Water Environment Federation: Washington, DC, USA, 1999.

Rauch, T., & Drewes, J. E. (2004). Assessing the removal potential of soil-aquifer treatment systems for bulk organic matter. Water Science and Technology, 50(2), 245–253.

Rauch, T., & Drewes, J. E. (2005). Quantifying biological organic carbon removal in groundwater recharge systems. Journal of Environmental Engineering, 131(6), 909–923.

Rauch, T., & Drewes, J. E. (2006). Using soil biomass as an indicator for the biological removal of effluent-derived organic carbon during soil infiltration. Water Research, 40, 961–968.

Reed PM, Minsker BS. Striking the Balance: Long-Term Groundwater Monitoring Design for Multiple Conflicting Objectives. J Water Resour Plan Manag. 2004;130(March/April):140-149.

Report No. 094 - Expo sure of the Population of the United States and Canada from Natural Back Ground Radiation, National Council on Radiation Protection and Measurements, NCRP 94, Bethesda, Md., USA, 1987

Rigby M, Prinn RG, Fraser PJ, Simmonds PG, Langenfelds RL, Huang J, et al. Renewed growth of atmospheric methane. Geophys Res Lett 2008; 35: L22805.

Romanak, K.D., Bennett, P., Yang, C., Hovorka, S.D., 2012. Process-based approach to CO2leakage detection by vadose zone gas monitoring at geologic CO2storage sites. Geophys. Res. Lett. 39 (15).

Roslev, P. and G. M. King. 1996. Regulation of methane oxidation in a freshwater wetland by water table changes and anoxia. Fems Microbiology Ecology 19:105-115.

Rossum, J.R., 1975. Checking the accuracy of water analyses through the use of conductivity. J. Am. Water Works Assoc. 67, 204–205.

Sanislav T, Mois G, Miclea L. An approach to model dependability of cyber-physicalsystems. Microproc Microsyst 2016; 41:67–76.

Schafer, A., Ustohal, P., Harms, H., Stauffer, F., Dracos, T., Zehnder, A., 1998. Transport of bacteria in unsaturated porous media. Journal of Contaminant Hydrology 33 (1e2), 149e169.

M.G. Schaap, F.J. Leij, M.T. van Genuchten ROSETTA: A computer program for estimating soil hydraulic parameters with hierarchical pedotransfer functions J. Hydrol., 251 (2001), pp. 163-176, 10.1016/S0022-1694(01)00466-8.

Schlesinger, W.H., 1997. Biogeochemistry: an analysis of global change. 2nd ed Academic Press, San Diego, California.

Shuang, X., QingLiang, Z., LiangLiang, W., LiNa, W., & ZhiGang, L. (2007). Fate of secondary effluent dissolved organic matter during soil-aquifer treatment. Chinese Science Bulletin, 52(18), 2496–2505.

Sciarra A., Cinti D., Pizzino L., Procesi M., Voltattorni N., Mecozzi S., Quattrocchi F. Geochemistry of shallow aquifers and soil gas surveys in a feasibility study at the Rivara natural gas storage site (Po Plain, Northern Italy) Applied Geochemistry 34 (2013) 3–22

Sciarra A., Cantucci B., Abu Zeid N., Vaccaro C., Quattrocchi F. 2014. Geochemical and Geomorphological Analyses on Liquefaction Occurred During the 2012 Emilia Seismic Sequence In "Engineering Geology for Society and Territory – Volume 5: Urban Geology, Sustainable Planning and Landscape Exploitation", Part XV Off-Fault Coseismic Surface Effects and Their Impact in Urban Areas pp 945 - 950,

Scrocca D., Carminati E., Doglioni C. & Marcantoni D. (2007) - *Slab retreat and active shortening along the central-northern Apennines*. In: LACOMBE O., LAVÉ J., ROURE F. & VERGES J. (Eds.), Thrust belts and Foreland Basins: from fold kinematics to hydrocarbon systems. Frontiers in Earth Sciences, Springer, 471-487.

Segers, R. 1998. Methane production and methane consumption: a review of processes underlying wetland methane fluxes. Biogeochemistry 41:23-51.

Serpelloni E., Anzidei M., Baldi P., Casula G. & Galvani A. (2005) - Crustal velocity and strain-rate fields in Italy and surrounding regions: new results from the analysis of permanent and non-permanent GPS networks. Geophys. J. Int., 161, 861-880, doi: 10.1111/j.1365-246x.2005. 02618.x, 1-20.0

Singh, B.K., Bardgett, R., Smith, P., Reay, D.S., 2010. Microorganisms and climate change: terrestrial feedbacks and mitigation options. Nature Reviews Microbiology 8, 779e790.
Stein, V.B., J.P.A. Hettiaratchi, Methane oxidation in three Alberta soils: influence of soil parameters and methane flux rates, Environmental Technology, 22 (1) (2001), pp. 101-111

Singh, R.; Singh, S.P. Development of a low cost wireless temperature monitoring system of industrial and research application. Int. J. Curr. Eng. Technol. 2015, 5, 355–361.

Siosemarde, M., Kave, F., Pazira, E., Sedghi, H., Ghaderi, S.J., 2010. Determine of constant coefficients to relate total dissolved solids to electrical conductivity. World Acad. Sci. Eng. Technol. 70, 258–260.

Sitaula, B. K., and L. R. Bakken. 1993. N2O release from spruce forest soil, relation with nitrification, CH4 uptake, temperature, moisture and fertilization. Soil Biol. Biochem. 25:1415-1421.

Shindell, D., et al. (2012). Simultaneously mitigating near-term climate change and improving human health and food security. Science, 335(6065), 183–189.

Šimůnek, J. and J. W. Hopmans, Modeling compensated root water and nutrient uptake, Ecological Modeling, doi:10.1016/j.ecolmodel.2008.11.004, 220(4), 505-521, 2009.

Solomon, S., Qin, D., Manning, M., Chen, Z., Marquis, M., & Averyt, K. B., et al. (Eds.). (2007). Climate Change 2007: The Physical Science Basis. Contribution of Working Group I to the Fourth Assessment Report of the Intergovernmental Panel on Climate Change. New York: Cambridge Univ. Press

Somov A., Wildfire safety with wireless sensor networks, ICST Transactions onAmbient Systems 11 (2011), e4 1–11.

Somov A., A. Baranov, A. Savkin, M. Ivanov, L. Calliari, R. Passerone, E. Kar-pov, A. Suchkov, Energy-aware gas sensing using wireless sensor networks, in: G.P. Picco, W. Heinzelmann (Eds.), Proceedings of the 9th European Con-ference on Wireless Sensor Networks (EWSN 2012), volume 7158 of LectureNotes in Computer Science, pp. 245–260, Trento, Italy, February 15–17, 2012, Springer-Verlag, Berlin/Heidelberg.

Standard EN 50194:2000: Electrical Apparatus for the Detection of CombustibleGases in Domestic Premises. Test Methods and Performance Requirements,2000.

Stange, F., K. Butterbach-Bahl, H. Papen, S. Zechmeister-Boltenstern , C. Li, and J. Aber. 2000. A process-oriented model of N2O and NO emissions from forest soils, 2. Sensitivity analysis and validation. J. Geophys. Res. 105(D4):4385-4398.

Strazisar, B.R., Wells, A.W., Diehl, J.R., Hammack, R.W., Veloski, G.A., 2009.Near-surface monitoring for the ZERT shallow CO2injection project. Int. J.Greenhouse Gas Control 3 (6), 736–744.

Sun AY, Nicot JP, Zhang X. Optimal design of pressure-based, leakage detection monitoring networks for geologic carbon sequestration repositories. Int J Greenh Gas Control. 2013;19:251-261.

Sundh, I., C. Mikkelä, M. Nilsson, and B. H. Svensson. 1995. Potential aerobic methane oxidation in a Sphagnum-dominated peatland—Controlling factors and relation to methane emission Soil Biology and Biochemistry 27:829-837.

Szabo, K.S., Jordan, G., Horv_ath, A., Szab_o, C., 2013. Dynamics of soil-gas radon concentration in a highly permeable soil based on a long-term high temporal resolution observation series. J. Environ. Radioact. 124, 74e83.

Tanner, A.B., 1980. 1980. Radon migration in the ground: a supplementary review, in proceedings of Natural Radiation Environment III. In: Gesell, T.F., Lowder, w. M. (Eds.). National technical Information Service, Springerfield, Va, pp. 5e56. U. S. Dep. of Comm. Rep. CONF. 780422.

Toze, S., Hanna, J., Smith, T., Edmonds, L., McCrow, A., 2004. Determination of water quality improvements due to the artificial recharge of treated effluent. In: Steenvoorden, J., Endreny, T. (Eds.), International Symposium on Wastewater Re-Use and Groundwater Quality. Int Assoc Hydrological Sciences, Wallingford, UK, pp. 53e60.

Trautz, R.C., Pugh, J.D., Varadharajan, C., Zheng, L., Bianchi, M., Nico, P.S., Spycher,N.F., Newell, D.L., Esposito, R.A., Wu, Y., Dafflon, B., Hubbard, S.S., Birkholzer, J.T., 2013. Effect of dissolved CO2on a shallow ground-water system: acontrolled release field experiment. Environ. Sci. Technol. 47 (1), 298–305.

Trefry M.G., Muffels Ch.: FEFLOW: a finite-element ground water flow and transport modeling tool. Ground Water, 45, 525–528, 2007.

Trevathan, T.; Johnstone, R.; Chiffings, T.; Atkinson, I.; Bergman, N.; Read, W.; Theiss, S.; Stevens, T. SEMAT—The next generation of inexpensive marine environmental measurement and monitoring Systems. Sensors 2012, 12, 9711–9748. [CrossRef] [PubMed].

UNEP, United Nations Environment Programme, (2011). *World Conservation Monitoring Centre*. Retrieved from: http://www.unep-wcmc.org/aboutWCMC/

Van Genuchten, M.Th.1980.Aclosed-formequationforpredictingthe hydraulic conductivity of unsaturated soils. Soil Sci. Soc. Am. J. 44:892–898.

V. Jelicic, S. Member, M. Magno, D. Brunelli, G. Paci, L. Benini, Context-adaptive multimodal wireless sensor network for energy-efficient gas monitoring, IEEE Sens. J. 13 (2013) 328–338.

V.V. Volkov, J. Van Landuyt, K. Marushkin, R. Gijbels, C. Férauge, M.G. Vasi-lyev, A.A. Shelyakin, A.A. Sokolovsky, LPE growth and characterization ofInGaAsP/InP heterostructures: IR light-emitting diodes at 1.66 m. Applicationto the remote monitoring of methane gas, Sensors and Actuators A: Physical62 (1997) 624–632.

Vanderzalm, J., Page, D., Barry, K., Dillon, P., 2010. A comparison of the geochemical response to different managed aquifer recharge operations for injection of urban storm water in a carbonate aquifer. Applied Geochemistry 25 (9), 1350e1360.

Vaughan, H., Brydges, T., Fenech, A., Lumb, A. (2001). Monitoring long-term ecological changes through the Ecological Monitoring and Assessment Network: Science-based and policy relevant. *Environmental Monitoring and Assessment 67*: 3–28.

Vasilyev, A.V., Zhukovsky, M.V., 2013. Determination of mechanisms and parameters which affect radon entry into a room. J. Environ. Radioact. 124, 185e190.

Visconti, F., De Paz, J.M., Rubio, J.L., 2010. An empirical equation to calculate soil solution electrical conductivity at 25 _C from major ion concentrations. Eur. J. Soil Sci. 61, 980–993.

Viswanathan, M. N., Al Senafy, M. N., Rashid, T., Al-Awadi, E., & Al-Fahad, K. (1999). Improvement of tertiary wastewater quality by soil aquifer treatment. Water Science and Technology, 40(7), 159–163.

Vreeburg, J. H. G., 2007. Discoloration in drinking water systems: a particular approach. PhD thesis, Technische Universiteit Delft, The Netherlands.

Xia F. Wireless sensor technologies and applications. Sensors 2009;9(11):8824–30.

Walid, D., S. Pistre, A. Kneppers, M. Bakalowicz, W. Najem 2011. Karst and artificial recharge: Theoretical and practical problems A preliminary approach to artificial recharge assessment. Journal of Hydrology, 408: 189-202.

Walter, K. M., L. C. Smith, and F. S. Chapin. 2007. Methane bubbling from northern lakes: present and future contributions to the global methane budget. Philosophical Transactions of the Royal Society a-Mathematical Physical and Engineering Sciences 365:1657-1676.

Wang, J. S., J. A. Logan, M. B. McElroy, B. N. Duncan, I. A. Megretskaia, and R. M. Yantosca. 2004. A 3-D model analysis of the slowdown and interannual variability in the methane growth rate from 1988 to 1997. Global Biogeochemical Cycles 18.

Wang Z, Small MJ. A Bayesian approach to CO2 leakage detection at saline sequestration sites using pressure measurements. Int J Greenh Gas Control. 2014;30:188-196.

Wentworth, C.K., 1922. A scale of grade and class terms for clastic sediments. J. Geol. 30, 377–392.

Westerhoff, P., & Pinney, M. (2000). Dissolved organic carbon transformations during laboratory-scale groundwater recharge using lagoon-treated wastewater. Waste Management, 20, 75– 83.

Wickert, A. The Alog: Inexpensive, open-source, automated data collection in the field. Bull. Ecol. Soc. Am. 2014, 95, 166–176. [CrossRef].

Widomski M., Iwanek M., Stępniewski W.: Implementing anisotropy ratio to modeling of water flow in layered soil. Soil Science Society of America Journal, 2013, 77(1), 8–18.

Wilkening, M., 1980. Radon transport processes below the Earth's surface. In: The Natural Radiation Environment, III. Tech. Inf. Center, U.S. Dept. of Energy, Springfield, pp. 90– 104.

Winkler, R., Ruckerbauer, F., Bunzl, K., 2001. Radon concentration in soil-gas: a comparison of the variability resulting from different methods, spatial heterogeneity and seasonal fluctuations. Sci. Total Environ. 272, 273e282.
Whalen, S. C. 2005. Biogeochemistry of methane exchange between natural wetlands and the atmosphere. Environmental Engineering Science 22:73-94.

W.-W. Chang, T.-J. Sung, H.-W. Huang, W.-C. Hsu, C.-W. Kuo, J.-J. Chang, Yi-T.Hou, Yi-C. Lan, W.-C. Kuo, Yu-Y. Lin, Y.-J. Yang, A smart medication system usingwireless sensor network technologies, Sensors and Actuators A: Physical 172(2011) 315–321.

Wiersma, G.B. (Ed.) (2004). *Environmental Monitoring.* Boca Raton, FLA: CRC Press.

Wrucke, C.T., and Wilson, R.F., 1957, Geologic map of the Boulder quadrangle, Boulder County, Colorado: US Geological Survey Geologic Quadrangle Map OF 67-281, scale 1:24,000.

Xue, S., Zhao, Q., Wei, L., & Rena, N. (2009). Behavior and characteristics of dissolved organic matter during column studies of soil aquifer treatment. Water Research, 43, 499–507.

Yang C, Hovorka SD, Treviño RH, Delgado-Alonso J. An Integrated Framework for Assessing Impacts of CO2 Leakage on Groundwater Quality and Monitoring-Network Efficiency: Case Study at a CO2-EOR Site. Environ Sci Technol. 2015;49:8887-8898.

Yang Y-M, Small MJ, Ogretim EO, Gray DD, Wells AW, Bromhal GS, Strazisar BR. A Bayesian belief network (BBN) for combining evidence from multiple CO2 leak detection technologies. Greenh Gases Sci Technol. 2012;2(3):185-199.

Yang, Y.J., Haugh, R., Goodrich, J., 2009. Real-time contaminant detection and classification in a drinking water pipe using conventional water quality sensors: techniques and experimental results. Journal of Environmental Management 90 (8), 2494-2506.

Yun-zheng, P. I., & Jian-long, W. (2006). A field study of advanced municipal wastewater treatment technology for artificial groundwater recharge. Journal of Environmental Sciences, 18(6), 1056–1060.

Zafrir, H., Barbosa, S.M., Malik, U., 2012. Differentiation between the effect of temperature and pressure on radon within the subsurface geological media. Radiat. Meas. 49, 39e56. http://dx.doi.org/10.1016/j.radmeas.2012.11.019.

Zhang, J., Huang, X., Liu, C., Shi, H., Hu, H., 2005. Nitrogen removal enhanced by intermittent operation in a subsurface wastewater infiltration system. Ecological Engineering 25 (4), 419e428.

Zhao Ch., Wang Y., Chen X., Li B.: Simulation of the effects of groundwater level on vegetation change by combining FEFLOW software. Ecological Modelling, 187, 341–351, 2005.

Zienkiewicz O.C., Taylor R.L., Nithiarasu P.: The finite element method for fluid dynamics. Elsevier Butterworth-Heineman, Oxford 2005a.

Zienkiewicz O.C., Taylor R.L., Zhu J.Z.: The finite element method. Its basis and fundamentals. Elsevier Butterworth-Heineman, Oxford 2005b.

Zhou, X., Lakkaraju, V.R., Apple, M., Dobeck, L.M., Gullickson, K., Shaw, J.A.,Cunningham, A.B., Wielopolki, L., Spangler, L.H., 2012. Experimentalobservation of signature changes in bulk soil electrical conductivity inresponse to engineered surface CO2leakage. Int. J. Greenh. Gas Control 7,20–29.

Zhuang, Q., Melillo, J. M.,McGuire, A.D., Kicklighter, D.W., Prinn, R. G., Steudler, P. A., et al. (2007). Net emissions of CH4 and CO2 in Alaska: Implications for the region's greenhouse gas budget. Ecological Applications, 17(1), 203–212.

Ziska, L.H., Moya, T.B., Wassmann, R., Namuco, O.S., Lantin, R.S., Aduna, J.B., Abao Jr., E., Bronson, K.F., Neue, H.U., Olszyk, D., 1998. Long-term growth at elevated carbon dioxide stimulates methane emission in tropical paddy rice. Global Change Biology 4, 657e665.

Websites, each one has a number as specified in the text and in the previous articles:

[1] https://ti.tuwien.ac.at/ecs/teaching/courses/mclu/theory-material/Microcontroller.pdf

[2] http://www.me.umn.edu/courses/me2011/arduino/arduinoGuide.pdf

[3] www.arduino.it

[4] Expanding the Vision of Sensor Materials (1995) Chapter: Chapter 1: Introduction to Sensors, page 9 – 17.

www.durridge.com/products_rad7.shtml

www.etgrisorse.com/en/Products/etg-mca-100-syn-p-2/

http://www.libelium.com/

[9] http://www.arduino.it

[10] https://www.raspberrypi.org

[11] https://www.adafruit.com

[12]http://www.epanorama.net/newepa/2016/02/20/arduino sensors-interfacing/

[13] https://www.sparkfun.com/products/9404

[14]http://www.robotdomestici.it/joomla/component/virtuemart/robotica-domotica/sensori/sensori-generici/co2-sensor-arduino-compatible

[15] http://www.robot-domestici.it

[16] www.droboticsonline.com

[17] https://www.sparkfun.com/tutorials/253

[18] https://www.libelium.com

[39] http://www.lnec.pt/en/research/research-infrastructures/fluvial-hydraulics-experimental-facility/